Titre: Title:	Hydraulic Performance and Biogeochemical Functions in Soil Treatment Units for Onsite Wastewater Treatment: Phosphorus and Nitrogen Removal
Auteur: Author:	Sorour Sheibani
Date:	2026
Type:	Mémoire ou thèse / Dissertation or Thesis
Référence: Citation:	Sheibani, S. (2026). Hydraulic Performance and Biogeochemical Functions in Soil Treatment Units for Onsite Wastewater Treatment: Phosphorus and Nitrogen Removal [Thèse de doctorat, Polytechnique Montréal]. PolyPublie. https://publications.polymtl.ca/73631/

POLYTECHNIQUE MONTRÉAL

affiliée à l'Université de Montréal

Hydraulic Performance and Biogeochemical Functions in Soil Treatment Units for Onsite Wastewater Treatment: Phosphorus and Nitrogen Removal

SOROUR SHEIBANI

Département des génies civil, géologique et des mines

Thèse présentée en vue de l'obtention du diplôme de *Philosophiæ Doctor*

Génie civil

Février 2026

POLYTECHNIQUE MONTRÉAL

affiliée à l'Université de Montréal

Cette thèse intitulée :

Hydraulic Performance and Biogeochemical Functions in Soil Treatment Units for Onsite Wastewater Treatment: Phosphorus and Nitrogen Removal

présentée par **Sorour SHEIBANI**

en vue de l'obtention du diplôme de *Philosophiæ Doctor*

a été dûment acceptée par le jury d'examen constitué de:

Sarah DORNER, présidente
Dominique CLAVEAU-MALLET, membre et directrice de recherche
Frédéric PITRE, membre et codirecteur de recherche
Maria PRIETO-ESPINOZA, membre
Christopher KINSLEY, membre externe

DEDICATION

This dissertation is dedicated to my parents, Saham and Sara, who never stopped believing in me, even from continents away, and to my husband, Benyamin, who has stood by me through every up and down.

ACKNOWLEDGEMENTS

I would like to express my sincere gratitude to my supervisor, Prof. Dominique Claveau-Mallet, for her guidance, support, and trust throughout my PhD. I am also deeply grateful to my co-supervisor, Prof. Frédéric Pitre, for his invaluable input and help at different stages of this project.

I would like to sincerely thank Michelle Nasrallah, Benoît Courcelles, Eric Rosa, and Brahim Maylal for their valuable contributions as co-authors of the first article. Their expertise, insightful discussions, and constructive feedback greatly strengthened the scientific quality of this work.

I would like to thank the Polytechnique Montréal technicians, Samuel Chénier and Éric Turgeon for their assistance with the soil characterization experiments, Gabriel St-Jean for constructing the experimental set-up, and Mélanie Bolduc and Ayat Farahat for their help with the analytical analyses. Finally, I would like to express my sincere appreciation to my friends at Polytechnique Montréal for their support and companionship throughout this journey.

The project was funded by the Ministère de l'Environnement, de la Lutte contre les changements climatiques, de la Faune et des Parcs (MELCCFP), the Natural Sciences and Engineering Research Council of Canada (NSERC; grant numbers ALLRP 570383-21 and RGPIN-2021-02934), and the Canada Research Chair in Decentralized and Small-Scale Water Treatment (grant number 950-232871). This work was also supported by a doctoral scholarship (B2X) from the Fonds de recherche du Québec - Nature et technologies (FRQNT).

RÉSUMÉ

Les systèmes de traitement des eaux usées sur place (Onsite Wastewater Treatment Systems, OWTS) constituent la principale option d'assainissement pour les habitations rurales et isolées qui ne sont pas raccordées à un réseau d'égout. Dans ces systèmes, les unités de traitement du sol (Soil Treatment Units, STU) assurent une étape de polissage, au cours de laquelle l'effluent infiltré est censé éliminer la matière organique et atténuer les nutriments avant qu'ils n'atteignent les eaux souterraines ou de surface. Pourtant, il reste difficile d'expliquer comment les choix de conception, les stratégies de chargement et les propriétés des milieux filtrants contrôlent conjointement la rétention du phosphore (P) et les transformations de l'azote (N) dans les systèmes réels. Cette thèse comble cette lacune en intégrant des études de terrain, des expérimentations en laboratoire, des modèles numériques et des analyses microbiologiques afin de développer une compréhension mécaniste, pertinente pour la conception, du rôle de la charge hydraulique, des caractéristiques de l'effluent et du fonctionnement biogéochimique piloté par l'humidité sur le devenir à long terme du P et du N dans les STU.

Pour atteindre cet objectif, la thèse combine quatre étapes complémentaires. Pour chaque étape, un chapitre a été préparé. Le chapitre 3 (article 1) visait à évaluer si des STUs construites avec des sables d'emprunt importés dans les sédiments peu perméables de la Ceinture d'argile peuvent simultanément satisfaire les exigences de performance hydraulique tout en limitant les rejets de P vers les milieux récepteurs. Cet objectif a été abordé au moyen d'une étude de cas multi-sites portant sur des STUs recevant des effluents secondaires en Abitibi-Témiscamingue (Québec), combinant des approches de terrain, de laboratoire et de modélisation afin d'évaluer la performance hydraulique et les rejets de P. Les inspections de terrain de 26 systèmes ont montré que seulement deux présentaient des signes d'inondation en surface, indiquant que la majorité des unités respectaient les attentes hydrauliques sous les charges et conditions climatiques actuelles. En revanche, l'échantillonnage des effluents de 12 systèmes a révélé que neuf rejetaient du P vers des fossés routiers, avec des concentrations en aval dépassant occasionnellement 35 mg/L, soit plusieurs ordres de grandeur au-dessus des critères québécois de qualité des eaux de surface (0,03 mg/L). Les essais de sorption en laboratoire ont montré que les sables d'emprunt présentaient de faibles capacités de sorption du P (de l'ordre de quelques dizaines de mg P par kg de matériau), et les simulations réalisées avec COMSOL Multiphysics ont indiqué que ces capacités seraient épuisées en moins d'un an sous des charges hydrauliques représentatives, entraînant une percée du

P vers les milieux récepteurs. La modélisation de scénarios a également montré que des connexions de sortie hydrauliquement robustes vers les fossés de drainage peuvent résister à des épisodes de précipitations extrêmes sans défaillance en surface, mais que les rejets systématiques de P demeurent une préoccupation majeure.

En s'appuyant sur ce diagnostic à l'échelle des systèmes concernant les rejets de P, le chapitre 4 visait à déterminer comment le développement de biofilms dans la zone de colmatage des filtres à sable modifie les mécanismes d'atténuation du phosphore lors du traitement des effluents de fosses septiques (STE). Cet objectif a été abordé à l'aide d'expériences contrôlées en colonnes couplées à des extractions séquentielles du P. Les résultats ont suggéré que la croissance des biofilms génère des sites de sorption supplémentaires, prolongeant l'élimination à court terme du P au-delà de ce qui est prédit par les isothermes de sorption obtenues sur sable propre. L'étude souligne la nécessité de distinguer explicitement les fractions de P stables et réversibles lors de l'évaluation des performances des milieux filtrants et du traitement des eaux usées. Globalement, la capacité de sorption s'est révélée largement réversible, soulevant des préoccupations quant à la remobilisation du P lors de perturbations hydrauliques ou chimiques et à ses implications pour l'eutrophisation des milieux en aval.

Le chapitre 5 (article 2) visait à déterminer comment la porosité remplie d'eau et la rétention d'humidité contrôlent le transport de l'oxygène, la structure rédox et l'élimination couplée du carbone et de l'azote dans les STUs. Cet objectif a été abordé à l'aide de deux colonnes de sable de 1 m conçues pour reproduire des STUs conformes à la réglementation québécoise et recevant des STE. Les colonnes étaient remplies de milieux sableux contrastés : un sable grossier avec peu de rétention capillaire et une conductivité hydraulique élevée, et un sable plus fin, plus rétenteur en eau, présentant une conductivité plus faible mais une porosité totale similaire. Le suivi de l'humidité a montré que la colonne grossière maintenait une faible porosité remplie d'eau et un drainage efficace, tandis que la colonne fine développait une porosité élevée remplie d'eau sous l'effet de la capillarité et une saturation de surface induite par les biofilms. Les deux milieux ont permis une élimination de la demande chimique en oxygène (DCO) supérieure à 90 %, mais l'augmentation de la rétention d'humidité a limité le renouvellement de l'oxygène. Dans la colonne de sable grossier, l'oxygène dissous (OD) en sortie dépassait 2,5 mg/L et l'azote ammoniacal influent (NH_4^+-N) était oxydé en azote nitrique (NO_3^--N), conduisant à une élimination moyenne de l'azote total (NT) d'environ 36 %, mais avec un effluent riche en NO_3^--N. À l'inverse, dans la

colonne plus rétentrice en eau, l'OD en sortie se stabilisait autour de 0,8 mg/L, tandis que l'élimination du NT doublait presque (≈67 % en moyenne, atteignant >98 % lors de la saturation tardive de surface), avec des concentrations nettement plus faibles de NO_3^--N dans l'effluent, indiquant un couplage plus étroit entre nitrification et dénitrification. Ces résultats montrent que, dans des conditions réglementaires réalistes, la rétention d'humidité exerce un contrôle de premier ordre sur la structure rédox et la performance d'élimination de l'azote des STUs.

Le chapitre 6 visait à relier la structure des communautés microbiennes résolues en profondeur et leur potentiel fonctionnel aux régimes hydrologiques et rédox contrastés observés dans les deux colonnes de sable. Cet objectif a été abordé en intégrant un volet microbien et fonctionnel, reposant sur le séquençage des amplicons du gène de l'ARNr 16S et l'inférence fonctionnelle à l'aide de PICRUSt2, le long de la profondeur des mêmes colonnes. Les profils communautaires résolus en profondeur ont montré que les deux colonnes hébergeaient des phyla dominants similaires en surface, mais que la diversité et la composition divergeaient fortement avec la profondeur : le sable grossier perdait rapidement en richesse, tandis que le sable rétenteur en eau maintenait des communautés diversifiées plus en profondeur. Ces résultats indiquent que les milieux plus humides redistribuent les substrats vers la profondeur, soutenant une biomasse active dans les couches inférieures. Les marqueurs fonctionnels inférés par PICRUSt2 ont également révélé un enrichissement marqué des gènes de nitrification et un potentiel de dénitrification limité à la surface de la colonne grossière, en cohérence avec une déplétion rapide de la DCO et un effluent riche en NO_3^--N. Dans la colonne plus fine, les marqueurs liés à la nitrification étaient plus uniformément distribués avec la profondeur, tandis que les gènes associés à la dénitrification présentaient une abondance relative plus élevée en surface. La biomasse plus active en profondeur a probablement favorisé une dénitrification supplémentaire et, par conséquent, une meilleure atténuation de l'azote total.

Pris dans leur ensemble, les quatre étapes de cette thèse suggèrent que les organismes de réglementation et les praticiens doivent dépasser une approche centrée uniquement sur les charges hydrauliques et les distances de séparation minimales, et plutôt : (i) exiger la caractérisation de la capacité et de la stabilité de sorption du P des sables d'emprunt et des milieux filtrants ; (ii) cibler explicitement une rétention d'humidité contrôlée et une stratification rédox intégrée sur toute la profondeur lors du choix et du dimensionnement des milieux ; et (iii) fonder les critères de conception et de suivi sur l'élimination à long terme du P et de l'azote vers les milieux récepteurs,

plutôt que sur des critères hydrauliques de court terme. Cette thèse propose ainsi un cadre évolutif pour la conception future des systèmes d'assainissement non collectifs basés sur le sol, afin de protéger à la fois les eaux souterraines et les eaux de surface contre la pollution nutritive.

ABSTRACT

Onsite wastewater treatment systems (OWTS) are the primary sanitation option for rural and remote households lacking sewer infrastructure. In these systems, soil treatment units (STUs) act as a polishing step, where infiltrating effluent is expected to remove organic matter and attenuate nutrients before reaching groundwater or surface waters. Yet it remains unclear how design choices, loading strategies, and media properties jointly control phosphorus (P) retention and nitrogen (N) transformations in real systems. This thesis addresses that gap by integrating field studies, laboratory experiments, numerical modelling, and microbiological analyses to develop a mechanistic, design-relevant understanding of how hydraulic loading, feed characteristics, and moisture-driven biogeochemical functions govern the long-term fate of P and N in STUs.

To achieve this objective, the thesis combines four complementary stages. For each stage, one chapter has been prepared. Chapter 3 (article 1) aimed to evaluate whether STUs constructed with imported borrow sands in low-permeability Clay Belt sediments can simultaneously meet hydraulic performance expectations while limiting P releases to receiving waters. This objective was addressed through a multi-site case study of STUs receiving secondary effluent in Abitibi-Témiscamingue, Québec, combining field, laboratory, and modelling approaches to assess hydraulic performance and P releases. Field inspections of 26 systems showed that only two exhibited surface flooding, indicating that most units met hydraulic expectations under current loading and climate conditions. In contrast, effluent sampling from 12 systems revealed that nine discharged P to roadside ditches, with downstream concentrations occasionally exceeding 35 mg/L, orders of magnitude above Québec surface-water guidelines (0.03 mg/L). Laboratory sorption tests demonstrated that the borrow sands had limited P sorption capacities (on the order of tens of mg P per kg of media), and COMSOL Multiphysics simulations indicated that these capacities would be exhausted in less than a year under representative hydraulic loads, leading to P breakthrough into receiving waters. Scenario modelling further showed that hydraulically robust outlet connections to drainage ditches can withstand extreme rainfall events without surface failure, but systematic P releases remain a critical concern.

Building on the system-scale diagnosis of P releases, Chapter 4 aimed to determine how biofilm development within the clogging zone of sand filters alters P attenuation mechanisms during septic tank effluent (STE) treatment. This objective was addressed using controlled column experiments

coupled with sequential P extraction. The results suggested that biofilm growth generated additional sorption sites, extending short-term P removal beyond what is predicted from clean-sand batch isotherms. The study argues for explicitly distinguishing stable from reversible P pools when evaluating media performance and for treating wastewater. Overall, the sorption capacity appeared largely reversible, raising concerns about P mobilization during hydraulic or chemical disturbances and its implications for downstream eutrophication.

Chapter 5 (article 2) aimed to determine how water-filled porosity and moisture retention govern oxygen transport, redox structure, and coupled carbon and nitrogen removal in STUs. This objective was addressed using two 1-m sand columns designed to emulate Québec-compliant STUs receiving STE. The columns were packed with contrasting sandy media: a coarser, freely draining sand with higher hydraulic conductivity, and a finer, moisture-retentive sand with lower conductivity but similar total porosity. Moisture monitoring showed that the coarse column maintained lower water-filled porosity and strong drainage, whereas the finer column developed capillary-driven high water-filled porosity and biofilm-driven surface saturation. Both media delivered >90% chemical oxygen demand (COD) removal, but increased moisture retention impeded oxygen replenishment. In the coarse sand column, effluent dissolved oxygen (DO) rose above 2.5 mg/L and influent ammonium nitrogen (NH_4^+-N) was oxidized to nitrate nitrogen (NO_3^-–N), yielding ~36% average total nitrogen (TN) removal but NO_3^--rich effluent. By contrast, in the moisture-retentive column, effluent DO stabilized near 0.8 mg/L, yet TN removal nearly doubled (~67% on average, increasing to >98% during late-stage surface saturation), with markedly lower NO_3^--N concentrations in the effluent, indicating tighter coupling of nitrification and denitrification. These results show that, within realistic regulatory constraints, moisture retention exerts first-order control on the redox structure and N removal performance of STUs.

Chapter 6 aimed to link depth-resolved microbial community structure and functional potential to the contrasting hydrologic and redox regimes identified in the two sand columns. This objective was addressed by coupling 16S rRNA gene amplicon sequencing with PICRUSt2-based functional inference along the depth of the same two columns. Depth-resolved community profiles showed that both columns hosted similar dominant phyla at the surface, but diversity and composition diverged sharply with depth: the coarser sand rapidly lost richness, whereas the moisture-retentive sand sustained diverse communities deeper in the profile. Therefore, moisture-retentive media redistributed substrate downward, sustaining active biomass at depth. PICRUSt2-inferred

functional markers further indicated enhanced enrichment of nitrification genes and only partial denitrification potential at the surface of the coarse column, consistent with fast COD depletion and NO_3^--N-rich effluent. In the finer column, nitrification-related markers were more uniformly distributed with depth, while denitrification-associated genes showed higher relative abundance at the surface. The more active biomass at depth likely supported further denitrification and consequently superior TN attenuation.

Taken together, the four stages in this thesis suggest that regulators and practitioners must move beyond a narrow focus on hydraulic loading and minimum separations, and instead: (i) require characterization of P sorption capacity and stability for borrow sands and filter media; (ii) explicitly target controlled moisture retention and depth-integrated redox stratification in media selection and sizing; and (iii) base design and monitoring standards on lifetime P and N removal to receiving waters, rather than on short-term hydraulic criteria alone. This thesis provides a scalable framework for the design of future soil-based OWTS so that they protect both groundwater and surface waters from nutrient pollution.

TABLE OF CONTENTS

LIST OF TABLES

LIST OF FIGURES

LIST OF SYMBOLS AND ABBREVIATIONS

16S rRNA - 16S ribosomal ribonucleic acid

ANOVA - Analysis of variance

ASS - atomic absorption spectroscopy

ASV - Amplicon sequence variant

BOD - Biochemical oxygen demand

cBOD - carbonaceous biochemical oxygen demand

Cc - Coefficient of curvature

C/N - Carbon-to-nitrogen ratio

CLR - Centered log-ratio (transformation)

COD - Chemical oxygen demand

COD/N - COD-to-nitrogen ratio

Cu - coefficient of uniformity

DADA2 - Divisive Amplicon Denoising Algorithm 2

DNA - Deoxyribonucleic acid

DO - Dissolved oxygen

EC - Electrical conductivity

EPS - Extracellular polymeric substances

HLR - Hydraulic loading rate

IC - inorganic carbon

KEGG - Kyoto Encyclopedia of Genes and Genomes

KO - KEGG Ortholog

N - Nitrogen

NH_4^+-N - Ammonium nitrogen

NO_2^--N - Nitrite nitrogen

NO_3^--N - Nitrate nitrogen

OC - Organic carbon

ortho-P - Orthophosphate

OWTS - Onsite wastewater treatment system

PCoA - Principal coordinates analysis

PCR - Polymerase chain reaction

PERMANOVA - Permutational multivariate analysis of variance

PICRUSt2 - Phylogenetic investigation of communities by reconstruction of unobserved states 2

RDA - Redundancy analysis

RMSD – Root mean square deviation

SEM - Scanning electron microscopy

STE - Septic tank effluent

STU - Soil treatment unit

TC - Total carbon

TN - Total nitrogen

TOC - Total organic carbon

TP - Total phosphorus

TSS - Total suspended solids

VWC - Volumetric water content

WFPS - Water-filled pore space

WRRF - Water Resource Recovery Facility

LIST OF APPENDICES

CHAPTER 1 INTRODUCTION

1.1 Definition of the problem

Treatment of domestic wastewater is essential to remove contaminants such as organic compounds and nutrients before they reach the environment. Domestic wastewater can be treated in centralized wastewater treatment plants or in decentralized onsite wastewater treatment systems (OWTSs), commonly known as septic systems (Gurpal et al., 2020). While centralized treatment predominates in cities and towns, isolated residences and small rural communities rely on decentralized systems.

Conventional septic systems are intended to prevent contaminants from entering freshwater resources. They consist of a septic tank, where primary treatment and solids separation occur, followed by a soil treatment unit (STU), also known as a drainfield, where secondary treatment takes place. In the septic tank, solids settle to form sludge at the bottom while fats and oils accumulate as a scum layer. Clarified effluent then infiltrates into the soil profile, where remaining contaminants are attenuated through filtration, sorption, and microbially mediated reactions as the effluent migrates toward groundwater (M. G. Lusk et al., 2017).

In Québec, STUs may be constructed as trenches, infiltration beds, or above-ground mounds depending on land availability and native soil hydraulic conductivity (MELCCFP, 2015, 2017). Where available area or native percolation rates are insufficient, wastewater may first be treated using an advanced secondary treatment system (e.g., sand filters, packaged units). The treated effluent is then discharged to a soil infiltration unit referred to in Québec regulations as a polishing field. This unit is designed to distribute the effluent from a secondary treatment system into the receiving soil to provide additional polishing and attenuation of contaminants before the effluent reaches groundwater.

Approximately 11% of Canadians rely on private wells for domestic water supply, and many of these households use OWTSs for wastewater treatment (Spoelstra et al., 2017). Nationally, about 30% of the Canadian population relies on groundwater as a drinking water source (Government of Canada, 2013). Therefore, the environmental performance of septic systems has direct implications for public health, groundwater safety, and freshwater ecosystem protection.

Microbial attachment to soil particles in STUs leads to the development of biofilm, which is essential for efficient wastewater treatment due to its high metabolic activity (He et al., 2021; Persson & Jansson, 2021). However, as biofilm thickens, it progressively reduces hydraulic conductivity and porosity, eventually generating clogging conditions (Brovelli et al., 2009; Rajabzadeh et al., 2015). These changes often develop slowly, altering oxygen transfer pathways, modifying redox conditions, and ultimately affecting nutrient fate. In severe cases, excessive clogging can cause a surface breakout.

OWTSs fundamentally depend on the ability of STUs to infiltrate effluent and remove contaminants in the unsaturated zone. Adequate unsaturated depth is critical as it enables oxygen replenishment and supports aerobic biodegradation processes. Events that induce prolonged saturation, such as biofilm-related hydraulic restriction, reduced drainage, elevated water tables, and intense rainfall, impede oxygen transfer and suppress aerobic organic matter degradation and nitrification (M. G. Lusk et al., 2017). In principle, an STU is expected to provide reliable hydraulic drainage, geochemical phosphorus sorption, and microbially mediated transformation of organic matter and nitrogen before effluent reaches groundwater or surface water. However, growing scientific evidence shows that these contaminants are not always effectively removed, even when systems appear hydraulically functional.

Phosphorus (P) in septic system effluent is of particular concern because very low concentrations can impair receiving waters. Concentrations as low as 0.03 mg P/L can trigger eutrophication (Smith et al., 2003). In most North American lakes, P is the primary limiting nutrient and the dominant driver of algal blooms (Schindler et al., 2016). Many studies have demonstrated that septic systems export phosphorus to adjacent surface waters (Bowes et al., 2010; Edwards & Withers, 2008). Unlike nitrogen, phosphorus removal relies predominantly on geochemical retention, meaning P attenuation is finite and its long-term security is uncertain.

Nitrogen (N) is another major contaminant released from septic systems. Excess nitrogen promotes eutrophication in receiving waters (Chambers et al., 2012) and concentrations above 10 mg N/L in drinking water pose documented health risks (M. G. Lusk et al., 2017).

Domestic wastewater typically contains 20–70 mg N/L, originating from human waste, food residues, and detergents (Rout et al., 2021). In contrast to P, N removal requires a sequence of microbially mediated transformations, nitrification followed by denitrification, which depend on

co-existing aerobic and anoxic conditions that are difficult to maintain simultaneously within the soil profile.

Agricultural runoff is widely recognized as the dominant source of nutrient inputs to surface waters. In this regard, the land application of manure and synthetic fertilizers has been estimated to account for a substantial proportion of P loading, approximately 72% of total P inputs in some regions, with areal export rates ranging from hundreds to several thousand kg P km^{-2} yr^{-1} (M. G. Lusk et al., 2017). However, the relative importance of nutrient sources varies among lakes depending on watershed characteristics and land use. In waterbodies with limited agricultural influence, aging or poorly functioning septic systems may represent a significant contributor. For example, Lombardo (2006) reported that septic systems can account for 4–55% of total P loads to lakes, and mass-balance analyses have documented cases in which septic effluent constituted the largest single source of P loading (Zurawsky et al., 2004). Regarding N, while inputs from septic systems are generally far smaller than those from agricultural sources, they can nonetheless constitute a significant source to groundwater and make a measurable contribution to overall watershed nitrogen loads (M. G. Lusk et al., 2017).

Regulatory frameworks for conventional OWTSs and STUs do not typically impose nutrient-based effluent limits. In Québec, for example, system approval and compliance are primarily evaluated on the basis of hydraulic design criteria, setback distances, and minimum unsaturated depth requirements rather than long-term nutrient discharge thresholds (LégisQuébec, 2022). Moreover, no numeric effluent standards are specified for N and P in conventional onsite systems, despite their recognized roles in eutrophication and groundwater contamination (LégisQuébec, 2022). Therefore, septic systems that appear fully functional, with no visible flooding, ponding, or failure, may nevertheless export significant loads of P and N to groundwater and surface drainage networks. Such nutrient leakage is persistent, difficult to detect, and environmentally consequential. Despite this, design standards in many jurisdictions have historically emphasized hydraulic infiltration capacity over long-term nutrient attenuation. As a result, regulatory compliance at installation does not ensure sustained environmental protection over the operational lifespan of the system.

1.2 Objectives and hypotheses

The purpose of this thesis is to advance a mechanistic understanding of how OWTSs perform, with a particular emphasis on hydraulic, geochemical, and microbiological factors that govern nutrient attenuation in STUs. To achieve this, the research integrates field observations, numerical modelling, laboratory experimentation, and microbial analysis across four complementary components. Together, these components aim to elucidate the pathways through which P and N are transformed, retained, or lost as septic tank effluent (STE) migrates through sand filters and drainfields.

The specific objectives of this research are structured as follows:

- Objective 1: Field-scale assessment of Abitibi-Témiscamingue STUs

The first objective was to evaluate the in-situ hydraulic performance and P attenuation behaviour of septic installations constructed in impermeable Clay Belt settings of Abitibi-Témiscamingue. The study aimed to determine whether these systems meet hydraulic expectations, particularly at heavy rainfall events, and to quantify the extent to which they release P to surface water networks. This objective was guided by the hypothesis that borrow-sand-based polishing fields generally satisfy hydraulic performance expectations, including during heavy rainfall events, yet exhibit limited long-term P attenuation due to the finite sorption capacity of the filter media. A complementary hypothesis was that observed P releases are primarily controlled by media adsorption capacity, system age, hydraulic loading rates, and design dimensions. To test these hypotheses, the prevalence and configuration of polishing fields were documented, operating conditions were characterized through sanitary inspections, and effluent P concentrations were measured in receiving roadside ditches. Numerical simulations were therefore used to relate measured P leakage to these controlling factors and to assess the consistency between field observations and process-based expectations. This objective was addressed in collaboration with the Groundwater Research Group at UQAT in accordance with a contract with the Ministry of the Environment, Ministère de l'Environnement, de la Lutte contre les changements climatiques, de la Faune et des Parcs (MELCCFP).

- Objective 2: Laboratory-scale investigation of P dynamics in the clogging zone

The second objective was to examine the geochemical basis of P retention within sand filter media, using a 1-m laboratory column operated under controlled STE loading over 13 weeks. Specifically, this objective assessed P attenuation evolution as biofilm developed, and determined how rapidly the initial P sorption capacity declines under STE loading. A key aim was to distinguish the relative contributions of virgin soil adsorption and biofilm-mediated retention within the near-surface "clogging zone," where chemical gradients emerge. The objective was guided by the hypothesis that P retention is dominated by adsorption to virgin sand surfaces, while biofilm development modifies the apparent retention behaviour. To test these hypotheses, the relative contribution of virgin soil adsorption was assessed within the chemically active clogging zone. This component further identified the mechanisms controlling eventual exhaustion in sand filters, leading to P breakthrough.

- Objective 3: Laboratory-scale assessment of hydrogeological control on organic carbon and nitrogen removal

The third objective was to investigate how media geological properties and capillary-driven moisture retention influence redox conditions and nitrogen processing in soil treatment units. This objective was guided by the hypothesis that differences in soil texture and pore structure regulate moisture retention, which in turn controls oxygen availability and redox stratification, leading to distinct pathways of organic carbon degradation and nitrogen transformation. To test this hypothesis, two parallel 1-m soil columns packed with contrasting sandy media were operated under identical hydraulic loading and fed with synthetic septic tank effluent (STE). This approach enabled direct assessment of how soil hydraulic properties govern oxygen diffusion and shape coupled carbon and nitrogen transformation processes under controlled but environmentally relevant conditions.

- Objective 4: Laboratory-scale examination of microbial and functional responses to moisture retention

The fourth objective was to examine how microbial community structure and functional gene potential respond to contrasting moisture regimes in soil treatment units. This objective was guided by the hypothesis that differences in moisture retention and associated redox conditions influence the spatial pattern of microbial communities and the distribution of functional genes involved in carbon and nitrogen cycling. It was further hypothesized that moisture-driven variations in biofilm

development alter the relative representation of nitrification- and denitrification-related pathways along the soil profile. To test these hypotheses, depth-resolved 16S rRNA gene sequencing and predictive metagenomic analyses were conducted on samples collected from 1-m laboratory columns operated under controlled STE loading over 13 weeks. These analyses evaluated the influence of soil moisture content on microbial community composition and functional potential. This integration sought to establish mechanistic links between hydrogeological conditions, microbial ecology, and nutrient fate.

These objectives seek to establish a solid understanding of how hydraulic behaviour, P sorption processes, N transformation dynamics, and microbial community evolution interact to control OWTSs' performance. This integrative structure enables the development of scientifically grounded strategies for improving the design, monitoring, and regulation of decentralized wastewater treatment systems in Québec and similar environments. Figure 1.1 visualizes different sections and objectives of this PhD project.

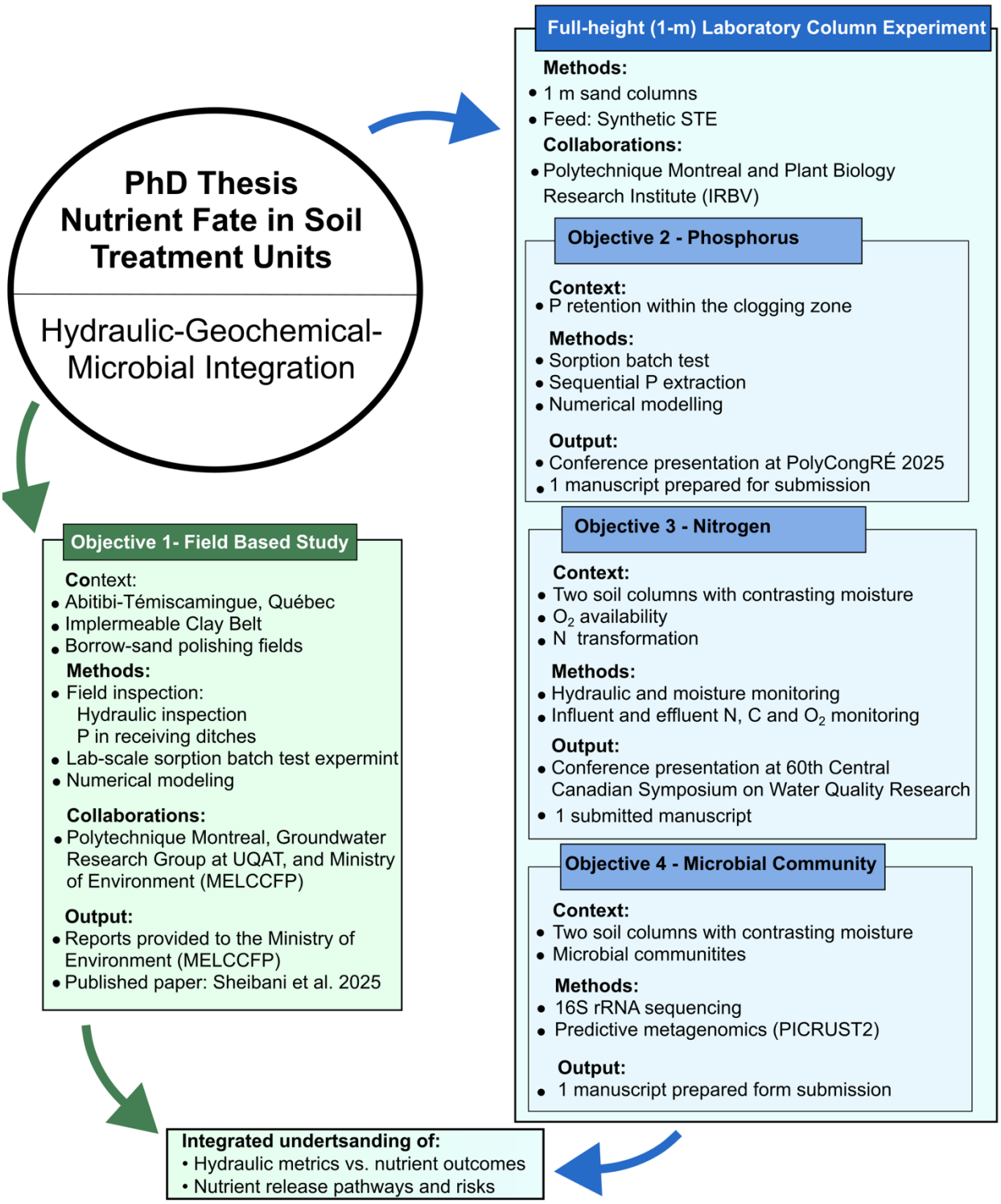

Figure 1.1 Visual synthesis of the PhD research framework on nutrient fate in soil treatment units.

1.3 Structure of the thesis

This dissertation is organized as an article-based thesis comprising four scientific manuscripts, framed by an introductory chapter, a literature review, a discussion and a concluding chapter. Chapter 1 presents the problem definition, and objectives of the work, while Chapter 2 reviews the literature on the fate of nutrients in STUs. The four manuscripts are presented in Chapters 3 to 6, Chapter 7 provides general discussion, and chapter 8 presents the overall conclusions and perspectives.

Each manuscript addresses one of the main objectives outlined in Section 1.2, targeting a distinct but complementary aspect of the hydraulic, geochemical, and microbiological processes governing nutrient fate in OWTSs. Together, they form a coherent framework for understanding nutrient attenuation in sandy STUs. The order of the presentation of the manuscripts is as follows:

- Chapter 3 – Phosphorus retention and hydraulic performance in borrow sand-based wastewater soil treatment units in impermeable settings: Case study in Abitibi-Témiscamingue, Québec (Manuscript 1)

This chapter provides a multi-site assessment of borrow-sand based STUs in the Clay Belt region of Abitibi-Témiscamingue. It evaluates hydraulic performance and P leakage to receiving ditches under real operating conditions. This manuscript has been published in the *Journal of Water Process Engineering*.

- Chapter 4 – Phosphorus Dynamics in the Clogging Zone of On-Site Sand Filters: Treatment Performance and Lifespan (Manuscript 2)

This chapter examines the geochemical processes controlling P retention in sand media. It combines batch adsorption experiments, a controlled column study, and reactive transport modelling to quantify P sorption capacity and its evolution during operation, with particular emphasis on the clogging zone and the role of biofilm development. Parts of the findings were presented at PolyCongRÉ 2025.

- Chapter 5 – Influence of Soil Moisture Distribution on Oxygen Availability and Nitrogen Removal in Onsite Wastewater Treatment Systems (Manuscript 3)

This chapter investigates how soil hydrogeological properties and capillary-driven moisture distribution influence oxygen availability, redox conditions and carbon and N removal rates. It is

based on two 1-m laboratory soil columns operated under identical hydraulic loading. This manuscript has been submitted to *Vadose Zone Journal* and is under review at the time of the submission of this thesis. Parts of the findings were presented at 60th Central Canadian Symposium on Water Quality Research.

- Chapter 6 – Microbial and Functional Responses to Moisture Retention in Soil Treatment Units: Implications for Nitrogen Transformation Pathways (Manuscript 4)

This chapter characterizes depth-resolved microbial communities and PICRUSt2-based functional pathways within the experimental columns. It links moisture regimes and redox gradients to microbial community structure, nitrogen cycling genes, and predicted functional capacities.

- Chapter 7 – General discussion

This chapter synthesizes the findings of the four manuscripts, examines their implications for the design and performance assessment of soil treatment units, and discusses their relevance for the regulation of decentralized wastewater treatment systems.

- Chapter 8 – Conclusions and Recommendations

This chapter concludes the thesis by summarizing the main outcomes of each manuscript and outlining the overall contributions of the work. It also identifies key directions for future research, with emphasis on improving the long-term sustainability of soil-based onsite wastewater treatment systems under realistic operating and environmental conditions.

CHAPTER 2 CONTEXT AND LITERATURE REVIEW

2.1 Hydraulic function of soil treatment units

2.1.1 Unsaturated flow and infiltration dynamics

The hydraulic behaviour of STUs is central to the performance of OWTSs because it governs effluent infiltration, oxygen transfer, and the residence time available for biogeochemical transformations. The unsaturated zone must provide sufficient air-filled porosity to enable oxygen diffusion, which is required for aerobic degradation of organic matter and nitrification (Luanmanee et al., 2001). Increases in soil moisture reduce gas diffusivity, as oxygen diffuses approximately 10,000× more slowly in water than in air. Thus, hydraulic conditions directly constrain the redox environment and the microbial processes responsible for nutrient removal.

Moisture retention within STUs is strongly controlled by soil texture and pore size distribution. Fine-textured soils retain more water at a given matric potential because of stronger capillary forces. In regions with shallow or perched water tables, capillary rise can increase water-filled pore space (WFPS), even when separation distances appear adequate (Gillham, 1984). In addition, climate change is intensifying heavy rainfall events, placing additional hydraulic stress on STUs, an aspect largely neglected in current design approaches (Intergovernmental Panel on Climate Change, 2021).

2.1.2 Implications for soil treatment unit’s design

Traditional STU design relies on percolation tests or saturated hydraulic conductivity to estimate infiltration capacity (Gill et al., 2007). However, these measurements do not capture unsaturated flow behaviour or moisture dynamics under real loading conditions. As wastewater percolates through the infiltrative surface, microbial populations colonize soil grains and form a biologically active clogging layer (biofilm) (Beal et al., 2005; Palmer et al., 2007). This layer traps suspended solids, retains organic matter, and contributes to pollutant removal, but it also reduces hydraulic conductivity (Siegrist & Boyle, 1987). Studies have shown that biomass development depends on the influent's quality and composition, loading rates, moisture content and temperature (Brady & Ray, 2002). Furthermore, the inlet regime of influent to the drain fields can play an influential role. The intermittent dosing prevents saturated conditions, allowing for aerobic biodegradation of

organic matter and nitrification (Brady & Ray, 2002). Field and laboratory studies have shown that, a mature biofilm layer can lead to reductions in hydraulic conductivity and porosity, resulting in water ponding in underground trenches, above the infiltration zone, while keeping the underlying soil unsaturated (Beal et al., 2005, 2006; Kanmani et al., 2014).

Hydraulic design is a central determinant of STU performance, since it controls oxygen availability and redox structure. The effects of moisture on treatment performance depend on its magnitude, duration, and interaction with biofilm development, soil texture, and loading conditions (M. G. Lusk et al., 2017). Prolonged or extreme saturation can severely limit oxygen diffusion and suppress aerobic treatment (Gill et al., 2009; Teerlink et al., 2012). Some experimental studies have linked elevated near-saturated conditions to increased risk of N releases (Kanmani et al., 2014). However, other work on septic plumes has shown that partial oxidation in the unsaturated zone can enhance overall N attenuation, provided suitable redox conditions and carbon sources are available (Robertson et al., 2023).

In practice, limited water accumulation within infiltration trenches or beds is not automatically considered a sign of system failure and is often tolerated, as long as the underlying soil profile remains at least partially unsaturated, oxygen diffusion is not completely impeded, and no surface breakout occurs (Beal et al., 2005; Gill et al., 2009). Under these conditions, the biofilm layer can improve effluent quality by increasing residence time and enhancing sorption and biodegradation (S. Chen et al., 2021).

Some areas worldwide are covered by clayey soils, making an impervious setting which is unfavorable for infiltration and promotes water saturation. For instance, in Canada, clay plains cover an area of 180,000 km^2 of Ontario and Québec (known as the Clay Belt). In this context, constructing STUs with borrow material is an option. For example, the University of Wisconsin designed an aboveground mound system with borrow coarse sand (Converse & Tyler, 1986). The system can be installed in permeable and impermeable settings and avoids ponding and side seepage when adequately designed (Converse & Tyler, 1986). Moreover, in Nova Scotia, sand filters are constructed with borrow fine and coarse sand in impermeable settings, with their effluent either infiltrating into the ground or reaching the surface (Ministry of Environment and Climate Change, 2022). Previous field studies suggest that the performance of onsite wastewater treatment

systems in Nova Scotia is acceptable in terms of the elimination of biological oxygen demand (BOD) and P (Havard et al., 2008).

2.2 Phosphorus fate and retention in soil treatment units

2.2.1 Phosphorus forms and transformations in septic systems

In residential areas, P appears in wastewater from toilets, laundry, and kitchens. Household products such as detergents are sources of P. Recently, laundry detergents with less or no P have been produced, and consequently, the P concentration in wastewater has reduced to 10 mg/L or even less (M. Lusk et al., 2011).

Phosphorus in wastewater exists as a phosphate compound (orthophosphate, polyphosphate, or organic phosphate). Orthophosphate (e.g., H_3PO_4, $H_2PO_4^-$, HPO_4^{2-}, and PO_4^{3-}) is the available reactive phosphorus, while polyphosphate (e.g., $P_2O_7^{4-}$ and $P_3O_{10}^{5-}$) is the linked orthophosphate molecules that will eventually break down to orthophosphate in water (M. G. Lusk et al., 2017). Organic phosphate (in sugar, phospholipids, and nucleotides) comes from human feces and food residues. Most of the phosphate that enters the drain field is in the form of orthophosphate (M. Lusk et al., 2011).

The total amount of P in wastewater can be classified into different phases; Dissolved phosphorus is soluble, while particulate phosphorus is bound to or a component of particles in wastewater (Reid et al., 2018). A fraction of P can also occur as colloidal P (Yang et al., 2021). A small amount of P (mainly particulate phosphorus) is eliminated in the septic tank due to the settling of sludge at the bottom of the tank (M. Lusk et al., 2011). Previous research suggested a P removal of almost 20%-30% in the septic tank (Lowe, 2010; McCray et al., 2005). Other than the settling of particulate P, no appreciable removal mechanism has been recognized for phosphorus in the septic tank (M. Lusk et al., 2011).

In drain fields, a fraction of organic P converts to orthophosphate, and a part of it directly adsorbs into soil grains (M. G. Lusk et al., 2017). The rest of the phosphorus concentration appears as orthophosphate and will either be taken up by plants, adsorb to soil grains, precipitate, or find its way toward groundwater (M. G. Lusk et al., 2017). Phosphorus is adsorbed into soil grains in the presence of positively charged ions such as Fe and Al ions (M. Lusk et al., 2011). Other factors that affect soil sorption capacity could be summarized as soil chemical and physical characteristics,

wastewater loading rates, chemical attributes, and pH (McCray et al., 2005; Persson & Jansson, 2021).

2.2.2 Measurement of soil phosphorus retention capacity

A wide range of engineered and natural materials has been evaluated as reactive media for P removal adsorption capacity in decentralized wastewater systems. Studies have tested substrates such as industrial slags, wollastonite, and various lightweight aggregates using laboratory batch assays, column experiments, and, in some cases, field-scale installations (Johansson Westholm, 2006). Many studies aimed to define the sorption capacities of different soils for P (e.g., Mechtensimer & Toor, 2017; Robertson et al., 2019). In a review paper, McCray et al. (2005) reported that the maximum sorption capacity of soils varies from 0 to 17600 mg/kg. As discussed earlier, precipitation is another type of elimination of P in drain fields. However, it is often lumped and considered together with sorption (McCray et al., 2005).

Sorption batch tests are commonly used to measure the sorption capacity of different filter media; The standard protocol includes exposing a known quantity of media to P solutions of various concentrations for 24 hours (ASTM International, 2016). However, some researchers claimed the results of these tests might contain some errors. For example, Hamisi et al., (2019) argued that these experiments fail to provide sufficient contact time and thus result in an underestimation of the adsorption capacity of the soil. They proposed that column tests are better alternatives. Moreover, batch tests results may vary due to differences in experimental design, influent chemistry, and hydraulic conditions, making direct comparison across studies difficult (Johansson Westholm, 2006).

Despite the limitations, batch tests remain widely used because they are relatively inexpensive, simple to implement, and provide rapid, screening-level estimates of sorption capacity, offering an initial indication of the suitability of different filter media. Langmuir isotherm and Freundlich isotherm are the two well-known isotherms that fit the adsorption of phosphorus in porous media (M. G. Lusk et al., 2017; McCray et al., 2005).

2.2.3 Phosphorus retention mechanisms and long-term stability in soil treatment units

Some studies have clearly shown that phosphorus retention in sand filters is governed primarily by reversible surface adsorption. Once the finite adsorption capacity of the media is exhausted, previously retained P can be released back into the percolating water, leading to elevated effluent concentrations. For instance, a column study examined P attenuation and leaching dynamics in sand filters receiving STE, highlighting the vulnerability of these systems to P breakthrough and mobilization under both routine loading and rainfall conditions (Wang et al., 2024). In this study, a complete P breakthrough occurred relatively quickly (within ~12–73 days, depending on sand age), and maximum P retention capacities were low (≈20–45 mg P kg^{-1}). Aged sands accumulated higher concentrations of Fe, Al, Ca, and Mg, enhancing their short-term P sorption relative to new media, but this did not prevent eventual depletion of available sorption sites.

The breakthrough behavior implies that sand filters may provide only temporary P removal and that long-term performance depends on media replacement. A field-scale study showed that newly constructed drainfields in sandy soils can retain most of the P from STE during the initial stages of operation (Mechtensimer & Toor, 2016). In the first year of operation, more than 95–99% of the applied P load was retained within the drainfield. Estimates based on measured sorption capacities showed that nearly one-fifth of the drainfield's P sorption capacity had already been consumed after the first year. Extrapolations suggested that, under continued loading, complete saturation could occur within approximately six years, at which point the risk of P breakthrough to shallow groundwater would increase sharply. This work highlights the strong short-term attenuation potential of sandy drainfields but also underscores their long-term vulnerability, raising concerns about the reliability of soils to protect groundwater.

Still, several studies report long-term, high P removal in STUs. These investigations suggest that additional mechanisms beyond reversible adsorption contribute to the sustained removal performance over extended periods. For example, a 33-year monitoring record from a seasonal-use septic system in Canada shows that P can be sustainably attenuated in the subsurface over multi-decadal timescales (Robertson et al., 2023). Throughout the monitoring period, soluble reactive P in the groundwater plume remained extremely low (average ≈0.08 mg L^{-1}), corresponding to

roughly 99% removal relative to the effluent, and most of this attenuation occurred within about 1 m of the infiltration pipes. Geochemical evidence indicated that long-term P removal was governed primarily by mineral precipitation rather than reversible sorption, with excess Fe and Al in the non-calcareous drainfield sediments supporting the formation of Fe– and Al–phosphate phases under acidic plume conditions.

A 30-year provincial review of 24 septic-system plumes in Ontario, across sites spanning a wide range of wastewater characteristics and geological settings, most systems exhibited strong attenuation in the shallow subsurface (Robertson, van Stempvoort, et al., 2019). Mean P removal within drainfields reached ~90% in non-calcareous sediments and ~66% in calcareous sediments, with combined drainfield + proximal plume removal averaging 97% and 69%, respectively. Mineral precipitation was the dominant long-term sink, evidenced by secondary P-rich coatings on sand grains at nearly all locations, indicating steady-state precipitation reactions occurring immediately beneath the infiltration pipes.

On the contrary, the secondary mechanisms contributing to long-term successful performance are site-specific and not always guaranteed. The long-term observations from the Ontario septic plume study showed no evidence of the "secondary," slow, or irreversible phosphorus attenuation processes (Robertson, 2008). Mechanisms such as diffusion of phosphate into mineral microsites, gradual transformation of sorbed P into more stable metal phosphate minerals did not measurably influence plume migration over 16 years. Instead, plume behavior was fully explained by rapid, reversible sorption, as reflected in a modest distribution coefficient derived from sediment desorption tests.

In practice, many field studies reported failed STUs from which P was released to the environment. some long-term examinations of P retention in soil-based treatment systems reveal that their capacity to immobilize P may be substantially lower than previously assumed. In a study of four community-scale infiltration beds that had been operating for 14–22 years, mass-balance calculations showed that, on average, only about 12% of the cumulative P load had been retained by the filter material, indicating limited long-term attenuation potential (Eveborn et al., 2012). Laboratory batch tests and geochemical modelling suggested that calcium phosphate precipitation

played a minimal role at most sites. Across the sites, the remaining P sorption capacity was small, reinforcing the view that soil treatment systems can lose their effectiveness over time.

Another investigations of STUs in Sweden further illustrate the limited long-term capacity of unsaturated subsoils to retain P from domestic wastewater. Across six systems ranging from 11 to 28 years old, the measured P accumulation in the subsoil (0.32–0.87 kg/m³) represented less than one-third of the estimated historical input, suggesting substantial losses over time (Eveborn et al., 2014). In the same study, column leaching tests demonstrated that accumulated P was readily mobilized when exposed to deionized water, with eluate concentrations reaching up to 6 mg/L, indicating that stored P is not necessarily stable under fluctuating hydrologic conditions.

Some studies confirm that biofilm improves the removal rate of P in soil. Rustige et al. (2003) argued that P removal in summer is more significant than in winter because of biomass growth in a constructed wetland in Germany. Other studies claimed that high organic carbon concentrations in infiltration-based treatment systems increase the biofilm growth and provide attachment sites for P (Hamisi et al., 2022).

Controversial studies have also been published. For example, an evaluation of 12 full-scale on-site wastewater treatment with seven out of eight systems failing to achieve the Swedish national guideline of <3 mg total P/L in the effluent, attributed the results largely to filter clogging and dilution by infiltrating extraneous water (Vidal et al., 2018). Their statistical analysis confirmed a strong positive correlation between effluent pH and P removal, but no relationship was found between influent organic carbon levels and P removal, suggesting that organic matter interference with precipitation processes was minimal under the generally high-pH conditions of these filters.

Overall, the divergent findings across laboratory studies, long-term field investigations, and full-scale system assessments highlight that P retention in soil-based treatment units is highly variable and governed by multiple, site-specific processes. While some systems exhibit sustained removal driven by mineral precipitation or favourable geochemical conditions, others rapidly exhaust their sorption capacity or mobilize previously stored P under fluctuating hydrologic or chemical regimes. These inconsistent outcomes underscore the need for further research that integrates multi-site field monitoring with controlled laboratory experiments to isolate the roles of media composition, redox conditions, hydrology, and biofilm development. Such combined efforts are

essential to more reliably link P retention mechanisms with their governing factors and to improve predictive assessments of long-term system performance.

2.3 Nitrogen fate and transformations in soil treatment units

2.3.1 Nitrogen forms and biogeochemical cycling in septic systems

In domestic wastewater, about 70%-80% of nitrogen (N) exists as ammonium nitrogen (NH_4^+-N), and the rest mainly exists as organic nitrogen (Li et al., 2017). The sum of NH_4^+-N and organic nitrogen is defined as total Kjeldahl nitrogen. The pH of domestic wastewater is close to neutral (pH=7); therefore, ammonia mainly exists in the form of NH_4^+-N (Lowe, 2010). In the septic tank, organic nitrogen is primarily converted to NH_4^+-N through ammonification; thus, most nitrogen (70-90% of total nitrogen) enters the soil treatment unit as NH_4^+-N (M. G. Lusk et al., 2017). In soil, organic nitrogen further transforms to NH_4^+-N via ammonification depending on soil composition, pH and temperature (Vymazal, 2007). In drainfields, approximately 10–50% of NH_4^+-N may adsorb to negatively charged soil particles, while the remaining fraction is primarily oxidized to nitrate (NO_3^--N) through aerobic nitrification (M. G. Lusk et al., 2017). Although NH_4^+ sorption can be a transient process and adsorbed NH_4^+-N may eventually be nitrified, a portion of adsorbed or fixed NH_4^+-N may not be readily available to nitrifying bacteria. A substantial fraction of fixed NH_4^+ (50–85%) may be unavailable or only slowly available to nitrifiers, potentially delaying nitrification (M. G. Lusk et al., 2017). Moreover, nitrification occurs under aerobic conditions, whereas under anaerobic conditions ammonium adsorption may persist (Beal et al., 2005). Minor fractions may also be assimilated by plants and microorganisms or lost through volatilization (M. G. Lusk et al., 2017).

Nitrification occurs in two stages by autotrophic bacteria (Hayatsu & Kosuge, 1993); first, ammonia converts to nitrite nitrogen (NO_2^--N) and then NO_2^--N converts to NO_3^--N. In both steps presence of oxygen and inorganic carbon is necessary (M. G. Lusk et al., 2017). NO_3^--N formed through nitrification can then be uptaken by plants and microorganisms, anaerobically (in the absence of oxygen) converted to nitrogen gas through denitrification or reach the groundwater (M. G. Lusk et al., 2017).

Several studies have reported that in the presence of oxygen (in the unsaturated zone), nitrifying bacteria, and inorganic carbon, complete nitrification is expected (Wilhelm, Schiff, & Robertson,

1994; Yamaguchi et al., 1996). On the other hand, denitrification is not always completed. If nitrate is not removed through denitrification, it will leach into groundwater resources. Organic carbon is the source of energy in denitrification.

2.3.2 Nitrogen removal and soil hydrogeological properties

A range of factors, including the type and intensity of wastewater loading, the age of the system, and the depth to the water table, have been examined for their influence on nitrogen attenuation in drainfields (e.g., Humphrey et al., 2021; Lusk et al., 2017; Robertson et al., 2021). Depending on these factors N removal rates vary. In one study, long-term monitoring of a seasonal-use septic system, representing roughly 80% removal relative to the septic tank effluent, demonstrated that nitrogen removal can remain stable over decades (Robertson et al., 2023). This study underscored that, under suitable hydrogeochemical conditions, conventional onsite systems are capable of sustaining substantial nitrogen removal over multi-decadal timescales, even without energy-intensive technologies or advanced operational controls (Robertson et al., 2023). On the other hand, some studies have shown that some traditional septic systems remove less than half of the total nitrogen they receive (Lotfikatouli et al., 2024; Pan et al., 2016).

Nitrification and denitrification highly depend on hydrogeological properties of soil. A field modeling study on percolation trenches showed that the intrinsic soil structure and hydraulic regime were the dominant controls on nitrogen transformations, underscoring that minimizing NO_3^--N leaching requires attention to site-scale soil and flow conditions (Zúñiga-Gutiérrez et al., 2025).

The degree of saturation is one key factor in controlling nitrification and denitrification (Berlin et al., 2014). In the absence of a sufficient unsaturated zone, nitrification will not occur. On the other hand, if the unsaturated zone is too deep, organic carbon will get oxidized and will not be available to the denitrifying bacteria (M. G. Lusk et al., 2017). A previous study revealed that denitrification is more likely to occur when soil is at least 60% saturated, and the air content is less than 10% (Brady & Ray, 2002).

In a lysimeter study, De & Toor (2015) investigated how hydrological and biogeochemical conditions in the vadose zone control the fate of effluent-borne nitrogen beneath drip-dispersal OWTS drainfields. Three large lysimeters with layered soil, and commercial sand received a daily dose of septic tank effluent via drip lines, and were instrumented with multi-probe sensors to track

water content, temperature, and electrical conductivity in sand and soil. Water-filled porosity was consistently higher in the soil layer (0.55–0.90) than in the sand (0.07–0.32), reflecting strong textural control on moisture distribution. Total N concentrations decreased from about 70 mg/L in the effluent to 27.4 mg/L in the leachate, with nitrification in the sand layer and denitrification in the soil layer contributing to N removal.

In a research experiment with loamy sand, sandy loam, and silt loam indicated that moisture distribution and residence time strongly influence N transformations (Beggs et al., 2011). A HYDRUS-2D model working based on nitrification and denitrification kinetics as functions of soil moisture, highlighted the sensitivity of denitrification to the soil moisture function. When the model was extended to account for generic soil types, the greatest total nitrogen losses (≈30–70%) were predicted for medium- to fine-textured soils and for occasions where slower percolation and capillary retention enhance denitrification under subsurface drip application.

Another modeling and laboratory study on agricultural soils demonstrated how strongly nitrogen transformations depend on soil moisture conditions, highlighting principles directly relevant to understanding N fate in unsaturated zones of STUs (Mekala & Nambi, 2017). Nitrogen transport experiments were conducted on two soils, a sandy soil and a loamy sand, under controlled moisture regimes spanning a wide range of WFPSs. The authors showed that nitrification was most effective at intermediate moisture levels (approximately 50–60% WFPS). At higher volumetric water contents (VWCs) (≥80% WFPS), oxygen limitation suppressed nitrification and promoted denitrification. Near-saturated conditions (≈96% WFPS) in the loamy sand yielded minimal nitrification but strong denitrification and substantial nitrogen losses.

Taken together, these studies demonstrate that N removal in onsite wastewater drainfields is governed far more by the hydrogeological setting and moisture regime of the soil than by system design alone. Although some systems achieve long-term, stable attenuation, others may perform poorly, even under similar loading. The reason is that soil structure, texture, and saturation dictate whether nitrification and denitrification can proceed. Overall, optimizing nitrogen removal in OWTS requires recognizing that soil hydraulic properties and moisture dynamics set the fundamental limits on treatment performance.

2.3.3 Biofilm-mediated nitrogen removal

The clogging layer formed due to the biofilm growth is one crucial factor. Biofilm plays a vital role in N removal. A mature biofilm layer can lead to clogged parts of the gravel layer and saturated or almost saturated parts in the trench while the overlying soil remains unsaturated (Brady & Ray, 2002). This variation in saturation may improve nitrogen removal. Moreover, hydraulic conductivity is decreased within the biofilm layer, leading to a longer residence time that can help the treatment process. Gill et al. (2009) argued that since the development of biomass in systems receiving septic tank effluent is more significant than in systems receiving secondary treatment effluent, the former system is capable of more efficient N removal. On the other hand, if the biomass section overgrows, a fully saturated zone develops, which may prevent nitrification. In such cases, the homeowners need to replace or unclog or replace the drain field.

A previous soil column study simulating SUTs examined how carbon availability at the infiltration surface, where biofilm growth is maximized, influenced nitrogen removal (Friedman et al., 2018). Columns were supplied with synthetic secondary effluent but operated at different influent C/N ratios (approximately 2 vs. 5). The low-C/N system was enriched in aerobic metabolisms, whereas the higher-C/N system exhibited a larger denitrification potential. The study showed that niche differentiation in biofilm with alternating oxic–anoxic conditions is critical for effective nitrogen removal.

A French study examining the performance of buried vertical sand filters highlighted that unlike NH_4^+-N, declining NO_3^--N levels were sensitive indicators of reduced aeration caused by developing clogging layers (Petitjean et al., 2016). The study therefore suggests NO_3^--N trends are effective for identifying early clogging in sand filters, offering a practical approach for anticipating performance deterioration in buried OWTSs.

Another recent study on sand highlighted the clogging layer still provided effective removal of biodegradable COD and NH_4^+-N and exhibited potential for simultaneous nitrification and denitrification (S. Chen et al., 2021). However, reduced moisture content at low loading rates created conditions less favorable for denitrification, leading to NO_3^-–N accumulation. The study argues that biofilm growth is an inherent, self-adaptive response to wastewater and that sustainability depends not on eliminating clogging, but on managing limited clogging to balance hydraulic function with long-term treatment efficiency.

Collectively, these studies show that biofilm development in STUs is a major control on N transformation patterns, with both beneficial and adverse effects depending on its extent and the resulting saturation profile. Overall, the literature suggests that biofilm formation is an unavoidable and often beneficial component of onsite treatment, but its growth must remain controlled. Sustainable long-term nitrogen removal depends not on preventing clogging, but on managing its development so that hydraulic function, oxygen supply, and redox stratification remain balanced.

2.4 Numerical modelling of soil treatment units

Flow in variably saturated porous media is often modelled using Richard's equation which was originally derived based on Darcy's law (L. A. Richards, 1931). Van Genuchten's model is the most widely used mathematical expression of the soil water retention curve that describes the relationship between the soil VWC and the capillary head in unsaturated porous media (van Genuchten, 1980). Researchers have used this approach to model soil treatment units with different properties.

Using the above-mentioned approach, researchers have studied different aspects of STUs. For example, a few numerical studies extended a one-dimensional reactive transport model for unsaturated soils by explicitly coupling water flow with multispecies transport of nitrogen species, dissolved oxygen (DO), dissolved organic carbon, and biomass (Berlin et al., 2014, 2015). In another numerical study, a groundwater-scale reactive transport model was constructed to represent the transformation and migration of inorganic nitrogen species in a saturated aquifer (Lee et al., 2006).

Some researchers used numerical models to model the fate of P in soil-based treatment systems. For this purpose, adsorption isotherms are usually considered. In one study, P removal in horizontal subsurface flow constructed wetlands was analyzed using a groundwater flow model (Liolios et al., 2015). Flow was simulated with the finite-difference code, coupled with solute transport, and sorption onto the porous medium was represented using a Freundlich-type sorption isotherm in linear form. Calibration against two years of experimental data yielded parameter sets for P adsorption parameters that produced acceptable agreement between simulated and observed P concentrations. The model was then used to explore how changes in design and operating conditions influence P removal efficiency.

Another process-based numerical model was used to assess how bioclogging affect hydraulics and contaminant removal in soil-based wastewater treatment systems (McCray et al., 2000). The simulated trench system included clogging layers at the base and sidewalls, with unsaturated flow and reactive transport of P sorption parameterized from literature data. Results showed that clogging reduces infiltration rates, increases the residence time, and thereby enhances removal of contaminants. Additional simulations comparing uniform versus focused STE loading indicated that uniform application increases residence times and improves treatment.

A long-term modelling study evaluated P removal in eight lateral flow sand filters treating STE using Langmuir, Freundlich, and linear isotherms, alone or combined with batch-derived Langmuir terms (Sinclair et al., 2014). Sorption behaviour in the longer, more heavily loaded 8-m LFSFs was best characterized by non-single-regime adsorption relationships, while the shorter, less stressed 5.5-m medium-sand units exhibited P retention patterns that were well captured by conventional equilibrium isotherm formulations.

Overall, these numerical studies show that flow and reactive transport models provide a powerful framework to dissect the coupled hydraulic and biogeochemical behaviour of soil treatment units. By explicitly representing variably saturated flow (via Richards' equation and van Genuchten–type retention functions), sorption/precipitation processes, and key reaction pathways, they allow systematic testing of design and operating scenarios and isolation of the effects of individual factors such as media texture, loading regime, oxygen supply, and clogging development. Such models are particularly valuable for exploring long-term performance and failure modes that are difficult to observe directly in the field, and they provide a quantitative basis for optimizing STU design and management to improve nutrient removal and protect downgradient receptors.

2.5 Microbial ecology of soil treatment units

Early studies on wastewater microbiomes relied on microscopy-based observations, which provided only coarse morphological information and could not resolve most bacterial taxa (Eikelboom, 1975; Gilbride et al., 2006). Subsequent culture-dependent methods allowed researchers to isolate specific functional groups; however, because the vast majority of environmental microorganisms are not readily cultivable, these approaches captured only a small

fraction of community diversity (Liss & Allen, 1992). More recently, the advent of molecular techniques provided the means to examine microbial communities without cultivation. The development of molecular techniques particularly those targeting the 16S rRNA gene, whose conserved and variable regions enable robust phylogenetic resolution, transformed the field by allowing direct characterization of microbial communities in wastewater and soil environments (Gilbride et al., 2006; Woes, 1987). More recently, metagenomic and high-throughput sequencing approaches have enabled not only taxonomic profiling but also the inference of functional potential within wastewater facilities.

To date, much of our understanding of how microbial communities influence treatment performance comes from studies on large, centralized wastewater treatment plants, where processes such as nitrification, denitrification, anammox, enhanced biological phosphorus removal, and floc or biofilm formation have been extensively examined (Criado Monleon et al., 2022; Daims et al., 2016; Sanz & Köchling, 2007). By comparison, only a limited number of investigations have examined microbial dynamics in decentralized treatment systems, and even fewer have focused directly on the STUs.

Tomaras et al. (2009) conducted one of the first studies on STUs microbiology. They used 16S rRNA gene sequencing and reported markedly lower phylogenetic diversity in STE than in the biofilm, and very few shared sequences between STE and biofilm communities, indicating that taxa carried in the effluent do not simply establish in the biofilm. Instead, the nutrient-rich STE appears to select for a distinct soil microbial assemblage during infiltration. Moreover, comparisons between soils receiving clean water and those receiving STE showed that the composition of the applied effluent strongly structures the resident microbiota, underscoring the role of STE loading in shaping STU microbial communities.

One study investigating depth-resolved bacterial communities in soil treatment areas showed that microbial assemblages can vary markedly with depth even within the same soil type (Amador & Atoyan, 2012). They argued that conventional systems implicitly assume that a suitable microbial community will self-establish and provide the necessary biochemical functions, regardless of soil texture or effluent characteristics, and designs therefore rarely consider microbiology explicitly. However, the large variability observed in OWTS performance, coupled with these documented

shifts in community structure, suggests that differences in bacterial assemblages that develop under long-term STE loading are a key, and often overlooked, source of functional variation. Linking community composition to specific treatment functions could improve the ability to predict system performance and inform adjustments to design and operation to selectively promote beneficial microbial processes.

Another detailed soil column study that combined chemical profiling with microbial community and functional analyses demonstrated that carbon availability is a major determinant of microbial structure and nitrogen-processing capacity (Friedman et al., 2018). Columns receiving higher C/N influent developed larger and more functionally diverse heterotrophic communities. Sequencing revealed that *Nitrospira* dominated across depths, surpassing the expected ammonia-oxidizing bacteria and *Nitrobacter*, and its distribution closely mirrored ammonium depletion and nitrate production, consistent with complete ammonia oxidation. Simultaneous nitrification and denitrification were concentrated in the upper layers where degradable carbon was abundant, whereas deeper zones were more carbon-limited. Overall, the study showed that microbial niche differentiation within biofilms is central to nitrogen removal performance, and that maintaining sufficiently high C/N ratios in applied effluent is critical for sustaining the microbial functions required for effective treatment.

A comparative field study examining biofilm communities in STUs receiving effluents with different levels of pre-treatment showed that influent quality strongly shapes microbial diversity and spatial organization (Criado Monleon et al., 2022). Systems receiving highly treated effluent from an aerobic rotating biodisc contactor supported richer and more diverse microbial communities than those receiving only partially treated septic tank effluent, reflecting the influence of lower and more stable carbon inputs on community assembly. Sequencing revealed pronounced shifts in phylum- and genus-level composition between the two influent types, with horizontal position along the trench exerting a stronger control on community structure than depth. Fully treated effluent promoted a higher relative abundance of denitrifying taxa, although the study emphasized that functional richness alone does not guarantee improved nitrogen attenuation; instead, the extent and maturity of the biofilm governed treatment potential by regulating hydraulic conductivity and thus metabolic activity. Overall, the work underscores that STU microbiomes do not develop uniformly but instead form distinct spatially structured biomes shaped by influent

quality and biofilm development, with important implications for pollutant attenuation and long-term system performance.

Another study comparing intermittently aerated and unaerated soils demonstrated that oxygen supply exerts a strong influence on the size and organization of microbial communities involved in wastewater treatment (Atoyan et al., 2013). Intermittent aeration consistently supported a larger active microbial biomass and higher richness. In contrast, unaerated soils harbored smaller and less diverse communities.

Studies examining leach field soils under contrasting moisture conditions show that microbial communities in STUs undergo substantial compositional shifts in response to wastewater loading and water saturation. Soils associated with leach fields host diverse microbial populations whose composition is not dictated solely by effluent inputs; rather, in situ conditions, especially moisture and the resulting oxygen availability, govern which taxa become established and active (Fernández-Baca et al., 2018). This aligns with column studies showing that moisture retention and depth-specific redox zones are key controls on the assembly and functioning of microbial communities responsible for carbon and nitrogen transformations in soil-based treatment systems (Fernández-Baca et al., 2018).

Fernández-Baca et al. (2019) assessed a pair of soil columns operated under well-drained versus flooded conditions, both 16S rRNA and functional-gene sequencing demonstrated that the microbial assemblages that developed during operation diverged strongly from those present in the original field soils. Community composition at the DNA level was strongly structured by soil moisture, indicating that redox and moisture gradients are dominant drivers of microbial assembly in STUs.

Taken together, these studies demonstrate that STU microbiomes are shaped far more by in situ physicochemical gradients than by the microbial composition of the influent. Across soil columns, and field systems, a consistent pattern emerges: moisture retention, oxygen availability, carbon supply, and depth-specific redox conditions dictate which taxa proliferate and which functional pathways dominate. These factors drive sharp vertical and horizontal stratification, promote the emergence of niche-specialized communities, and ultimately control the balance between nitrification, denitrification, carbon turnover, and biofilm development. Importantly, the marked

variability in community composition across soil types, influent qualities, and operational regimes challenges the long-standing assumption that a “suitable” microbial community will simply self-establish in all STUs. Instead, the literature clearly indicates that microbial communities in STUs do not converge toward a single stable state but assemble along environmental gradients that differ from system to system. This recognition underscores the need for mechanistic studies that directly link hydrogeological properties, microbial structure, and functional potential, an approach that motivates the column experiments presented in the following sections.

CHAPTER 3 ARTICLE 1: PHOSPHORUS RETENTION AND HYDRAULIC PERFORMANCE IN BORROW SAND-BASED WASTEWATER SOIL TREATMENT UNITS IN IMPERMEABLE SETTINGS: CASE STUDY IN ABITIBI- ABITIBI-TÉMISCAMINGUE, QUÉBEC

Journal of Water Process Engineering

Volume 74, April 22, 2025, Pages 107681

Coauthors: Sorour Sheibani[a]*, Michelle Nasrallah[a], Benoît Courcelles[a], Eric Rosa[b], Brahim Maylal[b] and Dominique Claveau-Mallet[a]

[a]Department of Civil, Geological & Mining Engineering, Polytechnique Montréal, 2900 Boulevard Édouard-Montpetit, Montréal, Québec H3T 1J4, Canada.

[b]Groundwater Research Group (GRES), Research Institute on Mines and Environment (RIME), Université du Québec en Abitibi-Témiscamingue (UQAT), 341 Rue Principale N, Amos, Québec J9T 2L8, Canada.

* Corresponding author. Email: sorour.sheibani@etud.polymtl.ca

Abstract

On-site wastewater treatment systems (OWTS), including soil treatment units (STUs), rely on effluent infiltration into local soils for treatment. However, in regions with impervious soils, this process becomes challenging. As a result, borrow sand is necessary for STU construction. For example, in the Abitibi-Témiscamingue region (western Québec, Canada), impervious sediments from the Clay Belt necessitate the use of such systems. This study evaluates the hydraulic performance and phosphorus retention capacity of borrow sand-based STUs through field inspections, laboratory experiments, and numerical modeling. Field inspections of 26 septic systems revealed that only 2 systems exhibited surface flooding, suggesting minimal hydraulic failure. However, sampling from 12 systems showed that 9 released phosphorus into the environment, with phosphorus concentrations exceeding 35 mg/L in the downstream ditches in some cases, which were far above Québec's surface water limit of 0.03 mg/L. Laboratory sorption tests demonstrated that the sands used in STUs had limited maximum P sorption capacities (88.49 and 17.12 mg/kg). Numerical simulations using COMSOL Multiphysics further indicated that P retention in the sand layer is likely to be exhausted within a year, leading to P migration into the

environment. Simulations also indicated that systems with properly designed outlets to a drainage ditch could maintain hydraulic performance during extreme rainfall events. These findings highlight the inadequacy of current borrow sand-based STU designs in ensuring long-term phosphorus retention. To mitigate environmental contamination, improved design strategies and management practices should be considered.

Keywords: Septic system within impermeable soils, Water saturation, Phosphorus elimination, Field inspection, COMSOL Multiphysics numerical simulations

3.1 Introduction

In sparsely populated areas, residences are not connected to centralized wastewater treatment plants. Instead, domestic wastewater is treated in decentralized onsite wastewater treatment systems (OWTSs). In a conventional OWTS, primary treatment takes place in a septic tank, and secondary treatment occurs in a downgradient soil treatment unit (STU) such as a drain field. However, if wastewater is not properly treated, septic systems can introduce contaminants such as organic chemicals, nutrients (phosphorus and nitrogen), and pathogens into the environment (e.g. Canter and Knox, 2017; Lusk et al., 2017). In Canada, approximately 25% of the population uses septic systems for wastewater treatment (Government of Canada, 2001), highlighting the importance of monitoring their performance.

In regions with clayey soils, including Canada's Clay Belt—covering 180,000 km² across Ontario and Québec—traditional STUs face significant challenges. These impervious soils restrict infiltration, reducing the effectiveness of treatment. In such environments, STUs constructed with borrow sand offer a practical solution to improve infiltration and wastewater treatment. For these systems to perform effectively, the unsaturated zone must facilitate oxygen diffusion, supporting aerobic microbial activity and the oxidation of pollutants such as organic carbon (e.g. Luanmanee et al., 2001). However, the impermeability of the underlying soils makes the design of the effluent discharge path crucial for maintaining hydraulic efficiency and preventing water accumulation or flooding.

Different designs have been developed for borrow sand-based STUs to address site-specific challenges. The University of Wisconsin, for example, developed an aboveground mound system using borrow coarse sand, which can be installed in both permeable and impermeable settings. These systems discharge effluent through infiltration into the soil and, when properly designed, prevent ponding and side seepage (Converse & Tyler, 1986). In Nova Scotia, sand filters are constructed with borrow fine and coarse sand in impermeable areas, with effluent either infiltrating the soil or discharging to the surface, depending on site conditions and system design (Ministry of Environment and Climate Change, 2022). Previous field studies suggest that the performance of onsite wastewater treatment systems in Nova Scotia is acceptable in terms of the elimination of biological oxygen demand (BOD) which suggests sufficient unsaturated depth (Havard et al.,

2008). Nevertheless, the hydraulic performance of STUs inevitably depends on local climatic and hydrogeological conditions. Consequently, further studies need to be conducted in various settings to test the applicability of treatment approaches and assess optimal design features. Moreover, the increase in recent intense rainfall events driven by climate change (Intergovernmental Panel on Climate Change, 2021), puts extra pressure on borrow sand-based STUs —a factor largely overlooked in existing designs. Therefore, studying the effective hydraulic performance of STUs has become crucial for enhancing resilience and ensuring reliable operation.

Phosphorus (P) is of particular concern in wastewater due to its role in eutrophication. Even small concentrations, as low as 0.03 mg/L, can trigger eutrophication in surface water (Smith et al., 2003). Studies confirm that septic systems contribute to P pollution in surface water bodies (e.g., Bowes et al., 2010; Edwards and Withers, 2008). A small amount of particulate P (typically 20 to 30% of total P) is removed in septic tanks during sludge settling (Lowe, 2010; M. Lusk et al., 2011; McCray et al., 2005). However, most dissolved P, primarily as orthophosphate, moves into the drain field, where it may be taken up by plants, interact with soil through sorption and precipitation, or migrate toward groundwater through advection-dispersion processes (M. G. Lusk et al., 2017). Sorption and precipitation, depending on the presence of positively charged ions and pH, are the primary physiochemical mechanisms leading to P elimination in STUs (Del Bubba et al., 2003).

Researchers have studied the suitability of sandy STUs in P removal through various approaches. Laboratory studies highlight the variability of P removal. Hamisi et al. (2022) reported an average P removal of about 80% in 0.6 m long sand-based columns operated for 300 days at a hydraulic load of 0.011 m/d. In contrast, Wang et al. (2024) found that P removal declined rapidly in 0.3 m sand filters as adsorption sites became saturated. P removal in their study ranged from 24 to 32% at higher hydraulic loads (0.049 m/d) and improved to 35 to 53% at lower loads (0.024 m/d), with complete breakthrough occurring in less than 75 days.

There are a few multi-site studies on real systems operating over the long term that also demonstrate contrasting outcomes. Robertson et al. (2019) investigated 24 OWTSs in Ontario, ranging from 8 to 45 years old, through plume monitoring. Their studied systems achieved an average P removal efficiency of 80%, which was attributed to mineral precipitation mechanisms and favorable soil chemistry. Among these systems, 10 were built on clay or granitic bedrock, relying on imported,

medium-coarse sand with 9 achieving over 75% P retention. In contrast, Eveborn et al. (2012) documented long-term failure, with P removal declining to around 12% in four sand-based STUs after 14 to 22 years of operation due to the saturation of adsorption sites. Their approach included sampling the filter beds and analysis of accumulated P. Similarly, Eveborn et al. (2014) evaluated six OWTSs (11 to 28 years old) in Sweden, four of which used imported sand over clay soils. They estimated removal rates below 30%. None of the abovementioned studies included investigations on the hydraulic performance of the systems.

Given the variability in P removal reported in previous studies and the limited research on the hydraulic performance and outlet design of systems within infiltration-preventive natural settings, further research is essential to understand how site-specific factors, material availability, design choices, and management practices influence the performance of borrow sand-based STUs. To our knowledge, this study is the first investigation to deepen the understanding of STUs built with borrow sand over clayey soils, focusing on both hydraulic performance and P removal. The reference area for this study is the Abitibi-Témiscamingue region, where many isolated households rely on OWTSs due to the rural setting. The widespread use of private wells for drinking water in this area further underscores the importance of preventing contamination from improperly treated septic effluent.

A novel, multi-faceted approach was employed to assess hydraulic performance and P removal efficiency, incorporating multi-site field inspections to identify STUs' failure risks in terms of P releases and flooding. To better understand the factors driving performance, the study included characterization of natural soils, laboratory tests to evaluate the adsorption capacity of two sands suitable for STU construction, and numerical simulations modelling P transport and water saturation across various real-world design scenarios. The new numerical framework integrates climate change considerations by simulating extreme rainfall events. Beyond performance evaluation, this study introduces a broadly applicable methodological framework for assessing site conditions and modelling wastewater treatment outcomes, offering practical guidance for the design, construction, and management of STUs in challenging environmental settings.

3.2 Methodology

3.2.1 Site description

The reference area of this study, the Abitibi-Témiscamingue region in western Québec, is depicted in Figure 3.1a along with silt and clay coverings. The hydrogeological environment of the study area is described in detail by (Cloutier et al., 2013, 2015, 2016) and Nadeau et al. (2018, 2015). Fine-grained glaciolacustrine sediments of Lake Barlow-Ojibway are found in this region. These varved sediments (centimetric alternations of subhorizontal layers of clay and silt) can reach thicknesses of over 50 m and cover over 38% of the region's municipalized territory (Cloutier et al., 2016).

The information regarding the original soil types (Figure 3.1b) and locations (Figure 3.1c) of 223 septic systems within the study area were obtained from municipal records. The aim was to study a large pool of data to establish the general context of septic systems in the study area. STUs of these systems are relevant to the septic installations addressed in this study. Soil types were defined based on the permeability categories defined by Québec's guidelines, further explained in section A.1. While a total of 14% of the studied systems were built in very permeable, permeable, and lowly permeable soils, 82% of the systems were built in impermeable soils (Figure 3.1b). The presence of lakes and rivers in Figure 3.1c, vulnerable to eutrophication, highlights the importance of P removal as a key objective. Additionally, in Québec, OWTSs' regulations prioritize P as the limiting nutrient of the local ecosystems.

In a conventional septic system, a septic tank is followed by a drain field, as shown in Figure 3.2a. However, more advanced septic systems include additional treatment steps. The target septic systems in Abitibi-Témiscamingue are advanced systems built in impermeable soil. Since the natural soil does not support infiltration, these systems include STUs as polishing fields constructed with borrow sand and are further classified into 3 categories based on the treatment chains.

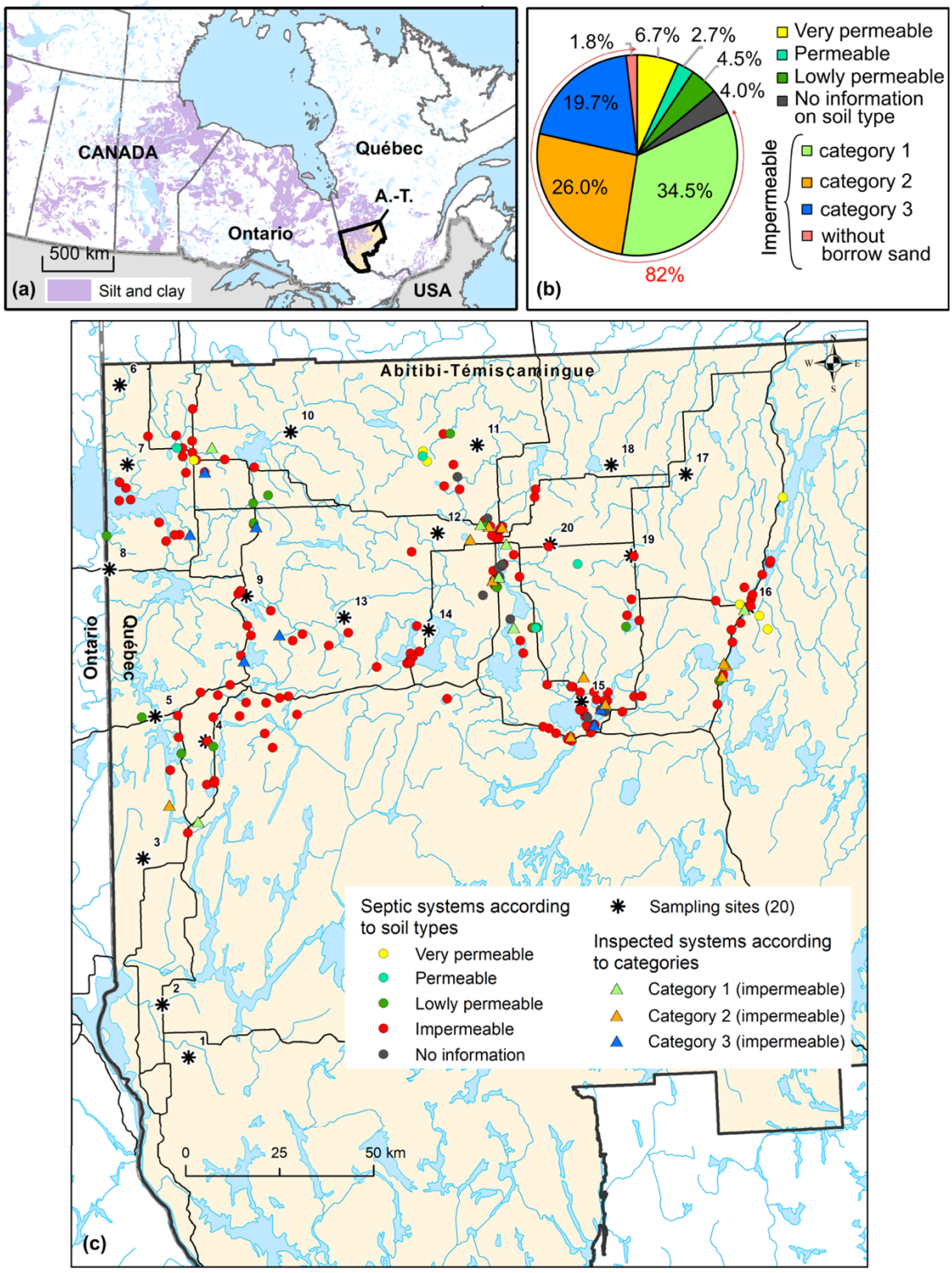

Figure 3.1 (a) Map of Abitibi-Témiscamingue in Québec, Canada and silt and clay coverings (Geological Survey of Canada, 2014, 2019; Veillette et al., 2005). (b) Classification of documented systems based on soil type and system category, (c) Location of documented systems with their settings' permeability, sampling sites and inspected systems.

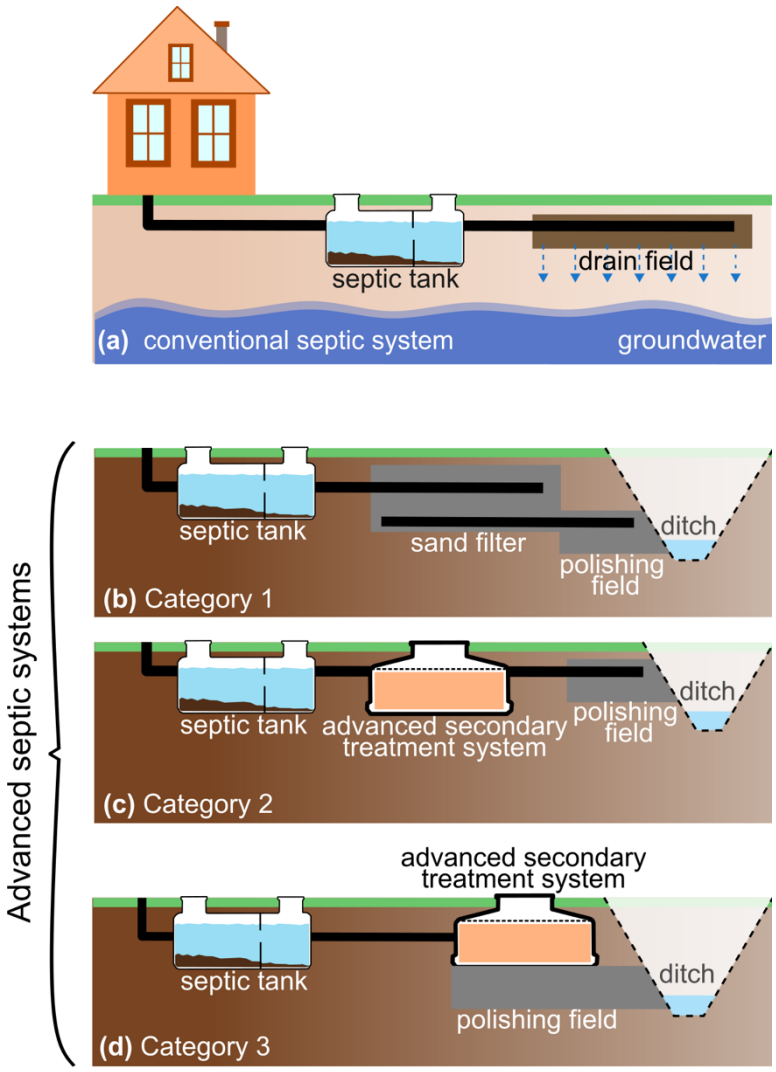

Figure 3.2 Schematic representation of septic system treatment chains. (a) Conventional septic system with a drain field. (b–d) Advanced septic systems found in Abitibi-Témiscamingue, which are constructed in impermeable soils and include a borrow-sand-based polishing bed. These systems are categorized into three types based on their treatment chain: (b) Category 1 – septic tank + sand filter + polishing bed, (c) Category 2 – septic tank + advanced secondary treatment + polishing bed, and (d) Category 3 – septic tank + advanced secondary treatment superimposed onto a polishing bed

In all studied systems, treatment chains start with a septic tank. Following this, some systems include a sand filter (Category 1), or an advanced secondary treatment system (Category 2). Other systems incorporate an advanced secondary treatment system superimposed on a polishing field (Category 3). All systems ultimately discharge into borrow-sand based polishing fields. In some septic systems, ditches were present downgradient of the polishing bed. The treatment chains in

these 3 categories are illustrated in Figure 3.2b, c and d. As shown in Figure 3.1b, among all 223 systems, 80% were installed in impermeable soil with borrow sand STUs, following one of the specified categories. The proportions of each system category are also shown in Figure 3.1b.

In comparison with a drain field, a polishing field is smaller in thickness and area but receives larger hydraulic loading rates [$L/m^2/d$]. Polishing fields and drain fields are constructed in trenches or infiltration beds (MELCCFP, 2015). Here, the studied polishing fields were built as polishing beds.

3.2.2 Field sanitary inspections

Sanitary inspections were conducted from July to August 2022. Twenty-six residences with septic systems including borrow sand polishing beds leading to ditches were targeted. These septic systems were chosen to encompass a variety of characteristics to reflect real-world conditions within the study area. The studied systems spanned all three main categories shown in Figure 3.2, with sizes ranging from 7 to 32 m^2, estimated hydraulic loads from 0.27 to 1.62 m^3/d (0.025 to 0.077 m/d), and ages between 2 and 17 years. They also included different inlet distribution methods, either gravity-fed or low-pressure systems. Further details about the inspected systems are provided in Table A.1. Gravity-fed systems and low-pressure systems are the main types of distribution of influent to soils in STUs (MELCCFP, 2017) and were further explained in, section A.4.

The hydraulic loads of the systems were estimated based on the number of residents and the wastewater production of 0.27 m^3/d per person (MELCCFP, 2017). The average occupancy rate, defined as the ratio of produced wastewater discharge to the system's full capacity according to local regulations (MELCCFP, 2017), was 45% in the inspected systems.

Septic systems were inspected for any sign of hydraulic failure (such as flooding). Water samples from ditches were collected at 2 points: (i) where polishing beds lead to ditches, and (ii) 5-10 m upstream from the polishing fields only if enough flow existed in the ditches. The plan of the sampling points is shown in Figure A.2. All samples were collected in triplicate. The location and categories of the inspected systems are shown in Figure 3.1c.

Samples were analyzed for total P concentration according to (MELCCFP, 2019). In short, samples were collected in plastic bottles and acidified to pH < 2 and then shipped to the laboratory and stored at 4°C. Next, samples were aliquoted into assay tubes, alongside standards and controls. Each tube received 120 µL of saturated potassium persulfate and was subjected to digestion in an autoclave and then cooled and assayed for absorbance.

The amount of released P was calculated as the difference in the average concentration of total P in the two sampling points as follows:

$$\text{Released P} = P_{polishing\ bed} - P_{upstream} \tag{3.1}$$

where $P_{polishing\ bed}$ [mg/L] and $P_{upstream}$ [mg/L] are the average total P concentrations at the level of polishing beds and upstream of the polishing beds respectively.

3.2.3 Sampling and analysis of natural soils

During the Fall of 2021, natural soil samples were collected at 20 sites covering several municipalities in Abitibi-Témiscamingue. The sampling points were not directly associated with individual septic systems but were chosen across the study area to capture the spatial variability of the clay deposit at the regional scale (sites shown in Figure 3.1c). At each site, 55 cm of the soil was excavated with an auger at first. Samples were then collected at depths of 55 cm to 70 cm also using an auger and weighed in the field. This depth corresponds to the approximate depth at which the STUs are constructed, ensuring that the soil characteristics at the relevant depth were studied. The procedure was repeated several times until 4 kg composite samples were obtained from each site. Samples were stored in tightly sealed plastic sampling bags, placed in rigid plastic buckets and carried to the Polytechnique Montreal geotechnical laboratory. All samples were stored in a refrigerator with humidity control prior to the tests.

The grain size distribution of samples was evaluated through sieve analyses conducted according to ASTM C136 (ASTM International, 2020) and clay content was estimated as the mass portion of particles smaller than 0.002 mm (García-Gaines and Frankenstein, 2015). Additionally, the soil type was determined according to Quebec's regulations (MELCCFP, 2017), further explained in section A.1.

3.2.4 Adsorption batch test

The adsorption tests were carried out on two sands that were likely to be used for the construction of the target STUs, to further investigate the factors influencing their performance in P removal. The first sand, identified as S1, comes from a quarry located in the city of Rouyn-Noranda in Abitibi-Témiscamingue, aligning with local resource availability and regional practices. The second sand, S2, is used in the preparation of concrete, further reflecting the types of sands commonly available and suitable for construction.

These two sands met the following criteria based on the regional regulations: (i) an effective particle size, d_{10}, between 0.25 and 1 mm, (ii) a uniformity coefficient, Cu, ≤ 4.5, (iii) less than 3% of particles smaller than 80 μm, and (iv) less than 20% of the particles larger than 2.5 mm (MELCCFP, 2015). Further justifications on S1 and S2 meeting the specifications are presented in section A.5.

Municipal wastewater often carries between 4 to 16 mg P/L (Metcalf et al., 1991). Here, solutions with P concentrations of 2, 5, 10, 15 and 20 mg/L, which covers a realistic range, were prepared by diluting a 100 mg P/L solution of KH_2PO_4 in Milli-Q water. In all solutions, 0.1 M potassium nitrate (KNO_3) was also added to maintain a constant conductivity of approximately 10 $\mu S/cm$ (Del Bubba et al., 2003).

The adsorption tests were carried out according to the ASTM D4646 standard (ASTM International, 2016). Sands were spread in a layer of 2-3 cm and air-dried for 7 days until a constant weight was achieved. Subsequently, 2 g of sand was added to the P solutions at a media/solution mass ratio of 1:20. Blank samples (P solutions with no sand) with the same concentrations were also tested. All samples were then placed in a rotary extractor for 24 h at a speed of 29 rpm, at a room temperature of 22 °C. After 24 h of agitation, the samples were allowed to settle for 1 hour. Then, samples were filtered through Whatman GF/C filters (47μm), and P concentrations were measured according to the USEPA PhosVer® 3 ascorbic acid method. The pH of all samples was measured before and after the test.

3.2.4.1 Isotherm modelling

Following the adsorption batch test, Freundlich and Langmuir isotherm equations were fitted to the adsorbed and equilibrium P concentrations. Freundlich's equation is:

$$c_a = k_F c^{b_F} \tag{3.2}$$

where c_a is the equilibrium mass of the adsorbate (P) per unit mass of adsorbent [g/kg], c is the adsorbate (P) concentration [mg/L] at equilibrium, and k_F [(g/kg) (L/mg) ^{b_F}] and b_F [-] are constants. Langmuir's equation is:

$$c_a = \frac{c k_L b_L}{1 + c b_L} \tag{3.3}$$

where k_L [g/kg] and b_L [L/mg] are constants. k_L denotes the maximum Langmuir adsorption capacity and b_L is related to the binding energy.

3.2.5 Numerical modelling

3.2.5.1 Conceptual Model, simulation scenarios and boundary conditions

In the polishing beds studied here, perforated pipes were placed in a layer of crushed stone within the borrow sand leading to a ditch (Figure 3.3). Water flow and P transport were modeled for different polishing beds (Table 3.1). General properties of all models were derived from the real systems in the study area. Additionally, the simulated models were designed to incorporate the range of variability observed in these systems. These variabilities include factors such as STU size, occupancy rates, shape (rectangular or square), and the adsorption capacity of the borrow sand used.

According to local criteria, the area of each polishing bed is based on the number of bedrooms in the residence, with larger residences requiring larger polishing beds (MELCCFP, 2015). To account for variation in size, the models include residences with 1 to 6 bedrooms. In all models, the areas of polishing beds were directly taken from local regulations (MELCCFP, 2015). We considered two occupancy rates: 100% occupancy, representing full capacity, and 45% occupancy, which is the average local rate. The occupancy rate directly affects the influent discharge to the

polishing beds. Based on the local regulation, the maximum discharge, applied at 100 percent occupancy, is 0.54 m³/d for a 1-bedroom residence and 3.24 m³/d for a 6-bedroom residence (MELCCFP, 2015). For 45% occupancy, the influent discharge is calculated as the product of the occupancy rate and the maximum inlet discharge.

Table 3.1 Characteristics of simulated polishing beds (number of bedrooms of residences, polishing bed area, occupancy rate, influent discharge, with of polishing bed, sand type, and rainfall intensity).

Model number	**Number of bedrooms**	**Polishing bed area, A_p [m^2]**	**Occupancy rate (%)**	**Influent discharge, Q_{inf} [m^3/d]**	**Width of polishing bed [m]**	**Sand type**	**Rainfall [mm/d]**
1*	1	7	100	0.54	2.4	S1	2.5
2	6	32	100	3.24	2.4	S1	2.5
3	6	32	100	3.24	5.66	S1	2.5
4	1	7	45	0.243	2.4	S1	2.5
5	6	32	45	1.458	2.4	S1	2.5
6	6	32	45	1.458	5.66	S1	2.5
7	1	7	100	0.54	2.4	S2	2.5
8	6	32	100	3.24	2.4	S2	2.5
9	6	32	100	3.24	5.66	S2	2.5
10	1	7	45	0.243	2.4	S2	2.5
11	6	32	45	1.458	2.4	S2	2.5
12	6	32	45	1.458	5.66	S2	2.5
13	1	7	100	0.54	2.4		78
14	6	32	100	3.24	2.4		78
15	6	32	100	3.24	5.66		78

* simulated in both 2D and 3D.

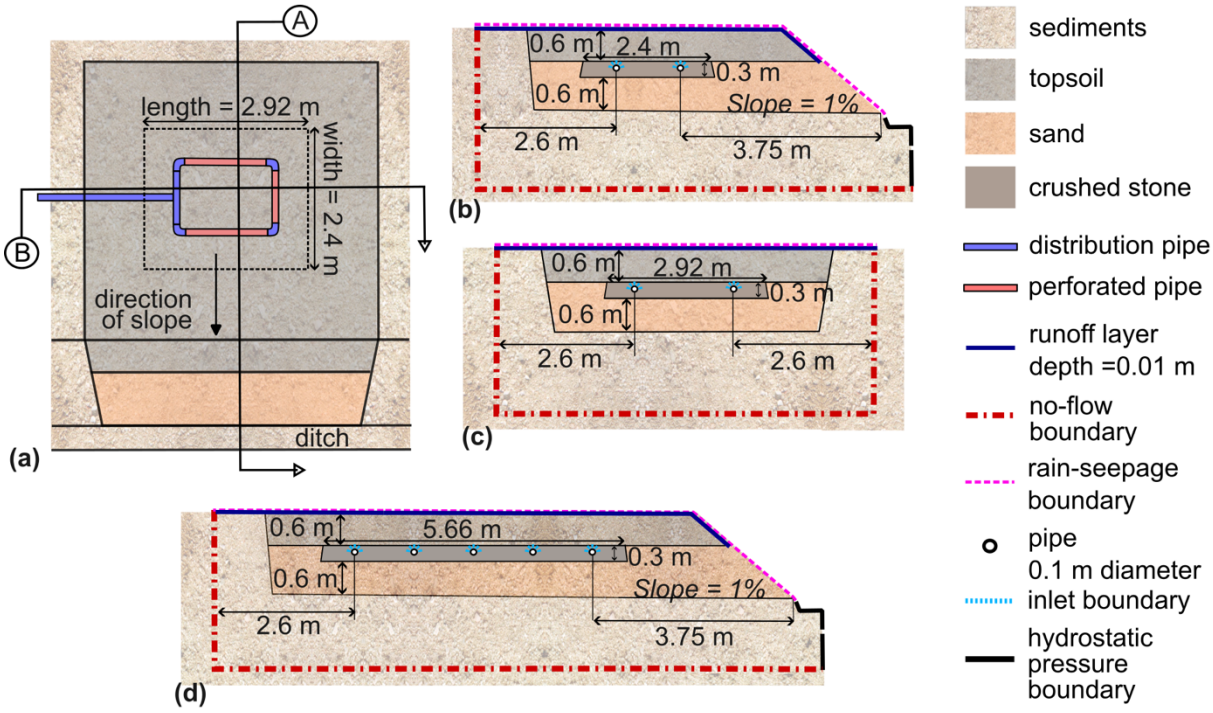

Figure 3.3 Simulated polishing beds and the implemented boundary conditions. (a) plan of a polishing bed for 1-bedroom residences. The dashed line shows the boundaries of the crushed stone layer. (b) Cross-section A simulated for polishing beds for 1-bedroom residences and rectangular polishing beds for 6-bedroom residences. (c) Cross-section B considered for 3D simulation of model 1. (d) Cross-section simulated for all square polishing beds for 6-bedroom residences.

Rectangular and square polishing beds were simulated for 6-bedroom residences to account for shape-related differences. In rectangular models, the width of the bed was set at 2.4 m to accommodate two pipes, and the length was calculated based on the required area. In square models, the width and length were equal, matching the total required area.

Model 1 represents the polishing bed for a 1-bedroom residence. Model 2 is a rectangular polishing bed for a 6-bedroom residence, with the same width as Model 1 but a longer length. Model 3 simulates a square polishing bed for a 6-bedroom residence to evaluate the effect of bed shape on performance. Models 4-6 replicate Models 1-3 but with 45% occupancy to account for the average occupancy rate identified during field inspections. Models 7-12 follow the same configuration as Models 1-6 but use S2 sand, which has a different P sorption capacity compared to the S1 sand used in the first six models.

In Models 1-12, average rainfall intensity was considered. To assess the hydraulic performance under extreme conditions, three additional models (Models 13-15) were included. These models exclude P transport and are subjected to torrential rainfall events to evaluate system performance under intense precipitation.

Two-dimensional models are frequently preferred to their 3-dimensional counterparts due to their less computational costs. Researchers usually apply dimensional contraction along the dimension in which the quantity of interest varies negligibly (Marafini et al., 2020). To the best knowledge of the authors, modelling STUs is generally done in 1D and 2D (e.g., Berlin et al., 2014; MacQuarrie et al., 2001). Here, in the case of sloped polishing beds, 2D simulations can be used to predict hydraulic integrity and the fate of contaminants. The reason is that wastewater disperses uniformly in the crushed stone layer and moves through the sand layer in the direction of the slope with negligible flow perpendicular to the slope. Therefore, for all 15 models, 2D simulations were performed. To further justify the use of 2D modeling, model 1 was simulated in 3D and compared to its 2D equivalent in section A.7. This approach led to the validation of 2D modelling in the context of this study.

Figure 3.3a represents the plan of a polishing bed for a 1-bedroom residence and Figure 3.3b and 3c exhibit cross-sections A and B. The surface area of the crushed stone layer corresponds to polishing bed's area. The crushed stone layer in cross-sections A and B represents the width and length of the polishing bed, respectively. Cross-section A is in the direction of the slope and was simulated for 2D models with 1 bedroom. The 3D simulation of model 1 was then conducted, considering the geometry of both cross-sections. Rectangular polishing beds designed for 6-bedroom houses have the same width as 1-bedroom models (Table 3.1), therefore, the cross-section of Figure 3.3b was simulated using the same geometry. Finally, the cross-section in Figure 3.3d was designed for square polishing beds associated with 6 bedrooms. The plans of polishing beds designed for 6-bedroom residences are provided in Figure A.4.

For models 1-12, simulations were performed in two steps. First, an average rainfall intensity of 2.5 mm/day, as suggested by Labonté-Raymond et al. (2020), was implemented, until a steady state was obtained. In the second step, the inflow from perforated pipes was introduced along with the rain inflow. Labonté-Raymond et al. (2020) highlighted that climate change has led to a significant

escalation in the intensity of extreme rainfalls in Abitibi-Témiscamingue in a way that a single-day rainfall of 77.8 mm in September 2018, surpassed the previously anticipated 100-year recurrence level. The final 3 models (models 13 - 15) were initially simulated using the average rainfall rate as well as the inlet flow from pipes until reaching a steady state and were then subjected to a 24-hour period of 78 mm rainfall along with the inflow from pipes.

Figure 3.3 shows all implemented boundary conditions. Low pressure distribution systems were considered and a uniform inflow through the upper half of the perforated pipes was implemented (further explained in section A.4). The inlet velocities were defined as:

$$\boldsymbol{n_v}.\boldsymbol{u_{2D}} = \frac{Q_{inf}}{86400 L_{1_{2D}} L_{2_{2D}}}$$

$$\boldsymbol{n_v}.\boldsymbol{u_{3D}} = \frac{Q_{inf}}{86400 L_{3D}^2} \tag{3.4}$$

where $\boldsymbol{n_v}$ is the outward normal vector, $\boldsymbol{u_{2D}}$ [m/s] and $\boldsymbol{u_{3D}}$ [m/s] are the 2D and 3D inlet velocities, Q_{inf} [m^3/d] is the influent discharge, $L_{1_{2D}}$ [m] is half of the perimeter of all pipes in the 2D cross-section, $L_{2_{2D}}$ [m] is the length of the polishing bed and L_{3D}^2 [m^2] is the lateral surface area of the upper half of perforated pipes in the 3D model. 86400 is the conversion factor.

The water depth in the ditch was set to 15 cm. Hydrostatic pressure was imposed to the boundaries below the water level. A mixed boundary condition was assigned to the boundaries above the water table as:

$$\boldsymbol{n_v}.\boldsymbol{u} = I + R_b(H_b - H) \tag{3.5}$$

where $\boldsymbol{u}$ [m/s] is the Darcy velocity, I [m/s] is the infiltration rate, R_b [s^{-1}] is the external resistance, H_b [m] is the total external head and H [m] is the total internal head at the boundary.

When the pressure is negative, the mixed boundary switches to $I = \text{rainfall rate}$ and $R_b = 0$. As the water table in the sand layer rises above the water level in the ditch, a seepage boundary forms where the saturated porous medium faces the air. An outward flux from the porous media to the

ditch occurs through this boundary. In this situation, $I = 0$ and R_b must be large enough to ensure that the boundary's pressure closely approximates atmospheric pressure (Chui & Freyberg, 2007).

It was assumed that rainfall completely infiltrates into the sand layer. However, lowly permeable sediments and topsoil can limit infiltration and entail runoff. To properly model the interaction of surface water and infiltration, a thin runoff layer was considered at the top of the sediments and topsoil. This layer serves as a transitional zone where rainfall can partially infiltrate while also allowing for surface runoff. The idea of incorporating a runoff layer into subsurface modelling was previously introduced and implemented (e.g., Chapuis, 2009; Weill et al., 2009). Details regarding the selection of the remaining no-flow boundaries are provided in section A.8.

An inlet P concentration of 5 mg/L was considered. This value is within the range of 3 - 7 mg P/L which was previously reported for secondary effluent (Banu et al., 2008). The initial P concentration within the polishing bed was established at zero.

3.2.5.2 Governing equations and parameters

Finite element-based software, COMSOL Multiphysics (COMSOL, 2019) was utilized for numerical simulations. Meshing used in the models and grid convergence are described in section A.9. The "Richards' equation" interface was used to model flow in variably saturated soil layers:

$$\frac{\partial \theta}{\partial t} + \nabla.(\boldsymbol{u}) = Q \tag{3.6}$$

where θ $[-]$ is the volumetric water content, $\boldsymbol{u}$ [m/s] is the Darcy velocity, and Q [s^{-1}] is a source/sink term. The Darcy velocity is defined as:

$$\boldsymbol{u} = -K_{sat} k_r \nabla\left(H_p + z\right) \tag{3.7}$$

where K_{sat} [m/s] is the saturated hydraulic conductivity, k_r[-] is the relative permeability, H_P [m] is the pressure head, and z [m] is the vertical coordinate. All soil layers were assumed to be homogenous and isotropic. The pressure head was addressed according to the water content (van Genuchten, 1980):

$$S_e = \begin{cases} \left(1 + \left|\alpha H_p\right|^n\right)^{-m} & H_p < 0 \\ 1 & H_p \geq 0 \end{cases}$$

$$\theta = S_e(\theta_s - \theta_r) + \theta_r$$

$$m = 1 - \frac{1}{n} \tag{3.8}$$

where S_e [-] is the effective saturation, θ_r [-] is the residual water content, θ_s [-] is the saturated water content which equals porosity, and α [m^{-1}], n [-] and m [-] are van Genuchten parameters. Relative permeability was defined as:

$$k_r = S_e^{0.5}(1 - (1 - S_e^{-m})^m)^2 \tag{3.9}$$

The hydraulic properties of the runoff layer were modelled using Richard's equation according to Chapuis (2009). In this layer, the relative permeability was set to 1, and the water content drops from 0.99 to 0.01 as the pore water pressure decreases from 0 to -1 Pa.

Porous media parameters were implemented as presented in Table 3.2. Further justifications are provided in section A.10.

Table 3.2 Porous media parameters used for modeling.

	Hydraulic conductivity K_{sat} [m/s]	**Porosity ε [-]**	**Residual water content θ_r [-]**	**van-Genuchten parameter α [m^{-1}]**	**van-Genuchten parameter n [-]**
Topsoil	3×10^{-6}	0.52	0.15	2.42	1.46
Sand	4.5×10^{-3}	0.39	0.03	12	2.5
Fine sediment	6×10^{-8}	0.54	0.26	4.53	1.51
crushed stone	2.5	0.52	0	20	2.2
Runoff layer	45	1	0	-	-

The “Transport of diluted species in porous media” interface was used to model the transport of wastewater P content by the advection-dispersion equation:

$$\frac{\partial(\theta c)}{\partial t} + \frac{\partial(\rho_b c_a)}{\partial t} - \nabla.\left((D_d + D_e)\nabla c\right) + \boldsymbol{u}.\nabla c = Q_c \tag{3.10}$$

where ρ_b [kg/m^3] is the dry bulk density of the soil, D_d [m^2/s] is the dispersion tensor, D_e [m^2/s] is the molecular diffusion coefficient, and Q_c [g/m^3/s] is the source/sink term. Longitudinal and transverse dispersivities and molecular diffusion coefficient were set to 0.01 m, 0.001 m and 1×10^{-9} m^2/s respectively. Langmuir adsorption isotherm was considered for modelling since it provides the maximum adsorption capacity, which is useful for analysis.

Soil bulk density was calculated as:

$$\rho_b = 2650(1 - \varepsilon) \tag{3.11}$$

where 2650 [kg/m^3] is a common value for soil particle density and ε [-] is the porosity.

Soils with larger particles have smaller specific areas and lower adsorption capacities (Khamehchiyan et al., 2007). Therefore, no adsorption capacity was attributed to crushed stone. The adsorption capacity of sand was defined based on experimental results. The impermeable sediment layer is expected to impede the infiltration of flow. As such, the adsorption capacity of sediments is unlikely to change the P removal pattern. For ease of convergence, a uniform adsorption capacity was assigned to sand and sediments.

The two mentioned interfaces were coupled to simulate wastewater transport through STU. Such an approach was successfully applied by Samsó et al. (2016).

The modelling framework did not explicitly account for potential biofilm development (bio-clogging). While biofilm formation may occur over time in soil treatment units, its extent is expected to remain limited in polishing beds receiving partially treated effluent. In addition, the sand media used in these systems is relatively coarse-grained, which promotes drainage and reduces the likelihood of substantial long-term reductions in hydraulic conductivity. The modelling results should therefore be interpreted within the scope of these assumptions.

3.2.5.3 Output variables

The following variables were calculated using the COMSOL Multiphysics post-processing tools:

- The inlet and outlet P load [g/day] was calculated as the total P flux that enters the polishing bed from the pipes and enters the ditch from the polishing bed, respectively. The 2D fluxes were multiplied by the length of the polishing beds to give comparable values.
- The average outlet P concentration [mg/L] in the outlet flux from the polishing bed to the ditch (at the seepage face boundary) was calculated.
- The lifetime of polishing beds was defined as the duration by which the outlet P load reached 80% of the inlet P load.

3.3 Results

3.3.1 Field inspections: Performance of septic systems with borrow sand-based polishing beds

Ground surface flooding, indicative of hydraulic failure, was observed solely in 2 systems out of the 26 studied septic systems. One possible factor could be that, unlike other systems, in one system, the bottom of the ditch is positioned at the same level as the bottom of the sand layer. Since the underlying sediments impede infiltration, this causes the sand layer to be flush with the accumulated water in the ditch, thereby increasing the likelihood of flooding. Additionally, the extended operational duration of the other system (installed in 2012) could also play a role in the observed outcome.

Nine properties had ditches without enough water for sampling. This could result from low wastewater production from households or deeper effluent percolation in some settings. Total P concentrations measured in water from the ditches of the rest of the septic systems are shown in Figure 3.4. Bars show the average values and error bars show the maximum and minimum data. In septic systems 1-12, water was present all through the ditches while in systems 13-17, water was only present downstream of the polishing beds. Nine systems out of the first 12 systems showed an increase in P concentration at the outlet of septic systems. Table 3.3 shows the released P from septic systems 1-12. The released P was > 9 mg/L in systems 1-3, > 1 mg/l in systems 4-7, but < 1 mg/l in systems 8 and 9.

To prevent eutrophication, the U.S. Environmental Protection Agency (EPA) has established guidelines that limit total P in flowing waters to a maximum of 0.1 mg/L (U.S. Environmental Protection Agency, 1986). In addition, Québec's environmental standards set a threshold of 0.03 mg/L for total P in surface waters (MENV, 2001). In the current study, all ditch samples contained P concentrations equal to or exceeding the 0.03 mg/L threshold. Furthermore, the observed P releases in the ditches, reaching up to 18.29 mg/L, underscores a significant P discharge that could potentially lead to adverse environmental impacts.

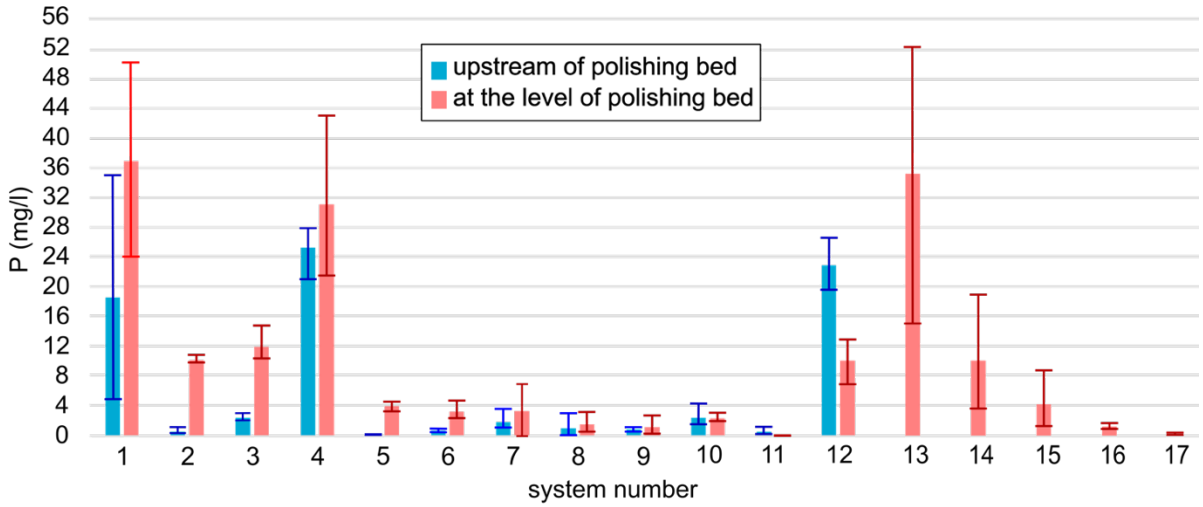

Figure 3.4 Phosphorus concentration upstream and at the level of the polishing beds in ditches.

In systems 10-12, the P concentration at the level of the polishing bed was smaller than the upstream concentration (negative values of released P). This could be due to P uptake by plants and microbes, presence of other sources of contamination, complex flow in the ditches, or the dilution of effluent at the outlet with any sort of uncontaminated water (e.g., rain water).

Sanitary inspections included diverse polishing beds from the three main categories, installed between 2009 and 2020, with both gravity-fed and low-pressure systems, 1 to 6 bedrooms, and varying occupancy rates. Differences in P removal performance can stem from the abovementioned properties and other factors such as P inlet from the household and the properties of the borrow sand. The average installation year of all 17 systems is 2015. Even relatively young systems such as systems 2 and 4, installed in 2018, show high P releases. Overall, sanitary inspections indicated

that the targeted septic systems have significant potential for releasing P into the environment, as evidenced by the increase in P concentration at the level of the majority of polishing beds.

Table 3.3 P released from septic systems.

System number	P released from septic system (mg/L)	System number	P released from septic system (mg/L)
1	18.29	7	1.49
2	9.59	8	0.50
3	9.47	9	0.32
4	5.86	10	-0.06
5	3.88	11	-0.55
6	2.53	12	-12.79

3.3.2 Characterization of native soil; particle distribution and permeability

The clay content exceeded 64% in 15 samples, with 4 samples ranging between 33% and 45%. Only one sample exhibited a clay content below 25%. Detailed particle distribution of the samples is presented in section A.11. Since the target area is located within the Clay Belt, the general clayey nature of the region is well known. Still, this quantitative data further characterized the site-specific soil properties critical for the design and performance evaluation of STUs. Despite this variability, all samples were classified as impermeable. The impermeability of this natural environment hinders infiltration, making the installation of SUTs with the natural soil impractical. Consequently, there is a need to utilize borrow sand for the construction of STUs. This is consistent with municipal records, indicating that many septic systems in the area have been constructed with borrow sand in impermeable soil.

3.3.3 Sand phosphorus adsorption isotherms

Freundlich and Langmuir isotherms parameters are reported in Table 3.4. Overall, both isotherms fitted well ($R^2 > 0.84$), although Freundlich isotherm provided a better fit for S1 ($R^2 > 0.94$). Figure 3.5 shows the experimental data and fitted isotherms.

The sand S1 has a greater sorption capacity compared to S2. The reason might be that S1 is more poorly sorted and contains more fines with greater surface areas for adsorption (Particle distribution curves in Figure A3). Additionally, pH measurements (pH values are detailed in section A.12) suggest that the mineral composition of the sands plays a role in adsorption efficiency. The initial solution pH ranged from 5.4 to 5.8, indicating slightly acidic conditions. After agitation, the pH of S2 samples remained in the acidic range (4.8–5.0), whereas S1 samples shifted to a near-neutral to slightly alkaline range (6.8–7.1). This difference suggests that S1 contains minerals capable of neutralizing acidity, whereas S2 lacks sufficient buffering capacity, maintaining an acidic environment.

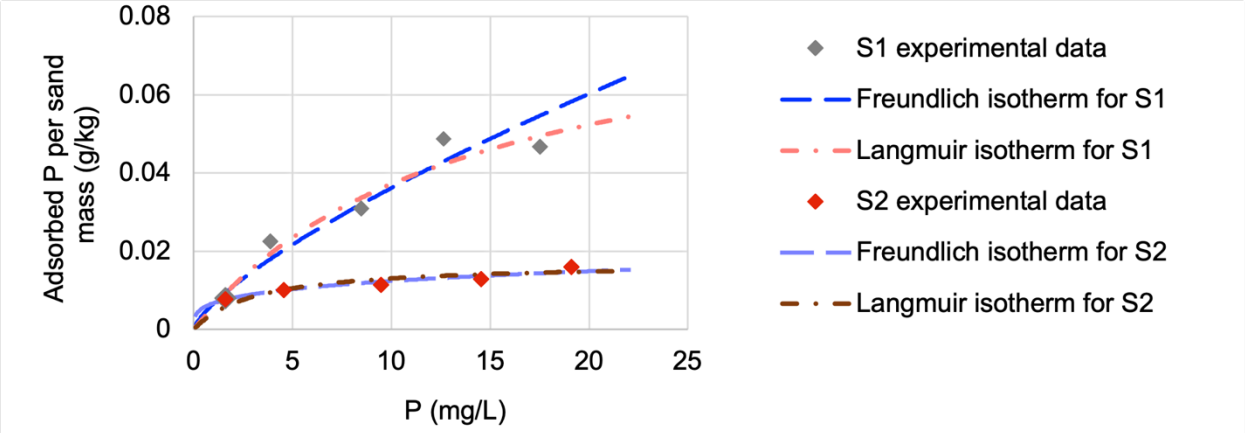

Figure 3.5 Adsorption experimental data and Freundlich and Langmuir isotherms for S1 and S2.

Table 3.4 Freundlich and Langmuir isotherm parameters for S1 and S2.

	Freundlich isotherm			**Langmuir isotherm**		
	k_F [g/kg(mg/L) ^{b_F}]	b_F [-]	R^2	k_L [mg/kg]	b_L [L/mg]	R^2
S1	6.627×10^{-3}	0.737	0.947	88.49	0.072	0.848
S2	6.715×10^{-3}	0.265	0.953	17.12	0.318	0.957

Previous studies indicate that the optimal pH range for phosphorus adsorption is 5–7. (Bai et al., 2017). While the initial solution pH was within this range, the post-agitation pH of S2 samples dropped below the optimal range, potentially reducing its adsorption efficiency. This highlights the

importance of mineral composition and pH buffering in phosphorus retention, further explaining the superior adsorption performance of S1.

3.3.4 Numerical simulation of polishing beds

In 2D simulations of models 1-12, following a steady-state saturation condition established with rain inflow, the water table reached stability within 100 days upon introducing inflow from pipes in addition to the rainfall inflow. This suggests a balance between water inflow, outflow, and storage within the system. Notably, our study employed an average rainfall rate. However, it important to acknowledge that in reality, seasonal variations lead to fluctuations in the water table.

Figure 3.6 shows the steady-state water tables for day 360 or 180. In all models, a seepage boundary face was established, extending from the water level in the ditch to a few centimeters above the sediment layers. The steady-state minimum unsaturated thicknesses below the crushed stone layer are presented in Table 3.5. Being designed for 6-bedroom buildings, models 2 and 3 show the lowest minimum unsaturated thicknesses among models 1-6. The average minimum unsaturated thicknesses in models 4-6 were greater than models 1-3, due to smaller influent discharge from the pipes. Models 7-12 are hydraulically identical to models 1-6. Maintaining the appropriate unsaturated thicknesses in the polishing bed is crucial to ensuring the sufficient oxygen levels required to support aerobic microorganisms and oxidation reactions. Here, the highly permeable sand layer was conductive to the efficient movement of water toward the ditch without a considerable water table rise. Given that the minimum thickness of the sand layer below the crushed-stone layer is 0.6 m (Figure 3.3), the sand layer remained mostly unsaturated. This finding is corroborated by field observations of rare flooding events and suggests the reliability of the models in predicting the hydraulic performance of the systems.

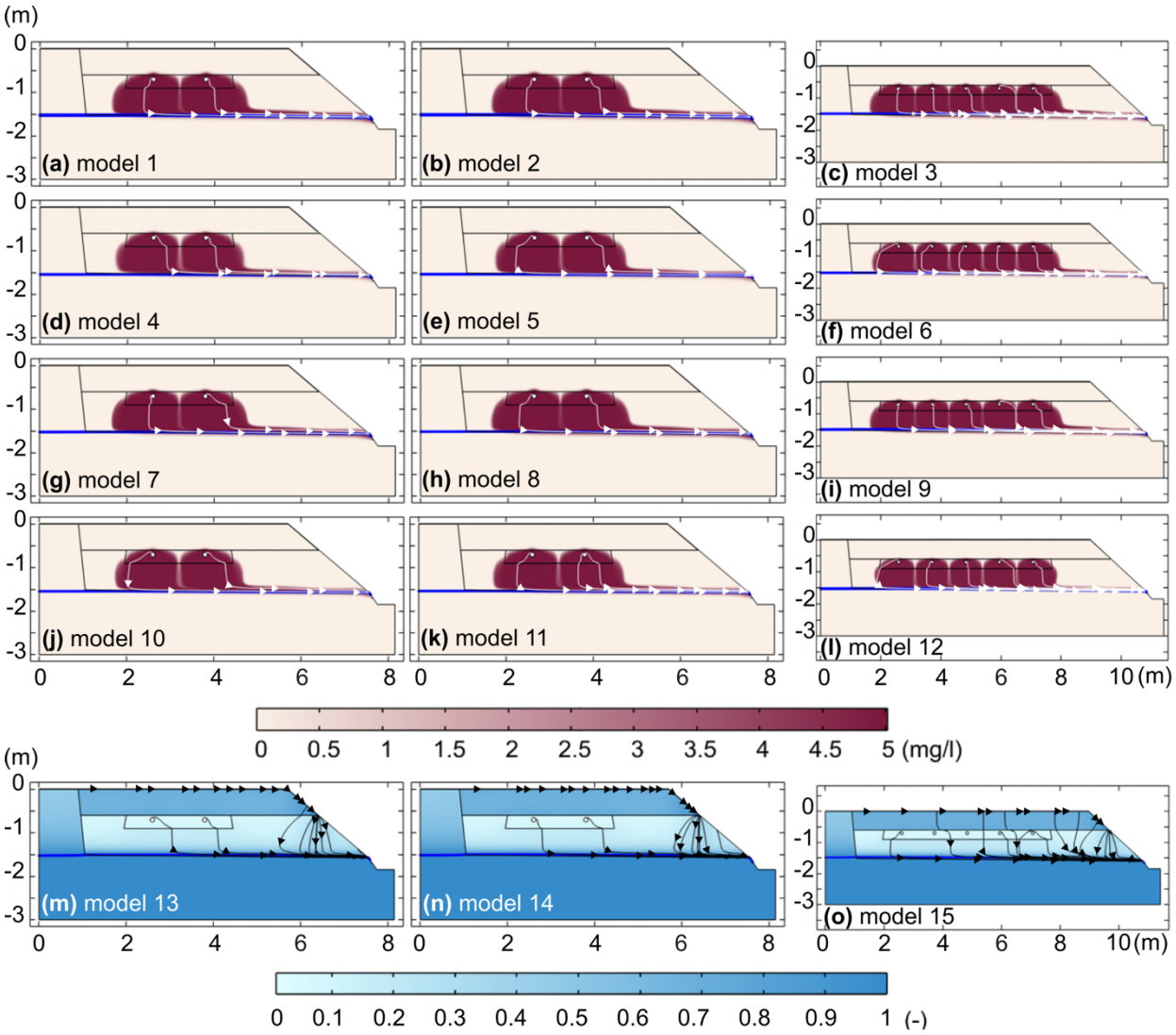

Figure 3.6 2D contour maps of phosphorus concentration, water table (blue line), and streamlines, (a-f) models 1-6 in day 360, (g-l) in models 7-12 in day 180. 2D contours of saturation degree and streamlines, (m-o) models 12-15 after 24 hours of heavy rain.

Figure 3.7a and b display the inlet and outlet P loads in models 1-12 and the lifetimes of polishing beds are reported in Table 3.5. Models 1-6 and 7-12 had approached P adsorption saturation by day 360 and 180, respectively. As shown in Figure 3.5, the P plume in all models at the time of saturation occupied the part of sand below the crushed stone as well as small minor parts above sediments towards the ditch. The evolution of P plume with time was further discussed in section A.13.

Figure 3.6m-o and the minimum unsaturated thicknesses of models 13-15 (Table 3.5) reveal that even during harsh rain events, the sand layer remained mostly unsaturated. The streamlines in Figure 3.6m-o showed that the infiltrating rainfall reaches the highly permeable sand layer and flows towards the ditch.

Table 3.5 Minimum unsaturated depths for models 1-15 and lifetimes for models 1-12.

Model number	Minimum unsaturated depth below crushed stone [m]	Lifetime [days]
1	0.6	110
2	0.59	85
3	0.56	68
4	0.62	243
5	0.61	180
6	0.6	145
7	0.6	50
8	0.59	39
9	0.56	30
10	0.62	99
11	0.61	78
12	0.6	67
13	0.58	-
14	0.58	-
15	0.55	-

Overall, numerical simulations suggests that all studied polishing beds have short P-sorption lifetimes, specifically less than a year. The implication is that systems operating beyond this timeframe would lead to reduced removal effectiveness and subsequent environmental releases. Moreover, the results of sanitary inspections of the studied STUs, revealing systematic phosphorus release from systems aged 2 to 17 years, confirm the trend of P release from systems. Therefore, the reliability of the models is supported by their consistency with real-world data, reinforcing their

validity for understanding P dynamics in these systems. The findings of numerical modelling explain the potential reasons behind the release of P, as observed in the field inspections.

The influent quantity and the sand available for P sorption led to variations in the calculated STU lifetimes. On average, the lifetimes of systems designed for 1 bedroom were 44% longer than those designed for 6 bedrooms. Rectangular beds and square beds have equivalent actual discharges and bed areas (surface area of the crushed stone layer). However, in comparison to square polishing beds, rectangular ones have greater bed lengths with identical distances from the edge of the crushed stone to the ditch (polishing beds' plans in Figure A.4) which gives more available sand beside the actual polishing bed. Consequently, rectangular polishing beds had 24% longer average lifetimes compared to square beds. The lifetimes of polishing beds performing at a 45% occupancy rate were on average 110% longer than those designed for full occupancy. Furthermore, the lifetimes of polishing beds constructed with S1 were 130% longer than polishing beds constructed with S2.

According to Figure 3.7c and d, the average outlet P concentration never quite reached the inlet P concentration of 5 mg/L despite increasing to reach close values. Within the same timeframe, the outlet P load almost matched the inlet P load. This outcome is the result of accounting for a dilution by a rainwater inlet discharge in addition to the inlet discharge from the pipes. While the rainwater did not change the total inlet and outlet P load, it diminished the P concentration in the outlet flux.

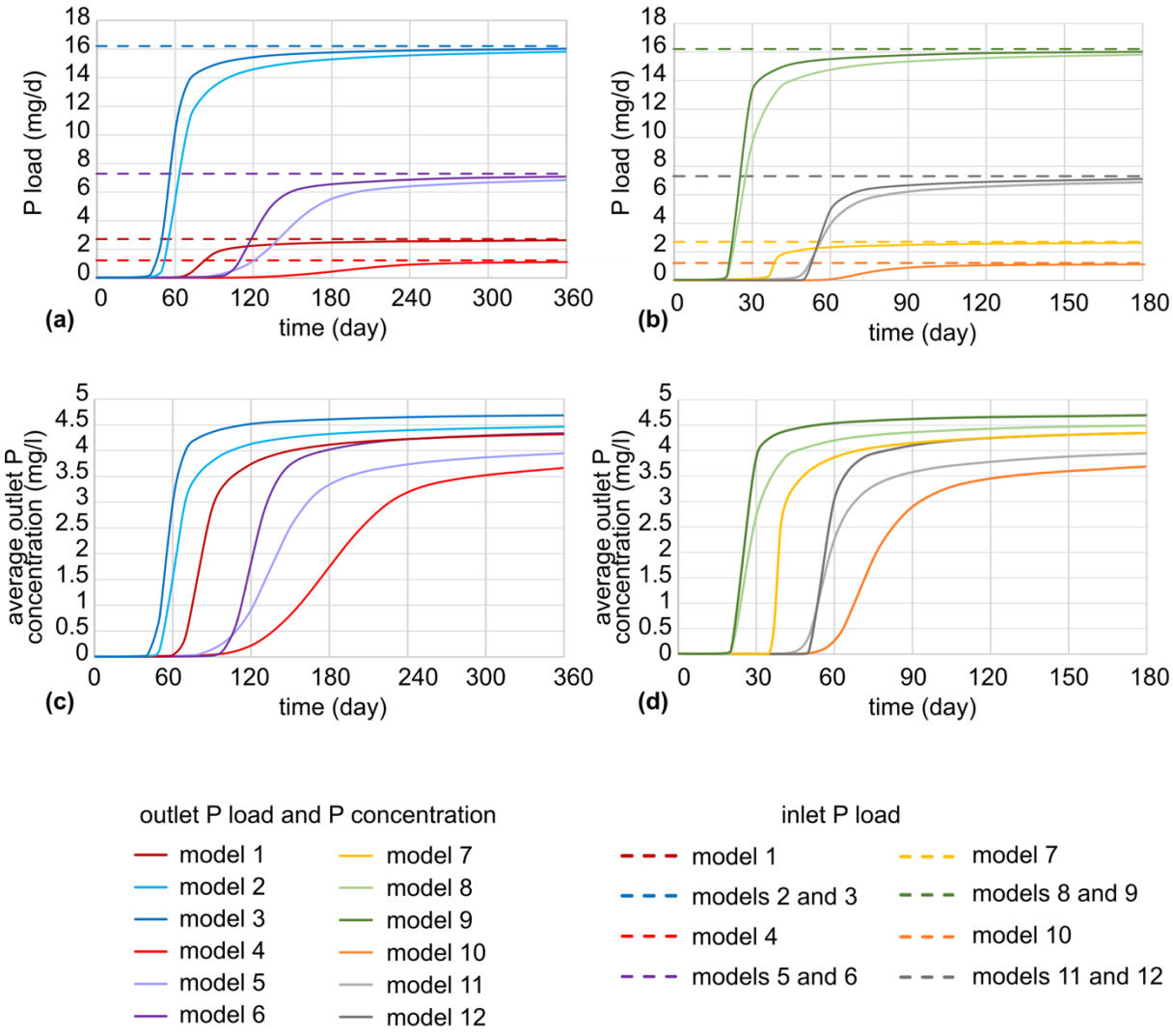

Figure 3.7 Inlet and outlet phosphorus load for (a) models 1-6 and (b) models 7-12. Average outlet phosphorus concentration for (c) models 1-6 and (d) models 7-12.

A mass balance approach quantifies the impact of rainfall-induced dilution on P concentrations. Assuming complete mixing of effluent from the polishing bed (p) and rainwater (r) in the downgradient ditch, the mass balance equation is expressed as: $c_p Q_p + c_r Q_r = c_t Q_t$ where c represents P concentration, Q represents discharge, and t refers to the mixture in the ditch. Given that rainwater does not contain P (c_r=0), the equation simplifies to $c_t = \frac{c_p}{\left(1+\frac{Q_r}{Q_p}\right)}$. Here, $1 + \frac{Q_r}{Q_p}$ represents the dilution factor, indicating the extent to which rainfall influences P concentrations in the ditch. Therefore, greater ratios of the rainwater discharge to the polishing beds' discharge led to lower outlet concentrations. Consequently, models designed for single bedroom and models

operating with occupancy-dependent actual discharges yielded lower final P concentrations. The total surface area exposed to rain is greater in rectangular beds than in square beds leading to rectangular polishing beds experiencing lower final outlet P concentrations. Finally, systems with S2 reached higher P outlet concentrations earlier than systems with S1 due to differences in sorption capacities. However, since the sorption capacity of sand isn't tied to discharges, it is not effective in the final outlet P concentrations.

Setting a threshold where rainfall-induced dilution is considered negligible, defined as $c_t > 0.9c_p$, results in $\frac{Q_p}{9} > Q_r$. For example, in model 1, where Q_p= 0.54 m^3/d, this condition leads to Q_r< 0.06 m^3/d. Assuming that rainfall on the surface area shown in Figure 3.3a (length =2.92 m and total width= 7.55 m) contributes to the ditch, with a surface area of 22 m², this corresponds to a rainfall intensity of 2.72 mm/day. This value is slightly higher than the average rainfall of 2.5 mm/day in the region (Labonté-Raymond et al., 2020), suggesting that typical rainfall events may have a limited impact on dilution. However, assuming the same surface area and a torrential rainfall of 78 mm/day leads to $c_t = 0.24c_p$ indicating that extreme precipitation can significantly reduce P concentrations. Since the study area experiences dry summers (Labonté-Raymond et al., 2020), rainfall-induced dilution is expected to be negligible during those periods but should not be overlooked in wet seasons, where it may play a crucial role in reducing P concentrations in the receiving environment.

3.4 Discussion

3.4.1 Key factors in the design of borrow sand-based STUs

Given the impermeability of the native soil in the target site, Abitibi-Témiscamingue, and the considerable hydraulic loads (higher than those typically applied to drain fields) imposed to the polishing beds, the native soil could not be used for efficient infiltration. As a result, the design of the outlet for the discharge from the STUs and its connection to surface water played a critical role in maintaining hydraulic performance and preventing flooding. Our system utilized a drainage ditch as the outlet, a design confirmed through numerical simulations to be effective under applied hydraulic loads (0.03 to 0.10 m/d) and rainfall of 2.5 mm/d.

Simulations further demonstrated that the implemented outlet design efficiently managed extreme rainfall conditions. During a modeled event with 78 mm/d of rainfall, the sand layer effectively directed water toward the ditch, maintaining unsaturated conditions and preventing waterlogging. This confirms that systems with well-designed drainage ditches offer a robust solution in impermeable settings, whereas designs relying on natural infiltration or piped outlets to surface water, as reported in previous studies (e.g., Converse and Tyler, 1986; Eveborn et al., 2014), may not perform as effectively under similar conditions with highly impermeable natural beds.

Two sands were selected based on availability and local regulations to reflect the materials likely used in STUs' installations. Maximum Langmuir adsorption capacities obtained from batch tests were 17.1 and 88.5 mg P/kg, aligning with previously reported values for sands used in other wastewater systems. For example, Florida and Danish sands reported ranges of 14 to 270 mg P/kg (Del Bubba et al., 2003; Kadlec & Wallace, 2008). In a literature review of previous studies, McCray et al. (2005) reported an average maximum P sorption capacity of 40 mg/kg (n=12) for sand which aligns with the capacities observed in this study. In general, natural soils with coarse grains generally show low P adsorption capacities (< 100 mg/kg); while other materials such as fly ash and red mud show higher adsorption capacities (>10 g/kg) (Cucarella & Renman, 2009).

The simulations revealed that the adsorption capacity of the sands was exhausted within less than a year, which corresponds with the P release observed during field inspections. In addition to adsorption capacity, other factors such as sand thickness also significantly influenced performance. The available sand thickness in this study was 0.6 m, whereas other borrow-sand-based STUs reported greater depths, such as 1 to 2 m in the study by Robertson et al. (2019) and over 0.8 m in the study by Eveborn et al. (2014).

Hydraulic loading rate is similarly crucial to P removal since it directly affects the input P to the system. The inspected systems operated with loads ranging from 0.025 to 0.077 m/d. Numerical simulations explored scenarios with 0.034 and 0.045 m/d based on a 45% occupancy rate and models simulated under full design capacity included hydraulic loads between 0.077 and 0.101 m/d. Previously, Robertson et al. (2019) observed successful P retention in borrow sand STUs under low hydraulic loads (less than 0.02 m/d). In contrast, Eveborn et al. (2014) documented

performance challenges at higher loads (up to 0.33 m/d), suggesting that the hydraulic loading rate could have contributed to the observed differences in system performance.

3.4.2 Recommendations for future system design and maintenance

To enhance P retention potential of future STUs, we recommend increasing the polishing bed size, both in depth and area. This approach provides more media available for P sorption and would extend the lifespan of P sorption. A sand thickness of at least 1.0 m and a hydraulic load limit of less than 0.03 m/d would provide improved long-term performance.

For the construction of future systems, pre-installation adsorption tests on potential borrow sands are recommended to estimate maximum sorption capacities. The choice of adsorbent should consider factors beyond availability and regulatory compliance, including the ability to maintain long-term performance, sustainability and environmental impact. In the context of this study, since the native soil is impermeable, the permeability of the filter material should be high enough. For instance, Cucarella & Renman (2009) categorized fly ash and red mud with high P adsorption capacities (> 10 g P/kg). However, their fine particle size (<0.15 mm) can cause hydraulic issues, making them unsuitable for the targeted systems of this study. While sands support hydraulic performance, which is essential for target systems in this study, their ability to retain P is not always efficient. It is recommended to use materials with capacities above 100 mg P/kg. If local sands fail to meet these criteria, incorporating P-sorbing alternatives and amendments should be considered.

As noted by McCray et al. (2005), some sands can achieve P adsorption capacities up to 1.3 g P/kg, which could be implemented in future systems to enhance P removal. Additionally, other natural materials, such as marine sediments, are rich in calcium and magnesium carbonates and have a high specific surface and a high porosity, which make them suitable candidates for P removal in wastewater treatment systems (Johansson Westholm, 2006). Shell sands have been reported to have P adsorption capacities of 14-17 g P/kg (Roseth, 2000). Another alternative is biochar, which can be produced from various organic waste materials, promoting sustainability and contributing to waste reuse. Iron- and calcium-impregnated biochar has been shown to achieve a P adsorption capacity of up to 3.21 g P/kg and can be used as an amendment layer to improve filter media in terms of P adsorption as demonstrated by Dalahmeh et al. (2020). Biochar’s large surface area,

high porosity, and ability to retain P make it a viable option for improving P retention and maintaining hydraulic performance.

Monitoring strategies are critical for early detection of system failures. Routine measurements at outlet ditches should be conducted to identify potential issues. Given that rainfall can dilute the effluent, as demonstrated by our numerical simulations, we recommend measuring both the discharge in the ditches and the P concentration to calculate P loads (P mass per unit time) rather than relying solely on concentration measurements. This approach is particularly important during wet seasons, where relying solely on concentration measurements may underestimate actual P transport. It is important to note that very few field studies accounted for dilution correction when estimating P removal (Wang et al., 2024). When early signs of P release are detected, maintenance actions should be undertaken promptly to prevent environmental impacts. Maintenance could include partial or complete replacement of the sand layer with virgin sand or the addition of P-sorbing amendments to enhance retention capacity.

In impermeable settings, proper outlet design, is essential to prevent waterlogging and maintain unsaturated conditions in the sand layer. Field inspections revealed that while most systems performed well, one case of flooding occurred due to improper ditch configuration. In this case, the bottom of the ditch was level with the sand layer, causing water to accumulate. Therefore, for future constructions, it is recommended that the ditch be positioned lower than the sand layer to prevent water accumulation and ensure effective drainage. Maintaining a stable water level in the ditch below the sand layer is also critical, as excessive water levels can lead to saturation and reduced system performance. To achieve this, it is recommended to build ditches with a slope along their length. This way, continuous flow away from the system could be achieved. Additionally, a slope at the bottom of the sand layer is necessary to direct infiltrated water toward the ditch efficiently. For example, in the studied cross-section (Figure 3.3b and 3d), a 1% slope was implemented to facilitate proper drainage and prevent water stagnation within the sand layer. These strategies can be broadly applied to the design and construction of borrow sand-based STUs in impermeable settings to enhance drainage efficiency and prevent hydraulic failures.

After construction, visual inspections of drainage ditches and regular monitoring of water levels in drainage ditches are crucial. While it is recommended to avoid P inspections immediately after

extreme rainfall events due to the potential underestimation of released P, it is advised to inspect systems for hydraulic performance during significant rainfall events. Signs of flooding or a sharp rise in water levels may indicate hydraulic performance issues. In such cases, deepening the ditch to make sure that the STU does not get flush with water in the ditch should be a priority.

Thoughtful outlet design and routine maintenance involve relatively low costs compared to the potential expense of system failures. While P-sorbing amendments or supplementary treatments may incur additional costs, their long-term benefits (such as reduced maintenance frequency and improved P retention) justify the investment. By implementing these strategies, STUs can be designed to achieve sustainable wastewater management in impermeable environments, safeguarding both groundwater and surface water quality.

3.5 Conclusions

This study provides a novel contribution to the understanding and optimization of borrow sand-based STUs in impermeable settings. Unlike STUs in naturally permeable soils, where deeper layers contribute to P removal and hydraulic performance, borrow sand-based systems overlaid clay-rich native soils with very low hydraulic conductivity. Accordingly, vertical infiltration into the native soil is expected to be minimal, and system performance is controlled primarily by processes occurring within the borrow-sand layer, including its finite adsorption capacity for phosphorus. In these installations, drainage ditches adjacent to the polishing fields provided controlled pathways for effluent collection, helping prevent waterlogging and surface overflow.

By integrating field inspections, experimental analyses, and numerical modeling, this study uniquely combines real-world observations with predictive tools to evaluate the dual challenges of hydraulic performance and P retention. Moreover, by addressing both hydraulic and hydrogeochemical challenges, this work provides a transferable framework for optimizing decentralized wastewater treatment systems in impermeable settings. The borrow sand-based polishing beds within the impermeable and clay-rich natural covering of Abitibi-Témiscamingue served as a case study. The following conclusions were drawn:

- Flooding, a common indicator of hydraulic failure, was rarely observed in polishing beds with proper designs that direct effluent toward drainage ditches. The sand layer in polishing beds remains mostly unsaturated even during extreme rainfall events.
- The sands used in this study, selected for availability and regulatory compliance, showed Langmuir adsorption capacities of less than 100 mg P/kg, aligning with values reported for natural soils with coarse grains.
- Relatively high P background concentrations were detected in the ditches downgradient from the septic systems. Still, a systematic release of P (up to 18.29 mg/l) caused by septic systems was detected.
- Insufficient sorption capacity of the borrow sands leads to systems getting saturated with P in less than a year. Early polishing beds' P saturation resulted in considerable P release from septic systems, rendering them ineffective for P removal.
- The findings suggest that current STU designs are ineffective for long-term P removal, necessitating design improvements and alternative materials with higher P sorption capacities.
- Rainfall can diminish the concentration of contaminants in the effluent of septic systems. It is crucial to monitor mass loads instead of relying on concentrations to avoid overrating systems' performances.
- 2D models are suitable for the successful modelling of hydraulic integrity in a sloped STU. Unlike 3D models, 2D models do not consider contaminants dispersion perpendicular to the STU slope. Nevertheless, this discrepancy does not lead to a systematic and significant difference.

This study is believed to shed light on the effectiveness of borrow-sand STUs within septic systems, provide critical insights for policymakers and researchers, and contribute to the development of sustainable wastewater treatment practices that safeguard both surface water and groundwater quality in challenging settings. Future work should focus on long-term monitoring of P desorption risks, the influence of bio-clogging and seasonal dynamics, the role of growing vegetation, and further refinement of outlet designs such as drainage ditches.

3.6 Acknowledgements

The authors thank Polytechnique Montreal technicians Samuel Chénier and Éric Turgeon for their help in soil characterization experiments and Mélanie Bolduc and Gabriel St-Jean for their help in phosphorus adsorption tests. We extend our gratitude to OBVAJ (Organisme de bassin versant Abitibi-Jamésie) for their effort in field inspections and data collection. We would also like to thank MELCCFP (Minstère de l'Environnement, de la Lutte contre les changements climatiques, de la Faune et des Parcs) for providing municipal documents and Patrick Morin for his effort in documenting municipal records. This project was funded by MELCCFP, the National Science and Engineering Research Council of Canada (grant number ALLRP 570383-21) and the Canada Research Chair in Decentralized and Small-Scale Water Treatment (grant number 950-232871).

CHAPTER 4 PHOSPHORUS DYNAMICS IN THE CLOGGING ZONE OF ON-SITE SAND FILTERS: TREATMENT PERFORMANCE AND LIFESPAN

4.1 Introduction

Onsite wastewater treatment systems (OWTS) are widely used for wastewater management in rural, sparsely populated, or remote regions where centralized treatment infrastructure is unavailable. In Canada, around 25% of the population depends on OWTSs (Government of Canada, 2001), while in the US, an estimated 60 million people rely on similar systems (Garcia et al., 2013). Although OWTS play a crucial role in decentralized wastewater treatment, concerns remain regarding their ability to effectively remove nutrients, particularly phosphorus (P), from wastewater before discharge into the environment.

Phosphorus (P) concentration in the effluent of OWTS is of particular concern because it can impair groundwater resources' quality at much lower concentrations than nitrogen (M. Lusk et al., 2011). Domestic wastewater contains P originating from human waste, food residues, laundry, and household cleaning products, especially detergents (M. G. Lusk et al., 2017). When discharged into natural water bodies, even low concentrations of P (as little as 0.03 mg/L) can lead to eutrophication, triggering excessive algal growth and ecosystem degradation (Smith et al., 2003). Consequently, P leaching from OWTS into groundwater and surface water is recognized as a significant environmental concern.

Sand filtration is commonly integrated into OWTS to reduce nutrient loads. These filters are used in various configurations, including natural sandy drainfields, borrow sand-based soil units, nitrogen removing biofilters, etc. (Eveborn et al., 2014; M. G. Lusk et al., 2017; Maleki Shahraki et al., 2021; Sheibani et al., 2025). While the use of sand filters is well established, their P removal performance has shown considerable variability across different studies. This variation is often attributed to differences in media properties and operational conditions (Sheibani et al., 2025).

Many researchers identified sorption, including both surface adsorption and mineral precipitation with metal ion, as the main mechanism for P removal in sand (Arias et al., 2001; Eveborn et al., 2014; Hamisi et al., 2022; Wang et al., 2024). In sand filters, P removal typically declines over time as the available reactive sorption sites become exhausted, eventually resulting in breakthrough

and leaching of phosphorus (Sheibani et al., 2025; Wang et al., 2024). However, other studies reported sustained P removal over extended periods, attributed to ongoing precipitation of Al, Fe, and Ca phosphates, as well as long-term conversion of P into more stable pools through secondary attenuation mechanisms (Robertson, 2008; Robertson, van Stempvoort, et al., 2019).

Batch sorption tests are widely used to estimate the P adsorption capacity of filter media, as implemented by various previous researchers (e.g., Cucarella & Renman, 2009; Del Bubba et al., 2003; Wang et al., 2024). These tests expose a known quantity of media to P solutions of various concentrations until equilibrium is reached. However, while batch tests are relatively cheap and easy to perform in a relatively short period, they do not account for the physical, chemical, or biological changes that occur when filter media are exposed to real wastewater.

This study provides detailed insights into phosphorus removal mechanisms in sand filters used in OWTSs. Specifically, it examines the reliability of batch adsorption tests for predicting filter performance and operational lifespan under conditions representative of septic tank effluent. A controlled 94-day column experiment, fed with synthetic wastewater at environmentally relevant P concentrations and hydraulic loading rates, was conducted to capture biofilm development, pH changes, and P dynamics. Results from the column study were compared against batch-derived sorption capacities, and both datasets were incorporated into reactive transport modeling to estimate filter longevity. This comparative framework allows assessment of whether standard batch parameters can reliably represent field-scale processes, while also identifying the influence of biofilm-induced sorption and its reversibility. By integrating experimental and modeling approaches, the study advances understanding of the mechanisms, limitations, and sustainability of P removal in sand-based OWTS.

4.2 Materials and methods

4.2.1 Laboratory column experiment

4.2.1.1 General properties and operation

The experimental setup consisted of a cylindrical column with a diameter of 0.3 m. To prevent sand migration and allow proper drainage, the bottom 0.1 m of the column was packed with gravel ranging from 1 to 7 mm in diameter. A grooved outlet pipe was installed at the base to collect the effluent uniformly. Above the gravel layer, the column was filled with 0.9 m of filter media.

Medium sand with particle sizes of <2 mm was used as the filter media in this study. The physical properties of the sand and the operational parameters of the column are summarized in Table 4.1. Saturated hydraulic conductivity was determined using the constant head method according to ASTM D2434 (ASTM International, 2022a), while particle density was measured following ASTM C128 (ASTM International, 2022b). Bulk density was obtained according to method ASTM C29 (ASTM International, 2023), and porosity was subsequently calculated from the ratio of particle density to bulk density using the relation:

$$\varepsilon = 1 - \frac{\rho_b}{\rho_p} \tag{4.1}$$

where ε [-] is the porosity, ρ_p [kg/m^3] and ρ_b [kg/m^3] are particle and bulk densities respectively.

The surface of the sand was covered with a 3–4 cm layer of pea gravel (6–12 mm) to secure the influent distribution tubing and reduce evaporation from the filter surface. A schematic representation of the column setup is provided in Figure 4.1a.

Table 4.1 Properties of the sand and the operation properties of the sand column

Properties of the sand	saturated hydraulic conductivity, K_{sat}	1.2×10^{-4} m/s
	porosity, ε	0.34
	bulk density, ρ_b	1800 kg/m^3
	median particle diameter (d_{50})	0.28 mm
Column operational parameters	Diameter	0.3 m
	Length	0.9 m
	hydraulic loading rate, HLR	0.027 m/d

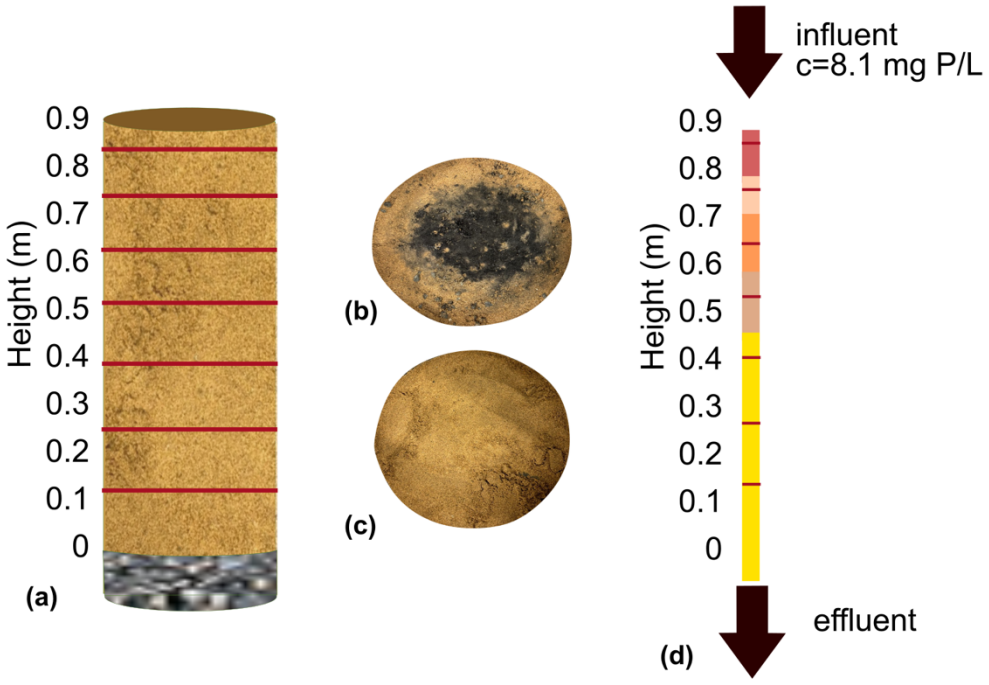

Figure 4.1 (a) Schematic of the 0.9 m sand filter. The red lines show the depths at which samples were collected during dismantling. (b) surface of the sand filter at the end of operation. (c) surface of the sand filter after removing the surface 1-2 cm layer. (d) Schematic representation of the 1-D domain used for numerical modelling. The red lines mark the sampling locations during dismantling, and each colored segment represents a zone assumed to have uniform properties matching those of the corresponding sample.

Prior to the start of the experiment, the sand column was conditioned by adding approximately 20 litres of tap water and allowing it to drain. This ensured some moisture retention in the sand filter and minimized initial flow irregularities. Following this pre-conditioning step, the column was fed with reconstituted synthetic septic tank effluent (STE) at a hydraulic loading rate of 0.027 m/day. The synthetic wastewater was prepared by dissolving the following constituents in 1 litre of tap water: 0.2–0.3 g sodium acetate, 0.15 g dextrose, and 0.15 g soy peptone as sources of organic carbon; 0.04 g K_2HPO_4 and 0.01 g KH_2PO_4 as P sources; and 0.13 g NH_4Cl as the primary nitrogen source. To introduce complex organic matter and promote natural microbial activities, 0.7 mL of primary sludge, collected from the St-Hyacinthe Water Resource Recovery Facility, immediately frozen upon collection, and thawed prior to use, was also added to each litre of feed solution. The use of synthetic wastewater is a common approach in laboratory-scale studies, as it minimizes the natural chemical fluctuations typically present in real wastewater, thereby enabling a more

controlled and mechanistic understanding of treatment processes. The synthetic effluent was freshly prepared and replaced every 5–6 days. It was kept in a cold room at 4℃ and pumped from there to the sand filter.

Feed and effluent samples were collected weekly throughout the experiment. pH was measured using a SevenExcellence S400 pH meter, following standard calibration procedures. Samples were analyzed for chemical oxygen demand (COD), total nitrogen (TN), total phosphorus (TP), and ammonium-nitrogen (NH_4^+-N) using Hach methods 8000, 10072, 10127, and 10205, respectively, following the manufacturer's instructions. In addition, subsamples were filtered through 0.45 µm membrane filters and analyzed for orthophosphate (ortho-P) and nitrate-nitrogen (NO_3^--N) using ion chromatography. All analyses were performed immediately after sample collection to prevent alterations in nutrient concentrations.

4.2.1.2 Dismantling, sample collection, and analysis

The column was dismantled after 94 days of continuous feeding. During dismantling, sand samples were collected from seven different heights along the column: 0.85, 0.78, 0.66, 0.54, 0.42, 0.28, and 0.14 m, as indicated in Figure 4.1. As shown in Figure 4.1b, a dark layer had formed on the surface of the sand column, attributed to biofilm accumulation. The uppermost 1–2 cm of the surface layer was discarded, and the first sample was taken from the underlying section, as illustrated in Figure 4.1c. All samples appeared visually uniform and indistinguishable from each other.

At each sampling depth, two sets of subsamples were collected. The first set of samples, approximately 900 g each, was sent to A & L Canada Laboratories Inc. (London, ON), an ISO/IEC 17025:2017 accredited analytical facility. Organic carbon (OC) content was determined as the difference between total carbon (TC), measured by dry combustion, and inorganic carbon (IC), quantified using a calcimeter. Soil pH was measured at a 1:1 solid-to-liquid ratio. The Mehlich 3 solution was used to extract reactive P from the samples.

The second set of samples, approximately 200–300 g of sand, was retained from each depth for subsequent analyses, including P adsorption and sequential extraction tests, as well as metal content determination. These samples were stored at 4 °C until analysis. For metal content, samples were first dried and ground using a shatter box. A mass of 0.2000 g was weighed and subjected to fusion

digestion. The resulting melt was dissolved and diluted in approximately 4% HNO_3. Concentrations of Fe, Mg, Ca, and Al in the sand samples were measured using atomic absorption spectroscopy (AAS) with a PerkinElmer Pinnacle 900F instrument.

4.2.2 Sequential phosphorus extraction

Sequential P extraction was performed to assess the desorbable P fraction in the used sand samples, collected during dismantling, using a modified version of the method originally proposed by Hedley et al. (1982) as adapted by Zohar et al. (2010). Briefly, an amount of moist sand equivalent to 0.5 g of dry soil was placed in a 50 mL centrifuge tube and mixed with 40 mL of extractant solution. The tubes were then placed on a rotary shaker at 35 rpm and agitated overnight (16 hours) at room temperature (~21 °C). After each extraction step, the tubes were centrifuged at 5000 rpm for 20 minutes to separate the supernatant from the solid phase. The clear supernatant was collected for P analysis, and the remaining solid was used in the subsequent extraction step. The extraction sequence consisted of three solutions applied in the following order: deionized water, 0.5 M $NaHCO_3$ (pH 8.5), and 0.1 M NaOH (pH 12). For each extract, TP and ortho-P were analyzed according to Hach methods 8190 and 8048 respectively following pH adjustment.

4.2.3 Phosphorus sorption batch test

P sorption tests were conducted on the virgin sand and all samples taken from the dismantled column to estimate the initial and remaining P sorption capacities, in accordance with ASTM D4646 (ASTM International, 2016). In short, a mother solution was prepared by spiking a 0.1 M KNO_3 solution (prepared with Milli-Q water) with equal molar ratios (~1.60 mmol) of KH_2PO_4 and K_2HPO_4, resulting in a P concentration of 100 mg P/L. This mother solution was then diluted with Milli-Q water to achieve P concentrations of 5, 7, 10, 12, and 15 mg P/L. The KNO_3 maintained a minimum electric conductivity. An amount of sand equivalent to 2 of dry soil was added to 40 ml of each of P solutions (soil-to-solution mass ratio of 1:20, consistent with standard protocols in soil science (Cucarella & Renman, 2009). The virgin sand was air-dried, but the used sand samples were moist. The moisture content of the used samples was determined gravimetrically by comparing the mass of moist subsamples with their corresponding oven-dried weights.

Blank samples (P solutions without soil) at the same concentrations were also prepared. All samples were placed in a rotary extractor at 29 rpm and maintained at room temperature (22°C).

After agitation, the samples were filtered through 0.45 μm filters and ortho-P concentrations were measured according to Hach method 8048. The pH of each solution was measured before and after the test. A common limitation of batch adsorption tests is the standard 24-hour contact time, which may not allow the system to reach equilibrium, potentially underestimating the true adsorption capacity (Hamisi et al., 2022). To address this, tests were conducted over varying durations until adsorption results stabilized, indicating steady conditions.

4.2.3.1 Isotherm modelling

After performing the adsorption batch test, the Langmuir isotherm model was applied to the adsorbed and equilibrium P concentrations. The model is expressed as:

$$c_a = \frac{c k_L b_L}{1 + c b_L} \tag{4.2}$$

where c_a [g/kg], represents the equilibrium mass of the adsorbate (P) per unit mass of adsorbent and c [mg/L] is the equilibrium concentration of the adsorbate (P). k_L [g/kg] indicates the maximum Langmuir adsorption capacity and b_L [L/mg] is associated with the binding energy constant.

4.2.4 Numerical phosphorus transport modelling

A time-dependent and one-dimensional model with a length of 0.9 m was developed in COMSOL Multiphysics (COMSOL, 2019). The 1-D mesh was generated automatically in COMSOL, with a maximum element size of 0.037 m. The model simulated P transport and retention via advection-dispersion coupled with adsorption as follows:

$$\frac{\partial(\varepsilon c)}{\partial t} + \frac{\partial(\rho_b c_a)}{\partial t} = \nabla.\left((D_d + D_e)\nabla c\right) - \boldsymbol{u}.\nabla c \tag{4.3}$$

where $\boldsymbol{u}$ [m/s] is Darcy flux imposed with the same value as HLR. These parameters were assigned values according to values reported in Table 4.1. D_d [m^2/s] and D_e [m^2/s] are the dispersion and diffusion coefficients, respectively set to 2×10^{-8} m^2/s and 10^{-9} m^2/s.

The initial condition was set to zero P concentration throughout the column. A constant inlet flux was applied at the top boundary with a P concentration of 8.1 mg/L **(**see Figure 4.1d**)**, corresponding to the average feed concentration as explained in section 4.3.1.

Adsorption was modeled using Langmuir isotherms**,** with parameters derived from batch adsorption tests (see section 4.2.3). The model was executed in two stages. In the first run, the initial adsorption capacity of clean sand was used, representing the expected performance of the sand filter based on the properties of the clean sand, prior to operation. In the second run, the adsorption capacity was updated to reflect that of the used sand samples. This simulation began at day 95, immediately following the conclusion of the physical column experiment, and represents the predicted performance of the sand filter after 94 days of operation, accounting for the P sorption capacity remaining in the media. The column was discretized into segments (see Figure 4.1d), each representing a zone around a sampling location assumed to have uniform adsorption characteristics, same as the corresponding soil sample.

4.3 Results and discussion

4.3.1 General performance of the sand filter

The characteristics of the influent and effluent from the sand column, in terms of chemical COD and nitrogen species, are presented in Figure 4.2. The influent COD averaged 390.6 ± 143.7 mg/L, which was significantly reduced to 10.4 ± 6.2 mg/L in the effluent, corresponding to an average removal efficiency of 97.4%. TN in the feed, primarily composed of organic nitrogen and NH_4^+-N, was 48.9 ± 4.7 mg/L. In contrast, the effluent TN was dominated by NO_3^--N at 35.4 ± 5.2 mg/L, indicating effective nitrification but only partial denitrification. The average TN removal rate was 35.9%. The feed characteristics align with typical concentrations observed in STE, and the observed effluent values and COD and TN removal efficiencies are consistent with expectations for well-aerated sand filters (Petitjean et al., 2016; S. Richards et al., 2016).

The concentration of ortho-P in the feed, shown in Figure 4.2, fell within the range of 8.1 ± 0.5 mg/L, which is in the realistic range observed in typical STE (S. Richards et al., 2016). The P concentrations in the synthetic feed showed only a minor difference of 0.11 mg P/L between TP and ortho-P, indicating that the synthetic feed contained P in the simple reactive form. This confirms the absence of significant amounts of organic or other forms of P. Accordingly, all P concentrations reported in this study refer specifically to ortho-P. During the experiment, the effluent concentration of ortho-P remained below the detection 0.06 mg P/L, indicating that all influent P was retained in the sand filter.

Several studies have shown that ortho-P is the dominant form of P in STE, and that more complex forms are often further converted to ortho-P during treatment in sand filters (M. G. Lusk et al., 2017; Mechtensimer & Toor, 2016; Wang et al., 2024). Additionally, in properly purged groundwater samples, the measured concentrations of TP and reactive ortho-P are nearly identical (Robertson, van Stempvoort, et al., 2019). Therefore, field studies on groundwater P leached from OWTSs, often focus solely on reactive form as the representative form of P (e.g., Robertson, 2008). This supports the representativeness of using ortho-P as the primary phosphorus form.

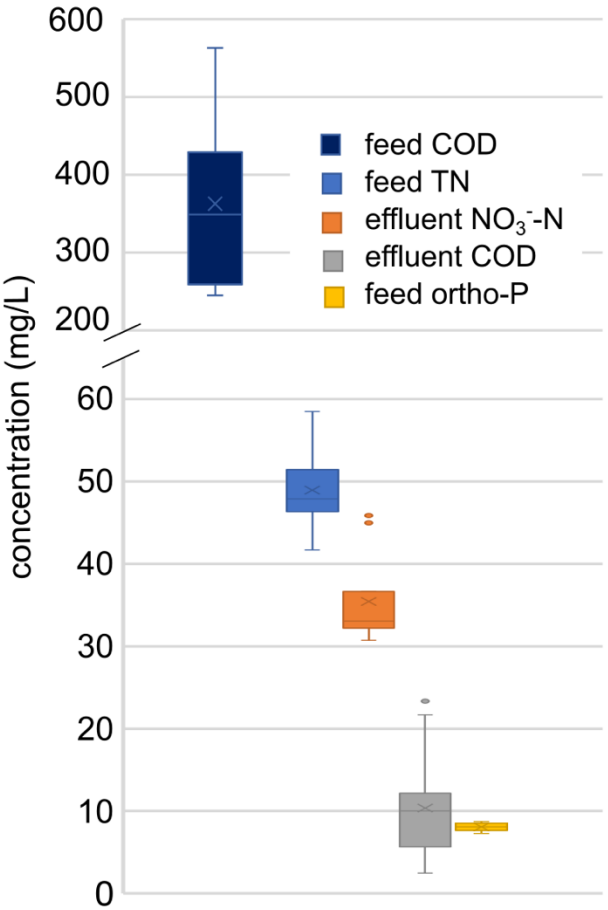

Figure 4.2 Feed concentrations of chemical oxygen demand (COD), total nitrogen (TN), and orthophosphate (ortho-P), and effluent concentrations of nitrate nitrogen (NO_3^--N) and COD.

While the synthetic feed lacks the chemical complexity of real wastewater, this simplification enables a more focused and mechanistic understanding of ortho-P behavior within the system. First,

the use of ortho-P in the feed mirrors the conditions of the batch sorption tests, facilitating direct and meaningful comparisons between batch and column experiments. Second, the near-constant P concentration in the synthetic feed, achieved through controlled synthetic feed, allows for a consistent inlet flux of P. This consistency enhances the reliability of comparisons between the experimental results from the sand filter and the model simulations, assuming a constant input condition as explained in section 4.2.4.

4.3.2 Sand phosphorus sorption capacity

4.3.2.1 Underestimation of phosphorus retention in batch sorption tests

Results from the batch experiments on virgin sand (Figure 4.3a) indicate that P uptake increased with contact time, approaching a plateau after 5 to 6 days. P adsorption is commonly described as a multi-stage process, beginning with a rapid phase dominated by surface reactions such as ion exchange and ligand exchange, followed by slower stages controlled by diffusion of phosphate into less accessible regions of the sediment matrix and other processes such as precipitation and reversible adsorption–desorption (Lai & Lam, 2009; Wang et al., 2024). The time required for sorption systems to approach equilibrium is strongly influenced by the physical characteristics of the sorbent material. Studies on sorption kinetics have shown that materials composed of very fine particles (diameter <0.15 mm) can reach equilibrium relatively quickly, often within only a few hours while materials with much larger particle diameters (approximately 2.5–10 mm) reported a substantial increase in phosphorus uptake when contact time was extended from 24 to 96 hours (Cucarella & Renman, 2009). Generally, the presence of internal pore structures also means that phosphate transport into the interior of the particles can be slow, so longer contact times may be required for the system to approach equilibrium due to processes such as intraparticle diffusion (Cucarella & Renman, 2009).

The results obtained in this study are consistent with the time-dependent sorption behavior described in the literature. As shown in Figure 4.3a, P uptake by the virgin sand approached a plateau after approximately 5–6 days, indicating that near-equilibrium conditions were reached within this timeframe. A substantial portion of adsorption occurred during the first 24 hours, reflecting the rapid initial sorption phase associated with readily available surface sites. However, adsorption continued to increase beyond the first day, demonstrating that equilibrium had not yet been achieved at 24 hours. The gradual increase in adsorbed P observed between days 1 and 5

likely reflects slower processes such as diffusion of phosphate ions into less accessible sorption sites within the sand matrix. These results underscore the importance of allowing adequate contact time in batch sorption tests, as shorter durations can lead to significant underestimation of the sand's true sorption capacity. Notably, many previous studies have overlooked the time dependency of sorption, often using a fixed and relatively short contact time of 24 hours without assessing whether equilibrium had been achieved.

Figure 4.3b compares the P sorption capacities of virgin sand and used sand collected from various heights within the column after 6 days of contact time. Sorption capacity varied with depth, reflecting differences in P exposure and retention during the column operation. The sample taken from the top of the column (0.85 m) exhibited the lowest sorption capacity because this section had experienced the highest P loading. However, the fact that some capacity remained suggests that the sorption sites were not fully saturated. Samples taken from intermediate heights (0.78, 0.66, and 0.54 m) showed similar and slightly higher capacities than the top sample, suggesting that P retention at these depths was somewhat lower, leaving more available sorption sites. The lowest samples, collected from 0.42, 0.28, and 0.14 m, also clustered together with relatively higher capacities than the top of the column. Still, the capacity of these lower samples was lower than the virgin sand.

The slightly lower sorption capacities observed in lower depths compared to virgin sand may be explained by the physical loss of fine particles during the early stages of column operation. Specifically, after packing the column and initiating feeding with tap water, turbid effluent was observed, indicating the washout of fines. Since fine particles typically offer greater surface area and thus enhanced sorption capacity, their removal may have led to a marginal decrease in overall P retention in these sections. Still, at influent concentrations of 8 mg P/L and below (the range tested in this experiment), the difference in sorption performance between these samples and the virgin sand remained relatively small (Figure 4.3b).

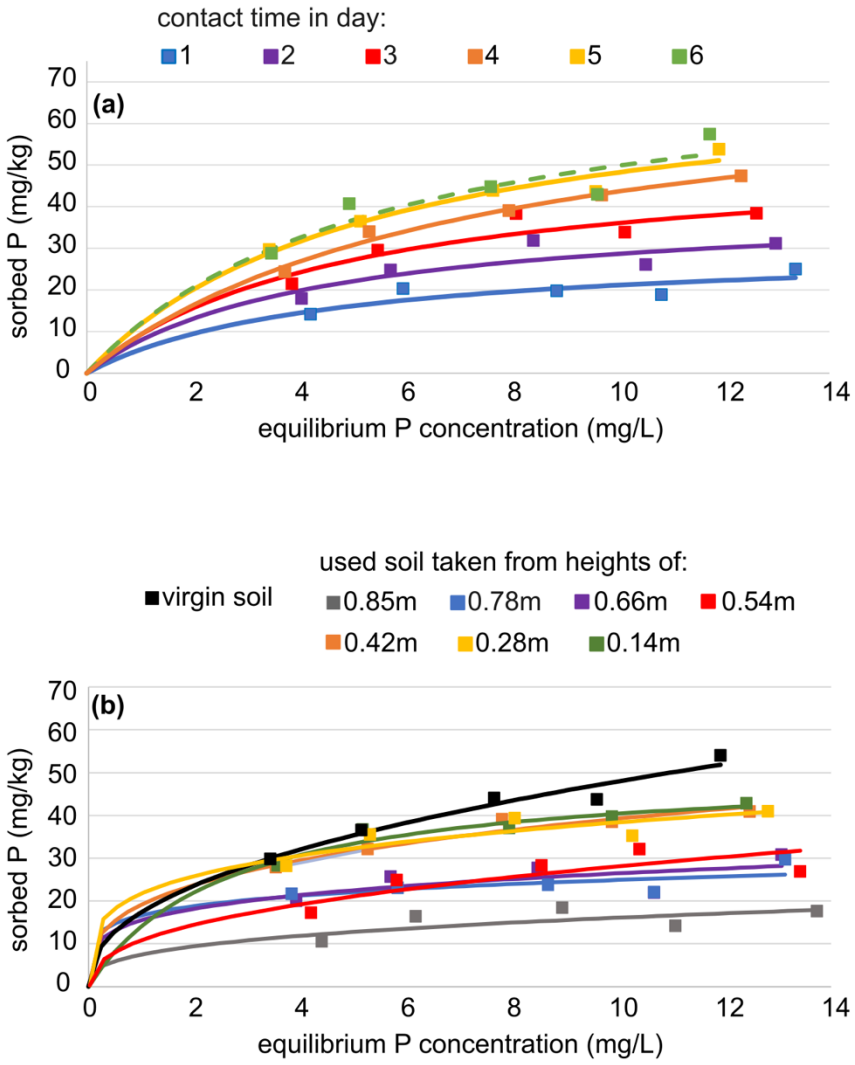

Figure 4.3 Phosphorus sorption experimental data and Langmuir isotherms for (a) virgin sand over contact durations ranging from 1-6 days. (b) virgin sand and used sand collected from various heights of the sand column with a contact duration of 6 days.

The Langmuir isotherm parameters for all tested samples are summarized in Table 4.2. For the virgin sand, a clear increasing trend in maximum sorption capacity is observed over time, with values approaching equilibrium in the final days, aligning with the trends described earlier. In the used sand samples, an overall increase in sorption capacity is seen from the top (0.85 m) to the bottom (0.14 m) of the column. The similar maximum sorption capacities observed among the intermediate samples (0.78, 0.66, and 0.54 m) and among the lower samples (0.42, 0.28, and 0.14 m) also align with the trends described earlier. Across all samples, the high coefficients of determination ($R^2 > 0.80$) indicate good fits of the Langmuir model to the experimental data.

Table 4.2 Langmuir isotherm parameters for virgin sand with 1-6 days of contact duration and used soil taken from various heights of the sand column with a contact duration of 6 days.

Virgin sand				**Used sand**			
contact time (days)	*k* (mg/kg)	*b* (L/mg)	R^2	used samples height in the column (m)	*k* (mg/kg)	*b* (L/mg)	R^2
1	30.54	0.22	0.84	0.85	20.69	0.33	0.82
2	40.89	0.23	0.87	0.78	30.82	0.45	0.87
3	53.58	0.21	0.91	0.66	32.14	0.46	0.82
4	74.24	0.13	0.96	0.54	36.92	0.29	0.85
5	74.26	0.18	0.94	0.42	50.11	0.36	0.99
6	77.45	0.18	0.84	0.28	45.85	0.50	0.96
				0.14	51.04	0.37	0.98

Previous researchers noted that the results of P sorption batch tests are also sensitive to pH (Cucarella & Renman, 2009). The objective of the batch test in this study was to reduce method-dependent variability and minimize discrepancies between batch and column experiments, thereby allowing for more meaningful comparisons. The pH of the initial phosphorus solutions in the batch test matched the pH range of the column influent (6.5–7.0 as shown in Figure 4.4), which is slightly acidic to neutral. This alignment ensured that pH-dependent adsorption behaviour remained comparable between the two tests. As seen in Figure 4.4, the pH range of the final solution after agitation with virgin sand (7.4-7.8) was close to the range of pH of the effluent (7.6-8.2) of the column test. The increase in the pH after contact with the sand in both experimental approaches is likely due to the dissolution of alkaline minerals from the sand matrix, which can raise the solution's pH.

Furthermore, as previous studies have shown that the adsorption capacity of filter media can vary with the initial concentration of the adsorbate (Cucarella & Renman, 2009), the batch test included

a range of initial P concentrations that cover the P concentration measured in the column feed (Figure 4.2 and Figure 4.3).

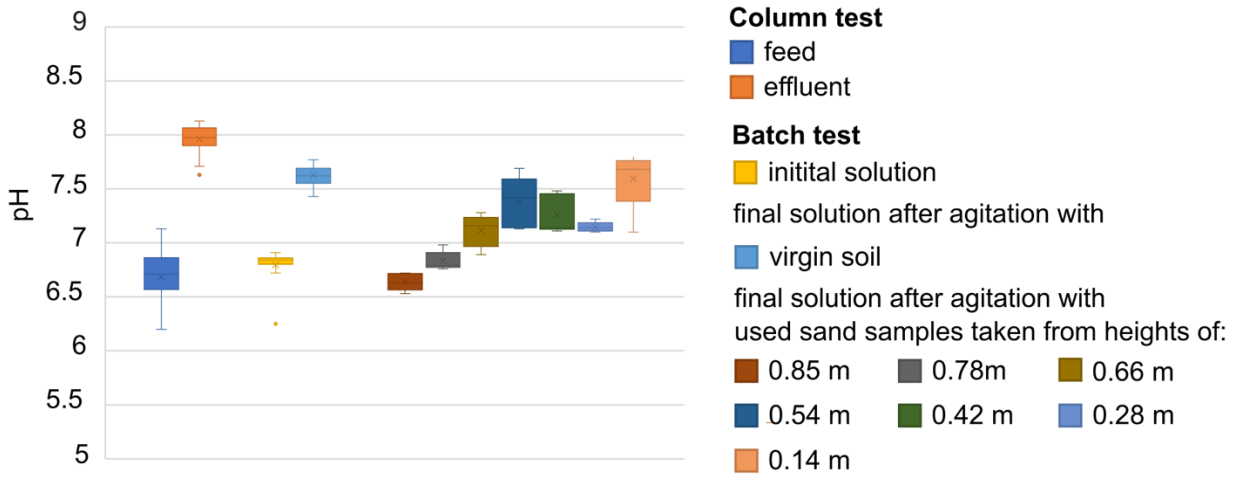

Figure 4.4 pH values measured in the feed and effluent of the column test, and in the initial and final solutions of batch sorption tests conducted on virgin sand and used sand collected from different depths of the column.

4.3.2.2 Shallow, reversible phosphorus retention in the sand column

Figure 4.5a shows the extracted P along the sand column using Mehlich-3 and sequential extraction methods. The sequential extraction data reflect ortho-P concentrations. TP was not plotted, as it exhibited minimal variation from ortho-P, with an average difference of only 2 mg/kg and a maximum of 7.8 mg/kg per extraction. This limited variability was expected since the column influent P was predominantly in the ortho-P form, as previously discussed.

Variations in the amount of P extracted from soil media are expected when using different extraction methods (Jalali & Jalali, 2016). Here, as seen in Figure 4.5a, some difference is seen in the P extracted according to the two methods. Nevertheless, both extraction methods consistently revealed markedly higher P concentrations at the top section of the column, suggesting that influent P was retained predominantly near the inlet zone. In contrast, the bottom three sampling depths (0.42, 0.28, and 0.14 m) exhibited minimal variation and low extracted P concentrations. Combined with their adsorption capacities (Figure 4.3b), which closely resemble those of the virgin sand, this suggests that the P detected at these lower depths represents background P content intrinsic to the original sand, rather than originating from the influent.

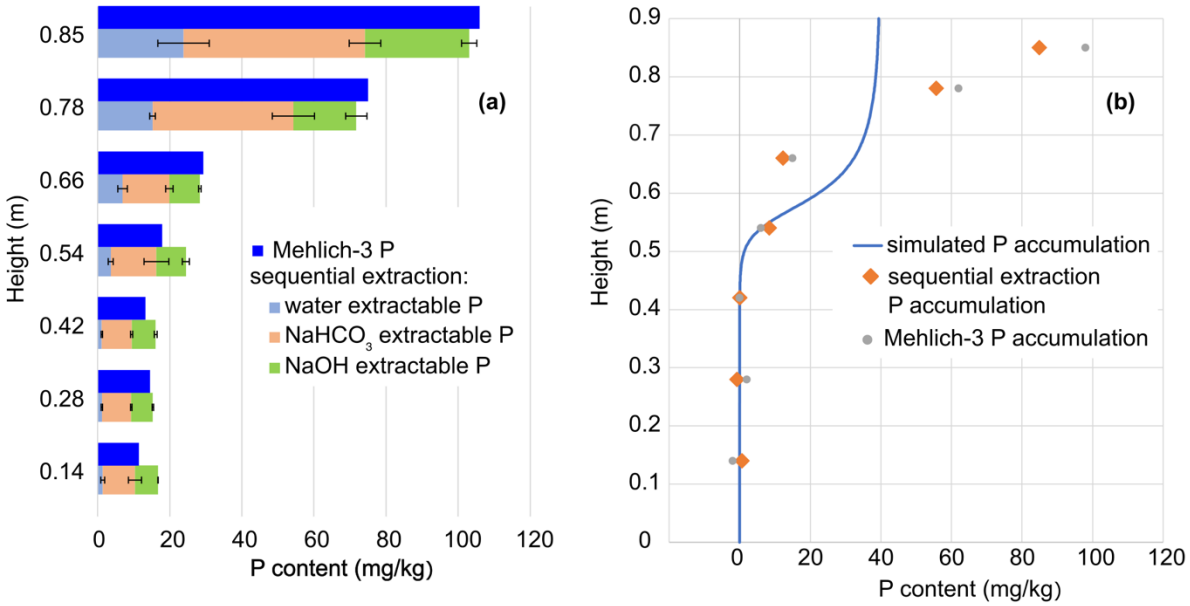

Figure 4.5 (a) Phosphorus extracted along the height of the sand column. (b) Comparison of measured and simulated phosphorus accumulation profiles along the sand column.

Mehlich-3 extraction is widely used to estimate the risk of P loss via runoff (C. J. Penn et al., 2018). As seen in Figure 4.5a, the high levels of Mehlich-3 extractable P at the top of the column suggest a potential for P release from this zone under surface flow conditions, highlighting a risk of desorption. In the sequential extraction method, water-extractable P represents the most labile and mobile pool. $NaHCO_3$ extractable P captures both labile and weakly adsorbed bound P, while NaOH targets more strongly adsorbed P (Zohar et al., 2010). Importantly, none of these fractions includes stable, insoluble P forms such as crystalline precipitates. These findings imply that a significant portion of the retained P was detected in labile extractable and desorbable pools, although part of the retained P may also be present in insoluble forms that were not quantified in this study. Consistently, previous studies reported that P sorption to soil media can be reversible, especially during rainfall or infiltration events (Wang et al., 2024). Furthermore, previous long-term studies on sand filters have shown that secondary attenuation mechanisms, such as the crystallization of soluble P into stable metal phosphate minerals, do not necessarily occur at all sites (Robertson, 2008).

Figure 4.5b presents the P accumulation profile along the sand column after 94 days of operation. The simulated P accumulation from the numerical model was obtained with the initial P content assumed to be zero, and includes both adsorbed and soluble P fractions. Experimentally, the added P retained at various column depths was calculated by subtracting the average extracted P in the lower section of the column (heights of 0.42, 0.28, and 0.14), which was assumed to represent background P, from the extracted P content at each sampling point.

Based on a mass balance approach, feeding with an influent solution containing 8.1 mg P/L over 94 days with a HLR of 0.027 m/d corresponds to approximately 1.45 g of P retained in the sand column. However, when calculating accumulated P using finite sections of the column corresponding to the sampling locations (as shown in Figure 4.1d), a slight overestimation of total retained P was observed, by 35% in the sequential extraction results and 43% in the Mehlich-3 extraction results. This discrepancy can be attributed to two factors. Firstly, the column was fed via a single inlet tube, which did not provide a perfect uniform distribution of influent across the column's cross-sectional area. Since all samples were taken from the center of the column, localized overestimation of P accumulation is likely due to non-homogeneous loading. Moreover, as discussed in section 4.3.4, soil pH varied along the column profile. Previous studies have shown that Mehlich-3 P extraction is highly pH-sensitive, with increasing extractability occurring when pH decreases from 7.5 to acidic values (C. J. Penn et al., 2018). In this study, the top section of the column had a pH of approximately 6.5. This pH is also within the range where P solubility and mobility tend to increase due to the transformation of more stable retention pools into labile forms (C. J. Penn et al., 2018). Still, these fractions remained retained within the sand matrix.

Figure 4.5b clearly demonstrates that P accumulation in the upper 0.25 m of the column exceeded the predicted values from the numerical model. In contrast, experimental P accumulation at the 0.66 m depth was lower than the simulated values. Therefore, the measured retained P was limited to a shallower depth in comparison with the model's prediction based on the initial sorption capacity of the sand. This indicates that the initial sorption capacity of the upper sand layer was likely saturated during the course of the experiment. However, continued exposure to septic tank effluent (STE) likely altered the surface chemistry of the media, possibly via the formation of new sorption sites, enabling further P retention in the top 0.25 m and preventing P leaking to deeper layers.

It is also important to note that the initial sorption capacity was determined using batch experiments, in which the sand particles were fully submerged and well-mixed, allowing maximum surface exposure to P. In contrast, in the column experiment, only a portion of the media surface is actively engaged in sorption due to flow channeling, saturation gradients, and diffusion limitations. Furthermore, using P solutions in the batch test isolates P, unlike wastewater, where other chemicals also compete for sorption sites (Cucarella & Renman, 2009). Therefore, batch tests typically overestimate field-scale or column-scale sorption capacities. However, in this case, the opposite was observed, greater P retention occurred in the column than predicted, further suggesting the development of additional sorption mechanisms or site activation over time, which were not captured in the initial batch-derived isotherm.

4.3.3 Lifetime predictions

The predicted breakthrough curve of the 0.9 m sand filter, based on the initial sorption capacity of the sand, is presented in Figure 4.6. The results indicate that the filter's lifetime would not exceed 340 days, at which point the effluent P concentration is expected to reach approximately 8 mg/L due to the complete exhaustion of available sorption sites. In contrast, the expected breakthrough curve for the used sand, which accounts for 94 days of actual operation plus the remaining sorption capacity measured in sand samples collected after dismantling, demonstrates that 94 days of operation had generated additional sorption sites in the upper section of the column, resulting in an extended lifetime of approximately 42 days beyond the original projection. It is noteworthy that 94 days represents a relatively short operational period; therefore, gaining an additional 42 days of lifetime, nearly half the duration of the initial operation, is a substantial improvement. However, when considered relative to the predicted total lifespan of approximately 340 days, this additional 42 days represents an increase of about 12%, indicating that the overall longevity of the system remains on the same order of magnitude. Still, longer-term operation could potentially lead to further changes in sorption capacity.

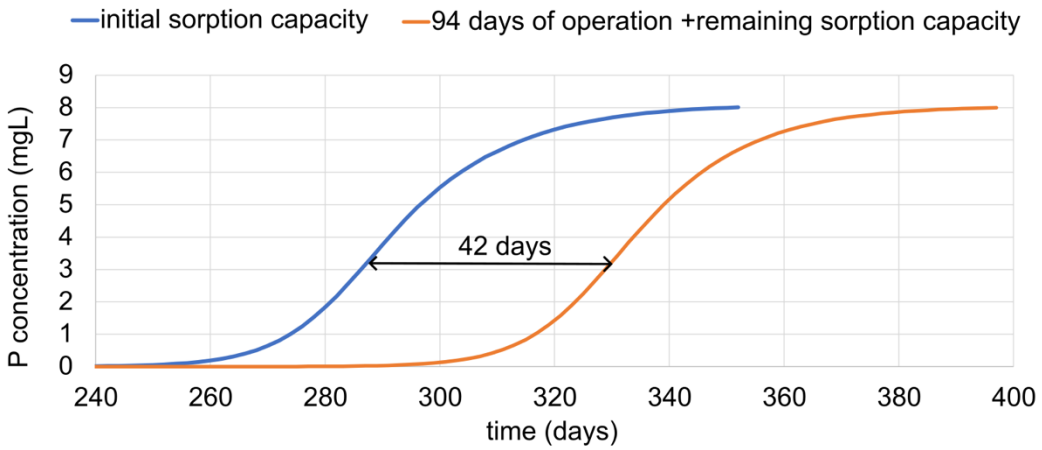

Figure 4.6 Predicted breakthrough curves of the sand filter based on the sorption capacity of the virgin soil and the used sand including 94 days of operation and the obtained remaining sorption capacity after dismantling.

4.3.4 Sand filter geochemical alterations

The sand filter operated for 94 days exhibited clear P retention in its upper section, where additional retention sites appear to have developed over time. In contrast, the lower section remained unaffected by P accumulation and preserved its initial sorption capacity, offering an opportunity for a geochemical comparison between the two layers. Figure 4.7 presents the biogeochemical properties of the sand filter across different depths, highlighting variations that reflect changes occurring during operation.

Organic carbon accumulation in the upper section is evident in Figure 4.7a. In sand filters treating wastewater, the growth of a clogging layer near the inlet is common, caused by the retention of suspended solids and biomass buildup (Rodgers et al., 2004). This clogging layer, characterized by elevated organic carbon content, can enhance P retention via two main mechanisms: The first mechanism is microbial P assimilation. In sand-based filtration systems, biological uptake is typically considered a minor pathway for long-term P removal, because microbial P storage reaches steady state relatively quickly, where the P uptake approximately equals the mineralized P (Eveborn et al., 2012; Liu & Davis, 2014). The second mechanism is biofilm-driven increase in sorption sites. Previous research suggested that biofilm and its extracellular polymeric substances (EPS) coat grain surfaces, creating additional binding sites for P. For example, Zhao et al. (2021) demonstrated under controlled batch-test conditions that sediment particles coated with EPS

exhibited 42–60% higher adsorption efficiency after six weeks of EPS development, depending on initial P concentration. They also observed up to a tenfold increase in Langmuir maximum adsorption capacity compared to uncoated sediments. Similarly, Chen et al. (2021) found that biofilm growth on sediments of different grain sizes increased P adsorption capacity by nearly an order of magnitude during the early rapid growth phase, before stabilizing. Despite these findings in controlled systems, the effect of naturally developed clogging layers on the initial P sorption capacity of sand filters treating wastewater has not been widely explored.

In our study, the extraction protocol targeted plant-available P associated with sorption sites, rather than intracellular or strongly mineral-bound P. Therefore, the observed increase in apparent adsorption capacity is most plausibly explained by additional sorption sites generated through biofilm development and EPS coverage of the sand surface. While some phosphorus may also be incorporated into microbial biomass or retained within the EPS matrix, these pools were not directly quantified in this study. Precipitation mechanisms may also contribute depending on local geochemical conditions; however, the extraction results primarily support adsorption-based retention. In addition, the synthetic influent contained phosphorus exclusively as ortho-P, which is soluble and readily reactive and not particulate; therefore, particulate P retention was not considered in this conceptual interpretation. This interpretation aligns with the results of Hamisi et al. (2022), who observed significantly higher P adsorption in sand columns fed with high-organic-strength wastewater compared to low-organic-strength feed. They also reported that this retention was reversible as P leached completely when the columns were exposed to natural rainwater. On the other hand, Vidal et al. (2018) found no relationship between influent organic content and P retention, but their feed contained less than 30 mg L^{-1} TOC (COD ≈ 110 mg L^{-1}), suggesting that such effects may only be detectable when organic loading is sufficiently high.

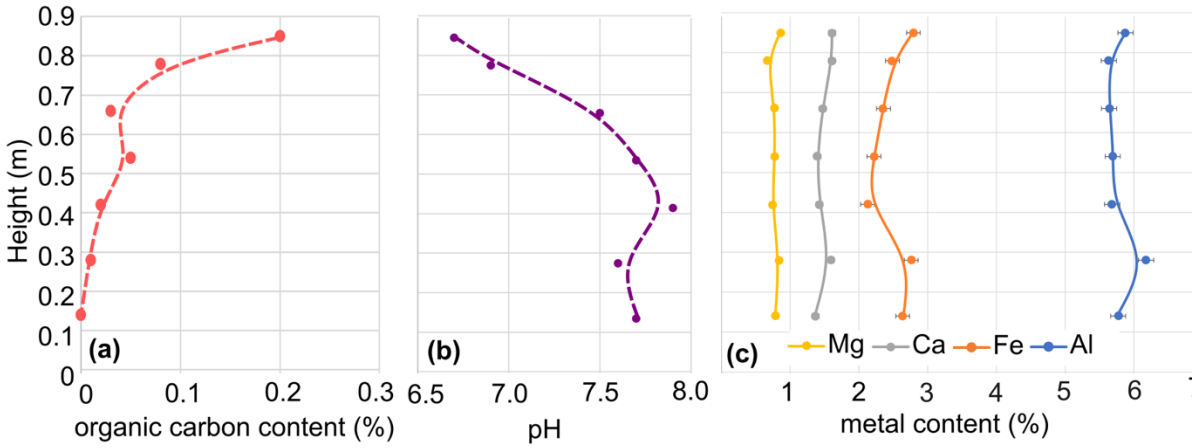

Figure 4.7 Biogeochemical profiles along the sand filter: (a) organic carbon content, (b) pH, and (c) total Mg, Ca, Fe, and Al contents.

As illustrated in Figure 4.7b, a pronounced decrease in pH occurred in the upper section of the sand column. Similar reductions have been observed in sandy soil units receiving STE (Eveborn et al., 2012, 2014), with likely causes including the generation of organic acids and the acidifying effect of nitrification (Eveborn et al., 2012; Maleki Shahraki et al., 2021; Peng et al., 2007). Results from the batch tests on used sand mirror this trend, showing that samples from the column's upper layers consistently reached lower final pH values than those from deeper layers, as shown in Figure 4.4.

Soil pH is a fundamental control on geochemical processes, influencing a wide range of reactions (C. Penn & Camberato, 2019). pH-dependent processes strongly regulate P retention in soils and sand filters. Under highly alkaline conditions (pH > 8), free hydroxide ions (OH^-) compete with phosphate for sorption sites on Fe oxides/hydroxides, whereas under acidic conditions (pH < 6), carbonate dissolution can release Ca-bound P back into solution (Morvannou et al., 2022). Maximum P solubility often occurs near pH 6.5 (C. J. Penn et al., 2018). Below this, Fe- and Al-bound P minerals tend to precipitate; above 6.5, Ca-P minerals are more likely to form (C. J. Penn et al., 2018). In the present case, wastewater exposure altered the sand filter pH from 7.5–8 down to 6.5–7 as shown in Figure 4.7b. Based on the above explanation, changes in pH may have promoted the transformation of some P from more strongly bound pools into more labile forms. The increase in extractable labile phosphorus still reflects P stored within the system and supports the interpretation that additional sorption capacity developed during operation.

Figure 4.7c illustrates the variations in Mg, Ca, Fe, and Al contents along the column. These concentrations are within the same order of magnitude as those reported by (Wang et al., 2024) for filter sand. Long-term accumulation of metals in soil treatment units has been documented in previous studies and is recognized as a mechanism that can enhance P retention (Eveborn et al., 2014; Wang et al., 2024). However, in the present study, given that the wastewater was synthetic, the influent composition was controlled, and the experimental duration was relatively short, such accumulation is unlikely to have occurred. This is supported by the absence of any clear metal enrichment in the upper section of the column, as shown in Figure 4.7c. Therefore, biofilm-induced P sorption remains the primary cause of enhanced P retention.

4.3.5 Environmental implications

Previous studies have reported a wide variability in the P sorption capacity of sands. For instance, sands from Denmark exhibited capacities ranging from 14 to 270 mg P/kg (Del Bubba et al., 2003), while a review by Wang et al. (2024) reported maximum sorption capacities of both commercial and natural sands in the range of 20–290 mg P/kg. In full-scale systems, Eveborn et al. (2014) found that the accumulated P in subsurface treatment systems fell between 120 and 228 mg P/kg, which aligns with the ranges observed in laboratory studies. These findings indicate that while sands can provide substantial short-term P retention, their removal capacity in the subsoil can be readily saturated under continuous loading. However, P removal capacity in the subsoil can be substantial.

The findings of this study contribute to understanding one of the mechanisms behind this: the addition of sorption sites as a result of biofilm growth. While biofilm growth is typically associated with eventual filter clogging, it can contribute positively to system sustainability by increasing available sorption sites. However, the extent of biofilm development is strongly influenced by the chemical characteristics of the influent. For example, septic tank effluent (STE) contains more organic matter, which promotes biofilm formation, compared to secondary treated effluent. In our previously published field study on sand filters receiving STE and SET, the lowest P release was observed in sand filters receiving STE (n = 3; average P release = 1.8 mg/L), whereas systems receiving secondary treated effluent showed higher release values (n = 9; average P release = 5.82 mg/L) (Sheibani et al., 2025).

The present study further demonstrates that even the additional sites created through biofilm growth are largely desorbable. While biofilm growth can enhance short-term P retention, the accumulated P remains vulnerable to remobilization. This risk is particularly concerning under extreme hydraulic events, such as heavy rainfall or flooding, which are expected to intensify with climate change (Tabari, 2020). Such events could accelerate P leaching, thereby increasing the risk of downstream loading and eutrophication in receiving waters.

4.4 Conclusion

This study indicates that sand filters used in OWTS can retain substantial amounts of P, with retention patterns potentially influenced by operational factors such as biofilm development. Reactive transport modelling based on the initial sorption capacity of the sand (measured through batch tests) predicted a lifespan of less than one year for a 0.9 m sand filter. However, experimental observations showed greater P accumulation than predicted, particularly in zones affected by biofilm development. These observations suggest that biofilm growth may contribute to additional sorption sites on sand grains, which could increase the apparent sorption capacity beyond that estimated from the virgin sand alone.

At the same time, the nature and stability of these additional retention mechanisms remain uncertain. Because retained P was detected in labile extractable pools, the long-term stability of the retained P is not guaranteed. As a result, hydraulic or geochemical disturbances could potentially influence P mobility under certain conditions. The differences observed between model predictions and experimental results highlight the importance of considering operational processes, including biofilm development and changes in surface properties, when estimating the P retention capacity and expected lifespan of sand filters receiving STE.

Improving the representation of these processes in predictive models could help refine estimates of system performance and support more effective management strategies, such as appropriate hydraulic loading rates and maintenance practices. Overall, the results suggest that understanding the interactions between hydraulic conditions, geochemical processes, and biofilm development is important for evaluating the long-term phosphorus retention potential of sand-based OWTS and for reducing the risk of P release to surrounding environments.

4.5 Acknowledgements

The authors thank Polytechnique Montreal technicians Samuel Chénier and Éric Turgeon for their assistance with the soil characterization experiments, Gabriel St-Jean for constructing the experimental set-up, and Mélanie Bolduc for helping with the analytical analyses. We would like to express our appreciation to Carmen Lulia Oniga for her help with batch sorption tests and to Adriana Liceth Alvarez De La Hoz for her help with results interpretation. We would also like to thank the Sewage treatment plant in Saint-Hyacinthe, Quebec for providing the primary sludge used in this project. This project was funded by the National Science and Engineering Research Council of Canada (grant number RGPIN-2021-02934) and the Canada Research Chair in Decentralized and Small-Scale Water Treatment (grant 950-232871). Sorour Sheibani was supported by Quebec Research Fund - Nature and Technologies (FRQNT) doctoral awards (B2X).

CHAPTER 5 ARTICLE 2: INFLUENCE OF SOIL MOISTURE DISTRIBUTION ON OXYGEN AVAILABILITY AND NITROGEN REMOVAL IN ONSITE WASTEWATER TREATMENT SYSTEMS

Submitted to Vadose Zone Journal on July 21, 2025

Coauthors: Sorour Sheibani[a*], Frédéric E. Pitre[b] and Dominique Claveau-Mallet[a]

[a] Department of Civil, Geological & Mining Engineering, Polytechnique Montréal, 2900 Boulevard Édouard-Montpetit, Montréal, Québec H3T 1J4, Canada.

[b] Institut de recherche en biologie végétale, Département de sciences biologiques, Université de Montréal and Jardin botanique de Montréal, 4101 Sherbrooke East, Montreal, QC, Canada

*corresponding author, email: sorour.sheibani@etud.polymtl.ca

Abstract

Onsite wastewater treatment systems rely on soil units for infiltration and contaminant removal; however, they are also recognized as significant sources of nitrogen release. This study evaluated how capillarity-driven soil moisture in the vadose zone affects dissolved oxygen (DO) and nitrogen transformations. Two one-m-high soil columns with a fixed water table at a depth of 0.9 m were fed with wastewater, simulating the vertical separation between the drainfield trench and groundwater. Column 1, filled with rapidly draining sand, exhibited a surface volumetric water content (VWC) of 0.09, whereas Column 2, with finer sandy soil, reached 0.19 surface VWC due to stronger capillarity. In Column 1, COD removal rate averaged 97.4%, the effluent dissolved oxygen (DO) increased to >2.5 mg/L, and an average total nitrogen (TN) removal of 35.9% was observed. In contrast, persistent moisture in Column 2 limited oxygen diffusion, stabilizing effluent DO at ~0.78 mg/L. Column 2 achieved 92.3% average COD removal, with effluent COD 18.2 mg/L higher than Column 1, and a higher average TN removal of 51.0%. Biofilm growth and ponding further decreased oxygen replenishment in Column 2. Consequently, slower nitrification promoted partial ammonium adsorption, and sustained anoxic conditions enhanced denitrification, raising TN removal from 64.8% to 98.8%. These findings highlight the trade-offs between nitrogen removal efficiency and oxygen availability, driven by moisture distribution. In real drainfields, minor influent accumulation at the trench is acceptable, while ground surface breakout of untreated

wastewater should be avoided. Therefore, careful design to balance treatment performance with long-term functionality is crucial.

Keywords: Onsite wastewater treatment systems, Nitrogen removal, Soil hydraulic properties, Wastewater infiltration in soil, Soil moisture content

5.1 Introduction

Domestic wastewater treatment methods vary widely. Centralized treatment plants typically serve urban areas, while onsite wastewater treatment systems (OWTSs), commonly known as septic systems, are used in isolated residences and small communities. OWTSs rely on effluent percolation in a soil treatment unit (STU) for treatment. OWTSs play a critical role in wastewater management, serving around 25% of the Canadian population (Government of Canada, 2001) and approximately 20% of the population in the U.S. (Garcia et al., 2013). However, system malfunction or inadequate treatment can lead to the discharge of pollutants, including nitrogen, into surrounding water resources. Nitrogen release from OWTSs to shallow groundwater is a major contributor to eutrophication and harmful algal blooms, posing serious threats to water quality, aquatic ecosystems, and public health (Chambers et al., 2012; Lapointe et al., 2017). This highlights the urgent need for effective design, monitoring, and management strategies to mitigate environmental impacts and protect water resources.

In conventional septic systems, wastewater undergoes primary treatment in a septic tank before flowing into a drainfield for secondary treatment. Approximately 70-80% of the total nitrogen (TN) in domestic wastewater exists as ammonium nitrogen (NH_4^+-N), with the remainder primarily as organic nitrogen (Li et al., 2017). Organic nitrogen is converted to NH_4^+-N through ammonification in both septic tank and drainfield (Gharoon & Pagilla, 2021). The nitrogen cycle continues in the drainfields with NH_4^+-N transformation into nitrate nitrogen (NO_3^--N) via aerobic autotrophic nitrification in oxygen-rich zones of the soil and then NO_3^--N being transformed into gaseous form via heterotrophic denitrification (Lusk et al., 2017). NO_3^--N removal is more complex, requiring oxygen-depleted conditions, along with adequate organic matter to serve as an electron donor (Lusk et al., 2017). While nitrification often occurs successfully (Rout et al., 2021; Teerlink et al., 2012), denitrification is not always completed, mainly due to the differing environmental requirements for nitrification and denitrification, and the depletion of organic matter in oxygen-rich zones, leading to suboptimal TN removal (Pan et al., 2016).

Concerns over nitrogen contamination from conventional septic systems have driven the development of more advanced treatment technologies to improve nitrogen removal. These systems often involve separating wastewater streams, recirculating nitrified effluent back into the septic tank, or incorporating external carbon sources for further treatment (Robertson et al., 2021).

Despite these innovations, conventional systems remain far more prevalent due to their lower cost, simpler installation, and reduced maintenance requirements. In some cases, increasing system complexity may also lead to the release of secondary by-products. For instance, treatment units that incorporate materials such as elemental sulfur or zero-valent iron can result in elevated concentrations of sulfate or iron species in groundwater (Lotfikatouli et al., 2024). Hence, continued research into the performance of conventional septic systems and their nitrogen attenuation capacity remains essential.

Many previous investigations reported less than 50% TN removal in conventional septic systems (Lotfikatouli et al., 2024; Pan et al., 2016). However, some other studies have reported considerably better efficiencies. For instance, a seasonal conventional-style septic system, constructed with imported sand over native sandy silt soil showed an 80% reduction in inorganic nitrogen (Robertson et al., 2023). Another study reported varying rates of inorganic nitrogen removal (ranging from zero to 91%) in the drainfields of 16 conventional septic systems in Canada (Robertson et al., 2021).

Different factors such as wastewater loading types and rates, system age, water table depth have been studied for their effect on nitrogen attenuation in drainfields (e.g., Humphrey et al., 2021; Lusk et al., 2017; Robertson et al., 2021). From a hydrogeological perspective, drainfields are always built in the unsaturated zone to provide enough supplies of oxygen for the degradation of organic matter. However, even in the unsaturated zone, soil moisture content plays a crucial role in oxygen transport and availability within soil, directly affecting nitrogen transformation processes. Higher volumetric water content (VWC) slows oxygen diffusion, promoting anoxic conditions (Teerlink et al., 2012; Wilhelm et al., 1994).

The physical straining of organic material and suspended solids initiates the attachment and growth of microorganisms on soil grains, forming a layer called biofilm composed of various microorganisms (Beal et al., 2005; Palmer et al., 2007). A mature biofilm layer can lead to reductions in hydraulic conductivity and porosity, resulting in water ponding in underground trenches, above the infiltration zone, while keeping the underlying soil unsaturated (Beal et al., 2005). Such changes could drastically affect oxygen transport and nitrogen cycling.

While most guidelines and previous studies focused on water table depths and the separation distance from trench bottom to water table, the influence of the moisture content distribution,

driven by natural soil properties and capillary action in the vicinity of the groundwater table, remains largely understudied. Some researchers have examined nitrification and denitrification rates under controlled soil moisture conditions. For example, Beggs et al. (2011) proposed that nitrification rates increased linearly when VWC ranged from 0.10 to 0.15 but declined at VWC levels between 0.26 and 0.45. Another study demonstrated that in sandy soil, nitrification occurs at 33-78% water-filled porosity, while denitrification becomes more pronounced at 57-70% water-filled porosity (Mekala & Nambi, 2017). However, while these studies provide valuable insight into nitrogen transformation under static moisture conditions, the impact of moisture distribution patterns and spatial variability, especially near the groundwater table, and the dynamic role of biofilm development in shaping oxygen availability and the overall nitrogen removal processes in drainfields remains poorly understood and requires further investigation.

Additionally, in soils with limited organic matter, denitrification relies on organic carbon (OC) from the septic tank effluent (STE) and its decomposition rate, which is influenced by soil hydrogeological characteristics and oxygen availability (Heatwole & McCray, 2007). While finer soils with anoxic conditions retain more organic carbon and promote denitrification (Lusk et al., 2017), the specific relationship between VWC and OC decomposition rates is not fully explored.

This study addresses key knowledge gaps by investigating how variations in VWC driven by hydrogeological properties, such as capillary actions and biofilm growth within sandy soils, influence oxygen availability and nitrogen and OC dynamics. To explore these interactions, two sandy soil columns with distinct capillary properties were subjected to an identical feed. This study provides new insights into optimizing STU design for enhanced nitrogen removal and long-term hydraulic performance, ultimately contributing to improved environmental management and regulatory strategies for reducing nitrogen transport to groundwater.

5.2 Materials and methods

5.2.1 Soil columns description and operation

In the province of Quebec, Canada, regulations permit the installation of drainfields for isolated residences by placing perforated pipes in an underground gravel trench, provided that the separation distance from the gravel trench bottom to the water table is at least 90 cm (LégisQuébec, 2022). The selected sands represented the two soil permeability classes permitted for infiltration systems under regulations: permeable soils with hydraulic conductivity in the range of 2×10^{-6} to

4×10^{-5} m s^{-1} and very permeable soils with hydraulic conductivity greater than 4×10^{-5} m s^{-1}, corresponding to the lower and upper bounds of the acceptable permeability range for drainfield installation. Following these guidelines, two soil columns (30 cm diameter, 1 m height) were constructed to simulate the zone beneath a trench, with a fixed water head at a height of 10 cm representing the water table.

As detailed in section B.1, this configuration equates to a total unsaturated depth of 1.8 m matching conditions found in many real-world systems: Robertson et al. (2021) and Humphrey et al. (2021) documented 21 drainfields in Ontario, Canada with water tables depths averaging 1.75 m (range 0.8–5 m) and 4 drainfields in North Carolina, USA, with water tables depths averaging 1.83 m (range 0.5–3.4 m), respectively. Figure 5.1 shows the column design.

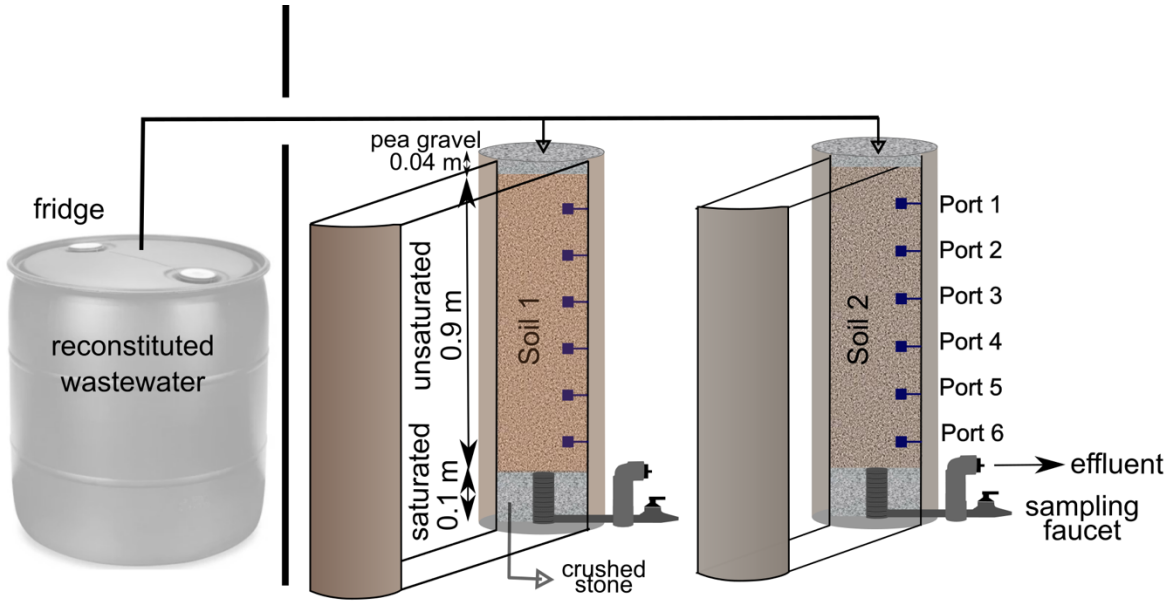

Figure 5.1 Schematic representation of the experimental setup showing the two soil columns being fed with reconstituted wastewater. Moisture/temperature probes are indicated by blue squares.

Each column was filled with a different soil type meeting the required hydraulic conductivities. Column 1 was filled with a sandy soil (Soil 1), characterized by larger grains and higher permeability. Column 2 was filled with another sandy soil with smaller grains and lower permeability. Specifically, Soil 2 is a homogeneous blend of 66% fine sand from the Gerard Therien sand quarry in northwestern Montreal, Quebec, and 33% fine moraine passing through a 0.315 mm sieve. Both soils are silica-rich, with silicon (Si) and oxygen (O_2) contributing more than

85% of the atomic composition. Both soils contained inorganic carbon (IC), while only Soil 2 had traces of organic carbon (OC).

Detailed geological properties of both soils are provided in Table 5.1. Saturated hydraulic conductivity was measured using the constant head method. Particle distribution is provided in section B.2. After filling the columns with dry soil, about 20 litres of tap water were gradually introduced from the top. The columns were then covered with plastic to minimize evaporation and left to drain for 14 days until outflow ceased. This allowed the moisture distribution within the columns to be governed by natural retention and capillary forces. Following this, wastewater was introduced. The columns were fed with wastewater over a 94-day period (~13 weeks). To avoid algae growth, both columns were covered using aluminum foil.

Table 5.1 Properties of the soils used in the study.

Properties	**Unit**	**Soil 1 (higher permeability)**	**Soil 2 (lower permeability)**
Saturated hydraulic conductivity, K_s	m/s	1.2×10^{-4}	5.3×10^{-6}
Mean porosity	-	0.32	0.33
Dry bulk density, ρ_b	kg/m^3	1809	1785
effective particle diameter, d_{10}	mm	0.1	0.05
Median particle diameter, d_{50}	mm	0.28	0.14
Coefficient of uniformity, C_u	-	3.25	4.57
Coefficient of curvature, C_c	-	1.04	1.66
Sand portion (mass of particles greater than 0.05 mm)	%	97.4	89.5
Inorganic carbon (IC)	g/kg	0.72	0.12
Organic Carbon (OC)	g/kg	-	0.2

The use of synthetic wastewater is a common approach in lab-scale studies. Here, synthetic wastewater inoculated with primary sludge, designed to mimic the characteristics of domestic STE, was used as the feed. The recipe for the feed is provided in section B.3 and the properties are shown in Table 5.2. STE can vary significantly in composition. A recent study by Richards et al. (2016) analyzing 32 STE samples reported a range of chemical oxygen demand (COD) values, from 48 to

5,514 mg/L. TN levels ranged from 11 to 146 mg/L, with NH_4^+-N being the predominant form, ranging from 2 to 144 mg/L. Total phosphorus concentrations varied between 1.13 and 132.49 mg/L and pH was measured between 6.37 and 7.68. The synthetic feed fell within all above-mentioned ranges and provided a good compositional control by avoiding the fluctuations typically observed in domestic STE, thereby enabling clearer interpretation of treatment performance.

Total Suspended Solids (TSS) in the influent were measured three times (in weeks 3, 6, and 10) using Whatman 934-AH glass microfiber filters (1.5 µm pore size), followed by drying the filters at 105°C for 24 hours to determine the dry weight. TSS of the feed was measured at 27.5 ± 10.3 mg/L which is within the acceptable range of STE based on Quebec's regulations (< 100 mg/L) (LégisQuébec, 2022).

Table 5.2 Reconstituted wastewater composition.

COD	391 ± 144
TSS	27.5 ± 10.3
pH	6.7 ± 0.2
alkalinity	141 ± 9.4
TN	47.8 ± 3.70
NH_4^+-N	36.6 ± 1.8
TP	8.07± 0.48

The concentration of sodium acetate, serving as organic matter content in the synthetic wastewater, was changed from 0.3 g/L to 0.2 g/L at the end of the 5th week of the experiment. Initially, a higher organic matter concentration was used to promote microbial establishment and growth within the soil columns. After the first five weeks, the recipe was modified to include a reduced concentration of organic matter, thereby lowering the COD of the influent. This phased approach aimed to help assess the long-term operational performance of the columns.

For isolated residences, Québec regulations establish a fixed design wastewater loading based on the number of bedrooms, corresponding to a typical infiltration rate of approximately 25 -30 L m^{-2} d^{-1}; therefore, wastewater was continuously pumped into the top of the columns at 0.027 m d^{-1}, the maximum permissible inflow rate to drainfields (LégisQuébec, 2022). Continuous feeding was

employed to maintain a simplified, controlled system with stable hydraulic conditions, minimizing the moisture fluctuations typically caused by different loading methods and dosing frequencies. This approach enables clearer interpretation of soil treatment processes by isolating the effects of the soil's inherent moisture distribution.

Each column featured wastewater entering from the top and exiting from the bottom. Inlet tubes were secured in a layer of 3-4 cm pea gravel (6-12 mm in size). Teros 12 probes were calibrated according to the manufacturer's method and embedded at six ports (labelled from Port 1 at the top to Port 6 at the bottom in Figure 5.1) at the heights of 0.88, 0.76, 0.64, 0.52, 0.38 and 0.24 m along the columns. The sensors reported volumetric water content (VWC), electrical conductivity (EC), and temperature every 15 minutes. At the bottom of each column, an effluent collection system was in place. The bottom 0.10 m sections of the columns were saturated and contained a grooved pipe that allowed the flow to enter the pipe once it reached this level. The flow then moved towards the effluent exit point at the bottom of each column, as shown in Figure 5.1. The sampling faucet remained closed except during sampling, ensuring that the bottom section of the columns stayed saturated, and the tube stayed without direct contact with the atmosphere. To prevent soil media washout, the bottom section was filled with washed crushed stone (1 to 7 mm in size; effective particle diameter, d_{10} = 1.3 mm; uniformity coefficient, C_u = 2.56).

The study was conducted using two full-scale laboratory columns (1 m height, 30 cm diameter) designed to reproduce representative field-scale hydraulic and biogeochemical conditions. Due to the large column dimensions and material requirements (>100 kg sand per column), the experimental design prioritized scale realism and hydraulic representativeness over column-level replication. The column dimensions were selected to reduce edge effects and spatial heterogeneity, enhancing internal representativeness of observed geochemical patterns.

5.2.2 Sample collection and analytical methods

5.2.2.1 Water quality analysis

Weekly samples of influent and effluent were taken from the inlet tube and exit points of the columns for analysis. All analytical procedures were performed directly after sampling and in accordance with the APHA standard methods (Rice et al., 2017). The pH was measured using a SevenExcellence S400 pH meter. The concentrations of NO_3^-N and nitrite nitrogen (NO_2^--N) were determined by filtering samples through 0.45 μm filters and analyzing them via ion

chromatography. Further tests were conducted using colorimetric test kits from HACH. NH_4^+-N was measured using the salicylate method (HACH Method 10205), and COD, commonly used to quantify organic material in wastewater (Metcalf et al., 1991), was measured following the USEPA dichromate digestion method (HACH Method 8000). From week 5 onward (after the microbial establishment period), TN was measured using the persulfate digestion methods (HACH Method 10072).

Additionally, effluent samples for DO measurement were drawn from the columns' sampling faucets using a syringe, ensuring minimal exposure to air. DO concentrations were measured immediately using a HACH HQ440D Multi-Parameter Meter.

5.2.2.2 Statistical analysis

To analyze trends, the Mann-Kendall test was applied to the moisture content time series, excluding the first two days due to the sharp initial increase in moisture content caused by the introduction of wastewater. This analysis was performed using Google Colab, an open-source Python environment.

The removal efficiency of COD and TN in both columns was calculated using the following formula:

$$Removal\ rate = 100 \times \frac{c_i - c_e}{c_i} \tag{5.1}$$

Where c_i [mg/L] represents the initial concentration of COD or TN in the influent, and c_e [mg/L] denotes the concentration in the effluent. To assess whether differences in the COD and TN removal rates between the two columns were statistically significant, both the Paired T-Test and the Wilcoxon Signed Rank test were applied, depending on the normality of the data. A significance level of $p < 0.05$ was used, with values below this threshold considered significant. These analyses were conducted using Microsoft® Excel for Mac, Version 16.87.

5.2.2.3 Soil Quality analysis

At the end of the experiment, seven samples (each about 900g) were collected from each column: one from the top 0.05 m and six from the locations where probes were embedded. These samples were sent to A & L Canada Laboratories Inc. (London, ON), an accredited facility meeting ISO/IEC

17025:2017 standards. Several key parameters were assessed for each sample. Total carbon (TC) was measured by combustion using a high-temperature furnace, which oxidizes the carbon in the sample to CO_2, followed by quantification. Inorganic carbon (IC) was determined using a calcimeter, which involves treating the sample with acid to release CO_2 from carbonate minerals, and the measurement of this gas. Samples were then subjected to a solution of KCL for extraction of NO_3^--N and NH_4^+-N content followed by measurements using colorimetric methods. pH was determined using a 1:1 water ratio.

5.2.3 Numerical modeling of soils hydrodynamic behaviour

In COMSOL Multiphysics (COMSOL, 2019), a 1-D model was developed to simulate the hydrodynamic behavior of flow in the top 0.90 m of the columns (where the target soils are located) using Richards' equation:

$$\frac{\partial \theta}{\partial t} = \frac{\partial}{\partial z}\left(K_{sat} k_r \left(\frac{\partial H_p}{\partial z} + 1\right)\right)$$
$$k_r = S_e^{0.5}(1 - (1 - S_e^{-m})^m)^2 \tag{5.2}$$

where θ $[-]$ is the volumetric water content, K_{sat} [m/s] is the saturated hydraulic conductivity, k_r [-] is the relative permeability, H_P [m] is the pressure head, z [m] is the vertical coordinate and S_e [-] is the effective saturation. The relation between pressure head and water content was detailed using the van Genuchten retention model, the most widely used mathematical expression of the soil water retention curve (van Genuchten, 1980):

$$S_e = \begin{cases} \left(1 + \left|\alpha H_p\right|^n\right)^{-m} & H_p < 0 \\ 1 & H_p \geq 0 \end{cases}$$
$$\theta = S_e(\theta_s - \theta_r) + \theta_r \tag{5.3}$$
$$m = 1 - \frac{1}{n}$$

where θ_r [-] is the residual water content, θ_s [-] is the saturated water content (equal to porosity), and α [m^{-1}], n [-] and m [-] are the van Genuchten parameters. Estimates of the Van Genuchten

parameters, α and n were obtained based on the mathematical equations proposed by Benson et al. (2014), using their particle distribution data. Other properties of the soils were specified according to Table 5.1. The 1-D mesh was built automatically with COMSOL Multiphysics with a maximum element size of 0.037 m.

In the initial step, a steady-state model was run to determine the moisture distribution along the columns, representing the initial condition at the onset of wastewater introduction. To achieve this, a no-flow boundary condition was imposed at the top of the 1-D domain, while a zero-pressure boundary condition was applied at the bottom of the 1-D domain, as illustrated in Figure 5.2.

In the second step, the results from the steady-state simulation were employed as the initial conditions for a time-dependent model, where the actual inflow rate from the column experiment was applied as the boundary condition at the top of the 1-D domain in Figure 5.2.. The model was used to predict soil moisture profiles in day 2, when biofilm had not yet developed. Thus, biofilm effects were not considered in the model. The simulated predictions were then compared to the measurements obtained from the soil columns.

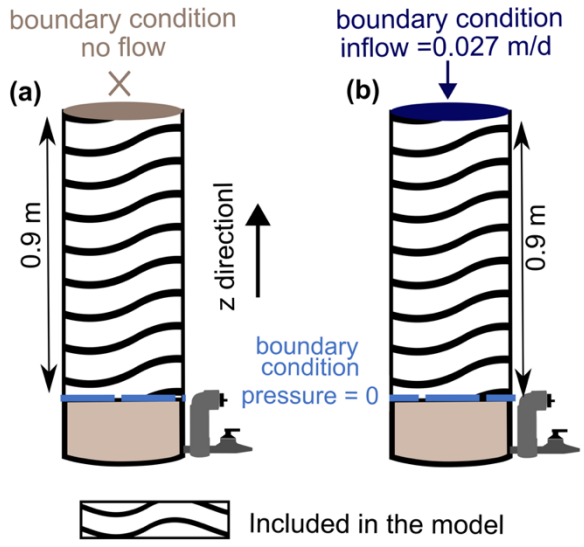

Figure 5.2 Boundary conditions applied in the 1-D numerical simulation of the soil columns during the (a) steady-state simulation, with a no-flow boundary condition at the top and a zero-pressure boundary condition at the bottom, (b) the time-dependent simulation, with an inflow at the top and a zero-pressure boundary condition at the bottom.

5.3 Results

5.3.1 Hydraulic performance of the soil columns

Moisture content distribution differed in Column 1 and 2. Figure 5.3a and c show the moisture content time series at various ports (Port 1 is at the top, Port 6 is at the bottom, and the others in between) in Column 1 and Column 2. Figure 5.3b and d show the initial and final moisture distribution along both columns. The moisture content at the bottom of both columns is nearly the same and close to their porosities (0.32 - 0.34). Initial VWC at Port 1 of Column 1 was observed at 0.11, while the upper section of Column 2 had a relatively higher initial VWC reaching 0.25 at Port 1. The soil columns were designed to simulate a water table at the same depth, and any differences in the initial moisture distribution between the two columns resulted from variations in the capillary effects.

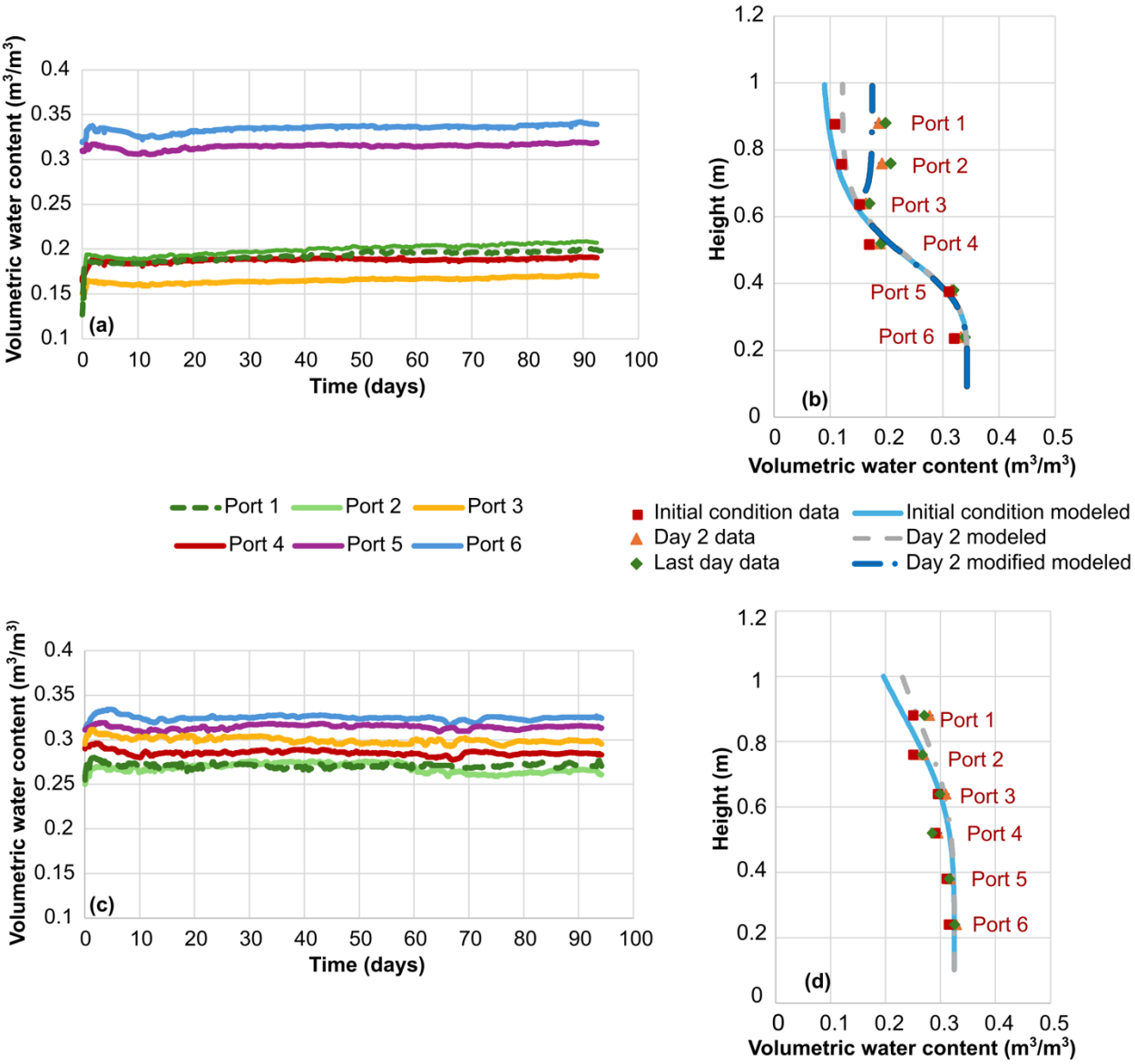

Figure 5.3 Moisture distribution along columns 1 and 2. (a) Time series of observed volumetric moisture content (VWC) at various depths in Column 1, (b) modelled and observed VWC along Column 1, (c) time series of observed VWC at various depths in Column 2 (d) modelled and observed VWC content along Column 2.

The Van Genuchten parameters for the two soils are listed in Table 5.3. Comparison of the modelled data with the initial conditions (Figure 5.3b and d) resulted in a good match with an RMSD of 0.020 for Soil 1 and 0.016 for Soil 2. Soil 1, with a high α and n, indicates a rapidly draining soil with a sharper transition from saturated to unsaturated conditions, as seen in Figure 5.3b. In contrast, Soil 2, with a lower α and n, represents a finer soil that retains more moisture and transitions more gradually between saturation states, as seen in Figure 5.3d.

Table 5.3 Obtained Van Genuchten parameters for Soil 1 and Soil 2.

	Van Genuchten parameters		residual water content, θ_r [-]
	α [m^{-1}]	n [-]	
Soil 1	2.5	4.9	0.07
Soil 2	1.2	4.5	0.06

An increase in VWC was measured in both columns immediately after the introduction of wastewater (Figure 5.3a and c). The model and the measured data confirm stabilization at Ports 1 and 2 after about a day. Figure 5.3b indicates that the modelled moisture content for day 2 (after stabilization) did not accurately match the data in the upper section of Column 1. To improve the model's accuracy, the hydraulic conductivity of the upper 0.35 m of the column was reduced to 10% of its original value. This adjustment significantly improved the modified model's fit with the observed data, achieving an RMSD of 0.017.

Wastewater typically exhibits lower fluidity and higher viscosity than pure water due to its suspended solids content, which can reduce the initial hydraulic conductivity of the infiltration media (Liu et al., 2021). This is a likely reason for the initial model's underprediction of moisture content in the top section and the better fit of the modified model with reduced hydraulic conductivity. As the flow continued, the suspended solids were gradually removed, resulting in purer water in the lower sections, where this moisture content increase was not observed. Another potential reason is the inlet design. The inflow was introduced via a tube, functioning as a point source, while the 1D model assumed a uniform inflow distribution across the surface. This discrepancy could lead to localized high VWC right below the inlet. Since the sensors were positioned at the column's center (aligned with the point source), their readings may have captured higher VWC values than would be expected with a more evenly distributed inflow. Overall, the observed VWC at Port 1 reached 0.18 after wastewater introduction.

Unlike Column 1, in Column 2 the modeled moisture distribution for day 2 matched the observed data well, with an RMSD of 0.019 (Figure 5.3d). The good agreement between modelled and observed moisture distribution in Column 2 may be attributed to the smaller pores in Column 2, which effectively filtered out suspended solids in the uppermost section, allowing purer water to reach the sensor at Port 1. Additionally, the finer texture of Soil 2 likely promoted a more uniform

flow across the surface, reducing localized variations in moisture distribution. Overall, distinct hydrogeological properties of the two soils resulted in different water retention capacities and infiltration regimes.

5.3.2 Evidence of biofilm growth

Visual evidence of biofilm formation on the surface of both columns was obtained using camera and scanning electron microscope (SEM) images, as described in section B.4. Within the biofilm-affected zone of an STU, an extracellular polymeric substance (EPS) matrix, produced as the by-product of microbial metabolism, surrounds microbial cells and increases water content, with the resulting rise in VWC serving as an indicator of gradual biofilm growth (McKinley & Siegrist, 2011; Knappe et al., 2020). Here, the Mann-Kendall test identified a meaningful increasing trend in moisture content at the two top ports of Column 1 (Ports 1 and 2), with the increasing trend leading to a rise in VWC exceeding 0.015 during the experiment period. Figure 5.3b shows that the final moisture contents at these ports were slightly higher than the measurements taken on day 2. Therefore, the upper 0.24 m of Column 1 supported biofilm growth. Neither of the other sensors in Column 1 showed an increase greater than 0.009 in VWC.

While Column 1 was consistently fed with wastewater at the initial inflow rate (0.027 m/d) throughout the entire experiment, Column 2 showed different behaviour. On day 62, minor ponding, with around 1-2 cm of water accumulation, was observed at the top of Column 2. To prevent an overflow and ensure the smooth running of Column 2 until the end of the experiment, the inflow rate of the pump was reduced by 15% to 0.023 m/d, which temporarily eliminated the ponding. However, ponding reappeared on day 70 and persisted until the end of the experiment. This was likely because the infiltration capacity of the uppermost section of Column 2 decreased over time due to the accumulation of suspended solids and the growth of the microbial population, further hindering the flow. It should be noted that this adjustment did not produce a significant change in moisture distribution along the column profile (Figure 5.3) and, therefore, did not introduce mechanistic differences in treatment performance.

Since the inflow rate for Column 2 was reduced at one point during the experiment, the data was analyzed in two phases: once for the period before the inflow change, and once for the period after. Neither analysis showed an increasing trend exceeding 0.010 in VWC, indicating that changes in moisture content in Column 2 were minimal and possibly within the range of natural variability or

sensor noise. A possible explanation is that shallow ponding in Column 2 altered moisture patterns: surface water accumulation can mask or dampen VWC changes measured at depth. Thus, even if biofilm growth was supported at below the depth of 0.12m, the sensors would show little response. This explains the lack of a significant increase in moisture content at any of the sensors' locations.

The accumulation of OC in the top section of both columns, as depicted in Figure 5.4, can be attributed to biofilm growth. As shown in Figure 5.4a, while both columns showed strong OC enrichment at the infiltrative surface, Column 2 generally exhibited lower OC overall, suggesting that its biofilm layer likely differed in composition from that of Column 1.

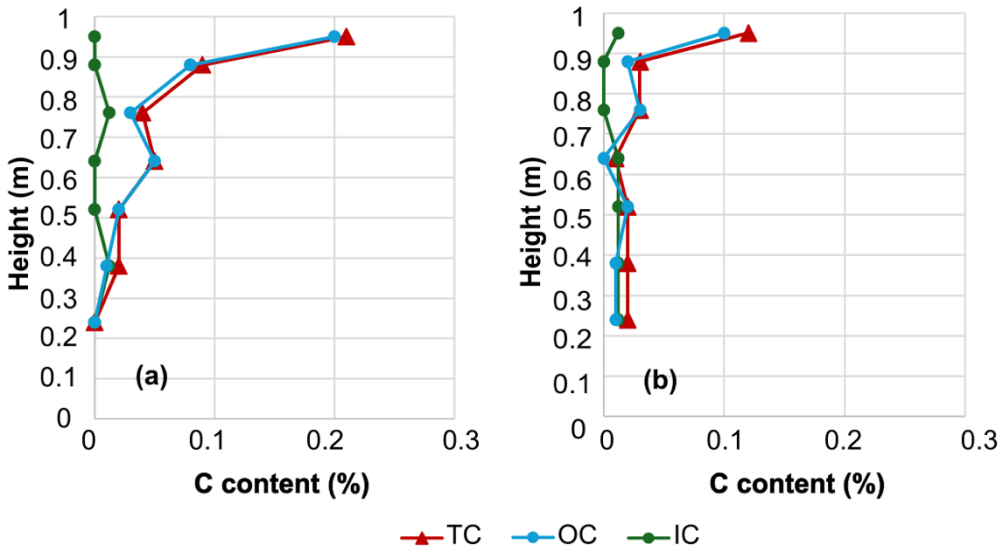

Figure 5.4 Distribution of total carbon (TC), organic carbon (OC), and inorganic carbon (IC) in the soil columns. (a) Column 1, and (b) Column 2.

5.3.3 Dynamics of dissolved oxygen, organic matter removal, and nitrogen transformations

The changes in DO concentrations in the effluent of both columns are presented in Figure 5.5. During the first 20 days, DO levels in both columns exhibited a similar trend, decreasing from approximately 2 mg/L to 1 mg/L, likely due to the establishment of a microbial population consuming available oxygen. After this period, however, DO levels in the effluent of Column 2 dropped further, becoming lower than those in Column 1. This difference may be attributed to the higher moisture content in Column 2, which impeded oxygen diffusion and replenishment.

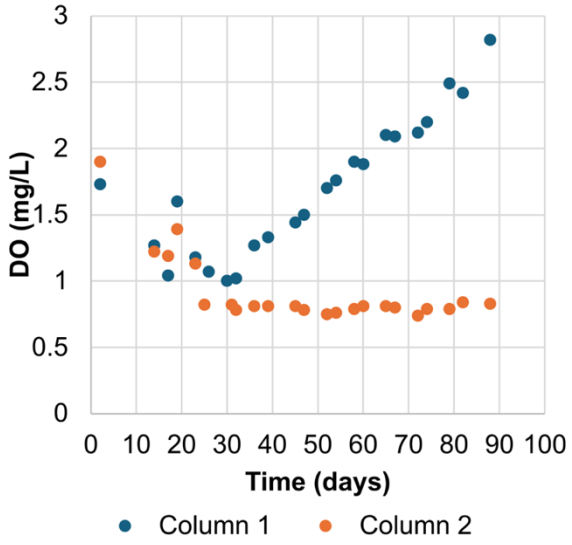

Figure 5.5 Columns 1 and 2 effluents dissolved oxygen (DO).

Following this initial phase, a decrease in the COD of the feed (Figure 5.6a) occurred due to a modification in the synthetic wastewater recipe (as described in section 5.2.1). In response to the reduced oxygen demand, the DO concentration in the effluent of Column 1 gradually increased, eventually reaching approximately 2.7 mg/L, indicating the dominance of aerobic conditions. In contrast, the DO levels in the effluent of Column 2 remained relatively stable at around 0.78 mg/L, showing no significant response to the reduced COD in the feed. The higher VWC at the top section of Column 2 (Figure 5.3) decreased air-filled porosity and restricted oxygen diffusion, combined with biofilm development and the resulting minor ponding at the surface in the final weeks of the experiment (week 10 to 13), likely restricted oxygen diffusion throughout the column. Consequently, despite the reduction in feed COD, oxygen replenishment remained limited, leading to persistently lower DO concentrations in the effluent of Column 2.

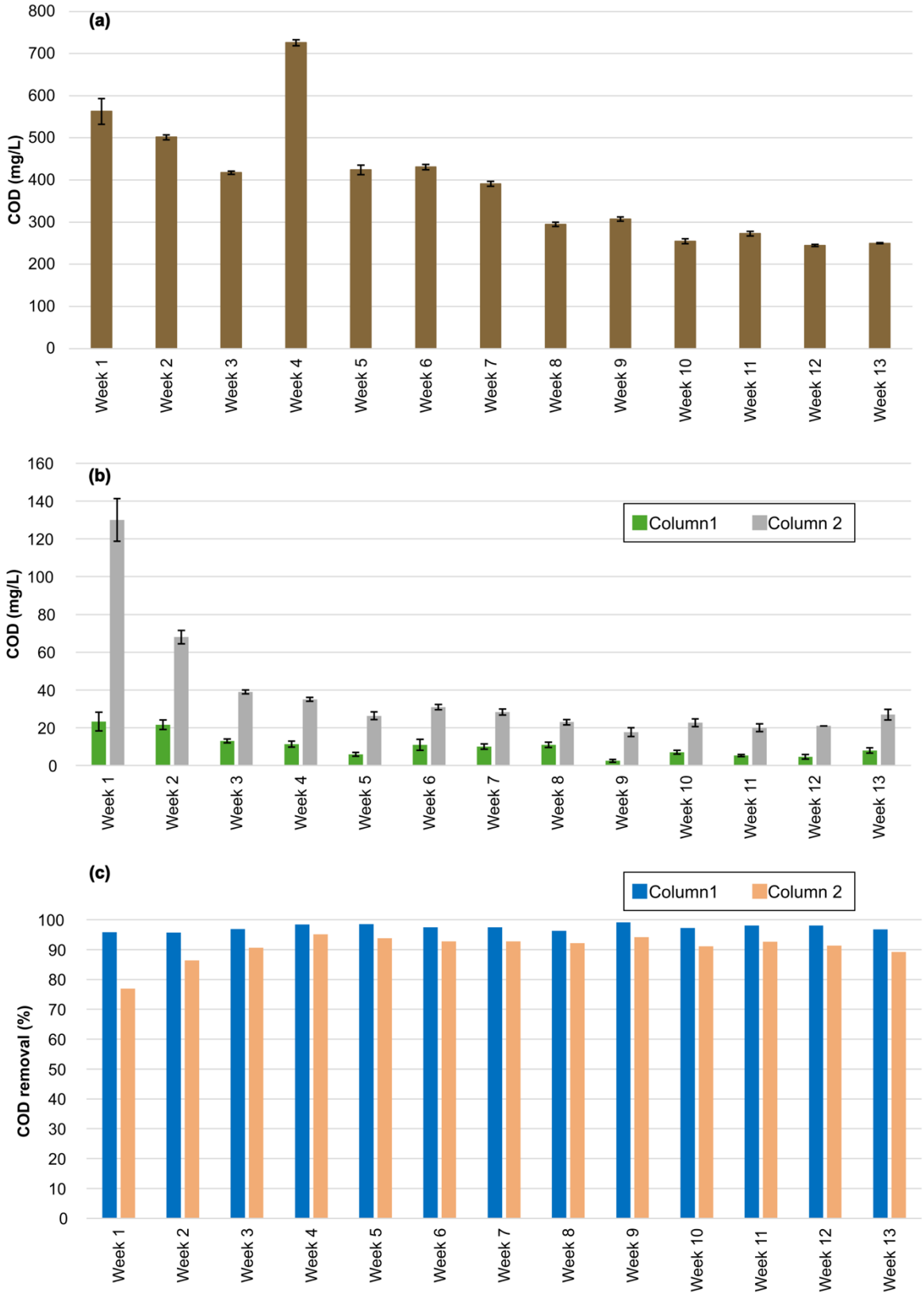

Figure 5.6 (a) chemical oxygen demand (COD) in the feed, (b) columns 1 and 2 effluent COD, and (c) COD removal rates in columns 1 and 2.

The effluent COD of Column 1 started from 23.3 mg/L in week 1 and decreased to 13.0 mg/L by week 3 and remained low throughout the experiment (Figure 5.6b) due to sufficient oxygen availability. Column 1 achieved high COD removal rates of 97.4 ± 1.1% with effluent COD averaging 10.4 ± 6.2 mg/L (Figure 5.6b and c) throughout the experiment. In contrast, Figure 5.6b depicts that Column 2 initially showed a higher effluent COD of 130 mg/L in week 1, with a lower removal rate of 76.9% (Figure 5.6c), likely due to limited oxygen availability which led to slower establishment of heterotrophic microbes. However, from week 3 onwards, as the microbial community became established, effluent COD decreased to an average of 26.5 ± 6.6 mg/L (Figure 5.6b), and removal rates improved to 92.4 ± 1.7% (Figure 5.6c). Nevertheless, the COD degradation rate in Column 2 remained lower than in Column 1, with a portion of the feed's degradable COD persisting in Column 2, suggesting that higher moisture content is associated with slower COD removal rates. In fact, between weeks 3 and 13, the effluent from Column 2 contained, on average, 18.3 mg/L of COD more than Column 1. The observed difference in removal efficiency between the two columns is statistically significant with $p < 0.05$.

Inorganic nitrogen species differed in the influent and effluent of both columns (Figure 5.7a). In the influent, NH_4^+-N was the dominant nitrogen form, whereas in the effluent of both columns, NO_3^--N became predominant, indicating active nitrification. The concentration of NO_2^--N in all samples remained mostly below the detection limit of 0.04 mg N/L, highlighting its high reactivity and transient nature (Essandoh et al., 2013).

Effluent NH_4^+-N concentrations in Column 1 were predominantly below the detection limit of 0.015 mg N/L, demonstrating nearly complete NH_4^+-N removal. In contrast, Column 2 exhibited minor NH_4^+-N levels, beginning at 0.022 mg N/L in week 1 and gradually increasing to 0.179 mg N/L by week 13. Despite this increase, Column 2 still achieved over 99% NH_4^+-N removal.

The comparison of TN concentrations (Figure 5.7b) with inorganic nitrogen levels (Figure 5.7a) reveals that the influent contained approximately 9.8 ± 3.5 mg/L of organic nitrogen. Notably, TN concentrations in the effluents were not significantly higher than the sum of NH_4^+-N and NO_3^--N, indicating that organic nitrogen was effectively degraded in both columns.

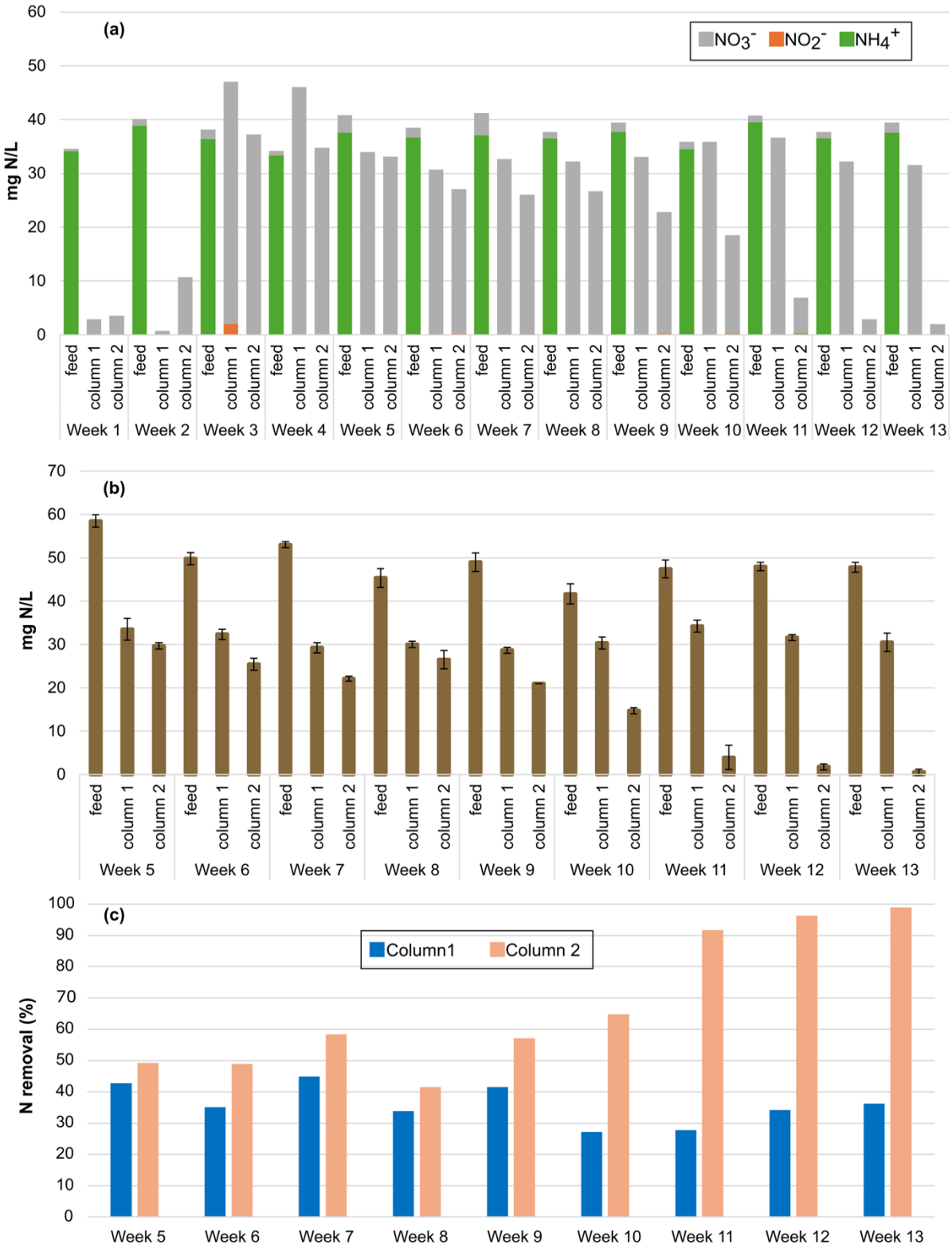

Figure 5.7 (a) Inorganic nitrogen species in the feed and columns 1 and 2 effluent, (b) Total nitrogen (TN) in the feed and columns 1 and 2 effluent, and (c) TN removal rates in columns 1 and 2.

During the initial two weeks, both columns displayed relatively low NO_3^--N concentrations in their effluents (Figure 5.7a) likely due to NH_4^+-N adsorption to soil or microbial assimilation as suggested by previous studies (Friedman et al., 2018; Wu et al., 2009). However, from week 3 until the end of the experiment, the NO_3^--N concentration in Column 1 effluent stabilized at an average of 35.4 ± 5.3 mg N/L. From week 5 onwards, Column 1 achieved an average TN removal rate of 35.9 ± 6.2% (Figure 5.7c). The average removal efficiency was slightly higher during weeks 5 to 9 (39.6± 4.9%) compared to weeks 10 to 13 (31.3 ± 4.5%), which may be the result of lower COD in the feed during the final weeks (Figure 5.6a).

The nitrogen contents along the vertical profiles at the time of dismantling, shown in Figure 5.8a, depict that the content of NH_4^+-N was consistently low throughout the column. The relatively high content of NO_3^--N observed at the top (Figure 5.8a) suggests elevated rates of nitrification. The NO_3^--N content in Column 1 initially decreased with depth until reaching a height of approximately 0.76 m, after which it began to increase again toward the last sampling port. This trend strongly correlated with the moisture content profile of the column (correlation factor = 0.72, see Figure 5.3). This similar pattern suggests that NO_3^--N concentration remained relatively stable along the column, indicating minimal NO_3^--N removal. Lack of significant NO_3^--N removal at sections with higher VWC, which typically favours denitrification, possibly resulted from the rapid depletion of COD. Furthermore, despite the saturation of the bottom section, it still contained substantial DO (Figure 5.5), impeding denitrification. Partial denitrification likely occurred in the biofilm-affected upper section of the column, where biofilm growth created localized low-oxygen zones and COD was still available.

As shown in Figure 5.7, from week 3 onwards, Column 2 consistently achieved higher TN removal than Column 1, with lower effluent NO_3^--N concentrations. However, the results can be divided into two periods: (i) week 3 to week 9, which is the period before the onset of surface ponding and (ii) week 10 towards the end of the experiment, which corresponds to the period with surface ponding. In period 1, Column 2 showed a relatively stable performance similar to Column 1. During this period, its effluent NO_3^--N averaged 29.5 ± 5.4 mg/L, about 6.7 mg/L lower than Column 1, indicating enhanced denitrification. This performance corresponded to an average TN removal of 51.0% from week 5 to 9. This suggests that the higher moisture retention in Column 2, reduced oxygen availability, and slower COD degradation promoted denitrification. From week 10 onward, Column 2 showed a steady decline in effluent NO_3^--N, reaching 1.8 mg/L by week 13.

Correspondingly, TN removal improved from 64.8% in week 10 to over 98% in week 13 (Figure 5.7c). This enhancement is likely due to further oxygen limitation caused by surface ponding. The observed difference in TN removal efficiency between the two columns throughout the experiment is statistically significant with $p < 0.05$.

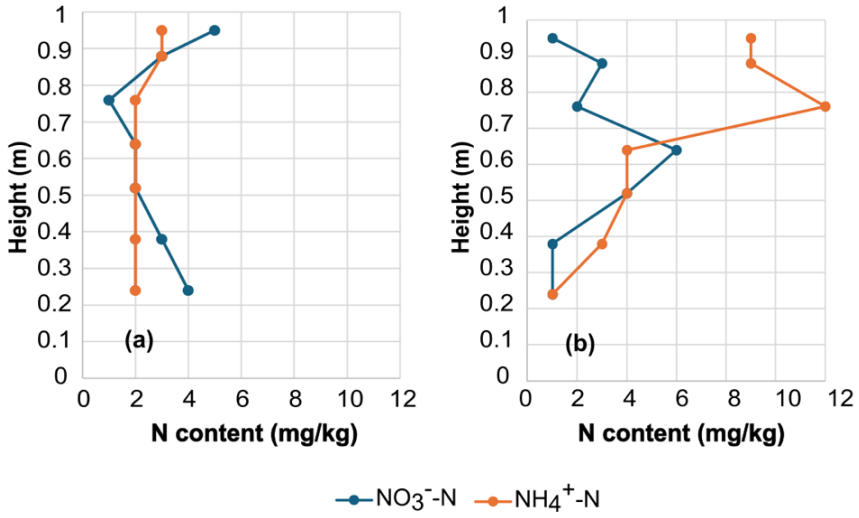

Figure 5.8 Distribution of inorganic nitrogen species contents in the soil columns. (a) Column 1 and (b) Column 2.

According to the nitrogen profile in Column 2 (Figure 5.8b), at the top of the column, NH_4^+-N content increased with depth, peaking at approximately 0.76 m, with values reaching 12 mg/kg. The equivalent concentration of NH_4^+-N in the pore water at this level is approximately 80 mg N/L, which is considerably higher than the inlet concentration of NH_4^+-N (Figure 5.7a). This suggests that, as a result of reduced DO, not all of the nitrogen in the feed followed the nitrification and denitrification path; instead, a portion of NH_4^+-N appeared to be adsorbed onto soil grains in the upper section. NO_3^--N in Column 2 was relatively low near the top 0.20 m and rose at deeper sections below the height of 0.76 m (equivalent to the depth of 0.24 m), suggesting slower nitrification rates compared to Column 1. Below the height of 0.64 m (equivalent to the depth of 0.36 m), NO_3^--N decreased, suggesting active denitrification. Environmental factors such as pH, alkalinity, and temperature are further discussed in section B.5.

5.4 Discussion

5.4.1 Soil moisture and nitrogen removal in drainfields

This study highlights the role of capillary-driven moisture content in the unsaturated zone in determining DO levels in deeper sections of drainfields within OWTSs. Moisture retention in soil, described by van Genuchten parameters, is driven by soil particle size distribution. Coarser soils with larger pore sizes typically exhibit higher α values, indicating more rapidly draining soils, whereas the breadth of particle sizes also largely affects the values of n and α (Benson et al., 2014). A broader range of particle sizes increases air entry suction (lower α) and leads to a more gradual transition from saturated to unsaturated conditions (lower n), enhancing capillary rise above the water table (Benson et al., 2014). Here, both tested soils in this study are sandy, but Soil 2 has a higher coefficient of uniformity (C_u) as reported in Table 5.1 and exhibits a more pronounced retention effect. Therefore, soil texture is not the only predictor; soil particle distribution and the breadth of soil particles also play a crucial role. It should be noted that while in the soil columns studied here, the main reason for variations in moisture content was the capillary forces, in real systems, precipitation pattern, soil heterogeneity, and system design (e.g., loading method and dosing frequency) influence moisture distribution.

In terms of nitrogen attenuation, the oxygen diffusion rate is a critical factor in differentiating between nitrification and denitrification (Lusk et al., 2017). Previous studies pointed out that while nitrification occurs in a wide range of degrees of saturation, its rate increases when VWC decreases (Beggs et al., 2011; Mekala & Nambi, 2017). The results of this study are generally consistent with this finding. In Column 1, the model predicted a low surface VWC of 0.09 (Figure 5.3b), before the introduction of the inflow, and elevated rates of nitrification were observed.

Some studies on nitrogen removal in soils receiving STE and naturally rich in OC often overlooked COD removal rates and their impact on nitrogen removal and reported elevated denitrification rates at higher degrees of saturation (Beggs et al., 2011; De & Toor, 2015; Mekala & Nambi, 2017). On the other hand, many nitrogen transport studies in septic systems assumed that denitrification is limited beneath the unsaturated soil zone of a drainfield due to the depletion of available labile carbon sources (Lusk et al., 2017). The findings of this study suggest that soil hydrogeology and

water content play a crucial role in COD degradation rates. This is especially significant in soils that lack naturally occurring organic carbon, such as those tested in this study (Table 5.1).

Both soil columns received the same influent with a COD/N ratio of 6.4±1.2 from weeks 5 to 13. The required COD/N ratio for effective denitrification is known to range from 3.5 to 4.5, with an optimal range between 6 and 11 (Lotfikatouli et al., 2024). Hence, the influent to both columns fell within the optimal range. However, similar to nitrification, COD degradation was rapid in Column 1 hindering denitrification in the saturated section. On the other hand, Column 2, even at its normal operation prior to surface ponding, demonstrated better nitrogen removal rates.

Stronger capillary effects in Column 2 led to slower degradation rates of COD, leaving more COD in the effluent. Still, a high COD removal rate, exceeding 92%, with effluent COD below 35 mg/L, was achieved. These results align with the Canadian National Performance Standards, which require treated effluent discharged to natural water bodies to contain no more than 25 mg/L of carbonaceous biochemical oxygen demand (cBOD), typically equivalent to about half the COD (Government of Canada, 2012). Therefore, even in slower-draining soils, substantial COD removal is plausible. This is in line with the findings of previous studies suggesting that in the absence of oxygen, heterotrophic bacteria naturally switch to the next most energy-efficient electron acceptor (such as NO_3^--N), and thereby STUs maintain resilience against COD release (Petitjean et al., 2016).

Previous researchers pointed out that partial oxidation of the influent in drainfields provides a better condition for N removal. A sign of partial oxidation in STUs could be the coexistence of NO_3^--N and NH_4^+-N. Robertson et al. (2023) observed the co-occurrence of NO_3^--N and NH_4^+-N in a groundwater plume, in the vicinity of a conventional-style septic system and reported high nitrogen removal rates of approximately 80%. In another study, Gill et al. (2009) reported up to 89% nitrogen removal in subsurface environments receiving STE when both NH_4^+-N and NO_3^--N were present. In contrast, sites receiving secondary treated effluent with dominant NO_3^--N showed only about 50% nitrogen loss. The findings of this study complement these insights by highlighting the role of soil moisture content in promoting such conditions and suggest a trade-off between drainage efficiency, oxygen replenishment, and nitrogen removal performance.

5.4.2 Biofilm-mediated trade-offs in drainfields

The development of a clogging zone in STUs was traditionally only associated with hydraulic failures of the septic system (Knappe et al., 2020; Zhao et al., 2009). In severe cases, clogging leads to effluent backing up into the septic tank or seeping to the ground surface, resulting in aesthetic problems, exposure to pathogens, and contamination of surface water due to landscape runoff (McKinley & Siegrist, 2011). Excessive clogging potentially hinders oxygen replenishment and the nitrification process, eventually leading to an accumulation and release of NH_4^+-N. However, under moderate conditions, reduced infiltration rates can be tolerated. As shown in section B.1, in conventional systems, STUs with perforated pipes placed in underground gravel trenches, minor effluent ponding within the gravel trench is normal and does not compromise treatment as long as unsaturated conditions persist below the trench to support aerobic degradation (Beal et al., 2005; Gill et al., 2009).

Clogging zone has also been reported to improve the treatment performance of STUs. It plays a key role in promoting uniform effluent distribution across the designated STU (Knappe et al., 2020). The findings of this study suggest that inflow distribution in Column 1 was less uniform compared to Column 2. Therefore, coarser-textured soils, like those in Column 1, particularly benefit from biofilm growth, as it helps effluent distribution. Moreover, Chen et al. (2021) suggested that the clogging zone plays a central role in removing organic matter and nitrogen. Biofilm layer plays a vital role in facilitating simultaneous nitrification and denitrification processes (Chen et al., 2021; Friedman et al., 2018). In another study, Gill et al. (2009) found lower potential nitrogen loading from septic systems to groundwater in sites receiving STE compared to sites receiving secondary-treated effluent, which are associated with less pronounced biofilm growth.

In this study, the increased moisture content at the top sensors (0.12 m and 0.24 m depth) in Column 1, associated with biofilm growth, was not found to substantially alter oxygen availability. On the other hand, in the second phase of operation of Column 2, the reduced infiltration capacity caused due to biofilm growth led to surface ponding, substantially altering the oxygen availability as evidenced by the sharp changes in TN removal. Such changes led to slower rates of nitrification. While nitrification is considered the dominant mechanism for NH_4^+-N removal in STUs, previous studies highlighted NH_4^+-N adsorption to soil particles or microbial assimilation as potential

removal processes (Friedman et al., 2018). For silt and sand, a considerable adsorption capacity of 0.08 to 0.1 g NH_4^+-N/kg soil has been reported (Shahraki et al., 2020). Researchers have noted that in anaerobic soils, where nitrification does not occur, NH_4^+-N is more likely to be absorbed by the soil (Beal et al., 2005). The results from this study suggest that, as observed in Column 2, higher VWC and effluent accumulation in drainfields' trenches enhance NH_4^+ adsorption. Under these conditions, partial adsorption of NH_4^+-N combined with slower COD degradation, which enhances denitrification, helps reduce the potential leaching of mobile NO_3^--N into groundwater resources.

While the results of this study suggest that minor ponding in the gravel trenches of drainfields may benefit the overall performance of OWTSs, appropriate design criteria and regular monitoring are essential to prevent excessive clogging that could lead to system backups or surface breakouts (further explained in section B.1).

The results of this study should be interpreted in light of the simplifications made. The 1-D soil columns operation in 13 weeks presents a simplified simulation of drainfields. However, they could not fully simulate the complex 3-D hydrogeochemical mechanisms occurring in real systems. Thereby, the patterns of biofilm development and the associated risks may not be fully captured. Nevertheless, the takeaway from this study is the key role of moisture content in balancing oxic and anoxic processes within STUs. While maintaining hydraulic function is critical, some reduction in oxygen availability, such as that caused by biofilm growth, may enhance the overall treatment efficiency.

5.5 Conclusions

This study advances the understanding of how hydrogeochemical conditions and biofilm growth influence infiltration dynamics and nitrogen removal in STUs within OWTSs. It highlights a key trade-off in OWTS design: In conventional-style drainfields constructed at well-drained soils with lower degrees of saturation, nitrification occurs rapidly at the surface, but fast COD degradation and air-filled porosity enhance oxygen replenishment, avoiding the sustained anoxic conditions needed for complete denitrification, resulting in low to moderate overall nitrogen removal. On the other hand, limited oxygen diffusion resulting from increased moisture retention and/or water ponding at the drainfield gravel-filled trench caused by biofilm growth leads to slower nitrification rates, allowing NH_4^+-N to penetrate deeper layers and undergo partial adsorption onto soil particles. Additionally, slower COD degradation and sustained anoxic conditions enhance denitrification,

leading to reduced leaching potential of NO_3^--N into groundwater resources. These findings underscore the importance of balancing hydraulic function and redox conditions to optimize nitrogen removal while maintaining system sustainability.

Future research should explore long-term operational strategies, variable inlet rates, and intermittent operation to enhance system resilience in passive treatment systems. Understanding these interactions is crucial for developing sustainable OWTSs that maximize nitrogen removal while maintaining stable infiltration over time. These findings contribute to reducing nutrient pollution in groundwater and supporting the long-term sustainability of decentralized sanitation systems.

5.6 Acknowledgements

The authors thank Polytechnique Montreal technicians Samuel Chénier and Éric Turgeon for their assistance with the soil characterization experiments, Gabriel St-Jean for constructing the experimental set-up, and Mélanie Bolduc and Ayat Farahat for their help with the analytical analyses. We would also like to thank the Sewage treatment plant in Saint-Hyacinthe, Quebec for providing the primary sludge used in this project. This project was funded by the National Science and Engineering Research Council of Canada (grant number RGPIN-2021-02934) and the Canada Research Chair in Decentralized and Small-Scale Water Treatment (grant 950-232871). Sorour Sheibani was supported by Quebec Research Fund - Nature and Technologies (FRQNT) doctoral awards (B2X).

CHAPTER 6 MICROBIAL AND FUNCTIONAL RESPONSE TO MOISTURE RETENTION IN SOIL TREATMENT UNITS: IMPLICATIONS FOR NITROGEN TRANSFORMATION PATHWAYS

6.1 Introduction

Onsite wastewater treatment systems (OWTSs) provide essential, decentralized sanitation for millions of households in rural and remote areas where centralized sewers are impractical. In the conventional configuration, wastewater undergoes primary settling in a septic tank, and the septic tank effluent (STE) is then distributed to a subsurface soil treatment unit (STU, or a drainfield in the conventional configuration). In more advanced systems, the STU receives effluent that has undergone further treatment in units following the septic tank. Within the unsaturated drainfield, filtration, sorption, and microbially mediated reactions attenuate organic matter, nutrients, and pathogens before percolation to groundwater (Lusk et al., 2017). When poorly sited, designed, or maintained, OWTSs can release organic matter and nutrients to underlying aquifers and adjacent surface waters, contributing to oxygen depletion, eutrophication, and nitrate contamination that poses risks to human health and ecosystems (Gao et al., 2019; Lusk et al., 2017; Ward et al., 2018).

Within the unsaturated STU, wastewater dosing seeds the infiltrative surface with cells, particulates, and dissolved substrates, promoting the development of a biofilm (biomat) composed of microorganisms and extracellular polymeric substances. This layer traps suspended solids, reduces local permeability, and steepens moisture and redox gradients (Beal et al., 2005). Although biofilm formation is often viewed as a hydraulic liability, it also functions as a reactive zone; by modulating residence time, oxygen supply, and carbon availability, the biofilm help regulate coupled carbon and nitrogen transformations (e.g., Gill et al., 2009; Knappe et al., 2020; Rauch-Williams & Drewes, 2006).

Most work linking treatment performance to microbial communities has focused on large, centralized wastewater treatment plants, with detailed characterization of nitrification, denitrification, anammox, enhanced biological phosphorus removal, and floc/biofilm development (Criado Monleon et al., 2022; Daims et al., 2016; Sanz & Köchling, 2007). In contrast, relatively few studies have studied the microbiology of decentralized systems, particularly within STUs themselves. Tomaras et al. (2009) were among the first to apply molecular tools in STUs,

demonstrating that biofilm communities differ from those in STE, highlighting in situ selection. Subsequent work has explored spatial patterns but remains fragmentary. For example, Amador & Atoyan (2012) observed strong depth-stratified shifts in bacterial communities in sand, sandy loam, and clay receiving synthetic STE, yet provided limited taxonomic resolution and no direct functional interpretation. Criado Monleon et al. (2022) reported that units receiving fully treated effluent exhibited higher microbial richness and diversity than those receiving only partially treated flows, and detected little depth effect; however, their cores extended only ~7.5 cm below the infiltrative surface, likely under-sampling vertical gradients and obscuring deeper stratification.

Emerging evidence points to a central role of substrate and oxygen supply in structuring STU microbiomes. Influent C/N ratio has been shown to shape both process rates and community composition, with more carbon-rich feeds supporting distinct aerobic/anaerobic functional potentials (Friedman et al., 2018). Intermittent aeration and redox cycling can increase active biomass and enhance richness and diversity (Atoyan et al., 2013). More broadly, STUs operate as moisture-structured bioreactors: air-filled pores sustain oxygen diffusion and nitrification, whereas elevated water-filled pore space slows oxygen transport and increases residence time, favouring denitrification and other anaerobic processes (Beggs et al., 2011; Lusk et al., 2017; Mekala & Nambi, 2017; Teerlink et al., 2012). Recent work in STUs has further linked soil moisture and redox to functional guilds, showing that volumetric water content can correlate with methanogenesis markers and explain substantial variation in microbial community structure (Fernández-Baca et al., 2018, 2019).

Despite these advances, key gaps remain for onsite STUs: (i) a lack of depth-resolved microbial surveys conducted under characterized hydraulic and moisture regimes; (ii) limited mechanistic integration of microbial community structure with moisture-driven redox niches and biofilm development; and (iii) scarce information on how these interactions shape the potential for nitrogen transformation pathways that control nitrate release risks.

Here, we address these gaps using two 1-m sandy soil columns designed to simulate STUs receiving synthetic STE under controlled hydraulic loading. The columns were packed with contrasting sandy media that produced distinct moisture retention profiles via capillary effects, thereby creating different oxygen and residence-time regimes. Using 16S rRNA gene amplicon sequencing and PICRUSt2-based functional inference, we aimed to: (i) characterize bacterial

community structure across depth under contrasting moisture regimes; (ii) evaluate putative functional capacities relevant to carbon and nitrogen cycling; and (iii) embed these patterns within a coupled hydrologic–biogeochemical framework emphasizing the role of biofilm formation, moisture distribution, and redox stratification in governing treatment performance. Collectively, this work advances a field-relevant understanding of how media properties and biofilm evolution shape STU microbiomes and the conditions needed to reliably attenuate nitrogen in decentralized sanitation systems.

6.2 Materials and methods

6.2.1 Experimental setup and feeding strategy.

Two soil columns were constructed to simulate drainfield conditions following Quebec's regulatory standards (MELCCFP, 2015), which require soils with a minimum saturated hydraulic conductivity of 2×10^{-6} m/s and at least 90 cm of unsaturated depth. Each column was 1 m in height and 30 cm in diameter. A 10 cm saturated zone was maintained at the base, leaving 90 cm of unsaturated soil above, as shown in Figure 6.1a.

Full description of the experimental setup was provided in a parallel research study (Sheibani et al., 2025). In short, the experimental columns were packed with two sandy soils that differed in texture and hydraulic behaviour. The first column contained a coarser sand, characterized by larger grain sizes ($d_{10} \approx 0.10$ mm; $d_{50} \approx 0.28$ mm) and relatively high hydraulic conductivity ($\sim 1.2 \times 10^{-4}$ m/s). The second column was filled with a finer-textured material composed of 66% sand from the Gerard Thérien quarry blended with 33% fine moraine, resulting in smaller effective particle diameters ($d_{10} \approx 0.05$ mm; $d_{50} \approx 0.14$ mm) and lower conductivity ($\sim 5.3 \times 10^{-6}$ m/s). Soil porosities were similar (0.32–0.33), but the finer soil exhibited a higher coefficient of uniformity, reflecting its broader particle size distribution and greater capacity to retain water through capillary forces.

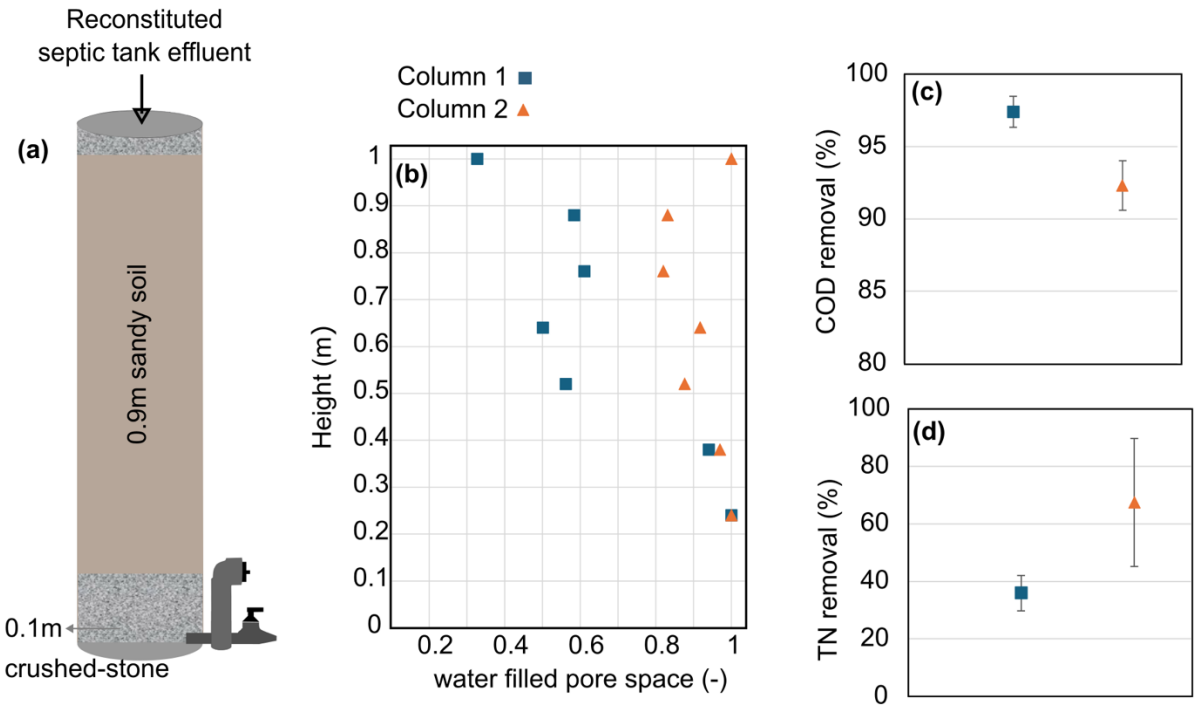

Figure 6.1 Experimental soil column setup and performance. (a) Schematic of the 1 m-high columns (b) Water-filled pore space along the columns at the end of the experiment, highlighting stronger moisture retention in Column 2. (c) COD removal efficiencies in both columns, and (d) Total nitrogen removal efficiencies in both columns. Adapted from (Sheibani et al., 2025)

Once packed with dry soil, both columns were fed with tap water and then allowed to drain to steady-state conditions. To prevent evaporation and light exposure, the columns were sealed with plastic and wrapped in aluminum foil. A pea gravel layer (3–4 cm thick, 6–12 mm size) was placed at the surface to secure influent tubing. Next, the plastic covers were removed, and the two columns were continuously supplied with synthetic wastewater formulated to replicate septic tank effluent. The recipe included a synthetic primary effluent inoculated with primary sludge sourced from the St-Hyacinthe water resource recovery facility, to better reproduce the complexity of real STE and stimulate microbial activity. Carbon sources (0.2–0.3 g sodium acetate, 0.15 g dextrose, and 0.15 g soy peptone) together with phosphorus amendments (0.04 g K_2HPO_4 and 0.01 g KH_2PO_4) and a nitrogen source (0.13 g NH_4Cl), and 0.7 mL of primary sludge, frozen immediately after sampling, and thawed before use, were added to each litre of feed. To ensure feed stability, wastewater was stored at 4°C and renewed every five days. Organic strength was adjusted through the study: a higher carbon load (0.3 g/L sodium acetate) was used during the initial five weeks to encourage microbial colonization, followed by a lower concentration (0.2 g/L) to reflect typical long-term conditions. The experimental run lasted 93 days (January–April 2024).

Influent loading was set at 0.027 m/day, the regulatory maximum, and was reduced slightly if ponding occurred on the surface. Flow entered from the top and exited at the base through a bottom crushed-stone-packed drainage section connected to an effluent outlet, as shown in Figure 6.1a. Controlling the chemical composition of the influent, together with continuous feeding, helped avoid the complexities of real wastewater systems and allowed for a clearer interpretation of the underlying mechanisms driving treatment performance.

Calibrated TEROS-12 probes were positioned at six depths along the unsaturated profile (0.88–0.24 m) to capture water dynamics. The water-filled pore space (WFPS) at the surface of columns was determined gravimetrically by comparing the mass of intact soil samples collected at dismantling with their corresponding oven-dried weights. Influent and effluent samples were collected weekly throughout the experiment. The pH was measured with a SevenExcellence S400 pH meter after calibration with standard buffers. Chemical oxygen demand (COD), total nitrogen (TN), and ammonium nitrogen (NH_4^+-N) were analyzed using Hach Methods 8000, 10072, and 10205, respectively, following the manufacturer's protocols. Nitrate nitrogen (NO_3^--N) was determined by ion chromatography after filtration through 0.45 μm membranes.

6.2.2 Dismantling, sample collection, and soil analysis

After 94 days of continuous operation, the soil columns were dismantled for microbial analysis. From both columns, samples were taken from four depths: the surface, and approximately 12, 24, and 36 cm below the surface. At each depth, three replicate samples of ~20 g were collected, yielding a total of 12 samples per column. All soil samples were immediately stored at –20 °C until subsequent analysis.

From each sampling location, ~900 g of soil was collected from each column and submitted to A&L Canada Laboratories Inc. (London, Ontario), an ISO/IEC 17025:2017-accredited facility. Total carbon (TC) was quantified by high-temperature combustion. Mineral nitrogen was extracted with 1M KCl and analyzed calorimetrically for NO_3^-–N and NH_4^+–N. Soil pH was measured in a 1:1 soil:water slurry as reported by the laboratory.

6.2.3 DNA extraction,16S rRNA gene sequencing

Frozen soil samples were thawed gradually in a cooler over several hours prior to processing. From each bulk sample, subsamples of approximately 200-250 mg were taken for DNA extraction.

Genomic DNA was isolated using the Qiagen DNeasy kit following the manufacturer's instructions. Extracted DNA was stored at -20 °C until shipment to the Center of Excellence in Research on Orphan Diseases - Fondation Courtois (CERMO-FC), Université du Québec à Montréal (Montréal, QC, Canada), where amplification and 16S rRNA gene sequencing were performed.

The bacterial 16S rRNA gene was amplified across the V5–V6 region using the 799F/1115R primers: 799F, 5′-AACMGGATTAGATACCCKG-3′, and 1115R, 5′-AGGGTTGCGCTCGTTG-3′ (Blakney et al., 2024). Amplicons were sequenced at CERMO-FC (UQAM, Montréal, QC, Canada) on an Illumina MiSeq with paired-end 2×300 bp chemistry. Dual-indexed, demultiplexed FASTQ files were provided by the facility. Negative (no-template) PCR controls were included and yielded very low read counts, indicating no detectable contamination.

6.2.4 Bioinformatics processing

We processed reads with the bioinformatic dada2 v1.34.0 pipeline (Callahan et al., 2016) in R 4.4.3 (R Core Team, 2025). In short, primers were removed using Cutadapt v5.1 (Martin, 2011). Reads were then quality filtered, removing PhiX contamination, eliminating sequences containing ambiguous bases, and truncating forward and reverse reads to 250nt and 180nt**,** respectively. Forward reads with more than 2, and reverse reads with more than 4 errors were also discarded. Sequences were dereplicated and denoised with dada (pool=TRUE) to infer amplicon sequence variants (ASVs). Paired reads were merged, and chimeras were removed. Taxonomic assignment used DADA2's naive Bayesian classifier against the SILVA v132 database (Callahan, 2018). ASVs classified as non-bacterial, or as mitochondria or chloroplast, were then excluded from downstream analyses.

Rarefaction curves were computed using the vegan v2.7-1 package to visualize sequencing depth versus observed richness (Oksanen et al., 2025). Finally, the phyloseq R package was used for the production of alpha diversity and beta diversity plots (McMurdie & Holmes, 2013). We did not rarefy because subsampling would discard substantial information and rarefying has been shown to be statistically unjustifiable (McMurdie & Holmes, 2014). To assess differences between the two soil columns across sampling depths, we applied a two-way ANOVA to the alpha diversity data, followed by Tukey HSD post-hoc comparisons across Depth × Column groups and additional depth-wise pairwise t-tests between columns at each sampling depth.

For the production of beta diversity plots, we applied a centered log-ratio (clr) transformation to sequencing counts using the microbiome R package (L. Lahti & S. Shetty, 2019). Euclidean distances of the clr-transformed data (Aitchison distance; Aitchison et al., 2000) were then used for principal coordinate analysis (PCoA). This approach better accounts for compositional data with variable library sizes (Gloor et al., 2017). Differences in community composition were tested using PERMANOVA (Anderson, 2017). This was implemented via adonis2 in the vegan R package with 999 permutations on Aitchison distances, including Column, Depth, and their interaction as fixed factors. Next, homogeneity of multivariate dispersion was assessed using betadisper and permutest. Finally, environmental drivers (pH, TC, WFPS, NH_4^+-N and NO_3^--N) were standardized (mean-centred and scaled to unit variance) and assessed with redundancy analysis (RDA) in CLR space; significance was tested via permutation ANOVA (999 permutations) for overall and marginal effects. All environmental drivers showed acceptable variance inflation factors (< 7), indicating that multicollinearity was not severe.

6.2.5 Predicting functional profiles

We predicted functional potential from 16S rRNA ASVs with PICRUSt2 to obtain per-sample KEGG Ortholog (KO) copy numbers (Douglas et al., 2020). Two ASVs with NSTI > 2.0 were excluded due to low proximity to sequenced reference genomes (Langille et al., 2013). The unstratified KO table was then converted to within-sample relative abundance (each KO divided by the sample total). KOs were mapped to the KEGG BRITE hierarchy using KO hierarchy file ko00001.keg (http://rest.kegg.jp/get/br:ko00001, accessed 16 October 2025) and KO abundances were summed to Level 2 and Level 1 categories per sample (Kanehisa et al., 2023). Where a KO belonged to multiple Level-2 categories, its abundance was fractionally apportioned across those categories to avoid double-counting. Non-functional catalogue branches (e.g., BRITE hierarchies; KEGG Level-1 A09180) and non-prokaryotic categories (e.g., Human Diseases, Organismal Systems, eukaryote-specific cellular community, and virus-specific branches) were excluded before aggregation. All downstream analyses were performed on within-sample KO relative abundances. We considered different nitrogen transformation pathways in soil according to a previous study (Nelson et al., 2016), and used tidyverse (Wickham et al., 2019) for data manipulation and visualization and pheatmap for heatmaps (R. Kolde, 2019).

6.3 Results

6.3.1 Soil columns' treatment Performance

A detailed description of the columns' performance regarding phosphorus, nitrogen, and COD removal, moisture distribution along each column, and effluent dissolved oxygen is provided in parallel research studies (Sheibani et al., 2025; Sheibani & Claveau-Mallet, 2025). In short, the influent contained on average 391 ± 144 mg/L COD and 47.8 ± 3.7 mg/L TN, with NH_4^+-N (36.6 ± 1.8 mg/L) as the dominant nitrogen species and ~9.8 mg/L present as organic nitrogen. These concentrations are within the range expected for domestic septic tank effluent (Richards et al., 2016).

Moisture measurements showed that the coarser sand retained less moisture, whereas the finer soil maintained higher values, confirming stronger moisture retention and slower drainage. Figure 6.1b shows the average WFPS within both columns on the last day of the experiment. The high WFPS observed in the lower section of the columns is attributed to capillary retention near the saturated section. The greater WFPS observed in the upper section of Column 2 is driven by stronger capillary effects related to the hydrogeological properties of the soil, which enhance moisture retention. In Column 2, the finer soil texture promoted localized accumulation of suspended solids and microbial biomass near the surface, which gradually reduced infiltration capacity. This resulted in minor ponding, observed as a shallow water layer during the later phase of operation. Therefore, the surface of Column 2 at the end of the experiment was saturated.

Column 1 showed rapid COD degradation, yielding effluent COD of 10.4 ± 6.2 mg/L and a high average removal efficiency of 97.4%. As shown in Figure 6.1c, TN removal was measured 35.9 ± 6.2%, (Figure 6.1d) with effluent dominated by NO_3^--N (~35 mg/L), while NH_4^+–N and organic nitrogen were almost entirely depleted. In contrast, Column 2 retained more moisture and experienced reduced oxygen diffusion, resulting in higher effluent COD concentrations (26.5 ± 6.6 mg/L) and slightly lower removal (92.4 ± 1.7%) as shown in Figure 6.1c. However, the anoxic conditions favoured denitrification, leading to substantially greater TN attenuation (67.4% on average, beginning from 49.3% and rising to >98% during late-stage ponding as shown in Figure 6.1d). Effluent from Column 2 showed persistently lower NO_3^--N levels compared to Column 1.

6.3.2 Microbial community overview

After quality filtering, a total of 800,730 reads were retained across all 24 samples. The distribution of reads was not uniform across depths, as shown in Figure C.1a. In both columns, surface samples yielded the highest number of reads, with averages exceeding 50,000 in Column 1 and 60,000 in Column 2. In Column 1, the deeper sections showed a marked decline, with average read counts falling below 10,000. In contrast, deeper sections of Column 2 maintained relatively high sequencing depth, averaging more than 40,000 reads.

Across all samples, 2,225 ASVs were detected. Species richness was strongly depth-dependent, particularly in Column 1, where deeper sections contained fewer than 100 ASVs (shown in Figure C.1b). By comparison, all other sampling depths, including the deeper section of Column 2, consistently supported more than 400 ASVs on average. Taxonomic annotation showed a gradual reduction in classification with increasing taxonomic resolution, with 1,189 ASVs identified at the genus level (Figure C.1c). Rarefaction curves for all samples approached a plateau, indicating that sequencing depth was sufficient to capture the majority of microbial diversity present (Figure C.2).

Alpha diversity patterns based on Shannon and Simpson indices are shown in Figure 6.2a. In Column 1, Shannon diversity declined with depth, indicating a loss of richness in deeper layers, whereas Column 2 exhibited higher and increasing Shannon values with depth. Simpson indices were uniformly high across samples, reflecting limited dominance by individual taxa; a slight decrease was observed at the bottom of Column 1, while Column 2 maintained consistently high evenness with depth. Two-way ANOVA revealed a significant Depth × Column interaction for both Shannon ($F_{3,16} = 22.1$, $p < 0.001$) and Simpson ($F_{3,16} = 7.27$, $p = 0.003$), indicating that vertical diversity profiles differed between columns. Depth-wise t-tests showed that Shannon diversity did not differ between columns at the surface (S; p_adj = 0.88), but Column 2 had significantly higher Shannon values at D1, D2, and D3 (p_adj = 0.026, 0.026, and 0.001), consistent with the strong depth-dependent decline in Column 1. For Simpson diversity, depth-wise t-tests revealed no significant between-column differences at any depth (all p_adj > 0.05), reflecting the small magnitude of evenness differences between media.

Tukey HSD comparisons reinforced the depth patterns observed in Shannon: within Column 1, Shannon diversity at D1, D2, and D3 was significantly lower than at the surface (p_adj = 0.037, 0.0001, 0.00026), while in Column 2, deeper layers were as diverse as or more diverse than the

surface. In contrast, Simpson Tukey HSD results showed only minor depth effects, detecting a small reduction at D2 in Column 1 ($p_{adj} = 0.011$) and no significant depth changes in Column 2, with statistically modest increases in evenness in Column 2 relative to Column 1 only at mid-depth. Overall, these results demonstrate that depth-dependent divergence between the two soil media is driven primarily by shifts in richness captured by Shannon, whereas evenness (Simpson) remains comparatively stable across depths in both columns.

Beta diversity plot is displayed in Figure 6.2b. PCoA (Axis 1 = 39.7%, Axis 2 = 11.5%) showed clustering of biological replicates. Surface communities from the two columns were relatively close, consistent with similar surface composition. In contrast, deeper sections (D1–D3) were clearly separated from surface samples along Axis 1, with an additional between-column separation at depth along Axis 2, suggesting that depth is the dominant structuring factor and column effects become pronounced in deeper horizons.

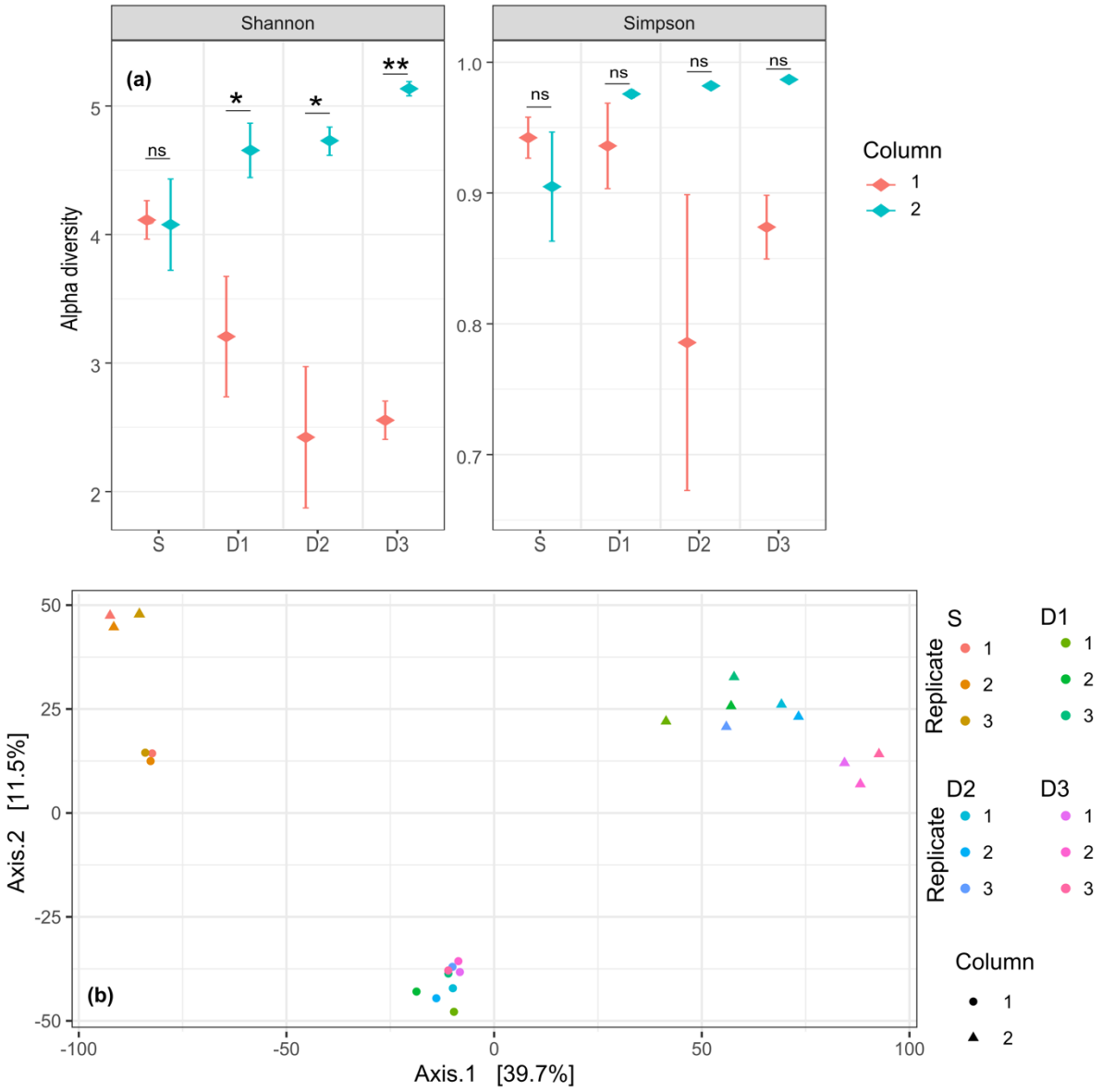

Figure 6.2 Alpha and beta diversity of bacterial communities across the surface (S) and depths of 12 cm (D1), 24 cm (D2), and 36 cm (D3) in Column 1 and Column 2. (a) Alpha diversity (Shannon, left; Simpson, right) by depth (S, D1–D3) for Columns 1 and 2. Points and error bars indicate mean ± SD. Asterisks denote significant differences between columns at a given depth based on t-tests with adjusted p-values ($p_{adj} < 0.05$; ns = not significant). (b) Beta diversity based on Aitchison principal coordinates analysis (PCoA; Axis 1 = 39.7%, Axis 2 = 11.5%). Points are colored by depth (S, D1–D3) and shaped by column.

PERMANOVA confirmed a significant Depth × Column interaction (Df = 3, F = 3.16, $R^2 = 0.171$, p = 0.001), indicating that the influence of depth on community composition differed between columns. Although replicates were tightly grouped overall, a dispersion test detected significant heterogeneity among Column × Depth groups (F = 8.08, p = 0.002), reflecting subtle differences

in within-group variability, particularly in deeper sections of Column 2. Accordingly, we interpret the PERMANOVA results cautiously, emphasizing contrasts that coincide with clear, directional separation in ordination space, with surface samples clustering together and deeper samples forming a distinct group.

6.3.3 Environmental drivers

The factors of pH, TC, WFPS, NH_4^+–N, and NO_3^--N have been considered as potential environmental factors shaping the microbial community used for RDA. Table C.1 reports the values used for analysis. As seen in Figure 6.3, the RDA was significant ($F_{5,18}$= 6.20, p = 0.001), indicating that the environmental predictors collectively explained a substantial fraction of community variation. Marginal permutation tests (999 permutations) showed that TC, WFPS, NH_4^+-N, and NO_3^--N each explained a significant portion of the variation in community composition ($p \leq 0.01$), whereas pH had no detectable marginal effect (p = 0.118).

In the RDA biplot (scaling 2 as shown in Figure 6.3), samples separate primarily by depth and column: surface (S) communities' group to the left, while deeper Column 2 samples plot toward the positive side of RDA1. Arrow directions indicate increasing values; accordingly, points lying further along the NH_4 arrow correspond to higher ammonium, and surface samples align with TC, consistent with expected near-surface accumulation. Together, this depicts a depth–column associated gradient structured chiefly by the environmental factors.

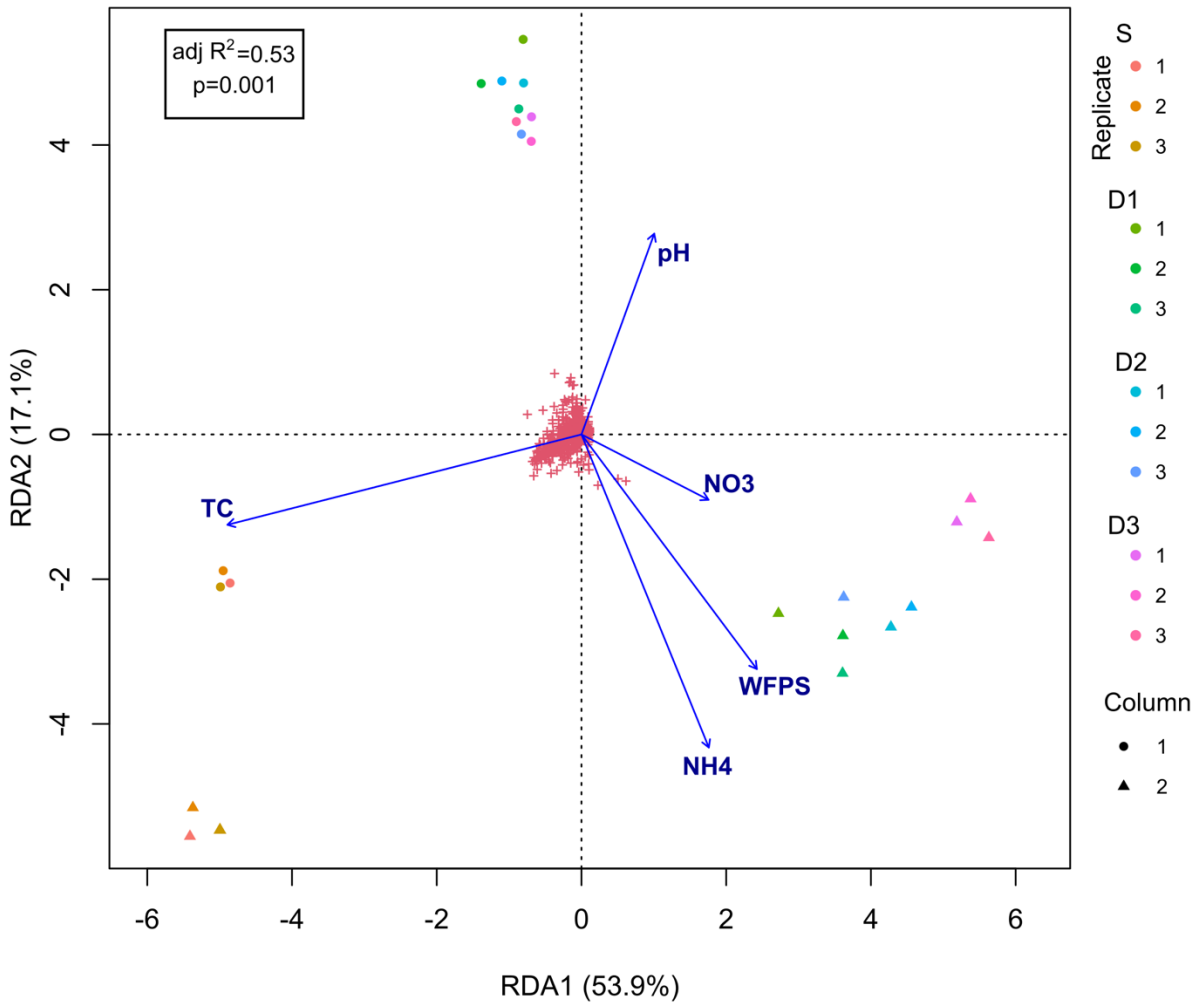

Figure 6.3 RDA of bacterial community composition constrained by environmental variables (scaling 2). Samples were annotated according to their sampling depths: samples from the surface (S) and depths of 12 cm (D1), 24 cm (D2), and 36 cm (D3) in Column 1 and Column 2. Points are colored by depth (S, D1–D3) and shaped by column. Arrows indicate increasing gradients of significant predictors; arrow length reflects correlation strength with the ordination.

6.3.4 Taxonomic composition and depth-dependent shifts

Bacterial communities were dominated by a limited number of phyla, with Proteobacteria, Chloroflexi, and Actinobacteria together accounting for more than 70 % of total sequences across all samples (Figure 6.4a). Minor contributions were observed from Bacteroidetes, Gemmatimonadetes, Firmicutes, Chlamydiae, Patescibacteria, Acidobacteria, and Lentisphaerae. The overall composition was broadly consistent between Columns 1 and 2; However, some differences were observed. Since the beta diversity plots (Figure 6.2b) showed clear clustering of surface samples and deeper samples, in Figure 6.5a-d, surface samples (Figure

6.5a and c) were separated from deeper samples (Figure 6.5b and d), and clear vertical stratification emerged. Proteobacteria and Actinobacteria were the dominant phyla at the surface, whereas Chloroflexi took over in the deeper section. At the surface, Column 1 contained a higher relative abundance of Actinobacteria, whereas in deeper layers, Chloroflexi were comparatively enriched in Column 2.

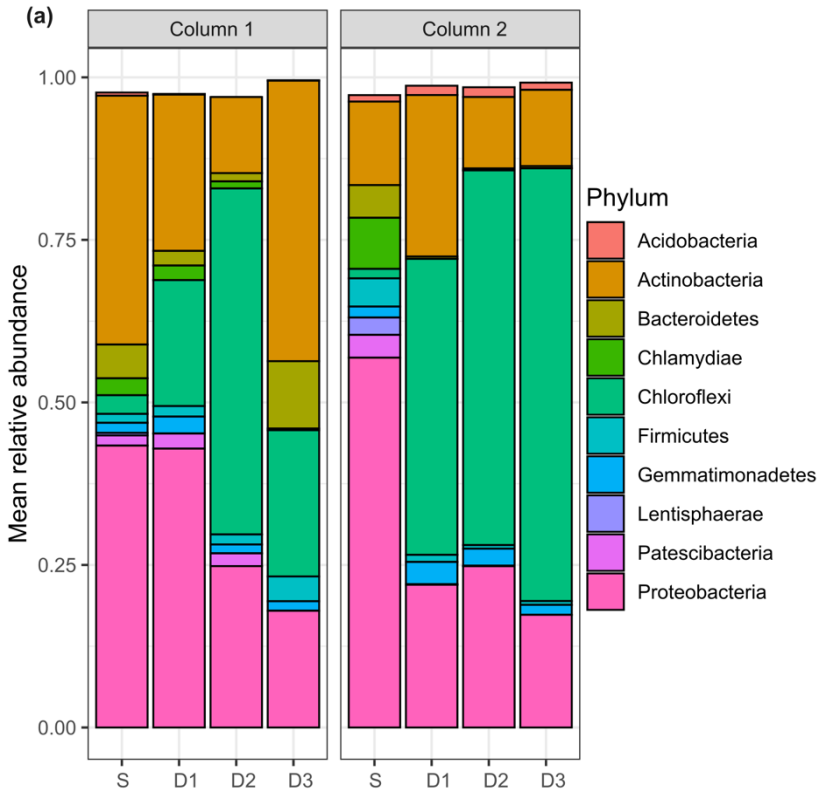

Figure 6.4 (a) Mean phylum-level bacterial community composition across the surface (S) and depths of 12 cm (D1), 24 cm (D2), and 36 cm (D3) in Column 1 and Column 2. (b) Mean genus-level bacterial community composition at the surface of Columns 1 and 2.

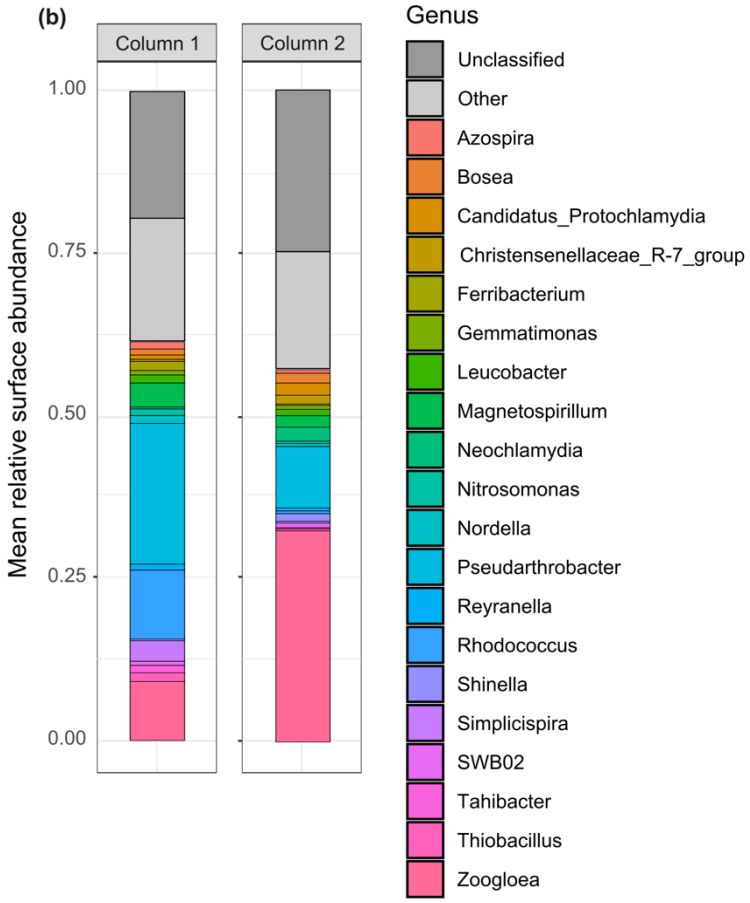

Figure 6.4 continued (a) Mean phylum-level bacterial community composition across the surface (S) and depths of 12 cm (D1), 24 cm (D2), and 36 cm (D3) in Column 1 and Column 2. (b) Mean genus-level bacterial community composition at the surface of Columns 1 and 2.

Surface bacterial communities were dominated by several genera (Figure 6.4b). Across both columns, *Zoogloea*, *Pseudarthrobacter*, and *Rhodococcus* were consistently abundant, accounting together for nearly 40 % of total reads. When comparing Columns 1 and 2 (Figure 6.5e and f), Column 1 exhibited higher representation of *Pseudarthrobacter* and *Magnetospirillum*, while Column 2 was enriched in *Zoogloea*. Unlike at the surface, a large fraction of sequences at depth could not be classified at the genus level, limiting ecological interpretation; these results are therefore not shown.

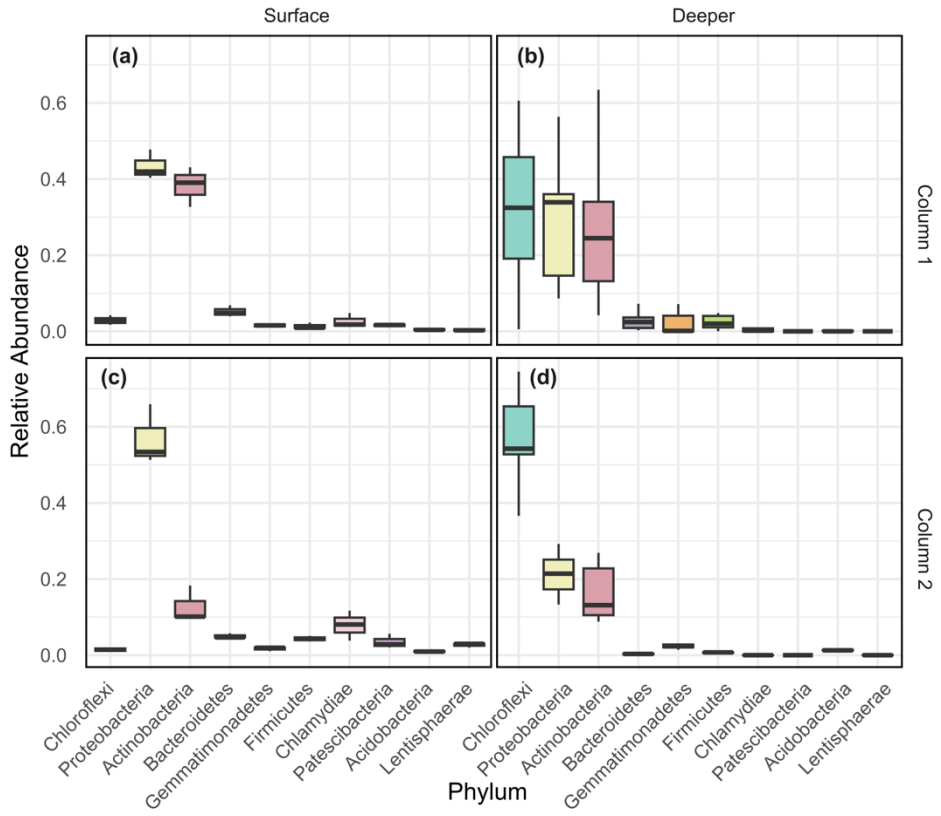

Figure 6.5 Distribution of dominant phyla in (a) surface samples from Column 1, (b) deeper samples from Column 1, (c) surface samples from Column 2 and (d) deeper samples from Column 2, distribution of dominant Genera in (e) surface samples from Column 1, and (f) surface samples from Column 2.

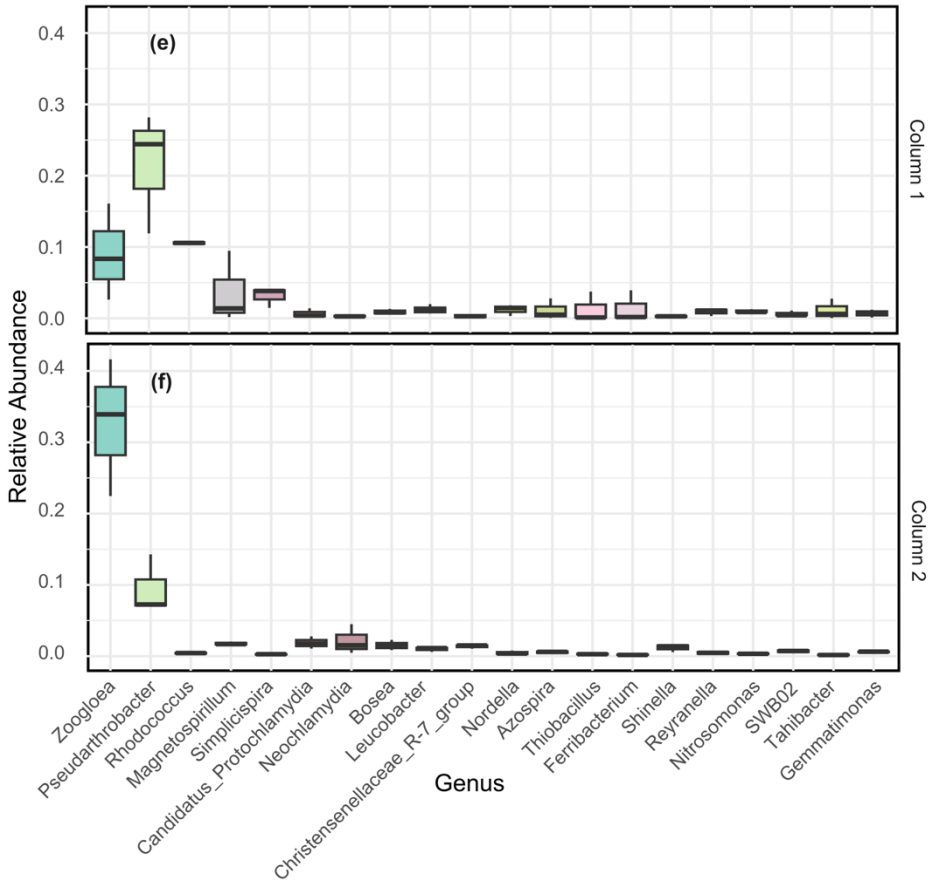

Figure 6.5 continued Distribution of dominant phyla in (a) surface samples from Column 1, (b) deeper samples from Column 1, (c) surface samples from Column 2 and (d) deeper samples from Column 2, distribution of dominant Genera in (e) surface samples from Column 1, and (f) surface samples from Column 2.

6.3.5 Predicted functional genes

PICRUSt2 infers gene potential from 16S profiles; it does not measure gene expression or process rates. Accordingly, all results below reflect potential capacity, not absolute activity. At KEGG Level 1, predicted functions were broadly similar across samples, with Metabolism dominating the community profile (61% ± 1.3%; Figure C.3). Surface samples showed slightly higher shares of Environmental Information Processing and Cellular Processes, whereas deeper sections shifted toward a more Genetic Information Processing and metabolism-centric composition. This vertical stratification was more pronounced in Column 2. At KEGG Level 2, Carbohydrate and Amino-acid metabolism together accounted for the largest fractions across samples (Figure C.4).

To highlight sample-wise deviations within each pathway, we also presented a row-wise z-score heatmap (Figure 6.6). In both columns, core metabolic categories (Energy, Carbohydrate, Amino-

acid metabolism) and Genetic Information Processing were relatively enriched at depth. In contrast, Environmental Information Processing and Cellular Processes were relatively enriched at the surface. This distinction is more pronounced in Column 2. Because z-scores represent within-pathway enrichment (not absolute magnitudes), these patterns indicate a redistribution of functional potential along depth rather than a change in total function. Notably, Carbohydrate and Amino-acid metabolism were lower at the surface of Column 2 than Column 1.

Predicted relative abundance of nitrogen-cycle marker genes is presented in Figure C.5. A row-wise z-score heatmap provided a clearer distinction among samples in Figure 6.7. Nitrification genes (amoABC and hao) were enriched at the surface of Column 1, whereas in Column 2 their enrichment was pronounced at depth. In contrast, genes associated with nitrate reduction (narI and napAB) and denitrification (nirKS, norBC and nosZ) showed their strongest enrichment at the surface. More specifically, the surface accumulation of denitrifiers seems to be more pronounced in Column 2. Deeper sections of Column 1 appeared noisier in both Figure 6.6 and Figure 6.7, whereas Column 2 exhibited a clearer stratification.

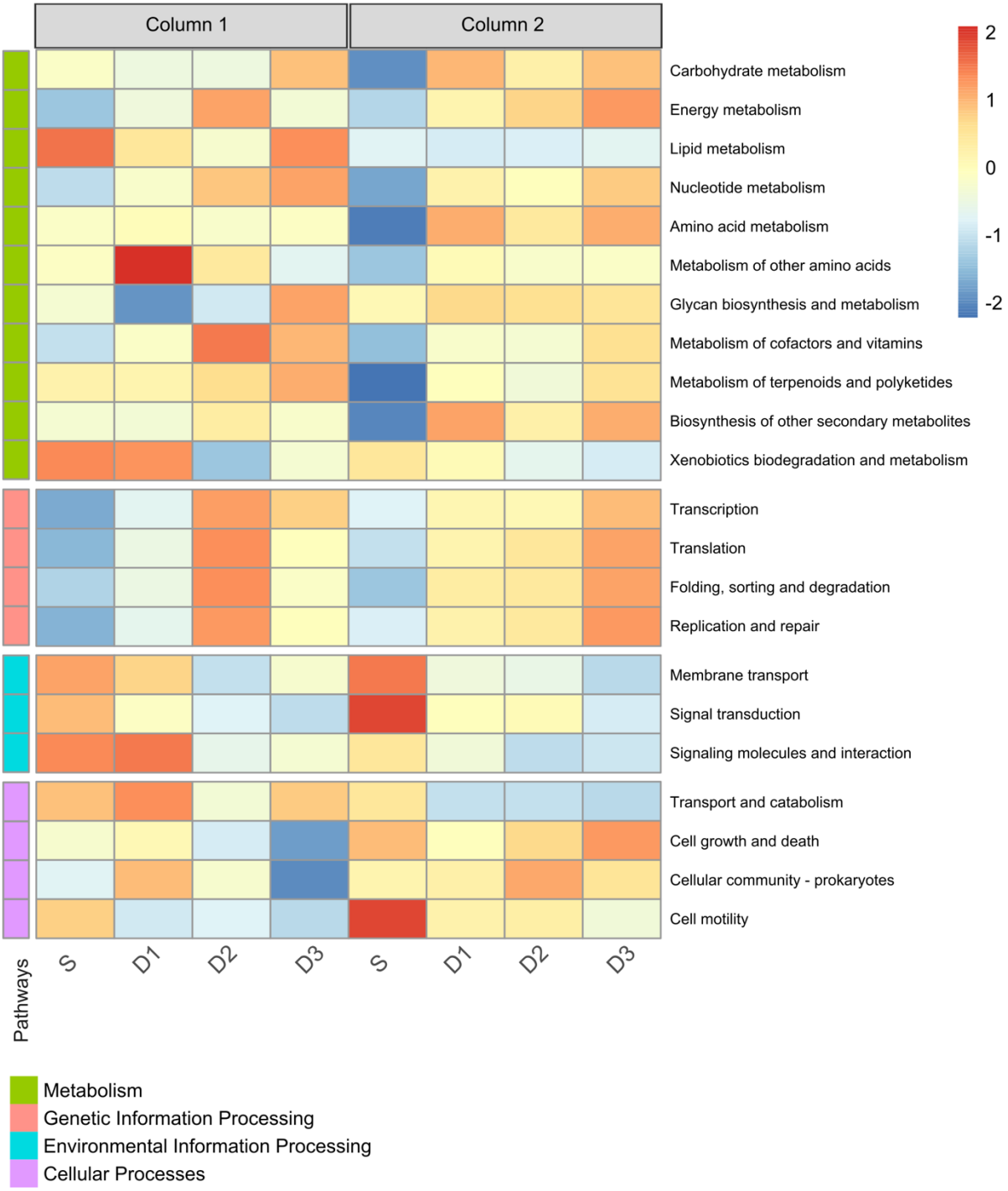

Figure 6.6 KEGG Level-2 functional profile (PICRUSt2). Cells show row-wise z-scores (mean relative abundance of each Level-2 pathway scaled to mean = 0, SD = 1) at the surface (S) and depths of 12 cm (D1), 24 cm (D2), and 36 cm (D3) in Column 1 and Column 2. Rows are pathways, grouped by their Level-1 parent

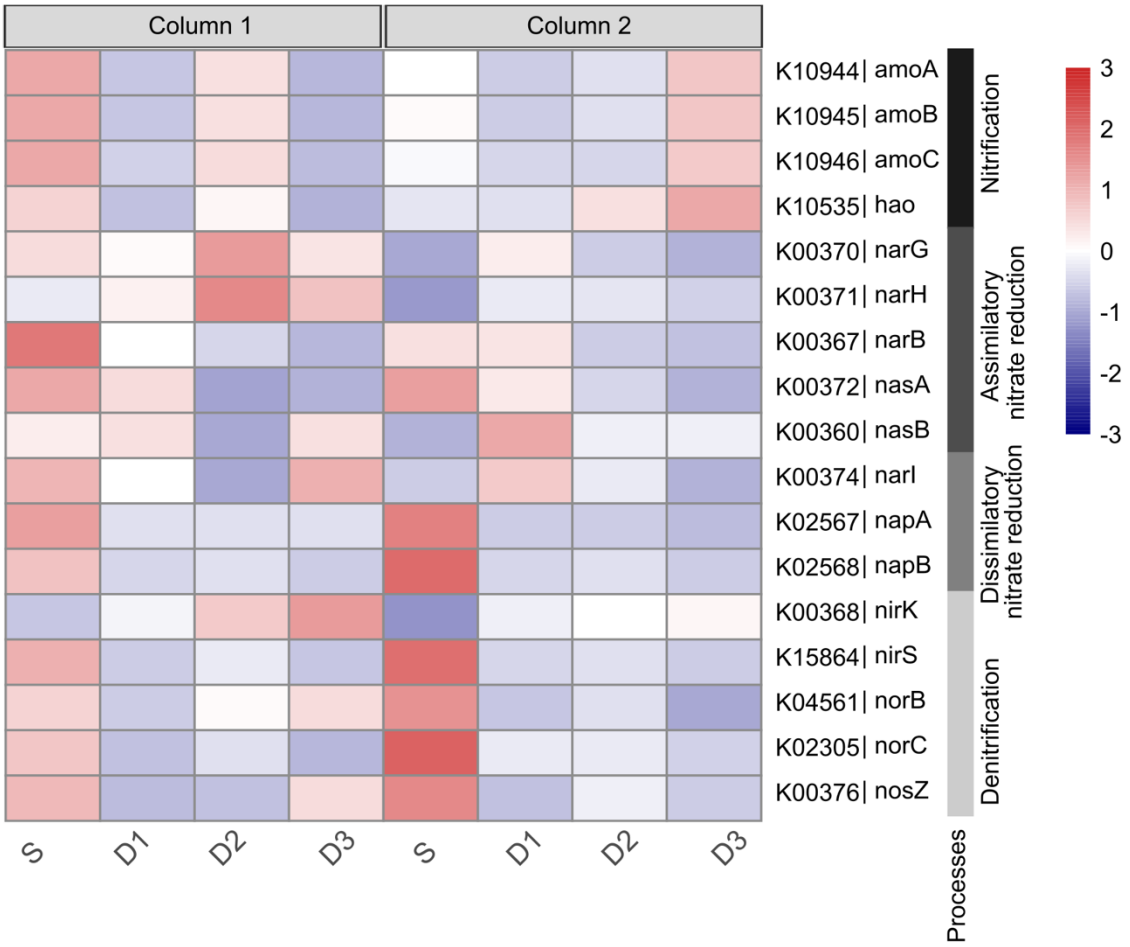

Figure 6.7 Nitrogen-cycle marker genes (KEGG KOs) predicted by PICRUSt2. Cells show row-wise z-scores (mean relative abundance of each KO scaled to mean = 0, SD = 1 across samples) at the surface (S) and depths of 12 cm (D1), 24 cm (D2), and 36 cm (D3) in Column 1 and Column 2, and grouped by process. Rows list KOs for nitrification (amoABC and hao), assimilatory nitrate reduction (narGHB and nasAB), dissimilatory nitrate reduction (napAB and narI), and denitrification (nirKS, norBC, and nosZ).

6.4 Discussion

6.4.1 Moisture retention shapes oxygen supply, substrate penetration, and functional stratification

The contrasting water-retention behavior of the two sands provides a mechanistic basis for the different redox environments inferred in the columns. As shown in Figure 6.1b, Column 2 sustained higher WFPS because capillary-driven moisture retention, combined with biofilm-induced reductions in surface hydraulic conductivity, promoted saturation. Within the soil column, this

reduced air-filled porosity acted as a barrier to gas transport. This implies that oxygen transfer from the surface into deeper pore space was more strongly limited in Column 2, favoring the development of micro-oxic to anoxic zones. This condition slowed COD degradation and discharged more effluent COD (Figure 6.1c). In contrast, the coarser, more freely draining sand in Column 1 maintained lower WFPS and higher gas permeability, allowing deeper oxygen penetration and a more oxidizing profile. Consequently, Column 1 supported faster COD removal and lower effluent COD (Figure 6.1c), consistent with stronger aerobic processing near the surface.

Previous studies have shown that, in both natural soils and wastewater-fed soils, microbial abundance generally declines with depth (Amador & Atoyan, 2012; Friedman et al., 2018). In our study, we confirm this overall pattern for drainfields, but we also show that the steepness and shape of the depth-related decline vary among systems. In this study, both experimental columns were packed with quartz sand, a low-nutrient medium with little background microbial DNA. This minimized indigenous microbial interference and allowed clearer identification of microbial communities that developed in response to wastewater exposure. Reduced labile carbon availability at depth in Column 1 plausibly explains the lower reads, ASVs, and richness in its deeper sections (section 6.3.2), constraining microbial proliferation. This is in line with the central role of carbon supply in structuring soil microbial richness and diversity (e.g., Q. Tian et al., 2021). In contrast, slower COD degradation in Column 2, caused by less available oxygen, permitted more organic carbon to percolate to deeper layers, sustaining microbial growth and resulting in higher richness. These patterns highlight how differences in substrate removal kinetics between columns influenced the vertical distribution of microbial communities.

Beta diversity plots (Figure 6.2b) depicted that the surface microbial community in both columns was relatively similar, meaning that the surface, exposed to air with high oxygen availability and identical feed, developed a relatively similar microbial community. However, as wastewater percolated down the columns, differences in moisture distribution, consequent oxygen availability, and COD degradation kinetics led to substantial differences.

Furthermore, this physical-biogeochemical coupling is also mirrored in the PICRUSt2-inferred functions. As suggested by PICRUST2 results, at KEGG Level 2, deeper sections of Column 1 displayed a relatively noisy functional profile, with a less pronounced trend (Figure 6.6). This is

consistent with lower biomass and substrate scarcity, which likely increased stochasticity in community assembly and inflated variance in PICRUSt2 predictions, rather than evidence of a strongly structured selection regime. In Column 2, the lower relative abundance of Carbohydrate and Amino-acid metabolism at the surface (Figure 6.6) is consistent with slower surface-driven COD degradation and greater substrate carry-over to depth, where these metabolic categories become more prominent. Accordingly, Column 2 exhibited a clearer vertical stratification (Figure 6.6), supporting the notion that more substrate reaches deeper layers and supports a more active and functionally coherent community.

Despite these column-specific differences, both systems share a common pattern: a relatively small shift from Genetic Information Processing and cellular functions near the surface toward core metabolic functions (Energy, Carbohydrate, Amino-acid metabolism) with depth (Figure C.3 and Figure 6.6). This suggests that surface communities, exposed to fresher, labile carbon and higher oxygen, allocate proportionally more to information processing and cellular functions, whereas deeper communities, experiencing lower oxygen and greater reliance on conserved metabolic pathways, show a metabolism-centric functional potential.

In interpreting these patterns, we note that the columns were fed a single, well-defined synthetic septic tank effluent. This simplified influent composition and loading history does not capture the full temporal variability of domestic wastewater, but it was chosen deliberately to isolate the effects of media-driven moisture retention on oxygen delivery and substrate penetration. By minimizing confounding variation in influent quality, the experiment provides a clearer mechanistic link between water retention, redox stratification, and the resulting hydraulic and biogeochemical responses. In full-scale systems, the infiltrative surface is typically overlain by 60–90 cm of unsaturated native soil, which buffers against oxygen limitation and surface expression. Consequently, localized saturation within the trench is generally tolerated, provided that the underlying soil profile remains unsaturated, oxygen diffusion is not completely impeded, and no surface breakout occurs (Beal et al., 2005; Gill et al., 2009).

6.4.2 Moisture-mediated redox shapes taxonomic stratification

The dominance of Proteobacteria, Actinobacteria, and Chloroflexi observed in our samples (Figure 6.4a and Figure 6.5a-d) aligns well with previous studies of wastewater-impacted environments, where these phyla typically represent a major fraction of the bacterial community. For example, Ibekwe et al. (2018) reported that in soils irrigated with wastewater, Proteobacteria and Actinobacteria were two of the three major phyla. In another study, Oluseyi Osunmakinde et al. (2019) reported that Proteobacteria, Actinobacteria, and Chloroflexi are among the four dominant phyla in wastewater treatment plants.

Chloroflexi are often considered oligotrophic organisms, typically thriving under conditions with limited carbon availability (Dragone et al., 2024). In contrast, Actinobacteria and Proteobacteria are generally regarded as copiotrophic taxa that respond positively to environments rich in organic carbon (Q. Tian et al., 2021). The vertical stratification observed in this study, characterized by higher relative abundances of Proteobacteria and Actinobacteria near the surface and an increase in Chloroflexi at depth (Figure 6.5a-d) reflects ecological gradients in substrate availability in deeper sections. Surface layers receive greater inputs of labile organic carbon, nutrients, and oxygen, favouring copiotroph taxa such as Proteobacteria and Actinobacteria. In contrast, deeper zones experience lower oxygen and energy availability, conditions under which slower-growing taxa (e.g., certain Chloroflexi lineages) are more competitive.

In our system, the stronger enrichment of Chloroflexi observed in Column 2 possibly reflects reduced oxygen availability, as many Chloroflexi can grow in low-oxygen or anaerobic conditions (Hug et al., 2013). Moreover, Actinobacteria are predominantly aerobic heterotrophs that thrive under well-oxygenated conditions (Barka et al., 2016), which may explain their higher abundance at the surface of Column 1 where oxygen diffusion was greater. Therefore, despite receiving the same STE, the soil properties are clearly shaping microbial community structure.

The surface prevalence of *Zoogloea*, *Pseudarthrobacter*, and *Rhodococcus* likely drove early carbon turnover at the surface. Members of these genera are generally classified as aerobic or facultative chemoorganotrophic bacteria, widely recognized for their ability to degrade a broad range of organic carbon compounds (Busse, 2016; Dugan et al., 1992; Muller et al., 2017; Nazari

et al., 2022). Therefore, their prevalence at the surface is consistent with the degradation of organics from the influent. *Zoogloea* is also well known for its production of extracellular polymeric substances (EPS) that stabilize aggregates and initiate biofilm formation (Tansel, 2018).

Between columns, the enrichment of *Zoogloea* in Column 2 reflects its adaptation to higher moisture retention and localized surface saturation. EPS-producing *Zoogloea* can trap suspended solids and thicken biofilms, contributing to the minor ponding observed in this column during later operation phases. Therefore, the surface conditions in Column 2 likely represent a realistic, functional biofilm equilibrium. On the other hand, increased *Magnetospirillum* in Column 1 is likely because better drainage maintained an unsaturated surface with micro-oxic niches adjacent to anoxic microsites (sharp oxic–anoxic interfaces), a setting that favours the growth of *Magnetospirillum* (Su et al., 2023).

6.4.3 Moisture retention shapes the spatial distribution of nitrification and denitrification markers

The compositional shifts point to complementary nitrogen pathways at the surface. In Column 1, more persistent oxic niches favored nitrification, as reflected by the PICRUSt2-inferred enrichment of surface nitrification markers (e.g., amoABC, hao, nxrAB; Figure 6.7). At the same time, surface denitrification potential was also detected in Column 1, consistent with biofilms creating micro-anoxic zones within bulk-oxic environments, enabling simultaneous nitrification–denitrification at the surface when COD is available (e.g. Friedman et al., 2018). This interpretation further supports the presence of micro-anoxic niches adjacent to oxic sites in unsaturated Column 1, as described in section 6.4.2.

On the contrary, in Column 2, nitrification-related markers were more distributed along the depth, consistent with slower surface nitrification, greater NH_4^+-N carry-over, and a more active community at depth that can sustain downstream nitrification and denitrification. The higher relative abundance of denitrification genes at the surface of Column 2 is plausibly tied to its Zoogloea-rich biofilms, whose EPS-mediated structure can thicken boundary layers and create O_2-limited microenvironments conducive to NO_3^--N reduction.

Taken together, these mechanisms align with the higher TN removal observed in Column 2 (Figure 6.1d): Column 1 likely experienced rapid surface nitrification and partial denitrification with weaker microbial activities at depth, yielding effluent rich in NO_3^--N. In contrast, in Column 2, beyond the partial nitrogen removal occurring at the surface, more moisture-retentive media promoted substrate delivery and micro-anoxia at depth, supporting co-occurring nitrification and denitrification along the column and thereby leading to more effective TN removal. Consistent with the multivariate pattern, the RDA biplot (Figure 6.3) placed deeper Column 2 samples in the direction of higher WFPS and NH_4^+-N. In practical terms, samples projecting farther along the NH_4^+-N and WFPS arrows correspond to the zones where carry-over of NH_4^+–N and micro-anoxia at depth are most likely, matching the more uniform nitrification markers in Column 2 and its higher TN removal.

6.5 Conclusions

Hydrogeological properties are a first-order control on how STUs partition carbon removal, nitrogen pathways, and microbiome structure. By operating two sand columns under identical synthetic STE loadings but with contrasting moisture-retention behaviour, we showed that media properties governing water-filled porosity and gas exchange fundamentally restructure both community composition and functional potential. The coarser, freely draining sand favoured oxygen penetration. In contrast, the finer, moisture-retentive sand in Column 2 developed elevated WFPS, which restricted gas exchange. These moisture-driven differences in redox provide the physical template on which the distinct microbial community and functional patterns emerge.

The finer, moisture-retentive sand sustained substantially higher ASV richness and evenness at depth, while the coarser sand rapidly lost richness with depth. Complementary beta-diversity patterns confirmed that communities were relatively similar at the surface across columns, but differences emerged and intensified with depth.

Surface communities in both columns were dominated by Proteobacteria and Actinobacteria, including *Zoogloea*, *Pseudarthrobacter*, and *Rhodococcus*, taxa associated with aerobic or chemoorganotrophic carbon degradation, which likely governed early COD removal. In the moisture-retentive sand, richer enrichment of *Zoogloea* at the surface likely enhanced EPS-rich biofilm development, intensifying oxygen diffusion limitation and favoring localized anoxia, consistent with stronger denitrification potential and improved TN removal. With depth, increased

representation of Chloroflexi, particularly in the finer sand, reflects selection for organisms adapted to low energy micro-oxic to anoxic conditions.

These taxonomic signals are mirrored by clear functional contrasts that reinforce the moisture-driven redox framework. Depth-resolved community profiles and PICRUSt2-inferred functional markers suggested that the coarser sand behaved as a shallow nitrifying filter with strong surface enrichment of nitrification markers, rapid surface COD removal, limited substrate transfer to depth, partial surface denitrification, and a NO_3^--N-rich effluent with only modest TN removal. In contrast, the finer, moisture-retentive sand slowed surface substrate degradation and nitrification, allowing COD and NH_4^+-N to be displaced to deeper, more reduced zones. This redistribution supported co-occurring nitrification and denitrification along the column, yielding slightly lower overall COD removal (still >90%) but nearly doubling average TN removal.

These findings support a coherent mechanistic framework in which moisture-retentive media transform STUs from thin aerobic filters into vertically extended bioreactors with more efficient TN attenuation. For onsite system design and regulation, media selection should explicitly target controlled moisture retention and depth-integrated redox stratification rather than maximizing drainage alone. Moderately more retentive sands that avoid full-profile saturation can enhance nitrogen removal and reduce NO_3^--N loading to groundwater while maintaining acceptable organic matter removal, offering a practical, mechanism-based lever to improve decentralized wastewater treatment performance. Field-scale validation and direct process-rate measurements should be addressed in future studies, but the hydraulic-microbial linkages resolved here provide actionable guidance for next-generation STU design criteria.

6.6 Declaration of generative AI use

During the preparation of this work the authors used ChatGPT to generate code in R. After using this tool, the authors reviewed and edited the content as needed and take full responsibility for the content of the article.

6.7 Acknowledgement

The authors thank Polytechnique Montreal technician Gabriel St-Jean for constructing the experimental setup. We would also like to thank Shayma Karray for her help in soil DNA extraction. This project was funded by the National Science and Engineering Research Council of

Canada (grant number RGPIN-2021-02934) and the Canada Research Chair in Decentralized and Small-Scale Water Treatment (grant 950-232871). Sorour Sheibani was supported by Quebec Research Fund - Nature and Technologies (FRQNT) doctoral awards (B2X).

CHAPTER 7 GENERAL DISCUSSION

7.1 Traditional controls on soil treatment units' performance

As discussed in section 2.1, conventional design and regulatory frameworks for STUs are primarily rooted in hydraulic considerations. Adequate unsaturated depth is typically treated as the central criterion for system approval, with the underlying assumption that sufficient aeration will ensure effective treatment. This assumption was explicitly tested in the first manuscript, where site visits and numerical modelling showed borrow-sand-based STUs in Abitibi-Témiscamingue met hydraulic expectations and showed no evidence of hydraulic failure, even under impermeable clay-belt settings. However, despite satisfactory hydraulic behaviour, substantial P discharges to receiving ditches were observed, demonstrating that hydraulic compliance alone does not guarantee environmental protection.

Nutrient removal has historically not been a primary design objective for conventional STUs. In many jurisdictions, explicit performance criteria for P and N are absent, and these systems are implicitly assumed to provide adequate nutrient attenuation as a by-product of infiltration through soil. The results of this thesis challenge that assumption by showing that nutrient fate is governed by mechanisms that are only weakly constrained by traditional hydraulic metrics.

7.2 Controls on phosphorus attenuation in soil treatment units: Apparent versus secure retention

Phosphorus retention, in particular, is fundamentally controlled by geochemical interactions between effluent P and the soil matrix. When stable precipitation reactions occur and P is incorporated into stable precipitates, sustainable long-term P removal may be achieved. However, such processes do not always play a role. In fact, when such processes are absent or even limited, P is retained primarily through reversible sorption and can ultimately be discharged to receiving waters, as observed in the field study presented in Chapter 3. These findings underscore the importance of characterizing P sorption capacity and stability prior to system installation in order to assess expected system lifespan and downstream risk.

The column study presented in Chapter 4 further demonstrated that even retained P can be highly reversible. Phosphorus was shown to be stored in loosely bound pools and therefore susceptible to remobilization under changing hydraulic or chemical conditions, even before sorption capacity was fully exhausted. This finding is particularly relevant in the context of climate-driven increases in extreme rainfall events, which can induce transient saturation, alter redox conditions, and promote P release. Together, the field and laboratory results indicate that apparent P removal should not be equated with secure long-term retention.

Sorption batch tests remain widely used because they are inexpensive and simple, but the results of this thesis show that they must be interpreted carefully. As demonstrated in Chapter 4, batch tests conducted on virgin sand can underestimate effective short-term P retention when biofilm development creates additional binding sites. However, this underestimation is conditional. When secondary-treated effluent with low organic carbon enters the STU, as in the systems studied in Chapter 3, biofilm growth is limited and batch tests are considered to provide a reasonable approximation of P retention behavior. In contrast, when septic tank effluent enters the STU directly, higher organic carbon loading stimulates biofilm growth and extracellular polymeric substance production, temporarily enhancing P retention beyond what batch tests predict.

Importantly, this biofilm-mediated retention does not necessarily translate into long-term stability. This distinction between apparent removal and secure removal provides a unifying explanation for the wide range of P removal efficiencies reported in the literature and reconciles apparently contradictory findings. Studies reporting rapid P breakthrough and those documenting decades-long retention are not mutually exclusive; rather, they reflect differences in media composition and dominant retention mechanisms.

7.3 Moisture-driven redox as a design variable for nitrogen removal

Nitrogen removal in STUs depends on a sequence of microbially mediated transformations that require the coexistence of oxic and anoxic conditions. Despite this, most design guidelines implicitly favor maximally aerated soils and treat moisture content as a secondary or even undesirable condition. The results presented in Chapters 5 and 6 demonstrate that this approach is incomplete and, in some cases, counterproductive.

Moisture retention emerged as a first-order control on redox structure and consequently oxic/anoxic reaction kinetics. In Chapter 5, soils with similar total porosity but different pore-size distributions developed markedly different water-filled pore space profiles. These differences persisted even under identical hydraulic loading and separation distances, highlighting the role of capillary forces in shaping moisture distribution. In regions with shallow groundwater or fine-textured soils, capillary rise can further increase water-filled pore space. Moreover, climate-driven changes in precipitation patterns, as discussed in Chapter 3, can deeply alter moisture distribution patterns within STUs.

In general, hydraulic compliance and oxygen availability do not equate to nitrogen protection. As shown in chapters 5 and 6, in highly aerated, freely draining media, rapid nitrification occurs near the infiltrative surface, but the lack of sustained anoxic zones and available carbon limits subsequent denitrification. This leads to nitrate-rich effluent, a pattern commonly observed in conventional systems and sometimes misinterpreted as successful treatment. The column experiments showed that deep denitrification might occur with controlled moisture retention that limits oxygen diffusion and redistributes substrates to depth.

The microbial analyses in Chapter 6 provided a mechanistic explanation for these observations. Moisture-retentive conditions supported a more spatially distributed and functionally diverse microbial community, with nitrification and denitrification potentials co-occurring across depth. In contrast, the freely draining column exhibited strong surface nitrification and limited denitrification potential at depth. These findings indicate that nitrogen removal in STUs is not primarily limited by reaction rates or microbial presence, but by the spatial alignment of redox conditions imposed by soil hydraulic properties.

7.4 The dual role of biofilm: hydraulic risk and biogeochemical opportunity for better nutrient removal

Biofilm development is traditionally viewed as a hydraulic liability in STUs, as it reduces permeability and can lead to surface ponding or breakout. While this risk is real and must be managed, the results of this thesis demonstrate that biofilm growth also plays a critical biogeochemical role that can enhance treatment performance when properly constrained.

Advanced secondary treatment systems, such as those examined in Chapter 3, discharge effluent with low organic carbon concentrations, resulting in limited biofilm development in downstream STUs. While this minimizes hydraulic risk, it also restricts opportunities for biofilm-mediated nutrient processing. In contrast, when septic tank effluent enters the STU directly, as in the column studies, biofilm growth increases near the infiltrative surface.

As shown in Chapter 4, this biofilm can temporarily enhance P retention by increasing sorption and sites. More importantly, Chapters 5 and 6 demonstrated that biofilm-induced reductions in permeability slow carbon oxidation and promote substrate transport to deeper zones, supporting a more active and diverse microbial community capable of enhanced nitrogen removal. Provided that sufficient unsaturated depth is maintained, effluent organic carbon concentrations can remain within acceptable limits while achieving substantially greater total nitrogen attenuation.

These findings point to an inherent trade-off. Complete suppression of biofilm growth may reduce hydraulic risk but can compromise biogeochemical performance, whereas uncontrolled biofilm accumulation can lead to system failure. This thesis suggests that limited, managed biofilm development represents a low-cost and sustainable pathway toward improved nutrient removal in onsite systems. Within this context, the absence of surface flooding is an insufficient performance metric.

7.5 Methodological considerations and implications for system design

The conclusions of this thesis are strengthened by the integration of multiple methodological approaches. Field surveys captured real-world system behavior and revealed discrepancies between hydraulic performance and nutrient outcomes. Controlled column experiments isolated specific processes and allowed direct manipulation of soil texture, biofilm growth and moisture regimes. Reactive transport modeling provided a framework for linking laboratory observations to long-term system behavior, while predictive metagenomics offered functional insight into microbial responses that cannot be resolved through chemistry alone.

Each method has intrinsic limitations. Field studies are constrained by site variability, laboratory experiments simplify complex systems, models rely on parameterization, and predictive metagenomics infers function rather than measuring activity directly. However, the convergence

of these independent approaches on the same controlling mechanisms, helps us better characterize the interacting hydraulic, geochemical, and microbial factors that govern nutrient fate in soil treatment units.

Taken together, the findings of this thesis suggest that future design and regulation of STUs must move beyond a narrow focus on infiltration capacity, and separation distances, and visible surface failures. Incorporating soil moisture retention characteristics, redox stability, and long-term nutrient fate into performance assessments is essential for protecting receiving waters.

CHAPTER 8 CONCLUSION AND RECOMMENDATIONS

8.1 Conclusions

The first manuscript (Chapter 3) evaluated the hydraulic behavior and P attenuation performance of borrow-sand-based STUs installed in impermeable clay-belt settings in Abitibi-Témiscamingue. Field inspections and numerical modelling showed that most systems met hydraulic expectations and exhibited no surface failure, even under challenging hydrogeological conditions. However, effluent monitoring revealed that many of these hydraulically compliant systems discharged substantial P loads to roadside ditches and surface waters. Laboratory sorption tests and reactive transport modeling demonstrated that the borrow sands used in these systems (with current media adsorption capacity, hydraulic loading rates, and design dimensions) had limited P retention capacity and that this capacity could be exhausted within relatively short timeframes. Together, these results showed that hydraulic functionality does not guarantee nutrient protection and highlighted the need to explicitly consider P retention capacity and longevity when designing and approving STUs in impermeable settings.

The second manuscript (Chapter 4) focused on P retention mechanisms within the biologically active clogging zone of sand filters receiving septic tank effluent. Column experiments combined with sequential P extraction revealed that P retention is dominated by adsorption and biofilm development can temporarily enhance P retention by creating additional binding sites. However, the retained P was shown to be largely reversible, residing in loosely bound pools that remained vulnerable to remobilization. This work demonstrated that biofilm-mediated P retention can extend short-term removal but does not necessarily provide long-term security. The results emphasized the importance of distinguishing between apparent P removal and stable retention when assessing filter performance and lifespan.

The third manuscript (Chapter 5) examined how soil texture and moisture retention influence oxygen availability, organic carbon degradation, and nitrogen transformations in STUs. Using two 1-m soil columns with contrasting hydraulic properties but similar total porosity, the study showed that moisture retention exerted a first-order control on redox structure, and nitrogen and carbon removal pathways. Freely draining media promoted efficient nitrification but resulted in nitrate-rich effluent and limited total nitrogen removal. In contrast, moisture-retentive media supported coupled nitrification and denitrification along the soil profile, leading to substantially higher total

nitrogen removal despite lower dissolved oxygen concentrations. These findings demonstrated that nitrogen attenuation in STUs is governed by moisture-driven redox architecture rather than by aeration alone.

The fourth manuscript (Chapter 6) added a microbial and functional dimension to the hydrogeochemical framework by characterizing depth-resolved bacterial communities and predicted metabolic pathways in the experimental soil columns. The results suggested that differences in moisture retention and associated redox conditions influence the spatial organization of microbial communities and the distribution of functional genes involved in carbon and nitrogen cycling. Moisture-retentive conditions supported more diverse and vertically distributed microbial communities, with functional potential indicative of enhanced nitrogen transformation processes, whereas freely draining conditions resulted in surface-dominated communities with reduced functional diversity at depth. The findings also confirmed that moisture-driven variations in biofilm development alter the relative representation of nitrification- and denitrification-related pathways along the soil profile. Collectively, these results provided biological support for the observed differences in nitrogen removal performance and demonstrated how soil moisture regimes shape microbial structure and function in STUs.

Collectively, the four manuscripts demonstrate that nutrient attenuation in STUs cannot be reliably inferred from hydraulic performance alone. Phosphorus retention depends on the stability of geochemical binding mechanisms, while nitrogen removal is controlled by moisture-driven redox structure and microbial activity. Biofilm development plays a dual role, representing both a hydraulic risk and a biogeochemical opportunity. Together, these findings highlight the need for design and regulatory approaches that explicitly account for long-term nutrient fate rather than relying solely on short-term hydraulic criteria. By demonstrating how hydraulic, geochemical, and microbial processes interact to control nutrient fate, this thesis contributes to a more mechanistic understanding of STU performance and provides a foundation for improving the sustainability of onsite wastewater treatment systems.

8.2 Future research directions

The findings of this thesis point to several important subjects for future research:

1. Long-term field monitoring of phosphorus stability

Extended monitoring of P retention and remobilization under dynamic hydraulic conditions, including extreme rainfall and seasonal water-table fluctuations, is needed to better assess long-term environmental risk.

2. Integration of moisture retention into STU design criteria

Future studies should develop design-oriented metrics that explicitly incorporate soil water retention properties and redox stability, rather than relying solely on saturated hydraulic conductivity or percolation tests.

3. Quantification of biofilm dynamics and thresholds

Research is needed to identify thresholds at which biofilm development shifts from beneficial to detrimental, particularly with respect to hydraulic performance versus nutrient removal.

4. Direct measurement of microbial activity

While predictive metagenomics provided valuable insight into functional potential, future work should incorporate direct measurements to directly link microbial activity with nutrient transformations.

5. Influence of influent chemical variability on biofilm and nutrient removal

Future research should examine how fluctuations in influent chemical properties (e.g., pH, C/N ratio, alkalinity) influence biofilm development and phosphorus and nitrogen removal in STUs, to better assess system resilience under realistic operating conditions.

6. Climate-change-driven impacts on STU performance

The influence of altered precipitation patterns, increased frequency of extreme events, and changing groundwater levels on nutrient fate in STUs warrants targeted investigation.

REFERENCES

Al- Fawzy, A. M., & Al- Mohammed, F. M. (2019). Dissipation of Energy of Flow by Conventional Type of Gabion Weir. *IOP Conference Series: Materials Science and Engineering*, *584*(1), 012038. https://doi.org/10.1088/1757-899X/584/1/012038

Amador, J. A., & Atoyan, J. A. (2012). Structure and Composition of Leachfield Bacterial Communities: Role of Soil Texture, Depth and Septic Tank Effluent Inputs. *Water*, *4*(3), 707–719. https://doi.org/10.3390/w4030707

Anderson, M. J. (2017). Permutational Multivariate Analysis of Variance. In *Wiley StatsRef: Statistics Reference Online* (pp. 1–15). Wiley. https://doi.org/10.1002/9781118445112.stat07841

Arias, C. A., Del Bubba, M., & Brix, H. (2001). Phosphorus removal by sands for use as media in subsurface flow constructed reed beds. *Water Research*, *35*(5), 1159–1168. https://doi.org/10.1016/S0043-1354(00)00368-7

ASTM International. (2016). *ASTM D4646-16, Standard Test Method for 24-h Batch-Type Measurement of Contaminant Sorption by Soils and Sediments*. https://doi.org/10.1520/D4646-03R08

ASTM International. (2020). *ASTM C136M, Standard Test Method for Sieve Analysis of Fine and Coarse Aggregates*.

ASTM International. (2022a). *Test Method for Permeability of Granular Soils (Constant Head)*. ASTM International. https://doi.org/10.1520/D2434-22

ASTM International. (2022b). *Test Method for Relative Density (Specific Gravity) and Absorption of Fine Aggregate*. ASTM International. https://doi.org/10.1520/C0128-22

ASTM International. (2023). *Test Method for Bulk Density (Unit Weight) and Voids in Aggregate*. ASTM International. https://doi.org/10.1520/C0029_C0029M-23

Atoyan, J., Staroscik, A., Nelson, D., Patenaude, E., Potts, D., & Amador, J. (2013). Microbial Community Structure of a Leachfield Soil: Response to Intermittent Aeration and Tetracycline Addition. *Water*, *5*(2), 505–524. https://doi.org/10.3390/w5020505

Bai, J., Ye, X., Jia, J., Zhang, G., Zhao, Q., Cui, B., & Liu, X. (2017). Phosphorus sorption-desorption and effects of temperature, pH and salinity on phosphorus sorption in marsh soils from coastal wetlands with different flooding conditions. *Chemosphere*, *188*, 677–688. https://doi.org/10.1016/j.chemosphere.2017.08.117

Banu, R. J., Do, K. U., & Yeom, I. T. (2008). Phosphorus removal in low alkalinity secondary effluent using alum. *International Journal of Environmental Science & Technology*, *5*, 93–98.

Barka, E. A., Vatsa, P., Sanchez, L., Gaveau-Vaillant, N., Jacquard, C., Klenk, H.-P., Clément, C., Ouhdouch, Y., & van Wezel, G. P. (2016). Taxonomy, Physiology, and Natural Products of Actinobacteria. *Microbiology and Molecular Biology Reviews*, *80*(1), 1–43. https://doi.org/10.1128/MMBR.00019-15

Beal, C. D., Gardner, E. A., Kirchhof, G., & Menzies, N. W. (2006). Long-term flow rates and biomat zone hydrology in soil columns receiving septic tank effluent. *Water Research*, *40*(12), 2327–2338. https://doi.org/10.1016/j.watres.2006.04.018

Beal, C. D., Gardner, E. A., & Menzies, N. W. (2005). Process, performance, and pollution potential: A review of septic tank - soil absorption systems. *Soil Research*, *43*(7), 781. https://doi.org/10.1071/SR05018

Beggs, R. A., Hills, D. J., Tchobanoglous, G., & Hopmans, J. W. (2011). Fate of nitrogen for subsurface drip dispersal of effluent from small wastewater systems. *Journal of Contaminant Hydrology*, *126*(1–2), 19–28. https://doi.org/10.1016/j.jconhyd.2011.05.007

Benson, C. H., Chiang, I., Chalermyanont, T., & Sawangsuriya, A. (2014). Estimating van Genuchten Parameters α and n for Clean Sands from Particle Size Distribution Data. *From Soil Behavior Fundamentals to Innovations in Geotechnical Engineering*, 410–427. https://doi.org/10.1061/9780784413265.033

Berlin, M., Kumar, G. S., & Nambi, I. M. (2014). Numerical Modeling on the Effect of Dissolved Oxygen on Nitrogen Transformation and Transport in Unsaturated Porous System. *Environmental Modeling & Assessment*, *19*(4), 283–299. https://doi.org/10.1007/s10666-014-9399-1

Berlin, M., Suresh Kumar, G., & Nambi, I. M. (2015). Numerical modeling of biological clogging on transport of nitrate in an unsaturated porous media. *Environmental Earth Sciences*, *73*(7), 3285–3298. https://doi.org/10.1007/s12665-014-3612-z

Blakney, A. J. C., Morvan, S., Lucotte, M., Moingt, M., Charbonneau, A., Bipfubusa, M., Gonzalez, E., & Pitre, F. E. (2024). Site properties, environmental factors, and crop identify influence soil bacterial communities more than municipal biosolid application. *Science of The Total Environment*, *926*, 171854. https://doi.org/10.1016/j.scitotenv.2024.171854

Bowes, M. J., Neal, C., Jarvie, H. P., Smith, J. T., & Davies, H. N. (2010). Predicting phosphorus concentrations in British rivers resulting from the introduction of improved phosphorus removal from sewage effluent. *Science of The Total Environment*, *408*(19), 4239–4250. https://doi.org/10.1016/j.scitotenv.2010.05.016

Brady, N. C., & Ray, R. W. (2002). *The nature and properties of soils* (14th ed.). Prentice Hall Inc.

Brovelli, A., Malaguerra, F., & Barry, D. A. (2009). Bioclogging in porous media: Model development and sensitivity to initial conditions. *Environmental Modelling & Software*, *24*(5), 611–626. https://doi.org/10.1016/j.envsoft.2008.10.001

Busse, H.-J. (2016). Review of the taxonomy of the genus Arthrobacter, emendation of the genus Arthrobacter sensu lato, proposal to reclassify selected species of the genus Arthrobacter in the novel genera Glutamicibacter gen. nov., Paeniglutamicibacter gen. nov., Pseudoglutamicibacter gen. nov., Paenarthrobacter gen. nov. and Pseudarthrobacter gen. nov., and emended description of Arthrobacter roseus. *International Journal of Systematic and Evolutionary Microbiology*, *66*(1), 9–37. https://doi.org/10.1099/ijsem.0.000702

Callahan. (2018). *Silva taxonomic training data formatted for DADA2 (Silva version 132)*. Zendo.

Callahan, B. J., McMurdie, P. J., Rosen, M. J., Han, A. W., Johnson, A. J. A., & Holmes, S. P. (2016). DADA2: High-resolution sample inference from Illumina amplicon data. *Nature Methods*, *13*(7), 581–583. https://doi.org/10.1038/nmeth.3869

Canter, L. W., & Knox, R. C. (2017). *Septic Tank System Effects on Ground Water Quality*. Routledge. https://doi.org/10.1201/9780203739877

Chambers, P. A., McGoldrick, D. J., Brua, R. B., Vis, C., Culp, J. M., & Benoy, G. A. (2012). Development of Environmental Thresholds for Nitrogen and Phosphorus in Streams. *Journal of Environmental Quality*, *41*(1), 7–20. https://doi.org/10.2134/jeq2010.0273

Chapuis, R. P. (2009). Numerical modeling of reservoirs or pipes in groundwater seepage. *Computers and Geotechnics*, *36*(5), 895–901. https://doi.org/10.1016/j.compgeo.2009.01.005

Chen, S., Dougherty, M., Chen, Z., Zuo, X., & He, J. (2021). Managing biofilm growth and clogging to promote sustainability in an intermittent sand filter (ISF). *Science of The Total Environment*, *755*, 142477. https://doi.org/10.1016/j.scitotenv.2020.142477

Chen, Y., Huang, L., & Li, X. (2021). Quantifying the biofilm effects on phosphorus adsorption of sediment. *Journal of Soils and Sediments*, *21*(2), 1302–1316. https://doi.org/10.1007/s11368-020-02851-5

Chui, T. F. M., & Freyberg, D. L. (2007). The use of COMSOL for integrated hydrological modeling. *In Proceedings of the COMSOL Conference* .

Cloutier, V., Blanchette, D., Dallaire, P. L., Nadeau, S., Rosa, É., & Roy, M. (2013). *Projet d'acquisition de connaissances sur les eaux souterraines de l'Abitibi-Témiscamingue (partie 1)*.

Cloutier, V., Rosa, É., Nadeau, S., Dallaire, P. L., Blanchette, D., & Roy, M. (2015). *Projet d'acquisition de connaissances sur les eaux souterraines de l'Abitibi-Témiscamingue (partie 2)*.

Cloutier, V., Rosa, E., Roy, M., Nadeau, S., Blanchette, D., Dallaire, P. L., Derrien, G., & Veillette, J. J. (2016). *Atlas hydrogéologique de l'Abitibi-Témiscamingue*. Presses de l'Université du Québec.

COMSOL. (2019). *COMSOL Multiphysics Reference Manual, version 5.5*.

Converse, J. C., & Tyler, E. J. ,. (1986). Wisconsin mound performance. *Small Scale Waste Management Project*, *345*.

Criado Monleon, A. J., Knappe, J., Somlai, C., Betancourth, C. O., Ali, M., Curtis, T. P., & Gill, L. W. (2022). Spatial Variation of the Microbial Community Structure of On-Site Soil

Treatment Units in a Temperate Climate, and the Role of Pre-treatment of Domestic Effluent in the Development of the Biomat Community. *Frontiers in Microbiology*, *13*. https://doi.org/10.3389/fmicb.2022.915856

Cucarella, V., & Renman, G. (2009). Phosphorus Sorption Capacity of Filter Materials Used for On-site Wastewater Treatment Determined in Batch Experiments-A Comparative Study. *Journal of Environmental Quality*, *38*(2), 381–392. https://doi.org/10.2134/jeq2008.0192

Daims, H., Lücker, S., & Wagner, M. (2016). A New Perspective on Microbes Formerly Known as Nitrite-Oxidizing Bacteria. *Trends in Microbiology*, *24*(9), 699–712. https://doi.org/10.1016/j.tim.2016.05.004

Dalahmeh, S. S., Stenström, Y., Jebrane, M., Hylander, L. D., Daniel, G., & Heinmaa, I. (2020). Efficiency of Iron- and Calcium-Impregnated Biochar in Adsorbing Phosphate From Wastewater in Onsite Wastewater Treatment Systems. *Frontiers in Environmental Science*, *8*. https://doi.org/10.3389/fenvs.2020.538539

De, M., & Toor, G. S. (2015). Fate of Effluent-Borne Nitrogen in the Mounded Drainfield of an Onsite Wastewater Treatment System. *Vadose Zone Journal*, *14*(12), 1–12. https://doi.org/10.2136/vzj2015.07.0096

Del Bubba, M., Arias, C. A., & Brix, H. (2003). Phosphorus adsorption maximum of sands for use as media in subsurface flow constructed reed beds as measured by the Langmuir isotherm. *Water Research*, *37*(14), 3390–3400. https://doi.org/10.1016/S0043-1354(03)00231-8

Douglas, G. M., Maffei, V. J., Zaneveld, J. R., Yurgel, S. N., Brown, J. R., Taylor, C. M., Huttenhower, C., & Langille, M. G. I. (2020). PICRUSt2 for prediction of metagenome functions. *Nature Biotechnology*, *38*(6), 685–688. https://doi.org/10.1038/s41587-020-0548-6

Dragone, N. B., Hoffert, M., Strickland, M. S., & Fierer, N. (2024). Taxonomic and genomic attributes of oligotrophic soil bacteria. *ISME Communications*, *4*(1). https://doi.org/10.1093/ismeco/ycae081

Dugan, P. R., Stoner, D. L., & Pickrum, H. M. (1992). The Genus Zoogloea. In *The Prokaryotes* (pp. 3952–3964). Springer New York. https://doi.org/10.1007/978-1-4757-2191-1_58

Edwards, A. C., & Withers, P. J. A. (2008). Transport and delivery of suspended solids, nitrogen and phosphorus from various sources to freshwaters in the UK. *Journal of Hydrology*, *350*(3–4), 144–153. https://doi.org/10.1016/j.jhydrol.2007.10.053

Eikelboom, D. H. (1975). Filamentous organisms observed in activated sludge. *Water Research*, *9*(4), 365–388. https://doi.org/10.1016/0043-1354(75)90182-7

Essandoh, H. M. K., Tizaoui, C., & Mohamed, M. H. A. (2013). Removal of dissolved organic carbon and nitrogen during simulated soil aquifer treatment. *Water Research*, *47*(11), 3559–3572. https://doi.org/10.1016/j.watres.2013.04.013

Eveborn, D., Gustafsson, J. P., Elmefors, E., Yu, L., Eriksson, A.-K., Ljung, E., & Renman, G. (2014). Phosphorus in soil treatment systems: Accumulation and mobility. *Water Research*, *64*, 42–52. https://doi.org/10.1016/j.watres.2014.06.034

Eveborn, D., Kong, D., & Gustafsson, J. P. (2012). Wastewater treatment by soil infiltration: Long-term phosphorus removal. *Journal of Contaminant Hydrology*, *140–141*, 24–33. https://doi.org/10.1016/j.jconhyd.2012.08.003

Fernández-Baca, C. P., Omar, A.-E. H., Pollard, J. T., & Richardson, R. E. (2019). Microbial communities controlling methane and nutrient cycling in leach field soils. *Water Research*, *151*, 456–467. https://doi.org/10.1016/j.watres.2018.12.036

Fernández-Baca, C. P., Truhlar, A. M., Omar, A.-E. H., Rahm, B. G., Walter, M. T., & Richardson, R. E. (2018). Methane and nitrous oxide cycling microbial communities in soils above septic leach fields: Abundances with depth and correlations with net surface emissions. *Science of The Total Environment*, *640–641*, 429–441. https://doi.org/10.1016/j.scitotenv.2018.05.303

Friedman, L., Mamane, H., Avisar, D., & Chandran, K. (2018). The role of influent organic carbon-to-nitrogen (COD/N) ratio in removal rates and shaping microbial ecology in soil aquifer treatment (SAT). *Water Research*, *146*, 197–205. https://doi.org/10.1016/j.watres.2018.09.014

Gao, Q., Blum, K. M., Gago-Ferrero, P., Wiberg, K., Ahrens, L., & Andersson, P. L. (2019). Impact of on-site wastewater infiltration systems on organic contaminants in groundwater

and recipient waters. *Science of The Total Environment*, *651*, 1670–1679. https://doi.org/10.1016/j.scitotenv.2018.10.016

Garcia, S. N., Clubbs, R. L., Stanley, J. K., Scheffe, B., Yelderman, J. C., & Brooks, B. W. (2013). Comparative analysis of effluent water quality from a municipal treatment plant and two on-site wastewater treatment systems. *Chemosphere*, *92*(1), 38–44. https://doi.org/10.1016/j.chemosphere.2013.03.007

García-Gaines, R. A., & Frankenstein, S. (2015). *USCS and the USDA soil classification system: Development of a mapping scheme*.

Gharoon, N., & Pagilla, K. R. (2021). Critical review of effluent dissolved organic nitrogen removal by soil/aquifer-based treatment systems. *Chemosphere*, *269*, 129406. https://doi.org/10.1016/j.chemosphere.2020.129406

Gilbride, K. A., Lee, D.-Y., & Beaudette, L. A. (2006). Molecular techniques in wastewater: Understanding microbial communities, detecting pathogens, and real-time process control. *Journal of Microbiological Methods*, *66*(1), 1–20. https://doi.org/10.1016/j.mimet.2006.02.016

Gill, L. W., O'Luanaigh, N., Johnston, P. M., Misstear, B. D. R., & O'Suilleabhain, C. (2009). Nutrient loading on subsoils from on-site wastewater effluent, comparing septic tank and secondary treatment systems. *Water Research*, *43*(10), 2739–2749. https://doi.org/10.1016/j.watres.2009.03.024

Gill, L. W., O'Súlleabháin, C., Misstear, B. D. R., & Johnston, P. J. (2007). The Treatment Performance of Different Subsoils in Ireland Receiving On-Site Wastewater Effluent. *Journal of Environmental Quality*, *36*(6), 1843–1855. https://doi.org/10.2134/jeq2007.0064

Gillham, R. W. (1984). The capillary fringe and its effect on water-table response. *Journal of Hydrology*, *67*(1–4), 307–324. https://doi.org/10.1016/0022-1694(84)90248-8

Gloor, G. B., Macklaim, J. M., Pawlowsky-Glahn, V., & Egozcue, J. J. (2017). Microbiome Datasets Are Compositional: And This Is Not Optional. *Frontiers in Microbiology*, *8*. https://doi.org/10.3389/fmicb.2017.02224

Government of Canada. (2001). *About your house, your septic system*. Canada Mortgage and Housing Corporation. https://publications.gc.ca/collections/collection_2011/schl-cmhc/nh18-24/NH18-24-34-2008-eng.pdf

Government of Canada. (2012). *Wastewater Systems Effluent Regulations (SOR/2012-139)*. https://laws-lois.justice.gc.ca/eng/regulations/SOR-2012-139/

Government of Canada. (2013). *Water sources: groundwater*. https://www.canada.ca/en/environment-climate-change/services/water-overview/sources/groundwater.htm

Gurpal, S. T., Mary, L., & Tom, O. (2020). Onsite Sewage treatment and Disposal systems : An Overview. Https://Edis.Ifas.Ufl.Edu/Publication/SS549.

Hamisi, R., Renman, A., Renman, G., Wörman, A., & Thunvik, R. (2022). Long-term phosphorus sorption and leaching in sand filters for onsite treatment systems. *Science of The Total Environment*, *833*, 155254. https://doi.org/10.1016/j.scitotenv.2022.155254

Hamisi, R., Renman, G., Renman, A., & Wörman, A. (2019). Modelling Phosphorus Sorption Kinetics and the Longevity of Reactive Filter Materials Used for On-Site Wastewater Treatment. *Water*, *11*(4), 811. https://doi.org/10.3390/w11040811

Havard, P., Jamieson, R., Cudmore, D., Boutilier, L., & Gordon, R. (2008). Performance and Hydraulics of Lateral Flow Sand Filters for On-Site Wastewater Treatment. *Journal of Hydrologic Engineering*, *13*(8), 720–728. https://doi.org/10.1061/(ASCE)1084-0699(2008)13:8(720)

Hayatsu, M., & Kosuge, N. (1993). Autotrophic nitrification in acid tea soils. *Soil Science and Plant Nutrition*, *39*(2), 209–217. https://doi.org/10.1080/00380768.1993.10416992

He, J., Dougherty, M., & Chen, Z. (2021). Numerical assessment of a soil moisture controlled wastewater SDI disposal system in Alabama Black Belt Prairie. *Chemosphere*, *263*, 128210. https://doi.org/10.1016/j.chemosphere.2020.128210

Heatwole, K. K., & McCray, J. E. (2007). Modeling potential vadose-zone transport of nitrogen from onsite wastewater systems at the development scale. *Journal of Contaminant Hydrology*, *91*(1–2), 184–201. https://doi.org/10.1016/j.jconhyd.2006.08.012

Hedley, M. J., Stewart, J. W. B., & Chauhan, B. S. (1982). Changes in Inorganic and Organic Soil Phosphorus Fractions Induced by Cultivation Practices and by Laboratory Incubations. *Soil Science Society of America Journal*, *46*(5), 970–976. https://doi.org/10.2136/sssaj1982.03615995004600050017x

Hodnett, M. G., & Tomasella, J. (2002). Marked differences between van Genuchten soil water-retention parameters for temperate and tropical soils: a new water-retention pedo-transfer functions developed for tropical soils. *Geoderma*, *108*(3–4), 155–180. https://doi.org/10.1016/S0016-7061(02)00105-2

Hug, L. A., Castelle, C. J., Wrighton, K. C., Thomas, B. C., Sharon, I., Frischkorn, K. R., Williams, K. H., Tringe, S. G., & Banfield, J. F. (2013). Community genomic analyses constrain the distribution of metabolic traits across the Chloroflexi phylum and indicate roles in sediment carbon cycling. *Microbiome*, *1*(1), 22. https://doi.org/10.1186/2049-2618-1-22

Humphrey, C. P., O'Driscoll, M., & Iverson, G. (2021). Comparison of Nitrogen Treatment by Four Onsite Wastewater Systems in Nutrient-Sensitive Watersheds of the North Carolina Coastal Plain. *Nitrogen*, *2*(2), 268–286. https://doi.org/10.3390/nitrogen2020018

Ibekwe, A. M., Gonzalez-Rubio, A., & Suarez, D. L. (2018). Impact of treated wastewater for irrigation on soil microbial communities. *Science of The Total Environment*, *622–623*, 1603–1610. https://doi.org/10.1016/j.scitotenv.2017.10.039

Intergovernmental Panel on Climate Change. (2021). *Climate Change 2021: The Physical Science Basis. Contribution of Working Group I to the Sixth Assessment Report of the Intergovernmental Panel on Climate Change (Chapter 11: Weather and Climate Extreme Events in a Changing Climate).*

Jalali, M., & Jalali, M. (2016). Relation between various soil phosphorus extraction methods and sorption parameters in calcareous soils with different texture. *Science of The Total Environment*, *566–567*, 1080–1093. https://doi.org/10.1016/j.scitotenv.2016.05.133

Johansson Westholm, L. (2006). Substrates for phosphorus removal—Potential benefits for on-site wastewater treatment? *Water Research*, *40*(1), 23–36. https://doi.org/10.1016/j.watres.2005.11.006

Judge, A. (2013). *Measurement of the hydraulic conductivity of gravels using a laboratory permeameter and silty sands using field testing with observation wells*. University of Massachusetts Amherst.

Kadlec, R. H., & Wallace, S. (2008). *Treatment Wetlands*. CRC Press. https://doi.org/10.1201/9781420012514

Kanehisa, M., Furumichi, M., Sato, Y., Kawashima, M., & Ishiguro-Watanabe, M. (2023). KEGG for taxonomy-based analysis of pathways and genomes. *Nucleic Acids Research*, *51*(D1), D587–D592. https://doi.org/10.1093/nar/gkac963

Kanmani, S., Gandhimathi, R., & Muthukkumaran, K. (2014). Bioclogging in porous media: influence in reduction of hydraulic conductivity and organic contaminants during synthetic leachate permeation. *Journal of Environmental Health Science and Engineering*, *12*(1), 126. https://doi.org/10.1186/s40201-014-0126-2

Khamehchiyan, M., Hossein Charkhabi, A., & Tajik, M. (2007). Effects of crude oil contamination on geotechnical properties of clayey and sandy soils. *Engineering Geology*, *89*(3–4), 220–229. https://doi.org/10.1016/j.enggeo.2006.10.009

Knappe, J., Somlai, C., Fowler, A. C., & Gill, L. W. (2020). The influence of pre-treatment on biomat development in soil treatment units. *Journal of Contaminant Hydrology*, *232*, 103654. https://doi.org/10.1016/j.jconhyd.2020.103654

L. Lahti, & S. Shetty. (2019). *microbiome R package*.

Labonté-Raymond, P.-L., Pabst, T., Bussière, B., & Bresson, É. (2020). Impact of climate change on extreme rainfall events and surface water management at mine waste storage facilities. *Journal of Hydrology*, *590*, 125383. https://doi.org/10.1016/j.jhydrol.2020.125383

Lai, D. Y. F., & Lam, K. C. (2009). Phosphorus sorption by sediments in a subtropical constructed wetland receiving stormwater runoff. *Ecological Engineering*, *35*(5), 735–743. https://doi.org/10.1016/j.ecoleng.2008.11.009

Lapointe, B. E., Herren, L. W., & Paule, A. L. (2017). Septic systems contribute to nutrient pollution and harmful algal blooms in the St. Lucie Estuary, Southeast Florida, USA. *Harmful Algae*, *70*, 1–22. https://doi.org/10.1016/j.hal.2017.09.005

Lee, M.-S., Lee, K.-K., Hyun, Y., Clement, T. P., & Hamilton, D. (2006). Nitrogen transformation and transport modeling in groundwater aquifers. *Ecological Modelling*, *192*(1–2), 143–159. https://doi.org/10.1016/j.ecolmodel.2005.07.013

LégisQuébec. (2022). *Règlement sur l'évacuation et le traitement des eaux usées des résidences isolées (RETEURI) [Regulation respecting the evacuation and treatment of wastewater from isolated dwellings]*.

Li, Y., Li, H., Xu, X., Xiao, S., Wang, S., & Xu, S. (2017). Fate of nitrogen in subsurface infiltration system for treating secondary effluent. *Water Science and Engineering*, *10*(3), 217–224. https://doi.org/10.1016/j.wse.2017.10.002

Liolios, K. A., Moutsopoulos, K. N., & Tsihrintzis, V. A. (2015). Numerical simulation of phosphorus removal in horizontal subsurface flow constructed wetlands. *Desalination and Water Treatment*, *56*(5), 1282–1290. https://doi.org/10.1080/19443994.2014.983550

Liss, S. N., & Allen, D. G. (1992). Microbiological study of a bleached kraft pulp mill aerated lagoon. *Journal of Pulp and Paper Science*, *18*(6).

Liu, C., Liu, F., Andersen, M. N., Wang, G., Wu, K., Zhao, Q., & Ye, Z. (2021). Domestic wastewater infiltration process in desert sandy soil and its irrigation prospect analysis. *Ecotoxicology and Environmental Safety*, *208*, 111419. https://doi.org/10.1016/j.ecoenv.2020.111419

Liu, J., & Davis, A. P. (2014). Phosphorus Speciation and Treatment Using Enhanced Phosphorus Removal Bioretention. *Environmental Science & Technology*, *48*(1), 607–614. https://doi.org/10.1021/es404022b

Lombardo, P. (2006). Phosphorus geochemistry in septic tanks, soil absorption systems, and groundwater. In *Phosphorus geochemistry Handbook*.

Lotfikatouli, S., Pan, Q., Wang, M., Russo, F. M., Gobler, C. J., & Mao, X. (2024). Effective nitrogen removal from onsite wastewater using a sequencing aerated biofilm reactor. *Journal of Water Process Engineering*, *60*, 105132. https://doi.org/10.1016/j.jwpe.2024.105132

Lowe, K. S. (2010). Influent Constituent Characteristics of the Modern Waste Stream from Single Sources. *Water Intelligence Online*, *9*. https://doi.org/10.2166/9781780403519

Luanmanee, S., Attanandana, T., Masunaga, T., & Wakatsuki, T. (2001). The efficiency of a multi-soil-layering system on domestic wastewater treatment during the ninth and tenth years of operation. *Ecological Engineering*, *18*(2), 185–199. https://doi.org/10.1016/S0925-8574(01)00077-5

Lusk, M. G., Toor, G. S., Yang, Y.-Y., Mechtensimer, S., De, M., & Obreza, T. A. (2017). A review of the fate and transport of nitrogen, phosphorus, pathogens, and trace organic chemicals in septic systems. *Critical Reviews in Environmental Science and Technology*, *47*(7), 455–541. https://doi.org/10.1080/10643389.2017.1327787

Lusk, M., Toor, G. S., & Obreza, T. (2011). Onsite Sewage Treatment and Disposal Systems: Phosphorus. *EDIS*, *2011*(8). https://doi.org/10.32473/edis-ss551-2011

Ly, D. K., & Chui, T. F. M. (2012). Modeling sewage leakage to surrounding groundwater and stormwater drains. *Water Science and Technology*, *66*(12), 2659–2665. https://doi.org/10.2166/wst.2012.496

MacQuarrie, K. T. B., Sudicky, E. A., & Robertson, W. D. (2001). Numerical simulation of a fine-grained denitrification layer for removing septic system nitrate from shallow groundwater. *Journal of Contaminant Hydrology*, *52*(1–4), 29–55. https://doi.org/10.1016/S0169-7722(01)00152-8

Maleki Shahraki, Z., Wang, M., Walker, H. W., Russo, F., Gobler, C., Heufelder, G., & Mao, X. (2021). A mechanistic understanding of the nitrification sand layer performance in a nitrogen removing biofilter (NRB) treating onsite wastewater. *Ecological Engineering*, *168*, 106271. https://doi.org/10.1016/j.ecoleng.2021.106271

Marafini, E., La Rocca, M., Fiori, A., Battiato, I., & Prestininzi, P. (2020). Suitability of 2D modelling to evaluate flow properties in 3D porous media. *Transport in Porous Media*, *134*(2), 315–329. https://doi.org/10.1007/s11242-020-01447-4

Martin, M. (2011). Cutadapt removes adapter sequences from high-throughput sequencing reads. *EMBnet.Journal*, *17*(1), 10. https://doi.org/10.14806/ej.17.1.200

McCray, J. E., Huntzinger, D. N., Van Cuyk, S., & Siegrist, R. (2000). Mathematical Modeling of Unsaturated Flow and Transport in Soil-based Wastewater Treatment Systems.

Proceedings of the Water Environment Federation, *2000*(12), 44–63. https://doi.org/10.2175/193864700784608667

McCray, J. E., Kirkland, S. L., Siegrist, R. L., & Thyne, G. D. (2005). Model Parameters for Simulating Fate and Transport of On-Site Wastewater Nutrients. *Ground Water*, *43*(4), 628–639. https://doi.org/10.1111/j.1745-6584.2005.0077.x

McKinley, J. W., & Siegrist, R. L. (2011). Soil Clogging Genesis in Soil Treatment Units Used for Onsite Wastewater Reclamation: A Review. *Critical Reviews in Environmental Science and Technology*, *41*(24), 2186–2209. https://doi.org/10.1080/10643389.2010.497445

McMurdie, P. J., & Holmes, S. (2013). phyloseq: An R Package for Reproducible Interactive Analysis and Graphics of Microbiome Census Data. *PLoS ONE*, *8*(4), e61217. https://doi.org/10.1371/journal.pone.0061217

McMurdie, P. J., & Holmes, S. (2014). Waste Not, Want Not: Why Rarefying Microbiome Data Is Inadmissible. *PLoS Computational Biology*, *10*(4), e1003531. https://doi.org/10.1371/journal.pcbi.1003531

Mechtensimer, S., & Toor, G. S. (2016). Fate, mass balance, and transport of phosphorus in the septic system drainfields. *Chemosphere*, *159*, 153–158. https://doi.org/10.1016/j.chemosphere.2016.05.084

Mechtensimer, S., & Toor, G. S. (2017). Septic Systems Contribution to Phosphorus in Shallow Groundwater: Field-Scale Studies Using Conventional Drainfield Designs. *PLOS ONE*, *12*(1), e0170304. https://doi.org/10.1371/journal.pone.0170304

Mekala, C., & Nambi, I. M. (2017). Understanding the hydrologic control of N cycle: Effect of water filled pore space on heterotrophic nitrification, denitrification and dissimilatory nitrate reduction to ammonium mechanisms in unsaturated soils. *Journal of Contaminant Hydrology*, *202*, 11–22. https://doi.org/10.1016/j.jconhyd.2017.04.005

MELCCFP. (2015). *Ministère de l'Environnement, de la Lutte contre les Changements Climatiques, de la Faune et des Parcs. Guide technique sur le traitement des eaux usées des résidences isolées (Partie B)*.

MELCCFP. (2017). *Ministère de l'Environnement, de la Lutte contre les changements climatiques, de la Faune et des Parcs, Guide pour l'étude des technologies conventionnelles de traitement des eaux usées d'origine domestique, chapitre 3*.

MELCCFP. (2019). *Ministère de l'Environnement, de la Lutte contre les changements climatiques du Québec, Centre d'Expertise en Analyse Environnementale du Québec, Détermination du Phosphore Total dans les Eaux Naturelles par Minéralisation au Persulfate : Méthode Colorimétrique Automatisée et Procédures Adaptées pour le Phosphore de Faible Concentration et à l'État de Trace*.

MENV. (2001). *Critères de qualité de l'eau de surface au Québec. Direction du suivi de l'état de l'environnement. Ministère de l'Environnement, Québec, QC*.

Metcalf, L., Eddy, H. P., & Tchobanoglous, G. (1991). *Wastewater engineering: treatment, disposal, and reuse* (Vol. 4). McGraw-Hill.

Ministry of Environment and Climate Change. (2022). *On-site Sewage Disposal Systems Standard*. https://novascotia.ca/nse/wastewater/docs/On-Site-Sewage-standard-June-2022.pdf

Moore, J. W., Schindler, D. E., Scheuerell, M. D., Smith, D., & Frodge, J. (2003). Lake eutrophication at the urban fringe, Seattle region, USA. AMBIO. *A Journal of the Human Environment*, *32*(1), 13–18.

Morvannou, A., Masson, M., Gautier, M., Bisone, S., Richard, L., Boutin, C., & Forquet, N. (2022). Fate of phosphorus from treated wastewater in soil-based constructed wetlands. *Science of The Total Environment*, *816*, 151589. https://doi.org/10.1016/j.scitotenv.2021.151589

Mriganka D., & Gurpal S. (2015). Fate of Effluent-Borne Nitrogen in the Mounded Drainfield of an Onsite Wastewater Treatment System. *Vadose Zone Journal*, *14*(12), 1–12. https://doi.org/10.2136/vzj2015.07.0096

Muller, E. E. L., Narayanasamy, S., Zeimes, M., Laczny, C. C., Lebrun, L. A., Herold, M., Hicks, N. D., Gillece, J. D., Schupp, J. M., Keim, P., & Wilmes, P. (2017). First draft genome sequence of a strain belonging to the Zoogloea genus and its gene expression in situ. *Standards in Genomic Sciences*, *12*(1), 64. https://doi.org/10.1186/s40793-017-0274-y

Nadeau, S., Rosa, E., & Cloutier, V. (2018). Stratigraphic sequence map for groundwater assessment and protection of unconsolidated aquifers: A case example in the Abitibi-Témiscamingue region, Québec, Canada. *Canadian Water Resources Journal / Revue Canadienne Des Ressources Hydriques*, *43*(2), 113–135. https://doi.org/10.1080/07011784.2017.1354722

Nadeau, S., Rosa, E., Cloutier, V., Daigneault, R.-A., & Veillette, J. (2015). A GIS-based approach for supporting groundwater protection in eskers: Application to sand and gravel extraction activities in Abitibi-Témiscamingue, Quebec, Canada. *Journal of Hydrology: Regional Studies*, *4*, 535–549. https://doi.org/10.1016/j.ejrh.2015.05.015

Nazari, M. T., Simon, V., Machado, B. S., Crestani, L., Marchezi, G., Concolato, G., Ferrari, V., Colla, L. M., & Piccin, J. S. (2022). Rhodococcus: A promising genus of actinomycetes for the bioremediation of organic and inorganic contaminants. *Journal of Environmental Management*, *323*, 116220. https://doi.org/10.1016/j.jenvman.2022.116220

Nelson, M. B., Martiny, A. C., & Martiny, J. B. H. (2016). Global biogeography of microbial nitrogen-cycling traits in soil. *Proceedings of the National Academy of Sciences*, *113*(29), 8033–8040. https://doi.org/10.1073/pnas.1601070113

Odong, J. (2007). Evaluation of empirical formulae for determination of hydraulic conductivity based on grain-size analysis. *Journal of American Science*, *3*, 54–60.

Oksanen, J., Simpson, G. L., Blanchet, F. G., Kindt, R., Legendre, P., Minchin, P. R., O'Hara, R. B., Solymos, P., Stevens, M. H. H., Szoecs, E., Wagner, H., Barbour, M., Bedward, M., Bolker, B., Borcard, D., Borman, T., Carvalho, G., Chirico, M., De Caceres, M., … Weedon, J. (2025). vegan: Community Ecology Package. In *CRAN: Contributed Packages*. https://doi.org/10.32614/CRAN.package.vegan

Oluseyi Osunmakinde, C., Selvarajan, R., Mamba, B. B., & Msagati, T. A. M. (2019). Profiling Bacterial Diversity and Potential Pathogens in Wastewater Treatment Plants Using High-Throughput Sequencing Analysis. *Microorganisms*, *7*(11), 506. https://doi.org/10.3390/microorganisms7110506

Palmer, J., Flint, S., & Brooks, J. (2007). Bacterial cell attachment, the beginning of a biofilm. *Journal of Industrial Microbiology & Biotechnology*, *34*(9), 577–588. https://doi.org/10.1007/s10295-007-0234-4

Pan, J., Yuan, F., Yu, L., Huang, L., Fei, H., Cheng, F., & Zhang, Q. (2016). Performance of organics and nitrogen removal in subsurface wastewater infiltration systems by intermittent aeration and shunt distributing wastewater. *Bioresource Technology*, *211*, 774–778. https://doi.org/10.1016/j.biortech.2016.03.133

Peng, J., Wang, B., Song, Y., Yuan, P., & Liu, Z. (2007). Adsorption and release of phosphorus in the surface sediment of a wastewater stabilization pond. *Ecological Engineering*, *31*(2), 92–97. https://doi.org/10.1016/j.ecoleng.2007.06.005

Penn, C., & Camberato, J. (2019). A Critical Review on Soil Chemical Processes that Control How Soil pH Affects Phosphorus Availability to Plants. *Agriculture*, *9*(6), 120. https://doi.org/10.3390/agriculture9060120

Penn, C. J., Rutter, E. B., Arnall, D. B., Camberato, J., Williams, M., & Watkins, P. (2018). A Discussion on Mehlich-3 Phosphorus Extraction from the Perspective of Governing Chemical Reactions and Phases: Impact of Soil pH. *Agriculture*, *8*(7), 106. https://doi.org/10.3390/agriculture8070106

Persson, G., & Jansson, M. (2021). *Phosphorus in freshwater ecosystems: proceedings of a symposium held in Uppsala, Sweden, 25–28 September 1985* (Vol. 48). Springer Science & Business Media.

Petitjean, A., Forquet, N., & Boutin, C. (2016). Oxygen profile and clogging in vertical flow sand filters for on-site wastewater treatment. *Journal of Environmental Management*, *170*, 15–20. https://doi.org/10.1016/j.jenvman.2015.12.033

Q. Tian, Y. Jiang, Y. Tang, Y. Wu, Z. Tang, & F. Liu. (2021). Soil pH and Organic Carbon Properties Drive Soil Bacterial Communities in Surface and Deep Layers Along an Elevational Gradient. *Frontiers in Mocrobiology*.

Qu, W., Suo, L., Liu, R., Liu, M., Zhao, Y., Xia, L., Fan, Y., Zhang, Q., & Gao, Z. (2022). Influence of Temperature on Denitrification and Microbial Community Structure and

Diversity: A Laboratory Study on Nitrate Removal from Groundwater. *Water*, *14*(3), 436. https://doi.org/10.3390/w14030436

R Core Team. (2025). *R: A Language and Environment for Statistical Computing* (4.4.3). R Foundation for Statistical Computing.

R. Kolde. (2019). *pheatmap: Pretty Heatmaps; https://CRAN.R-project.org/package=pheatmap*.

Rajabzadeh, A. R., Legge, R. L., & Weber, K. P. (2015). Multiphysics modelling of flow dynamics, biofilm development and wastewater treatment in a subsurface vertical flow constructed wetland mesocosm. *Ecological Engineering*, *74*, 107–116. https://doi.org/10.1016/j.ecoleng.2014.09.122

Rauch-Williams, T., & Drewes, J. E. (2006). Using soil biomass as an indicator for the biological removal of effluent-derived organic carbon during soil infiltration. *Water Research*, *40*(5), 961–968. https://doi.org/10.1016/j.watres.2006.01.007

Reid, K., Schneider, K., & McConkey, B. (2018). Components of Phosphorus Loss From Agricultural Landscapes, and How to Incorporate Them Into Risk Assessment Tools. *Frontiers in Earth Science*, *6*. https://doi.org/10.3389/feart.2018.00135

Rice, E. W., Bridgewater, L., & Eaton, A. D. (2017). *Standard methods for the examination of water and wastewater* (American Public Health Association eds., Ed.; 23rd ed.). American Public Health Association.

Richards, L. A. (1931). Capillary Conduction of Liquids Through Porous Mediums. *Physics*, *1*(5), 318–333. https://doi.org/10.1063/1.1745010

Richards, S., Paterson, E., Withers, P. J. A., & Stutter, M. (2016). Septic tank discharges as multi-pollutant hotspots in catchments. *Science of The Total Environment*, *542*, 854–863. https://doi.org/10.1016/j.scitotenv.2015.10.160

Robertson, W. D. (2008). Irreversible Phosphorus Sorption in Septic System Plumes? *Groundwater*, *46*(1), 51–60. https://doi.org/10.1111/j.1745-6584.2007.00389.x

Robertson, W. D., Elgood, R. J., Van Stempvoort, D. R., Brown, S. J., & Schiff, S. L. (2023). Nitrogen and Phosphorus Treatment Can Be Sustainable During on-Site Wastewater Disposal. *Groundwater*, *61*(4), 586–598. https://doi.org/10.1111/gwat.13316

Robertson, W. D., van Stempvoort, D. R., & Schiff, S. L. (2019). Review of phosphorus attenuation in groundwater plumes from 24 septic systems. *Science of The Total Environment*, *692*, 640–652. https://doi.org/10.1016/j.scitotenv.2019.07.198

Robertson, W. D., Van Stempvoort, D. R., & Schiff, S. L. (2021). Nitrogen Attenuation in Septic System Plumes. *Groundwater*, *59*(3), 369–380. https://doi.org/10.1111/gwat.13065

Rodgers, M., Mulqueen, J., & Healy, M. G. (2004). Surface Clogging in an Intermittent Stratified Sand Filter. *Soil Science Society of America Journal*, *68*(6), 1827–1832. https://doi.org/10.2136/sssaj2004.1827

Roseth, R. (2000). Shell sand: A new filter medium for constructed wetlands and wastewater treatment. *Journal of Environmental Science and Health, Part A*, *35*(8), 1335–1355. https://doi.org/10.1080/10934520009377039

Rout, P. R., Shahid, M. K., Dash, R. R., Bhunia, P., Liu, D., Varjani, S., Zhang, T. C., & Surampalli, R. Y. (2021). Nutrient removal from domestic wastewater: A comprehensive review on conventional and advanced technologies. *Journal of Environmental Management*, *296*, 113246. https://doi.org/10.1016/j.jenvman.2021.113246

Rustige, H., Tomac, I., & Höner, G. (2003). Investigations on phosphorus retention in subsurface flow constructed wetlands. *Water Science and Technology*, *48*(5), 67–74. https://doi.org/10.2166/wst.2003.0283

Sanz, J. L., & Köchling, T. (2007). Molecular biology techniques used in wastewater treatment: An overview. *Process Biochemistry*, *42*(2), 119–133. https://doi.org/10.1016/j.procbio.2006.10.003

Schindler, D. W., Carpenter, S. R., Chapra, S. C., Hecky, R. E., & Orihel, D. M. (2016). Reducing Phosphorus to Curb Lake Eutrophication is a Success. *Environmental Science & Technology*, *50*(17), 8923–8929. https://doi.org/10.1021/acs.est.6b02204

Shahraki, Z. M., Mao, X., Waugh, S., Lotfikatouli, S., Walker, H. W., Gobler, C., & Wanlass, J. (2020). Potential release of legacy nitrogen from soil surrounding onsite wastewater leaching pools. *Water Research*, *169*, 115241. https://doi.org/10.1016/j.watres.2019.115241

Sheibani, S., & Claveau-Mallet, D. (2025). Phosphorus Dynamics in the Clogging Zone of On-Site Sand Filters: Treatment Performance and Lifespan . *[Manuscript in Preparation]*.

Sheibani, S., Nasrallah, M., Courcelles, B., Rosa, E., Maylal, B., & Claveau-Mallet, D. (2025). Phosphorus retention and hydraulic performance in borrow sand-based wastewater soil treatment units in impermeable settings: Case study in Abitibi-Témiscamingue, Québec. *Journal of Water Process Engineering*, *74*, 107681. https://doi.org/10.1016/j.jwpe.2025.107681

Sheibani, S., Pitre, F., & Claveau-Mallet, D. (2025). Influence of Soil Moisture Distribution on Oxygen Availability and Nitrogen Removal in Onsite Wastewater Treatment Systems. *[Manuscript in Preparation])*.

Siegrist, R. L., & Boyle, W. C. (1987). Wastewater-Induced Soil Clogging Development. *Journal of Environmental Engineering*, *113*(3), 550–566. https://doi.org/10.1061/(ASCE)0733-9372(1987)113:3(550)

Sinclair, A., Jamieson, R., Gordon, R. J., Madani, A., & Hart, W. (2014). Modeling Phosphorus Treatment Capacities of On-Site Wastewater Lateral Flow Sand Filters. *Journal of Environmental Engineering*, *140*(2). https://doi.org/10.1061/(ASCE)EE.1943-7870.0000796

Smith, R. A., Alexander, R. B., & Schwarz, G. E. (2003). Natural Background Concentrations of Nutrients in Streams and Rivers of the Conterminous United States. *Environmental Science & Technology*, *37*(14), 3039–3047. https://doi.org/10.1021/es020663b

Spoelstra, J., Senger, N. D., & Schiff, S. L. (2017). Artificial Sweeteners Reveal Septic System Effluent in Rural Groundwater. *Journal of Environmental Quality*, *46*(6), 1434–1443. https://doi.org/10.2134/jeq2017.06.0233

Su, Q., Andersen, H. R., Bazylinski, D. A., & Jensen, M. M. (2023). Effect of oxic and anoxic conditions on intracellular storage of polyhydroxyalkanoate and polyphosphate in Magnetospirillum magneticum strain AMB-1. *Frontiers in Microbiology*, *14*. https://doi.org/10.3389/fmicb.2023.1203805

Tabari, H. (2020). Climate change impact on flood and extreme precipitation increases with water availability. *Scientific Reports*, *10*(1), 13768. https://doi.org/10.1038/s41598-020-70816-2

Tansel, B. (2018). Morphology, composition and aggregation mechanisms of soft bioflocs in marine snow and activated sludge: A comparative review. *Journal of Environmental Management*, *205*, 231–243. https://doi.org/10.1016/j.jenvman.2017.09.082

Teerlink, J., Martínez-Hernández, V., Higgins, C. P., & Drewes, J. E. (2012). Removal of trace organic chemicals in onsite wastewater soil treatment units: A laboratory experiment. *Water Research*, *46*(16), 5174–5184. https://doi.org/10.1016/j.watres.2012.06.024

Tomaras, J., Sahl, J. W., Siegrist, R. L., & Spear, J. R. (2009). Microbial Diversity of Septic Tank Effluent and a Soil Biomat. *Applied and Environmental Microbiology*, *75*(10), 3348–3351. https://doi.org/10.1128/AEM.00560-08

U.S. Environmental Protection Agency. (1986). *Quality criteria for water 1986, Report 440/5-86-001*.

van Genuchten, M. Th. (1980). A Closed-form Equation for Predicting the Hydraulic Conductivity of Unsaturated Soils. *Soil Science Society of America Journal*, *44*(5), 892–898. https://doi.org/10.2136/sssaj1980.03615995004400050002x

Vidal, B., Hedström, A., & Herrmann, I. (2018). Phosphorus reduction in filters for on-site wastewater treatment. *Journal of Water Process Engineering*, *22*, 210–217. https://doi.org/10.1016/j.jwpe.2018.02.005

Vidal, B., Kinnunen, J., Hedström, A., Heiderscheidt, E., Rossi, P., & Herrmann, I. (2023). Treatment efficiency of package plants for on-site wastewater treatment in cold climates. *Journal of Environmental Management*, *342*, 118214. https://doi.org/10.1016/j.jenvman.2023.118214

Vymazal, J. (2007). Removal of nutrients in various types of constructed wetlands. *Science of The Total Environment*, *380*(1–3), 48–65. https://doi.org/10.1016/j.scitotenv.2006.09.014

Wang, M., Zeng, F., Chen, S., Wehrmann, L. M., Waugh, S., Brownawell, B. J., Gobler, C. J., & Mao, X. (2024). Phosphorus attenuation and mobilization in sand filters treating onsite

wastewater. *Chemosphere*, *364*, 143042. https://doi.org/10.1016/j.chemosphere.2024.143042

Ward, M., Jones, R., Brender, J., De Kok, T., Weyer, P., Nolan, B., Villanueva, C., & Van Breda, S. (2018). Drinking Water Nitrate and Human Health: An Updated Review. *International Journal of Environmental Research and Public Health*, *15*(7), 1557. https://doi.org/10.3390/ijerph15071557

Weill, S., Mouche, E., & Patin, J. (2009). A generalized Richards equation for surface/subsurface flow modelling. *Journal of Hydrology*, *366*(1–4), 9–20. https://doi.org/10.1016/j.jhydrol.2008.12.007

Wickham, H., Averick, M., Bryan, J., Chang, W., McGowan, L., François, R., Grolemund, G., Hayes, A., Henry, L., Hester, J., Kuhn, M., Pedersen, T., Miller, E., Bache, S., Müller, K., Ooms, J., Robinson, D., Seidel, D., Spinu, V., … Yutani, H. (2019). Welcome to the Tidyverse. *Journal of Open Source Software*, *4*(43), 1686. https://doi.org/10.21105/joss.01686

Wilhelm, S. R., Schiff, S. L., & Cherry, J. A. (1994). Biogeochemical Evolution of Domestic Waste Water in Septic Systems: 1. Conceptual Model. *Ground Water*, *32*(6), 905–916. https://doi.org/10.1111/j.1745-6584.1994.tb00930.x

Wilhelm, S. R., Schiff, S. L., & Robertson, W. D. (1994). Chemical fate and transport in a domestic septic system: Unsaturated and saturated zone geochemistry. *Environmental Toxicology and Chemistry*, *13*(2), 193–203. https://doi.org/10.1002/etc.5620130203

Woes, C. (1987). Bacterial Evolution. *Microbiological Reviews*, *51*, 221–271.

Wu, J., Zhang, J., Jia, W., Xie, H., Gu, R. R., Li, C., & Gao, B. (2009). Impact of COD/N ratio on nitrous oxide emission from microcosm wetlands and their performance in removing nitrogen from wastewater. *Bioresource Technology*, *100*(12), 2910–2917. https://doi.org/10.1016/j.biortech.2009.01.056

Yamaguchi, T., Moldrup, P., Rolston, D. E., Ito, S., & Teranishi, S. (1996). Nitrification in porous media during rapid, unsaturated water flow. *Water Research*, *30*(3), 531–540. https://doi.org/10.1016/0043-1354(95)00206-5

Yang, B., Lin, H., Bartlett, S. L., Houghton, E. M., Robertson, D. M., & Guo, L. (2021). Partitioning and transformation of organic and inorganic phosphorus among dissolved, colloidal and particulate phases in a hypereutrophic freshwater estuary. *Water Research*, *196*, 117025. https://doi.org/10.1016/j.watres.2021.117025

Zhao, H., Zhang, Y., Tang, L., Cui, Z., Liu, B., Cheng, W., Guo, C., Liu, D., Gao, X., & Feng, H. (2021). Effect of extracellular polymeric substances on the phosphorus adsorption characteristics of sediment particles. *International Journal of Sediment Research*, *36*(5), 628–636. https://doi.org/10.1016/j.ijsrc.2021.02.005

Zhao, L., Zhu, W., & Tong, W. (2009). Clogging processes caused by biofilm growth and organic particle accumulation in lab-scale vertical flow constructed wetlands. *Journal of Environmental Sciences*, *21*(6), 750–757. https://doi.org/10.1016/S1001-0742(08)62336-0

Zohar, I., Shaviv, A., Klass, T., Roberts, K., & Paytan, A. (2010). Method for the Analysis of Oxygen Isotopic Composition of Soil Phosphate Fractions. *Environmental Science & Technology*, *44*(19), 7583–7588. https://doi.org/10.1021/es100707f

Zúñiga-Gutiérrez, J., Caballero-Chavarría, A., Zambrano, D., Ulate-Molina, R., & Masís-Meléndez, F. (2025). Nitrate leaching in an on-site wastewater system: Monitoring and modeling with HYDRUS 1D. *Journal of Water Process Engineering*, *70*, 107049. https://doi.org/10.1016/j.jwpe.2025.107049

Zurawsky, M. A., Robertson, W. D., Ptacek, C. J., & Schiff, S. L. (2004). Geochemical stability of phosphorus solids below septic system infiltration beds. *Journal of Contaminant Hydrology*, *73*(1–4), 129–143. https://doi.org/10.1016/j.jconhyd.2004.01.003

APPENDIX A: PHOSPHORUS RETENTION AND HYDRAULIC PERFORMANCE IN BORROW SAND-BASED WASTEWATER SOIL TREATMENT UNITS IN IMPERMEABLE SETTINGS: CASE STUDY IN ABITIBI-TÉMISCAMINGUE, QUÉBEC

This appendix provides supplementary information related to Chapter 3 (Article 1).

A.1 Soil type estimations

Québec's guidelines classify soil as very permeable, permeable, lowly permeable, and impermeable, each with a specific range of hydraulic conductivity: (i) very permeable (K > 4×10-5 m/s), (ii) permeable (2×10-6 m/s < K < 4×10-5 m/s), (iii) lowly permeable (6×10 7 m/s < K < 2×10-6 m/s), and (iv) impermeable (K < 6×10-7 m/s) where K is the hydraulic conductivity of the in situ soils. Various methods exist to determine soil type, including defining hydraulic conductivity through *in situ* and laboratory permeability tests and subsequently categorizing soil types based on the obtained hydraulic conductivity (MELCCFP, 2017). Another approach involves using the soil texture triangle to estimate soil type based on its particle size distribution (MELCCFP, 2017). Figure A.1 shows the correlation between the texture triangle and the 4 soil types. In this study, the samples collected from the field were plotted on the triangle as seen in Figure A.1 and their soil types were estimated using this method.

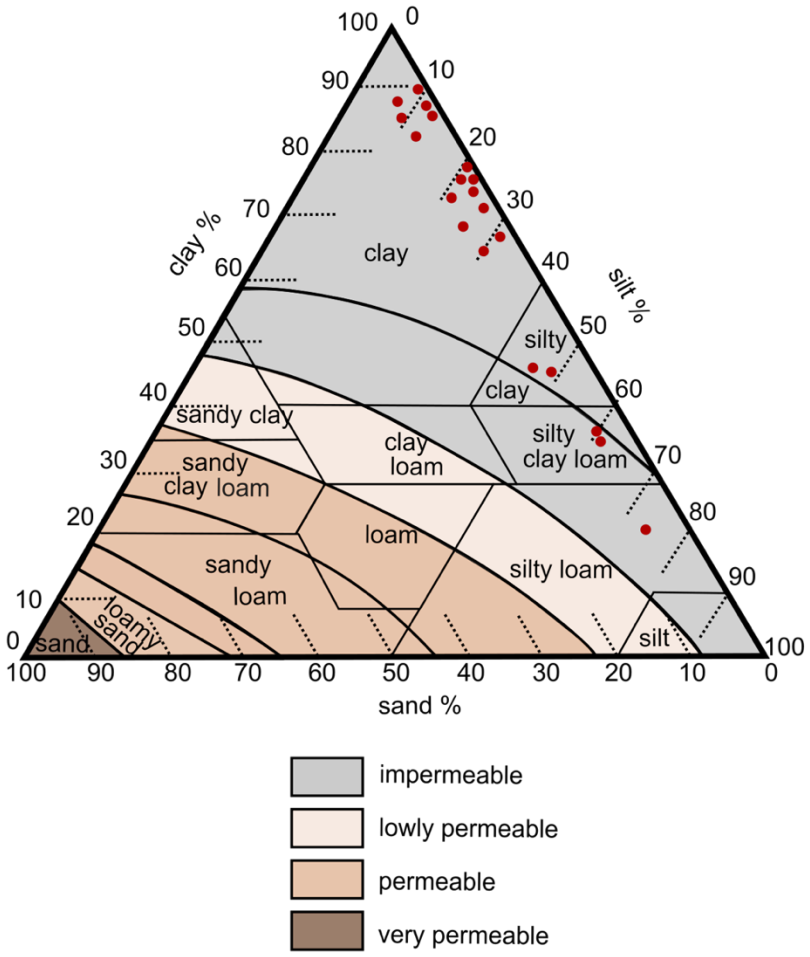

Figure A.1 Correlation between the texture triangle and impermeable, lowly permeable, permeable and very permeable soil (MELCCFP, 2017) and the plotted natural soil samples.

A.2 Sanitary inspection sampling points

The following figure shows the location of the ditch, the polishing bed leading to the ditch and sampling points in sanitary field inspections.

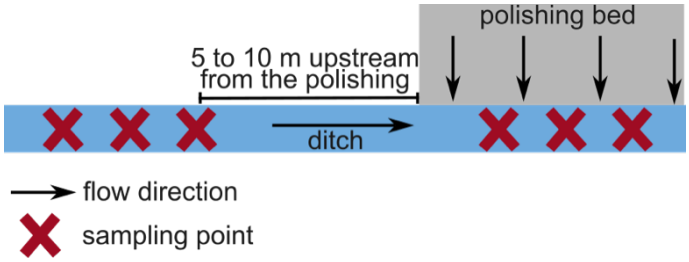

Figure A.2 Plan of sampling points in sanitary inspections.

A.3 Inspected systems

Table A.1 Characteristics of inspected systems (type of distribution of wastewater from the pipes, number of bedrooms of residences, number of residents, area, occupancy rate, installation year, and category of the septic system).

System number	Type of distribution	Number of Bedroom	Residents	Area (m^2)	Estimated hydraulic load (m^3/d)	Occupancy rate	Installation year	Category
1	Gravity-fed	3	2	16	0.54	33%	2009	2
2	Low-pressure	3	3	16	0.81	50%	2018	2
3	Low-pressure	3	2	16	0.54	33%	2006	3
4	Low-pressure	4	4	22	1.08	50%	2018	2
5	Low-pressure	5	4	27	1.08	40%	2014	1
6	Gravity-fed	4	2	22	0.54	25%	2005	3
7	Gravity-fed	4	2	22	0.54	25%	2019	1
8	Low-pressure	4	2	22	0.54	25%	2018	2
9	Gravity-fed	3	2	16	0.54	33%	2018	2
10	Low-pressure	2	2	11	0.54	50%	2017	2

Table A.1 continued Characteristics of inspected systems (type of distribution of wastewater from the pipes, number of bedrooms of residences, number of residents, area, occupancy rate, installation year, and category of the septic system).

System number	Type of distribution	Number of Bedroom	Residents	Area (m^2)	Estimated hydraulic load (m^3/d)	Occupancy rate	Installation year	Category
11	Low-pressure	2	1	11	0.27	25%	2015	3
12	Gravity-fed	3	2	16	0.54	33%	2019	1
13	Low-pressure	6	6	32	1.62	50%	2020	3
14	Low-pressure	2	2	11	0.54	50%	2018	2
15	Low-pressure	4	2	22	0.54	25%	2017	2
16	Low-pressure	3	2	16	0.54	33%	2011	2
17	Low-pressure	3	4	16	1.08	67%	2019	2
18	Low-pressure	4	2	22	0.54	25%	2020	3
19	Gravity-fed	4	5	22	1.35	63%	2017	1
20	Low-pressure	1	2	7	0.54	100%	2020	3
21	Gravity-fed	5	6	27	1.62	60%	2020	2

Table A.1 continued Characteristics of inspected systems (type of distribution of wastewater from the pipes, number of bedrooms of residences, number of residents, area, occupancy rate, installation year, and category of the septic system).

System number	Type of distribution	Number of Bedroom	Residents	Area (m^2)	Estimated hydraulic load (m^3/d)	Occupancy rate	Installation year	Category
22	Gravity-fed	4	4	22	1.08	50%	2018	1
23	Gravity-fed	3	3	16	0.81	50%	2013	2
24	Low-pressure	4	4	22	1.08	50%	2013	3
25	Low-pressure	4	2	22	0.54	25%	2015	1
26	Low-pressure	1	2	7	0.54	100%	2012	3

The hydraulic loads of the systems were estimated based on the number of residents and the wastewater production of 270 L/d (MELCCFP, 2017). Systems 7 and 16 demonstrated ground surface flooding.

A.4 Gravity-fed vs low-pressure distribution systems

In a gravity-fed system, a preferential flow forms at the nearest orifice to the supply pipe and therefore, the flow does not distribute evenly through pipes. On the other hand, low-pressure distributing systems distribute the flow almost evenly through the network by pressurizing. In reality, pipes are perforated, and the discharge comes out of holes with small areas. In a low-pressure distribution system, the water leaves the pipes upwards. In the modelling section, low-pressure distribution systems were simulated. To ease the numerical convergence, a uniform inflow through the upper half of the lateral area of pipes was considered.

A.5 S1 and S2 meeting specifications

To make sure that the specifications are met, the particle size distributions of 2 sand samples were obtained according to ASTM C136 (ASTM International, 2020) and presented in Figure A.3.

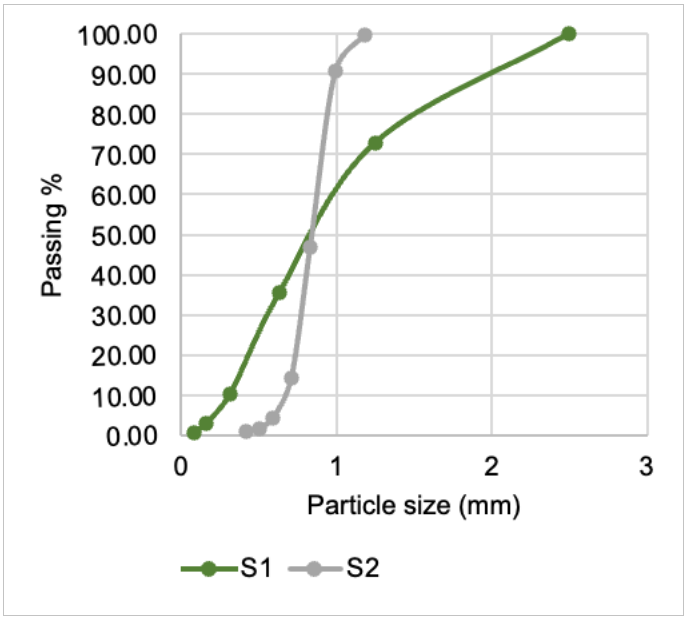

Figure A.3 Particle distribution curves of S1 and S2.

Table A.2 shows that both S1 and S2 met all specifications.

Table A.2 Sands specifications and their validations for S1 and S2.

Specification	Validation for S1	Validation for S2
0.25 mm < d_{10} <1 mm	d_{10} = 0.31	d_{10} = 0.66
C_u <4.5	C_u = 3.30	C_u = 1.33
Particles smaller than 80 μm < 3 %	Particles smaller than 80 μm = 0.57 %	No particles smaller than 80 μm
Particles bigger than 2.5 mm < 20%	No particles bigger than 2.5 mm	No particles bigger than 2.5 mm

A.6 Polishing beds plans

Figure A.4 exhibits the plans for rectangular and square polishing beds associated with 6-bedroom residences.

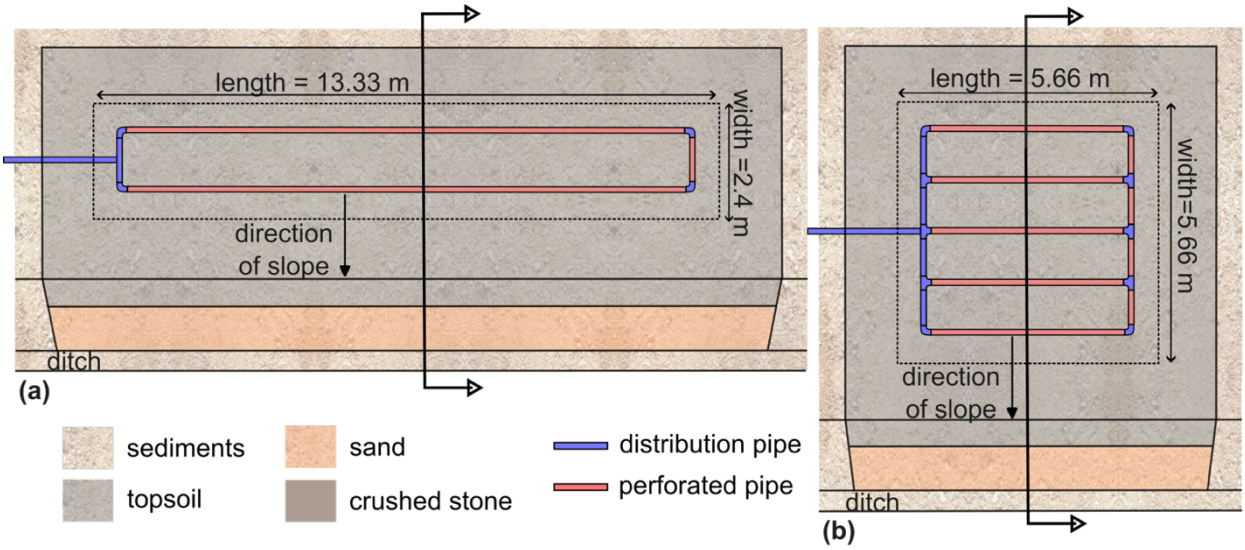

Figure A.4 Plan of polishing beds designed for 6-bedroom residences. (a) rectangular polishing bed and (b) square polishing bed. The dashed line shows the boundaries of the crushed stone layer.

A.7 3D modeling of polishing bed vs 2D

Figure A.5 illustrates the 3D simulation of model 1 in day 360. The horizontal blue plane represents the water table within the polishing bed and the P plume in Figure A.5a indicates the isosurface corresponding to a 4 mg/l P concentration (80% of the inlet concentration). The contaminant plume

saturated the crushed stone layer and extended downslope through the sand layer toward the ditch. While the equivalent 2D model yielded a lifetime of 110 days (Table 3.5), a relatively small content of P dispersed perpendicular to the slope resulted in a longer yet comparable lifetime of 160 days in the 3D model. The minimum unsaturated thickness in the 3D model was 0.61 m which is merely 1 cm greater than that of the 2D model (0.6 m, as in Table 3.5). Figure A.5b displays the P concentration contour in a cross-section extracted from the 3D model exhibiting a strong similarity to the configuration of the equivalent 2D model (Figure 3.6a). The 3D simulation demanded a substantial computation time of 46 hours, highlighting the practical advantage of opting for 2D simulations running in less than an hour.

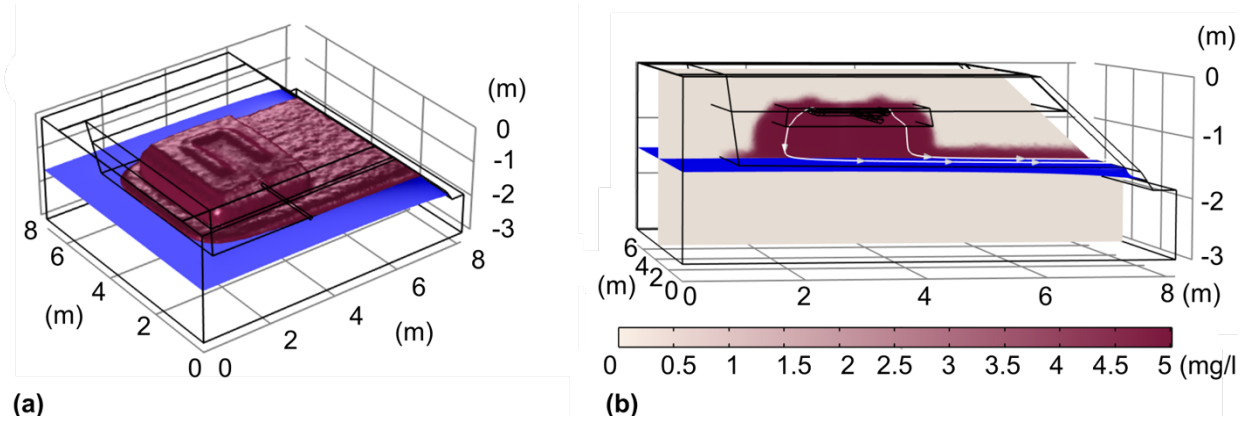

Figure A.5 Model 1 3D simulation in day 360. (a) Isosurface of 4 mg/l of phosphorus and water table and (b) water table, contour map of phosphorus concentration and streamlines in a cross-section.

Dispersion along the omitted dimension (the dimension perpendicular to the STU's slope) is not accounted for in the 2D model. This simplification is valid when flow and transport primarily occur within the modeled plane, but it may introduce inaccuracies in cases where lateral spreading is significant. Despite the overall agreement between 2D and 3D results, 3D modeling remains essential in situations where lateral contaminant dispersion cannot be neglected, such as in non-uniform subsurface flow conditions, heterogeneous media, or when assessing contaminant migration toward nearby water bodies or infrastructure. Although 3D simulations offer greater detail, their high computational cost (46 hours compared to under an hour for 2D) limits their practicality unless lateral transport is a key focus.

A.8 No flow boundaries in numerical modelling

In general, two types of no-flow boundaries were implemented; bottom no-flow boundaries and side no-flow boundaries. The bottom no-flow boundaries are deep enough to not affect the hydraulic integrity and transport of phosphorus. No-flow side-boundaries can imply the impermeability in the sediments layer which is realistic since the sediments layer is clayey in general. Additionally, the main hydraulic behavior of the polishing beds was in a way that highly permeable sand layer did not allow for water accumulation but instead helped forming an outlet flow towards the ditch. Also, the phosphorus (P) plume never approached these boundaries. Therefore, the location of the no-flow side-boundaries is not influential regarding the above-mentioned pattern.

A.9 Numerical meshing

Triangular mesh was built automatically with COMSOL Multiphysics. In 2D modelling, mesh size varied from 1.8×10^{-4} m to 0.02 m and in 3D modelling mesh size varied from 0.001m to 0.09 m. Different mesh sizes, spanning from twice as coarse to twice as fine as the size of the final mesh, were tested and revealed grid convergence, as the results remained consistent regardless of variations in mesh size.

A.10 Justification of porous media parameters used for modelling

Topsoil was considered to be loamy, representing a natural cover for the culture of grass, as commonly observed in backyards. Hodnett and Tomasella, (2002) tested 771 soils and derived values of van Genuchten parameters as well as porosity and residual water content. We used the average parameters they suggested for loam for topsoil. Topsoil's hydraulic conductivity was set in the range of permeable soil according to Québec's guidelines (MELCCFP, 2017).

Based on the particle size distribution of S1 and S2 sands, their hydraulic conductivities were estimated using Kozney-Carman, Hazen and Breyer formulas. These empirical formulas were shown to give the most precise estimations among available empirical formulas (Odong, 2007). The values of 1.22×10^{-3} and 7.88×10^{-3} m/s were obtained for S1 and S2, respectively. The value used in simulations is the average hydraulic conductivity of the two sands. For other properties of the sand, we referred to the study by Benson et al. (2014) in which the measured hydraulic properties of fine, medium, and coarse sand were presented based on their particle sizes. We used average values for sand samples with d_{60} and d_{10} values that compare to the sands used in our work.

The results of the sieve test conducted on the 20 samples collected from the field revealed that the sediment layer is impermeable. The imposed hydraulic conductivity for this layer was set to a low value suggesting impermeability. Other hydraulic properties of fine sediments were the values presented by (Hodnett and Tomasella, 2002) for clayey soil.

Crushed stone is composed of 20 mm particles. The hydraulic conductivity of crushed stone with 20 mm particles was estimated from (Judge, 2013) and the porosity was taken from (Al- Fawzy and Al- Mohammed, 2019). The residual water content was set to zero since the particles are large. Furthermore, since the crushed stone used in the infiltration beds is washed prior to usage, fine particles are not included, and the coarse particles produce low suction which means that the α parameter is relatively large. Also, the value of n, for soils with limited breadth of the particle size distribution, tends to be relatively high (Benson et al., 2014). Here, the highest value with which the models converge was used.

The runoff layer was addressed according to Chapuis (2009) with its hydraulic conductivity being 10^4 times greater than most permeable media in the model (sand), as suggested by Chapuis (2009).

A.11 Analysis of natural soil covering

Figure A.6 shows the particle size distribution curve of the 20 samples taken from the field.

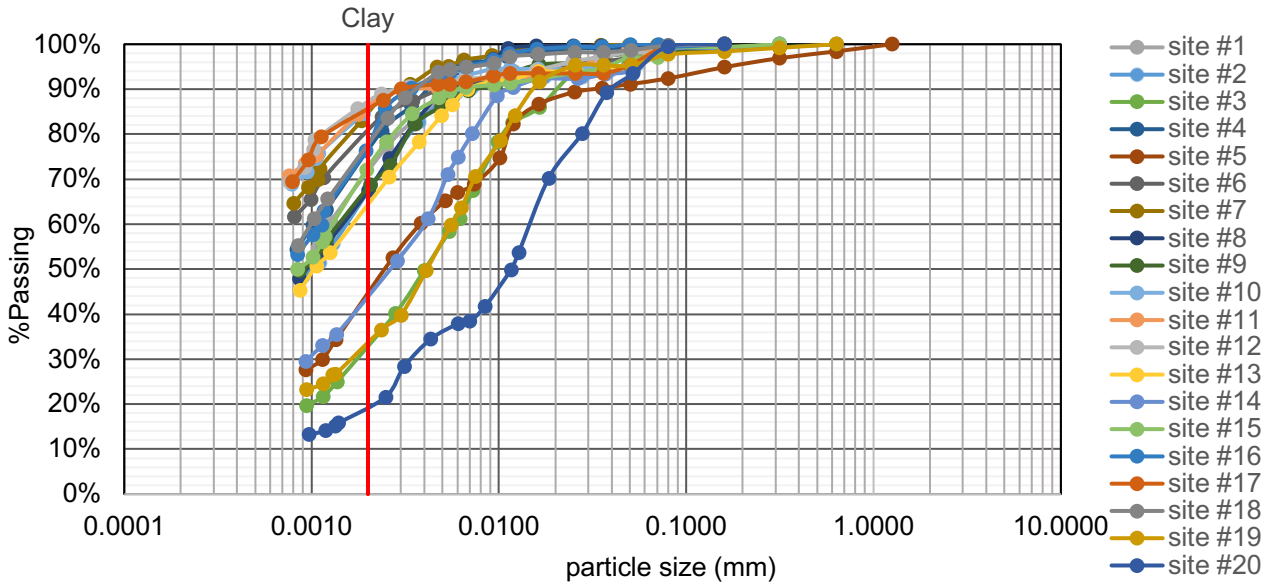

Figure A.6 Particle size distribution curves of the 20 soil samples.

A.12 pH in adsorption batch test

The pH in the initial solutions ranged from 5.4 to 5.8 (acidic solutions). After agitation, the pH measured in samples containing S2 were still in the range of 4.8 – 5.0 (acidic) while the pH of samples with S1 reached the range of 6.8 - 7.1 (alkaline). This difference could be due to the mineral compositions of different sands. Measured pH values are reported in Table A.3.

Table A.3 Initial pH of samples, and final pH of blank sample, samples with S1 and samples with S2.

Target concentrations mg P/L	Initial pH	Final pH		
		Blank samples	Samples with S1	Samples with S2
20.00	5.40	5.37	ND*	4.85
15.00	5.34	5.34	6.82	Nd*
10.00	5.47	Nd*	7.05	4.97
5.00	5.64	5.61	ND*	4.97
2.00	5.77	5.81	ND*	Nd*

Not determined (ND)

The pH was not measured for all the samples after the rotation period because the quantities of certain samples were limited and necessary to be able to make the required dilutions for concentration calculations.

A.13 Evolution of P plume

In Figure A.7, contour maps show the progression of P concentration in the polishing bed of model 1 throughout its lifespan. Similar patterns were observed in other models.

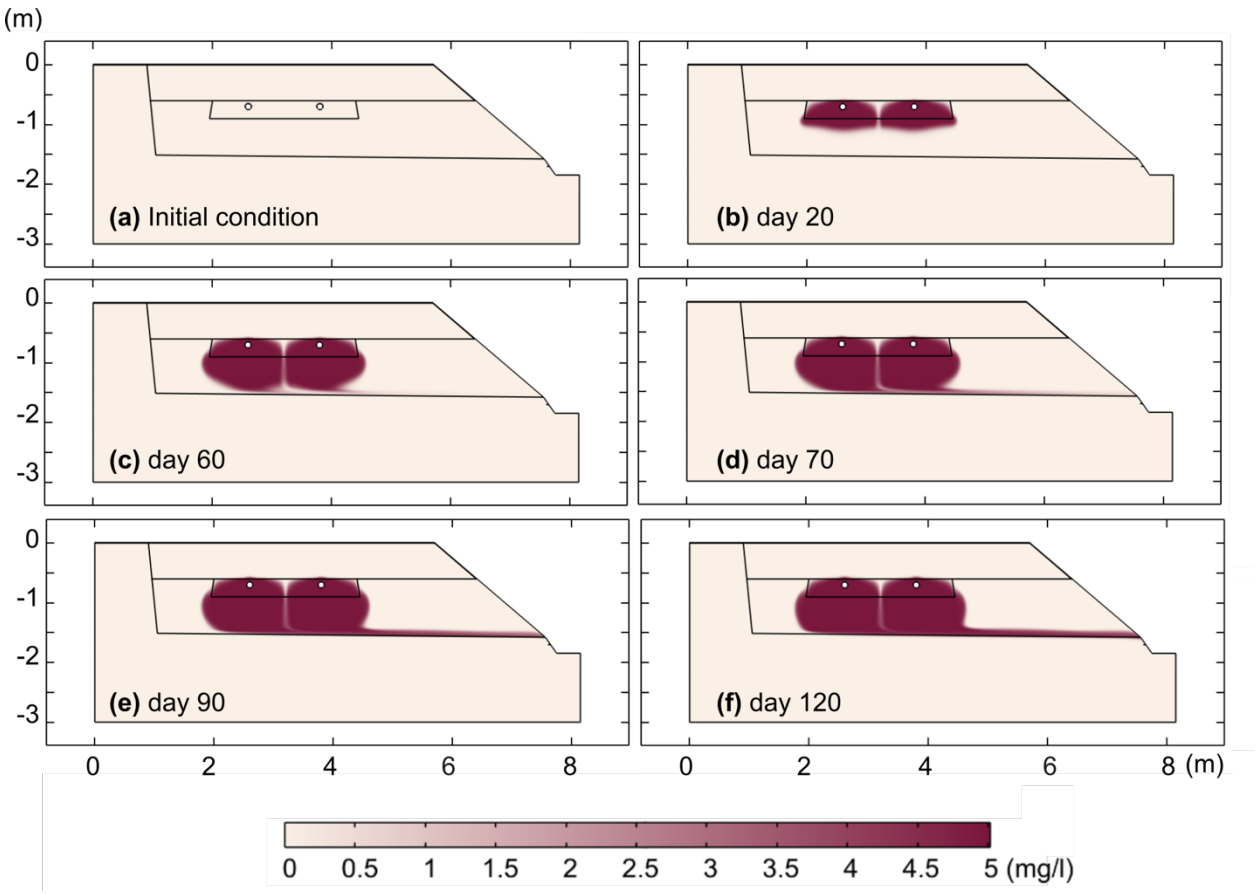

Figure A.7 Contour map of phosphorus concentration in (a) initial condition, (b) day 20, (c) day 60, (d) day 70, (e) day 90, and (f) day 120 of operation of polishing bed in model 1.

APPENDIX B: INFLUENCE OF SOIL MOISTURE DISTRIBUTION AND OXYGEN AVAILABILITY AND NITROGEN REMOVAL IN ONSITE WASTEWATER TREATMENT SYSTEMS

This appendix provides supplementary information related to Chapter 5 (Article 2).

B.1 Drainfield vertical configuration

The cross-section of a conventional drainfield conforming to Quebec's regulations is shown in Figure B.1a. To construct a drainfield, an underground trench is dug and filled with gravel. Perforated pipes are then placed in the gravel layer. The distance between the top of the drainfield trench to the ground level is 0.6 m, and the distance between the bottom of the trench to the groundwater level is 0.9 m. The whole unsaturated depth (water table depth) is 1.8 m. In this study, the 0.9 m unsaturated zone below the trench and 0.1 m of the saturated zone were simulated.

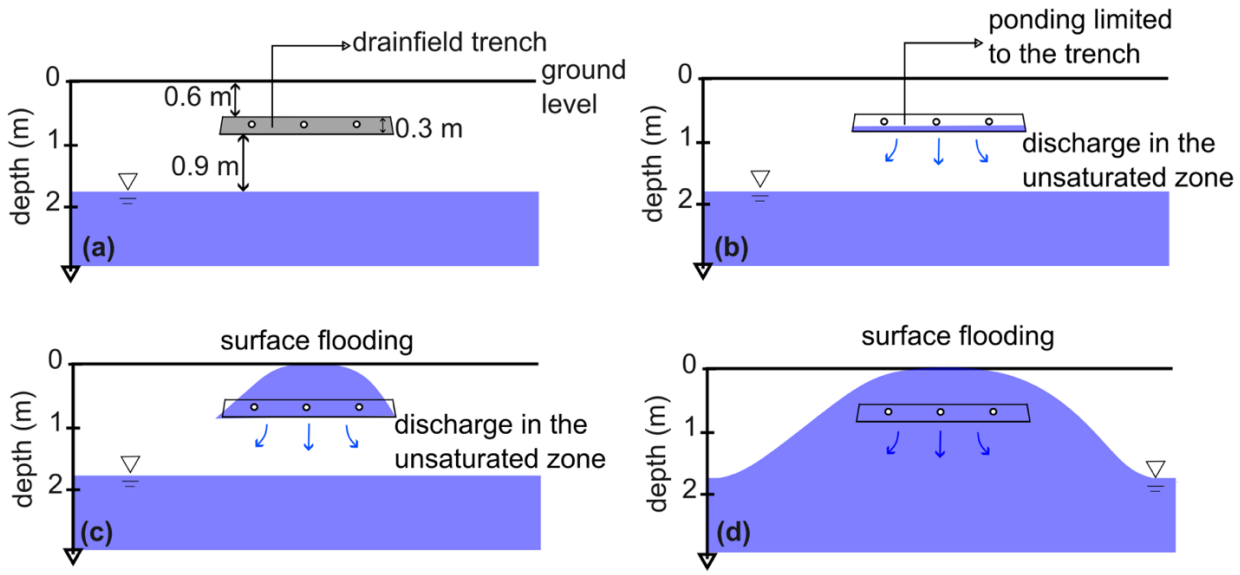

Figure B.1 Cross-section of a conventional drainfield (a) Vertical dimensions of a conforming drainfield installed above the water table, showing separation between trench bottom and groundwater. (b) Normal operation with minor ponding restricted within the trench and discharge occurring in the unsaturated zone. (c) Failing drainfield due to excessive biofilm development causing surface flooding. (d) Failing drainfield where hydraulic loading exceeds soil infiltration capacity, resulting in surface flooding.

When conditions are normal (Figure B.1b), wastewater percolates into the unsaturated soil, with ponding confined within the trench. In cases of excessive biofilm clogging (Figure B.1c) or

hydraulic overloading (Figure B.1d), the system can fail, leading to surface flooding and potential environmental and health hazards.

B.2 Soil particle distribution

Particle distributions of both soils were determined. To do so, 338.3 g of Soil 1 was sieved through a series of sieves ranging from 0.08 mm to 5 mm. Additionally, 376.1 g of Soil 2 underwent a combined sieve and hydrometer analysis. Figure B.2 shows the particle distribution of both soils.

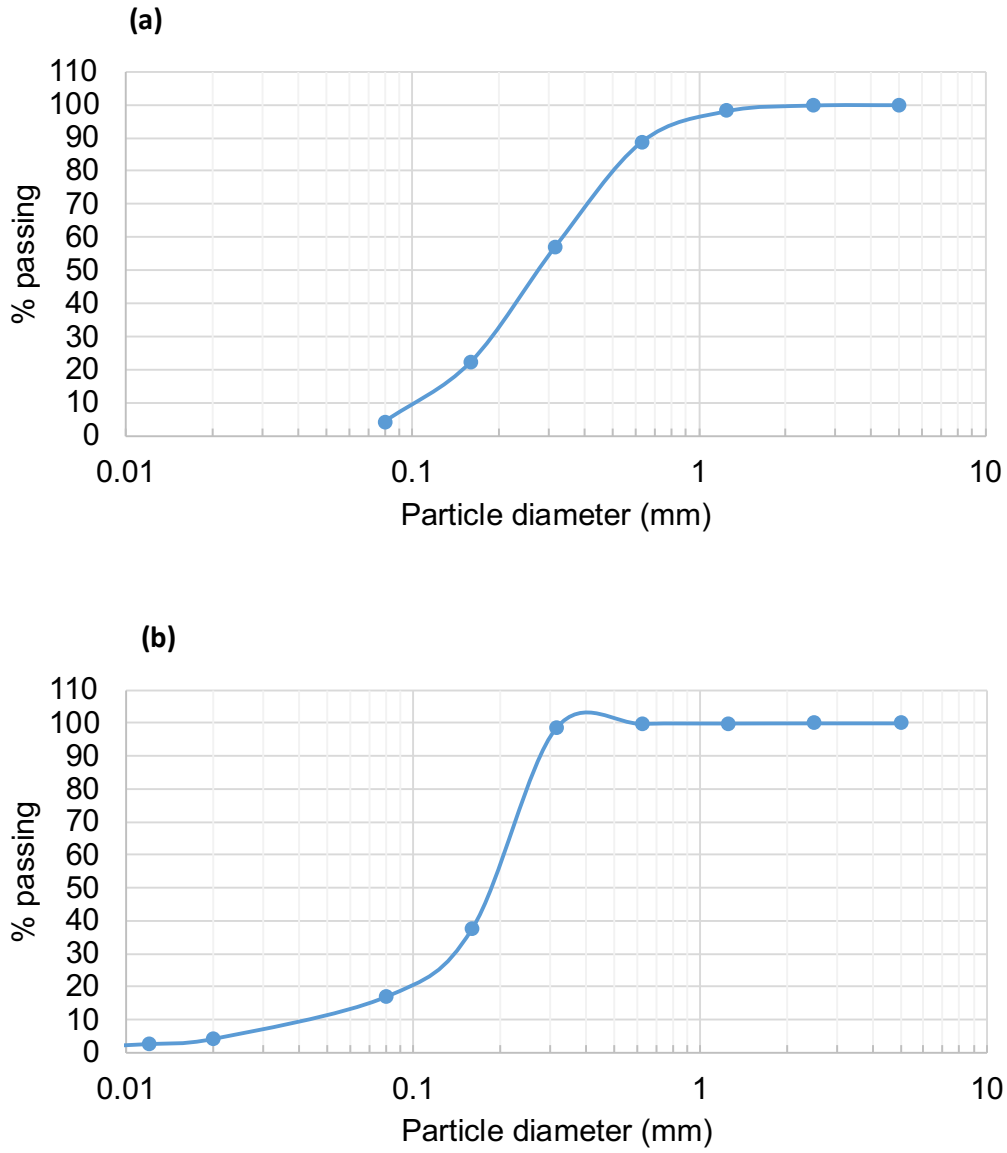

Figure B.2 Particle size distribution curve of (a) Soil 1, and (b) Soil 2.

B.3 Reconstituted wastewater preparation

The wastewater was prepared according to Table B.1, incorporating synthetic primary effluent inoculated with primary sludge from a Water Resource Recovery Facility (WRRF). The sludge originated from the St-Hyacinthe WRRF, Quebec. This facility was selected for its primary sludge, which contains fewer coagulants compared to other sources. Notably, at this WRRF, the contribution of industrial sources is primarily from food industries, thus sharing many characteristics with domestic wastewater. Primary sludge was divided into 14 ml subsamples in sterile plastic containers at the time of collection and stored at -20 °C. Feeding was done from a barrel kept at 4°C to prevent biological degradation of the wastewater and was renewed every 5 days. At each feed renewal, the desired primary sludge was thawed and added to the barrel.

Table B.1 Reconstituted wastewater recipe.

Ingredient of reconstituted wastewater	**Quantity**	**Ingredients of trace elements solution**	**Quantity**
Sodium acetate	0.3-0.2 g	EDTA	8 g
Dextrose	0.15 g	Iron (III) Chloride - FeCl3	3.6 g
Soy peptone	0.15 g	Boric acid - H_3BO_3	0.36 g
K_2HPO_4	0.04 g	Copper (II) Sulfate Pentahydrate - $CuSO_4.5H_2O$	0.072 g
KH_2PO_4	0.01 g	Molybdic acid sodium dihydrate - $Na_2MoO_4.2H_2O$	0.144 g
NH_4Cl	0.13 g	Potassium Iodide - KI	0.432 g
Primary sludge	0.7 mL	Cobalt (II) Chloride - $CoCL_2.6H_2O$	0.36 g
Traces elements solution	0.5 mL	Manganese (II) chloride tetra hydrate - $MnCl_2.4H_2O$	0.288 g
Tap water	1 L	Zink sulfate heptahydrate - $ZnSO_4.7H_2O$	0.288 g
		HCl 0.5M	1 mL
		Milli-Q water	1 L

B.4 Visual evidence of biofilm development

Camera images and scanning electron microscopy (SEM) was employed to compare the virgin soil with the soil from the top of the columns to detect any biofilm build-up. Intact samples were collected from the surface of the filters. All samples were oven-dried overnight, then mounted onto aluminum stubs using double-sided sticky tabs, and examined with a Hitachi TM4000-II SEM at a low electron voltage of 5 kV.

Camera images in Figure B.3 provide a visual comparison of the soil surface showing the presence of biofilm and the middle section. In Column 1, the surface soil (Figure B.3a) exhibits notable dark organic accumulation, indicating biofilm presence. This contrasts with the cleaner appearance of the middle section (Figure B.3b). In Column 2, the surface soil (Figure B.3e) shows dark organic accumulation, while the middle section (Figure B.3f) remained relatively clean. Camera images further illustrate that biofilm growth in Column 1 was primarily concentrated at the center of the cross-section, leaving the perimeter less influenced by biofilm development, which further supports the notion that wastewater infiltration in Column 1 predominantly occurred through the central portion of the column. In contrast, Column 2 exhibited a more uniformly distributed biofilm layer across the surface, which facilitated a more even spread of inflow and resulted in a broader infiltration pattern.

In column 1, SEM images confirm the presence of the biofilm on the surface (Figure B.3c), where particles appeared to have dark coatings. In contrast, the SEM image of virgin soil (Figure B.3d) shows clean, uncoated, smoother and more even soil particles. In Column 2, SEM imaging of the surface (Figure B.3g) reveals a rougher texture with aggregated particles, consistent with biofilm formation. The SEM image of virgin soil (Figure B.3h) shows cleaner, more angular particles. In both columns, the surface sand grains were visible, indicating that neither column experienced complete filling of voids due to excessive biofilm growth.

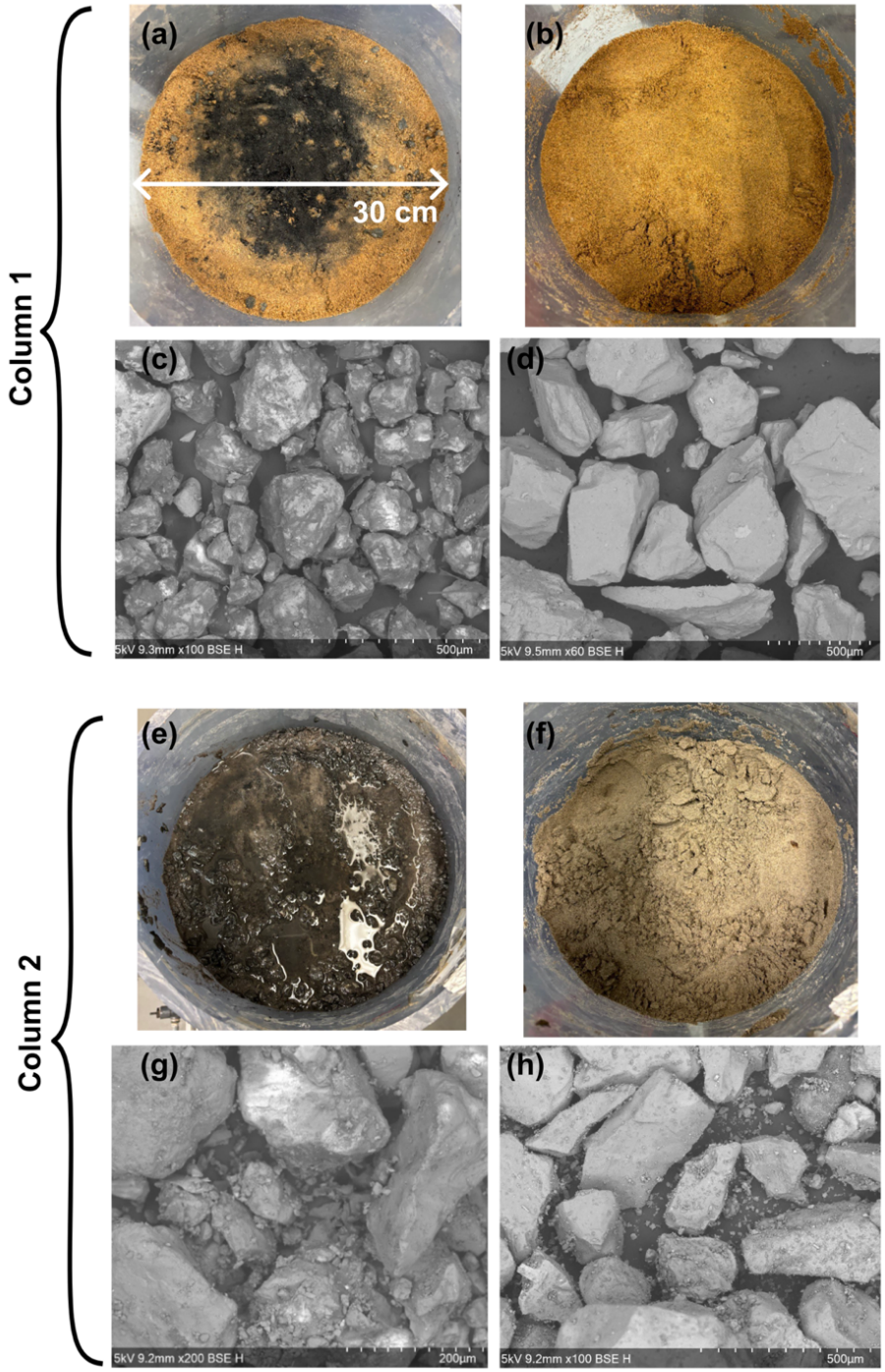

Figure B.3 Camera photography and SEM images of the soil with and without biofilm. (a) Camera photography of the surface of Column 1, (b) middle section of Column 1, (c) SEM image of the surface of Column 1, (d) virgin soil used in Column 1, (e) camera photography of the surface of Column 2, (f) middle section of Column 2, (g) SEM image of the surface of Column 2, and (h) virgin soil used in Column 2.

B.5 Environmental conditions

The mean pH of the feed was 6.7 ± 0.2, while the effluent pH averaged 7.9 ± 0.1 in Column 1 and 7.8 ± 0.3 in Column 2. Time series of pH of the influent and effluent is provided in Figure B.4. Within the soil, pH averaged 7.4 ± 0.4 in Column 1 and 7.1 ± 0.2 in Column 2. This pH range (6.5 to 8.1) created favourable conditions for both nitrification and denitrification processes (Vidal et al., 2023). The temperature in the columns varied from 22.7 to 26.1°C, which is close to the optimal range for nitrification (28–36°C) (Vidal et al., 2023) and denitrification (25–35°C) (Qu et al., 2022). Time series of temperature along the two columns is provided in Figure B.5.

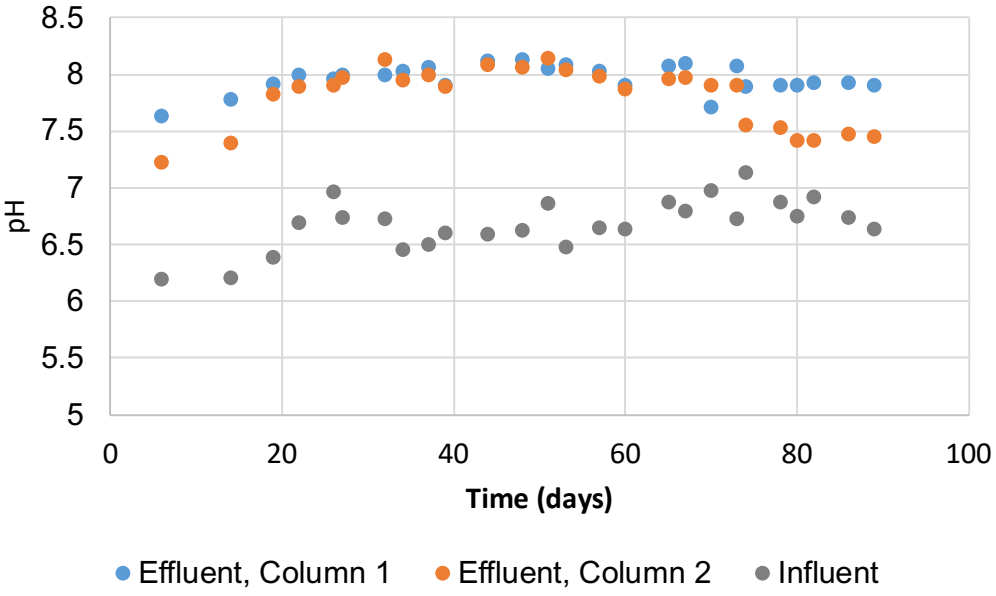

Figure B.4 pH of the effluents from Column 1 and 2 and the influent.

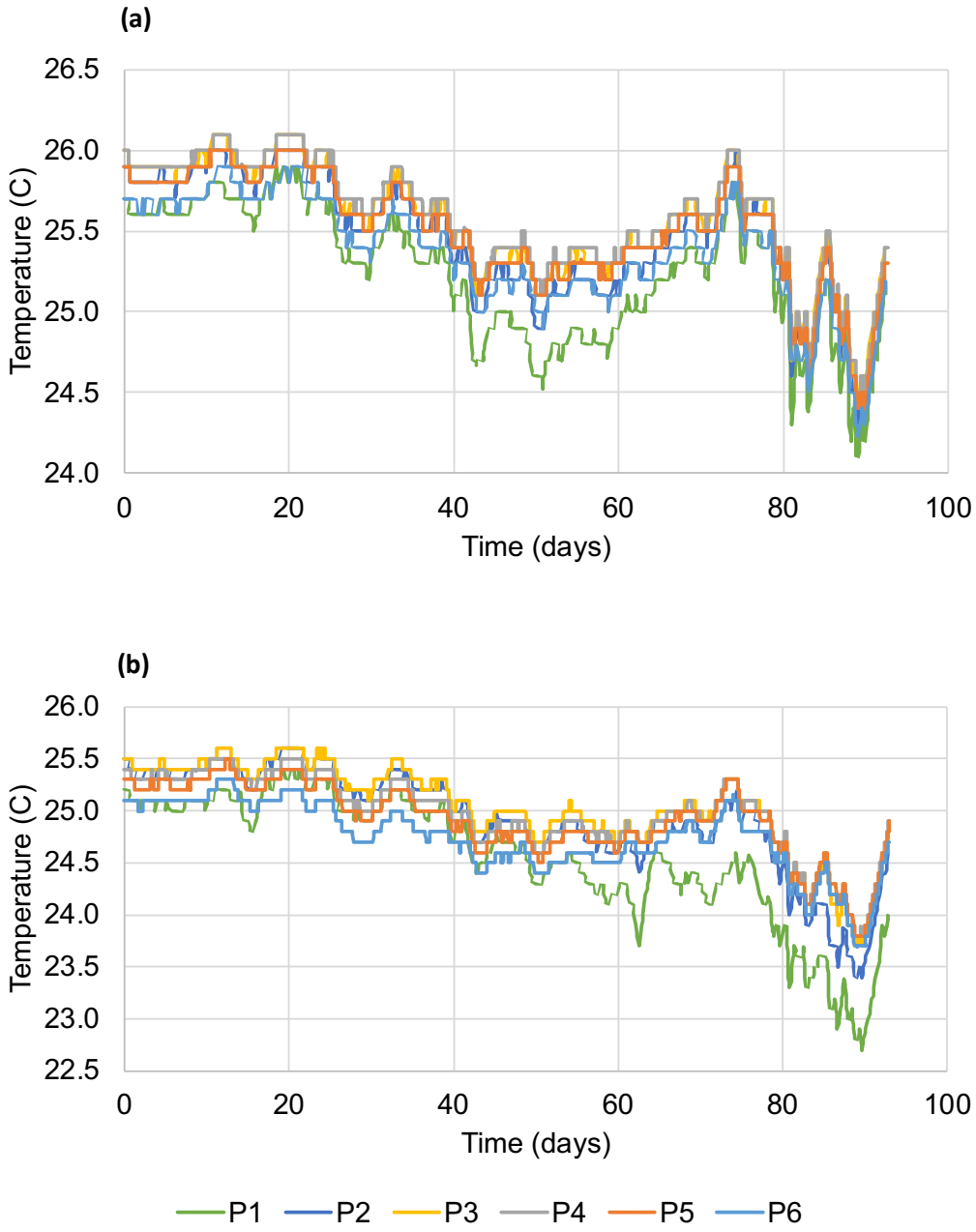

Figure B.5 Time series of Temperature measured at various depths along (a) Column 1 and (b) Column 2. Measurement points (P1–P6) are distributed from a height of 0.88 m (P6) to 0.24 m (P6), with intermediate points located in between.

During nitrification, each gram of NH_4^+-N consumes approximately 7.14 g of $CaCO_3$ alkalinity, while denitrification generates about 3.57 g of $CaCO_3$ per gram of NO_3^--N reduced, replenishing about half of the alkalinity lost during nitrification. Alkalinity was measured in weeks 6, 9, and 12

by titrating 50 mL samples with 0.02 N sulfuric acid to pH 4.5 and 4.2, calculated using the following equation:

$$Alkalinity\ \left(\frac{mg}{L}CaCO_3\right) = 20(2B - C) \quad \text{(B. 1)}$$

where B [mL] and C [mL] are the volumes of sulfuric acid consumed to reach pH 4.5 and 4.2 respectively.

The alkalinity levels in both the influent and effluent are presented in Table B.2. Despite the initial alkalinity limitations, nitrification was achieved in both columns, and alkalinity remained present in the effluent of both columns. The observed increase in effluent pH (Figure B.4) relative to the influent in both columns suggests that mineral dissolution within the soil contributed to enhancing systems' alkalinity. Moreover, The EC data from the embedded probes (Figure B.6) indicate a gradual increase in EC from the top to the bottom of the column, supporting the hypothesis of mineral dissolution occurring within the system.

In Column 2, the effluent alkalinity was higher than in Column 1, which is likely linked to higher denitrification rates. By week 12, when nearly complete TN removal was observed in Column 2, there was a corresponding increase in effluent alkalinity, further supporting the occurrence of denitrification.

Table B.2 Alkalinity levels measured in both the influent and effluent of the columns.

	Alkalinity (mg $CaCO_3$/L)		
	Influent	Column 1 effluent	Column 2 effluent
Week 6	133.9	97.3	114.7
Week 9	138.5	76.9	127.1
Week 12	151.9	77.5	253.4

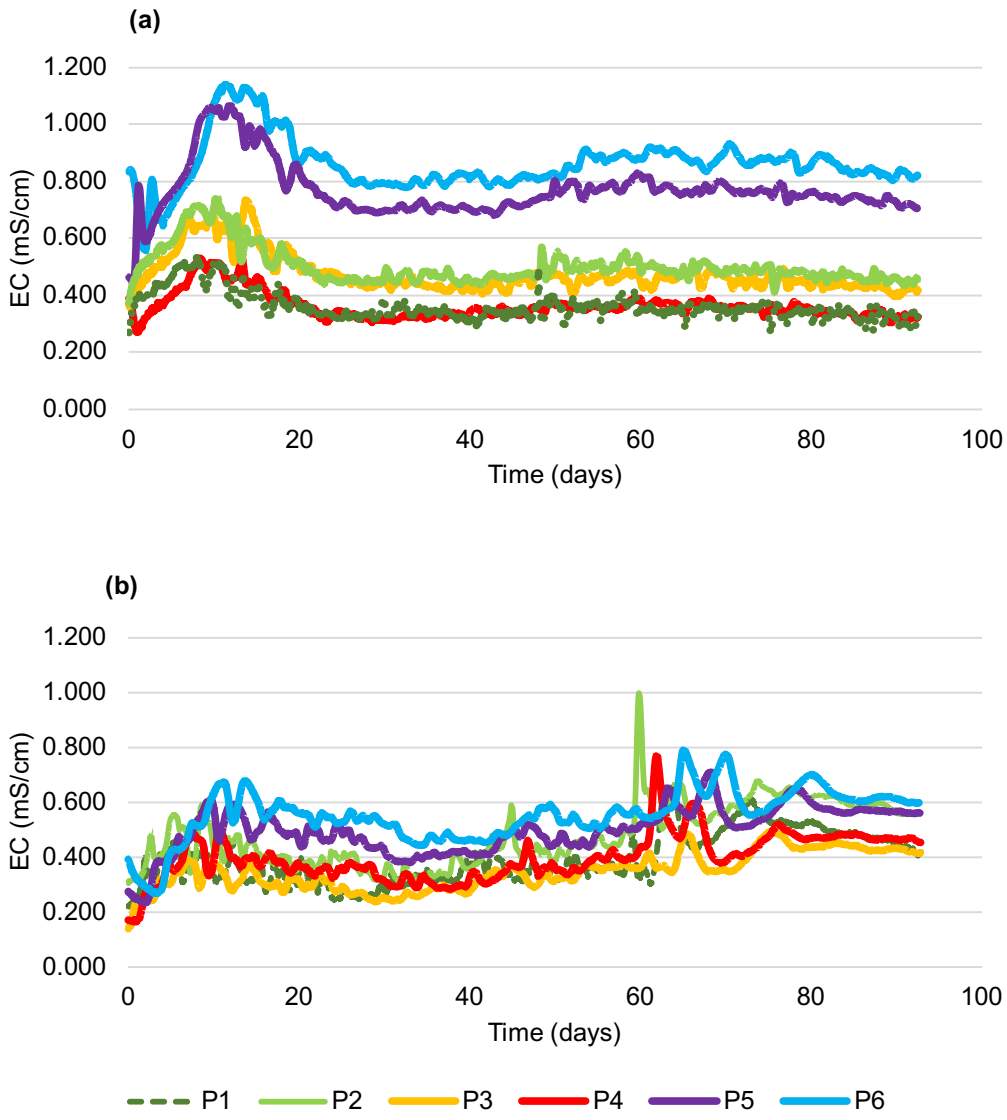

Figure B.6 Time series of electrical conductivity (EC) measured at various depths along (a) Column 1 and (b) Column 2. Measurement points (P1–P6) are distributed from a height of 0.88 m (P6) to 0.24 m (P6), with intermediate points located in between.

APPENDIX C: MICROBIAL AND FUNCTIONAL RESPONSES TO MOISTURE RETENTION IN SOIL TREATMENT UNITS: IMPLICATIONS FOR NITROGEN TRANSFORMATION PATHWAYS

This appendix provides supplementary information related to Chapter 6.

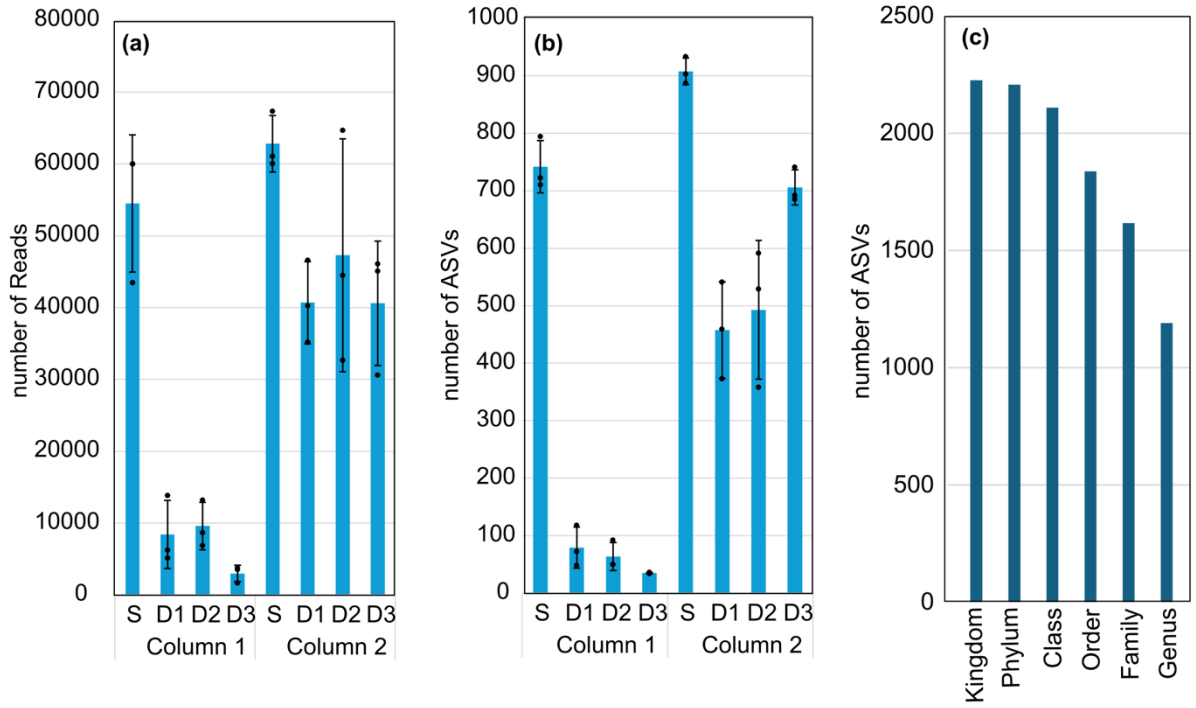

Figure C.1 (a) Sequencing reads across samples from the surface (S) and depths of 12 cm (D1), 24 cm (D2), and 36 cm (D3) in Column 1 and Column 2. Bars show mean read counts ± SD (n = 3), and points represent biological replicates. (b) Distribution of detected ASVs across samples. (c) Number of ASVs assigned to different taxonomic levels, from Kingdom to Genus.

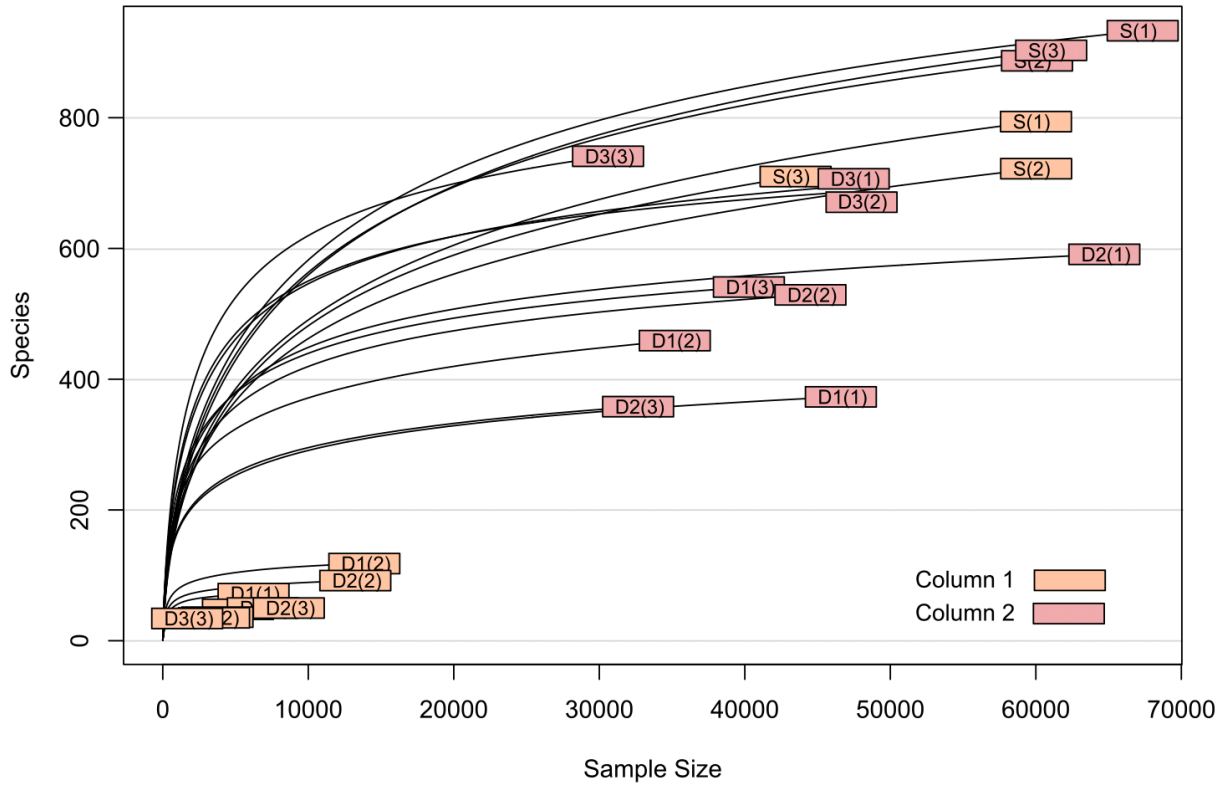

Figure C.2 Rarefaction curves showing observed ASV richness as a function of sequencing depth, with samples from Column 1 (orange shades) and Column 2 (pink shades). Curves are labelled according to sampling depth of S, D1, D2 and D3 and replicate number (1–3).

Table C.1 Environmental variables (pH, TC, WFP, NH_4-N, and NO_3-N), included in the RDA.

Depth (m)	Column	pH	TC (%)	WFP	NH_4-N (mg/kg)	NO_3-N (mg/kg)
surface	1	6.7	0.21	0.32	3	5
0.12	1	6.9	0.09	0.58	3	3
0.24	1	7.5	0.04	0.61	2	1
0.36	1	7.7	0.05	0.5	2	2
surface	2	7	0.12	1	9	1
0.12	2	7.1	0.03	0.83	9	3
0.24	2	7.3	0.03	0.81	12	2
0.36	2	6.9	0.01	0.91	4	6

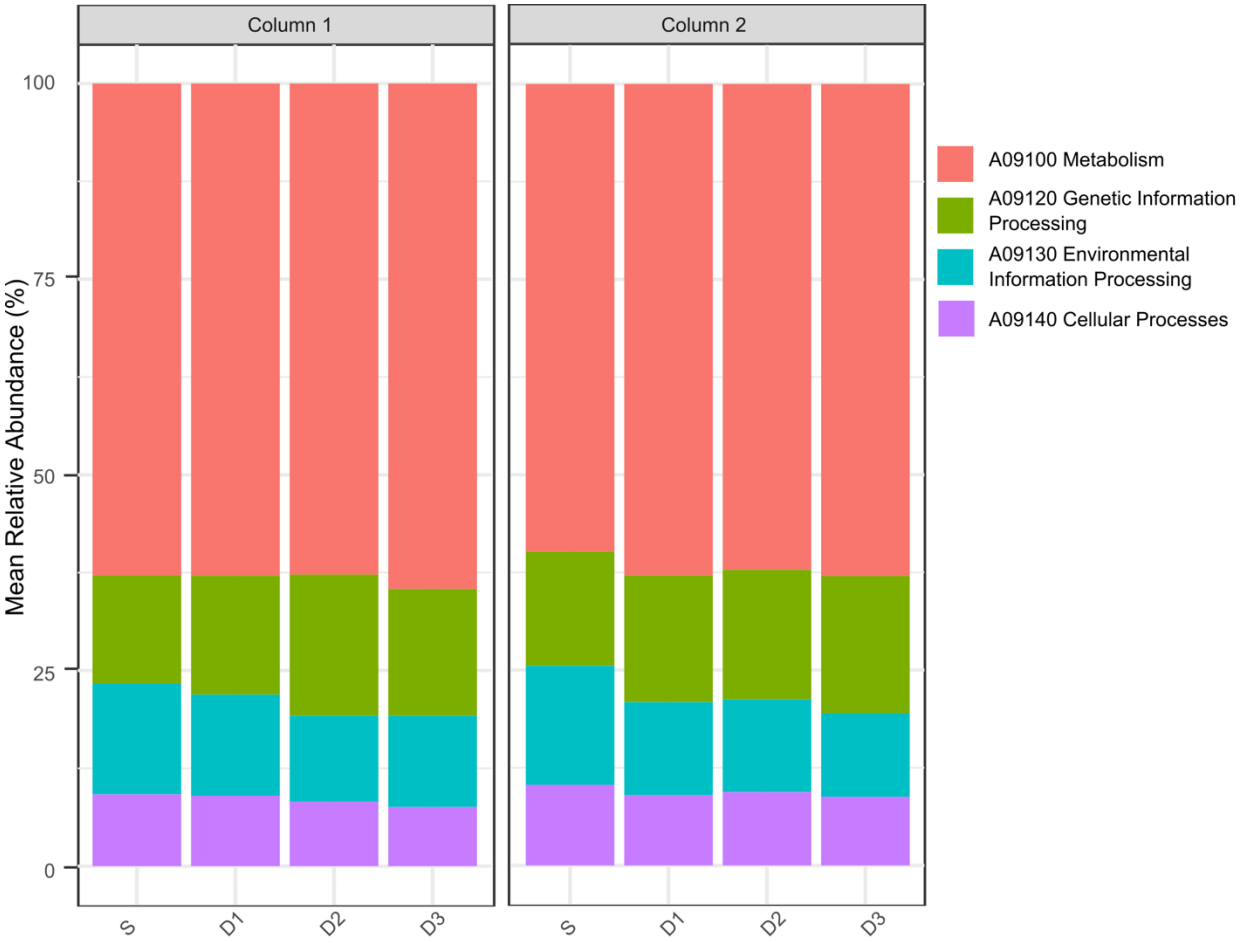

Figure C.3 KEGG Level-1 functional profile (PICRUSt2). Stacked bars show the mean relative abundance (%) at the surface (S) and depths of 12 cm (D1), 24 cm (D2), and 36 cm (D3) in Column 1 and Column 2.

Figure C.4 KEGG Level-2 functional profile (PICRUSt2). Cells show the mean relative abundance (%) of Level-2 pathways (color scale 0–10%) at the surface (S) and depths of 12 cm (D1), 24 cm (D2), and 36 cm (D3) in Column 1 and Column2. Rows are pathways, grouped by their Level-1 parent categories.

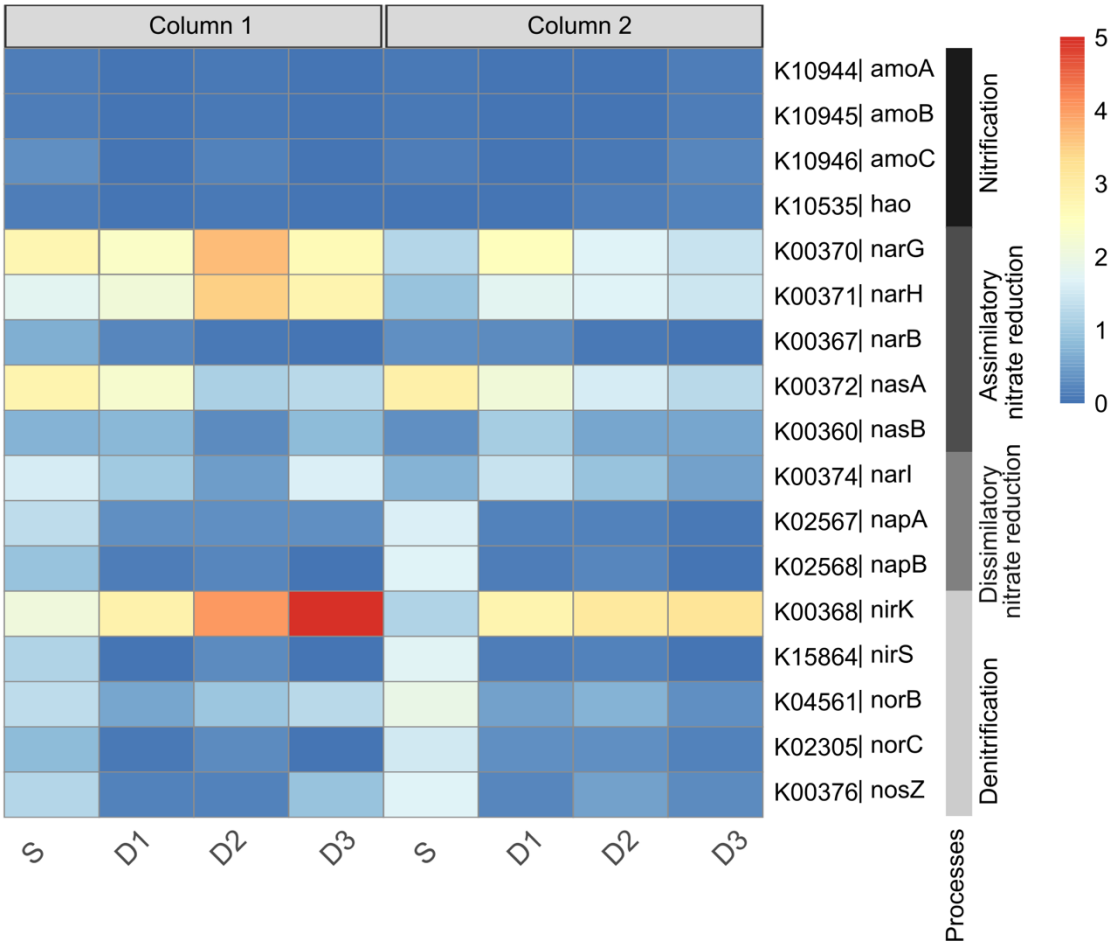

Figure C.5 Nitrogen-cycle marker genes (KEGG KOs) predicted by PICRUSt2. Cells show mean relative abundance (%) (color scale 0–5%) at the surface (S) and depths of 12 cm (D1), 24 cm (D2), and 36 cm (D3) in Column 1 and Column 2 and grouped by process. Rows list KOs for nitrification (amoABC and hao), assimilatory nitrate reduction (narGHB and nasAB), dissimilatory nitrate reduction (napAB and narI), and denitrification (nirKS, norBC, and nosZ).